ISSN 2518-1726 (Online),
ISSN 1991-346X (Print)

ҚАЗАҚСТАН РЕСПУБЛИКАСЫ
ҰЛТТЫҚ ҒЫЛЫМ АКАДЕМИЯСЫНЫҢ
әл-Фараби атындағы Қазақ ұлттық университетінің

Х А Б А Р Л А Р Ы

ИЗВЕСТИЯ

НАЦИОНАЛЬНОЙ АКАДЕМИИ НАУК
РЕСПУБЛИКИ КАЗАХСТАН
Казахский национальный университет
им. аль-Фараби

N E W S

OF THE NATIONAL ACADEMY OFSCIENCES
OF THE REPUBLIC OF KAZAKHSTAN
Al-Farabi Kazakh
National University

SERIES
PHYSICO-MATHEMATICAL

4 (332)

JULY – AUGUST 2020

PUBLISHED SINCE JANUARY 1963

PUBLISHED 6 TIMES A YEAR

ALMATY, NAS RK

«ҚР ҰҒА Хабарлары. Физика-математикалық сериясы».
ISSN 2518-1726 (Online), ISSN 1991-346X (Print)
Меншіктенуші: «Қазақстан Республикасының Ұлттық ғылым академиясы» РҚБ (Алматы қ.).
Қазақстан Республикасының Ақпарат және коммуникациялар министрлігінің Ақпарат комитетінде 14.02.2018 ж. берілген **№ 16906-Ж** мерзімдік басылым тіркеуіне қойылу туралы куәлік.
Мерзімділігі: жылына 6 рет.
Тиражы: 300 дана.

Редакцияның мекенжайы: 050010, Алматы қ., Шевченко көш., 28; 219, 220 бөл.; тел.: 272-13-19; 272-13-18, http://physics-mathematics.kz/index.php/en/archive

---

Типографияның мекенжайы: «NurNaz GRACE», Алматы қ., Рысқұлов көш., 103.

«Известия НАН РК. Серия физика-математическая».
ISSN 2518-1726 (Online), ISSN 1991-346X (Print)
Собственник: РОО «Национальная академия наук Республики Казахстан» (г. Алматы).
Свидетельство о постановке на учет периодического печатного издания в Комитете информации Министерства информации и коммуникаций Республики Казахстан **№ 16906-Ж**, выданное 14.02.2018 г.
Периодичность: 6 раз в год.
Тираж: 300 экземпляров.

Адрес редакции: 050010, г. Алматы, ул. Шевченко, 28; ком. 219, 220; тел.: 272-13-19; 272-13-18,
http://physics-mathematics.kz/index.php/en/archive

Адрес типографии: «NurNaz GRACE», г. Алматы, ул. Рыскулова, 103.

News of the National Academy of Sciences of the Republic of Kazakhstan. Physical-mathematical series.
ISSN 2518-1726 (Online), ISSN 1991-346X (Print)
Owner: RPA "National Academy of Sciences of the Republic of Kazakhstan" (Almaty).
The certificate of registration of a periodical printed publication in the Committee of information of the Ministry of Information and Communications of the Republic of Kazakhstan **No. 16906-Ж**, issued on 14.02.2018.
Periodicity: 6 times a year.
Circulation: 300 copies.

Editorial address: 28, Shevchenko str., of. 219, 220, Almaty, 050010, tel. 272-13-19; 272-13-18,
http://physics-mathematics.kz/index.php/en/archive

Address of printing house: «NurNaz GRACE», 103, Ryskulov str, Almaty.

NEWS
OF THENATIONAL ACADEMY OF SCIENCES OF THE REPUBLIC OF KAZAKHSTAN
PHYSICO-MATHEMATICAL SERIES
ISSN 1991-346X **https://doi.org/10.32014/2020.2518-1726.59**
Volume 4, Number 332 (2020), 5 – 12

UDC 538.95;
IRSTI 29.19.22

Zh.E. Ayaganov[1], M.T. Gabdullin[2], D.G. Batryshev[1,4], T.S. Ramazanov[1], N.R. Guseinov[2], Ray Baughman[3]

[1]Al-Farabi Kazakh National University, Almaty, Kazakhstan;
[2]National Nanotechnology Laboratory of Open Type, Al-Farabi KazNU, Almaty, Kazakhstan;
[3]The Alan G. MacDiarmid NanoTech Institute, University of Texas at Dallas, Richardson, USA;
[4]Kh. Dosmukhamedov Atyrau State University, Atyrau, Kazakhstan.
E-mail: zhanibek13@gmail.com

SYNTHESIS OF CARBON NANOTUBES WITH NI-TI CATALYST

Abstract. Carbon nanotubes have been of interest to the scientists for about 30 years due to their unique properties. Their use as a material for creating flexible conductive coatings, supercapacitors, batteries and solar cells is promising because of their excellent mechanical and electrical properties, as well as high electrochemical stability. In this paper, we consider one of the methods for the synthesis of carbon nanotubes on a Ni-Ti bimetallic catalyst on a silicon substrate. The effect of the thickness of the catalytic layer and the synthesis temperature on the quality of the obtained samples was studied. The synthesis was carried out by the CVD method as the most convenient technique with the possibility of a large yield of the final product. The obtained samples were studied by scanning electron microscopy and Raman spectroscopy. It was found that with an increase in the synthesis temperature and a decrease in the thickness of the catalytic layer, the crystallinity of the structure improves the number of defects in the structure decreases and structural ordering increases. The use of a catalyst and an adhesive metal layer, which was a barrier between the catalyst and the substrate, shows good results in improving the quality of the synthesis of nanotubes.

Keywords: carbon nanotubes, synthesis, chemical vapor deposition (CVD), catalyst, magnetron sputtering.

Introduction. A carbon nanotube is a hollow cylindrical structure with a diameter of one to several tens of nanometers, a length of one to several hundred micrometers or more, formed by carbon atoms and is a graphene plane rolled into a cylinder. For the first time, CNTs were systematically described by Sumio Iijima (NEC Corporation), who discovered them in 1991 as a by-product of the synthesis of fullerene C60 [1], and, almost simultaneously with it, the L.A. group Chernozatonsky [2]. Mention of the existence of unusual forms of carbon similar in morphology was encountered earlier [3, 4], however, these works did not receive further development.

Carbon nanotubes (CNTs) have many physical and chemical properties many of which are unique. CNTs have very high thermal conductivity [5,6], strength [7], and the tensile modulus is many times higher than that of steel. A wide range of electrical conductivity [8, 9] from semiconductor to metal makes them promising for creating conductors and pn junctions in nanoelectronics, for creating conductive high-strength composite materials and functional additives to polymers. The use of carbon nanotubes in various fields of science and technology is a promising task [10]. In addition, carbon materials, such as amorphous carbon or activated carbon, are widely used, and their replacement with CNTs in some cases gives a unique effect, limited only by the higher cost of CNTs compared to other carbon materials. Therefore, the development of effective methods for the synthesis of CNTs is a very urgent task.

CVD is a method with a high level of process control that allows you to control the growth location and geometric parameters of carbon tubes on any type of substrate [11]. To obtain an array of CNTs on the substrate surface, a seed layer is needed. A thin metal film acts as a seed layer, which is a catalyst for the growth of CNTs; mainly nickel, iron, and cobalt act as such metals. A catalyst film can be formed using

the methods of chemical deposition from a solution containing a catalyst, thermal evaporation, ion beam sputtering, or magnetron sputtering. The main issue of this work was to study the effect of a buffer layer, as well as the temperature dependence and thickness of the catalytic layer on the growth of CNTs.

Experiment. In this work, a bimetallic catalyst was used to synthesize CNTs. Its preparation included 2 stages: the deposition of a catalytic layer and the formation of nanoclusters. At the first stage, a thin layer of titanium with a thickness of 80 nm is deposited on the pre-cleaned substrate using the magnetron sputtering method. After that, 0.5 to 10 nm thick nickel layers were deposited using the second magnetron, which is in the same chamber. The thickness of the forming layer is adjusted according to the indications of quartz microbalances previously calibrated for the sputtered materials. The second stage is the formation of nanoclusters, which occurs during the replacement of the substrate from the cold zone of CVD the reactor to a hot one, pre-heated to the synthesis temperature. Within 5 minutes after the placement of the substrate into the hot zone, the catalyst film transforms into nanoclusters. The process takes place in a stream of hydrogen, which reduces the catalyst because thin metal films oxidize very quickly in the air. This is necessary for high catalytic activity. A longer heating duration leads to an increase in the particle size of the catalyst, which in turn affect the tubes' diameter. The synthesis of CNTs by the CVD method of was carried out in a tubular sealed quartz reactor at atmospheric pressure in a stream of hydrogen equal to 4 normal liters per hour (figure 1). The carbon source in the synthesis process was ethanol vapor. In the preparation stage for the synthesis, the chamber while heating was preliminary blown out with nitrogen for 10 minutes to remove oxygen, and only after that the hydrogen was let into the chamber. In addition, at the stage of the heating, the hydrogen passed through the bubbler previously blowing all the air out of volume unfilled with ethanol. The bubbler and the reaction zone of the chamber were cut out with valves, which were opened only at the time of synthesis. The flow of hydrogen passing through a bubbler carries the ethanol vapour into the reaction zone of the chamber, where under the high temperature the ethanol decomposes into carbon and hydroxyl group. The latter in turn combines with hydrogen, forming water vapor or interacting with an amorphous carbon formed in the process of the synthesis, oxidizing it this way and removing from the substrate increasing the catalyst activity time. We experimentally found out an optimal temperature for our chamber configuration. It ranges from 880°C to 950°C. Upon reaching the synthesis temperature, a stream of hydrogen is directed through a bubbler with ethanol at room temperature. Upon completion of the synthesis, the hydrogen flow is stopped and the bubbler is cut out with valve. Samples were taken into the cold zone. Subsequent cooling of the reactor took place in a stream of nitrogen. After taking the samples out the reactor, one can see that the substrates are covered with a soot.

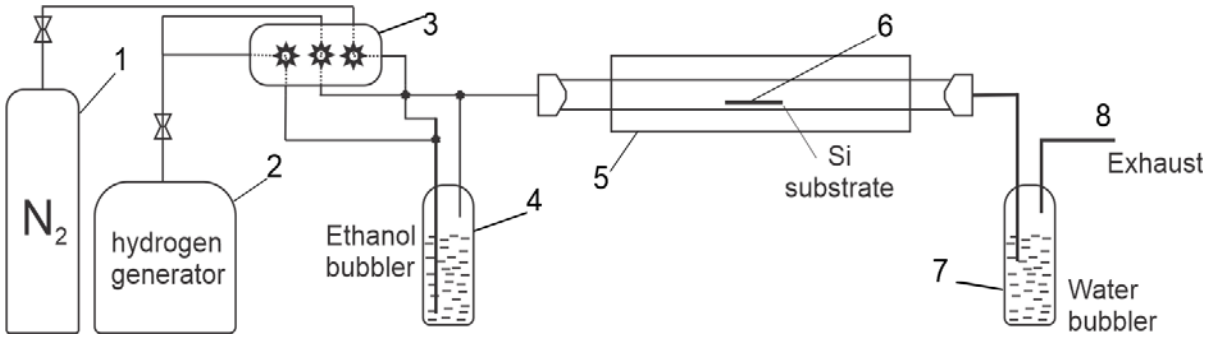

Figure 1 - The structure of the CVD installation for the synthesis of carbon nanomaterials.
1 - nitrogen gas, 2 - hydrogen generator, 3 - gas flow meters, 4 - bubbler with ethanol, 5 - tubular flow reactor, 6 - substrate, 7 - bubbler with water for gas purification, 8 - discharge to the atmosphere

Figure 2 shows silicon substrates coated with a nickel-titanium catalyst before and after the synthesis of CNTs by CVD. It is seen that after the synthesis the substrate surface with catalyst layer is covered with soot, which indicates the possible deposition of carbon nanostructures, including CNTs.

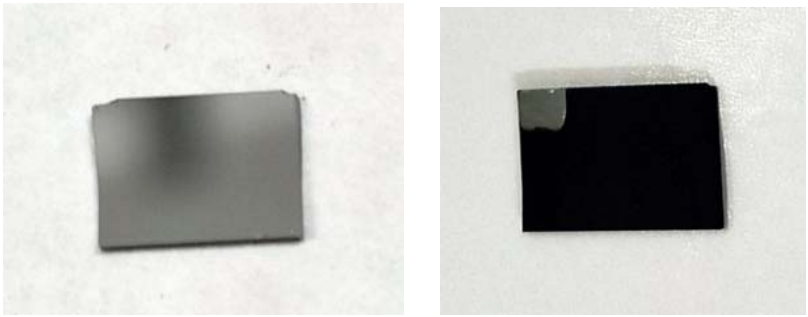

a b

Figure 2 - Silicon substrates with a nickel-titanium catalyst
(a) - before and (b) after synthesis of CNTs by CVD

Results and discussions. It is known from the literature [12] that the average size of catalyst nanoclusters formed after annealing depends on the thickness of the initial film, as well as the duration of heating of the substrate. During our experiments, it was found out that the synthesis temperature plays a key role in this process, because at different thicknesses of the deposited catalyst layer and at the same annealing temperature, the diameters of the tubes are the same. However, with an increase in the synthesis temperature, the diameter of CNTs decreases significantly. Using SEM analysis, talking about the diameter of the tubes is only conditional. However, this analysis shows a significant change in size with increasing temperature (figure 4-5).

To improve the quality of the synthesized CNTs, the so-called titanium buffer layer was used in this work. As the experimental results show, in the absence of a buffer layer during high-temperature heating, the silicon substrate material interacts with the catalyst, leading to the formation of nickel silicide islands [13] (figure 3a). As can be seen from Figure 3b, CNT growth occurs only on these areas. On the rest of the substrate, where no islands are formed, the catalyst loses its activity, possibly due to the diffusion process into the surface of the substrate (figure 3c).

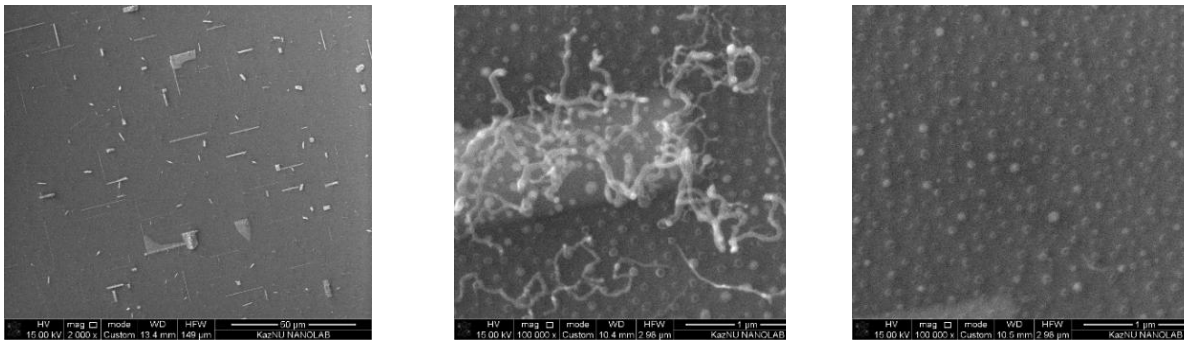

a b c

Figure 3 - The formed islands of nickel silicide (a) and selective growth of CNTs on it (b,c)

Thus, to prevent the diffusion of nickel into silicon and the formation of nickel silicide, a thin film of a titanium buffer layer was deposited on the silicon surface. Under the high temperature, a titanium-nickel alloy is formed, which subsequently exhibits high catalytic activity. An analysis of the results showed that an increase in the synthesis temperature affects the quality of the obtained samples. The properties of these samples were studied by scanning electron microscopy (figure 4-5) and Raman spectroscopy (figure 6). Raman signal of the synthesized products corresponds to a typical spectrum of multi-walled carbon nanotubes (MWCNTs) [14]. Analysis of the Raman data shows that with increase in the synthesis temperature, the quality of the obtained samples improves; this is evidenced by an increase in the G peak's intensity and a decrease of the D peak intensity (characterizing the defective structure).

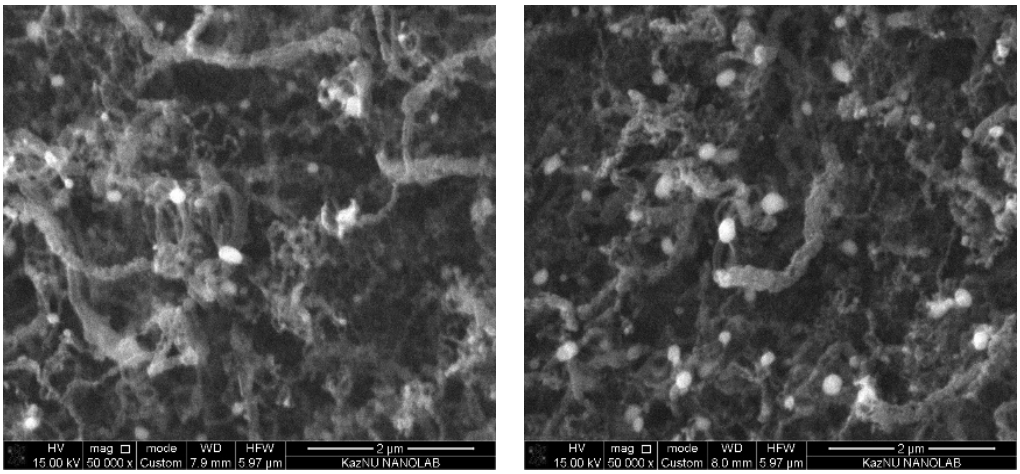

a – Ni (5 nm), Ti (80 nm) b – Ni (10 nm), Ti (80 nm)

Figure 4 - CNT samples synthesized at a temperature of 880°C and synthesis time t - 1 min

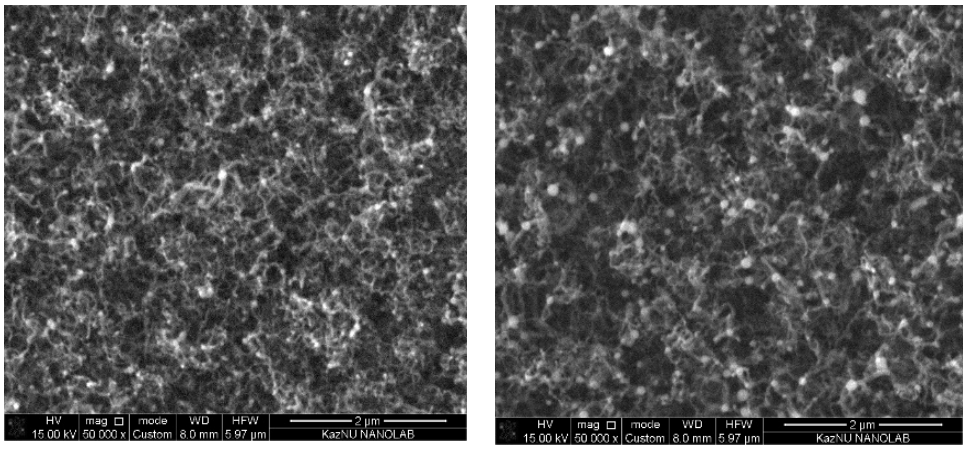

a – Ni (5 nm), Ti (10 nm) b – Ni (10 nm), Ti (80 nm)

Figure 5 - Samples of MWCNTs synthesized at a temperature of 950°C and synthesis time t - 1 min

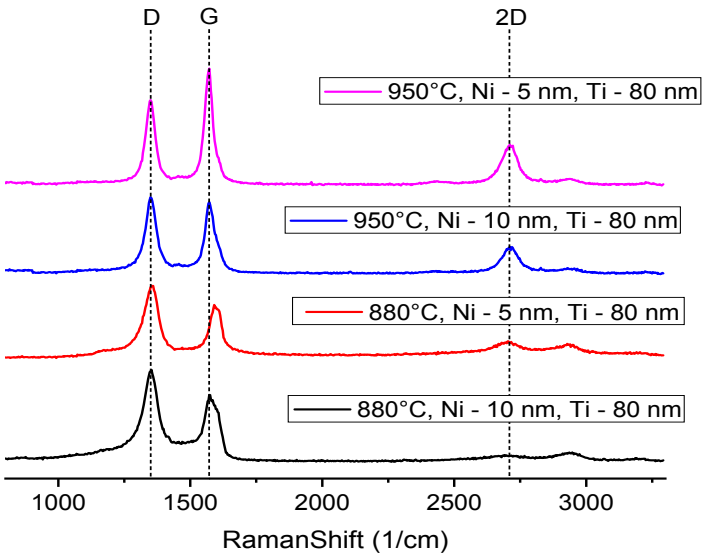

Figure 6 - Raman spectra of obtained MWCNTs

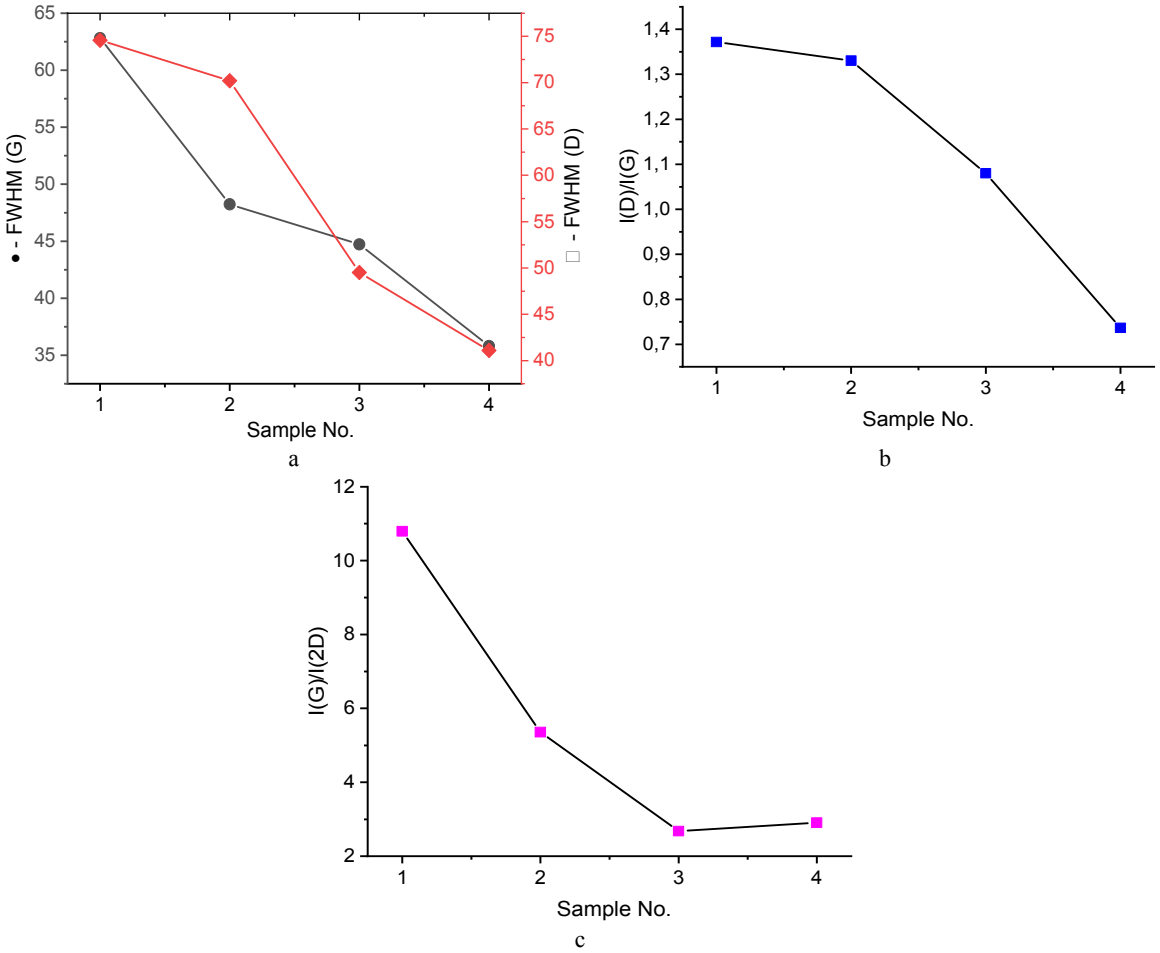

where No. 1 and No. 3 are samples of Ni (10 nm), Ti (80 nm), T = 880 and 950 °C, respectively,
No. 2 and No. 4 are samples of Ni (5 nm), Ti (80 nm), T = 880 and 950 °C, respectively

Figure 7 - Data analysis of the Raman spectra of CNTs

A more detailed analysis of the Raman spectra of CNTs is presented in figure 7. It can be seen that with increasing temperature and decreasing thickness of the catalytic layer, such trends are observed: narrowing of the half-width of the peaks (figure 7a), which indicates an increase in the crystallinity of the structure; a decrease in the intensity of peak D, which is represented by the ratio I(D)/I(G), indicating a decrease in the number of defects in the structure (figure 7b); a decrease in the ratio of G to 2D peaks' intensity, which indicates an increase in structural ordering in the mutual arrangement of atoms (figure 7c) [15-16]. Thus, it was shown in the work that the use of a titanium buffer layer allows to reach effective synthesis conditions, while the diameters and quality of synthesized CNTs depend not only on the thickness of the catalytic film but also on the synthesis temperature.

Conclusion. Due to its variability, the CVD method makes it possible to precisely control the growth of CNTs. By changing the synthesis parameters, one can control the yield and structural parameters of nanotubes. In this work, the influence of the synthesis temperature and the thickness of the catalytic layer on the growth of CNTs, as well as the role of the buffer layer, were demonstrated. An increase of synthesis temperature and a decrease in the thickness of the catalyst improves the crystallinity of nanotubes. The use of a catalyst and an adhesive metal layer, which was a barrier between the catalyst and the substrate, gave positive results in improving the effectiveness of the synthesis of nanotubes. It was previously assumed that the catalyst particles during preliminary annealing can dissolve in titanium and lose their catalytic activity; however, the formed Ti-Ni nanoclusters promoted the catalytic growth of CNTs.

Ж.Е. Аяғанов[1], М.Т. Ғабдуллин[2], Д.Ғ. Батрышев[1,4], Т.С. Рамазанов[1], Н.Р. Гусейнов[2], Р. Боуман[3]

[1]Әл-Фараби атындағы ҚазҰУ, Алматы, Қазақстан;
[2]Ашық түрдегі ұлттық нанотехнологиялық зертхана, әл-Фараби атындағы ҚазҰУ, Алматы, Қазақстан;
[3]Алан Дж. МакДиармида атындағы нанотехнология институты; Техас университеті, Даллас, Ричардсон, Техас, АҚШ;
[4]Х.Досмұхамедов атындағы Атырау мемлекеттік университеті, Атырау, Қазақстан

КӨМІРТЕКТІ НАНОТҮТІКШЕЛЕРДІ NI-TI КАТАЛИЗАТОРЫМЕН СИНТЕЗДЕУ

Аннотация. Отыз жыл бойы көміртекті нанотүтікшелер ерекше қасиетінің арқасында ғалымдарды қызықтырып келеді. Оларды икемді өткізгіш жабын, суперконденсатор, батареялар мен күн батареяларын жасау үшін материал ретінде пайдалану тамаша механикалық және электрлік қасиеттері арқылы әрі жоғары электрохимиялық тұрақтылығымен ерекшеленеді. Мақалада кремний субстратындағы Ni-Ti биметалды катализаторында көміртекті нанотүтікшелерді синтездеу әдістерінің бірін қарастырамыз. Каталитикалық қабаттың қалыңдығы мен синтез температурасының алынған үлгілердің сапасына әсері де зерттелді. CVD синтезді соңғы өнімнің үлкен шығымдылығы арқылы ықтимал ең қолайлы өндіріс әдісі ретінде жүргізді. Алынған үлгілер сканерлеуші электронды және Раман спектроскопиясы арқылы зерттелді. Синтез температурасының өсуі және каталитикалық қабаттың қалыңдығының азаюы негізінде құрылым кристалдылығының жақсаруы, ақау санының азаюы және құрылымдық реттіліктің жоғарылауы байқалды. Катализатор мен төсеніш арасындағы кедергі саналатын, катализатор мен металдың адгезиялық қабатын пайдалану, көміртекті нанотүтікшелер синтезінің сапасын жақсартуда оң нәтиже берді.

Көміртекті нанотүтікше – қуыс цилиндрлік құрылым, диаметрі бірнеше нанометрден басталып ондаған нанометрлерге дейін жететін, ұзындығы бір микрометрден жүздеген микрометрге дейін немесе одан да көп болатын, көміртек атомдарынан түзілген және цилиндрге оралған графен парақшасы. Алғаш рет КНТ жүйелі түрде Сумио Ииджима (Sumio Iijima NEC Corporation) сипаттады, ол оларды 1991 жылы С60 фуллерендер синтезінің жанама өнімі ретінде ашты және онымен бір мезгілде Л.А.Чернозатонскийдің тобы да сипаттаған. Морфологиясы көміртектің ұқсас ерекше формаларының бар екендігі туралы бұрын да кездестірілген, алайда бұл жұмыстар одан әрі дами алмады.

Көміртекті нанотүтікшелер (КНТ) көптеген физикалық және химиялық қасиеттерге ие, олардың көпшілігі ерекше болып келеді. КНТ өте жоғары жылу өткізгіштікке және беріктікке ие, ал созылу модулі болатқа қарағанда бірнеше есе жоғары. Жартылай өткізгіштен металға дейінгі электр өткізгіштіктің кең спектрі оларды наноэлектроникада өткізгіштер мен p-n жартылай өткізгіш құруға, өткізгіштігі жоғары берік композит материалдар мен полимерлерге функционалды қоспалар жасауға КНТ перспективалы етеді. Көміртекті нанотүтікшелерді ғылым мен техниканың әртүрлі саласында қолдану перспективалы тапсырма болып есептеледі. Сонымен қатар, көміртегі материалдары, мысалы, аморфты көміртек немесе активтендірілген көміртек, кеңінен қолданылады және оларды КНТ-мен алмастыру кей жағдайда ерекше эффект береді, алайда басқа көміртекті материалдармен салыстырғанда КНТ қымбат болғандықтан шектеледі. Сондықтан КНТ синтезінің тиімді әдістерін жасау өте өзекті болып саналады..

CVD – кез-келген субстратқа көміртек түтікшелерінің өсу орны мен геометриялық параметрлерін бақылауға мүмкіндік беретін жоғары технологиялық бақылау әдісі. Субстрат бетіне КНТ массивін алу үшін тұқым қабаты қажет. Жұқа металл қабыршағы тұқым қабаты ретінде әрекет етеді әрі КНТ өсуінің катализаторы болып саналады, негізінен металл ретінде никель, темір және кобальт қолдынылады. Катализатор қабыршағын алу үшін катализаторы бар ерітіндіден химиялық тұндыру, термиялық булану, иондық сәуленің шашылуы немесе магнетронның шашырау әдістерін қолдану арқылы қол жеткізуге болады. Бұл жұмыстағы басты мәселе КНТ өсуіне буфер қабатының болуы, сонымен қатар катализатор қабаттың қалыңдығы және синтез температурасына тәуелділік әсерін зерттеу.

Түйін сөздер: көміртекті нанотүтікшелер (КНТ), синтез, химиялық будың тұнбасы (CVD), катализатор, магнетронды шашырату.

Ж.Е. Аяганов[1], М.Т. Габдуллин[2], Д.Г. Батрышев[1,4], Т.С. Рамазанов[1], Н.Р. Гусейнов[2], Р. Боуман[3]

[1]КазНУ им. аль-Фараби, Алматы, Казахстан;
[2]Национальная нанотехнологическая лаборатория открытого типа, КазНУ им. аль-Фараби, Алматы, Казахстан;
[3]Нанотехнологический институт Алана Дж. МакДиармида, Техасский университет в Далласе, Ричардсон, Техас, США;
[4]Атырауский государственный университет имени Х. Досмухамедова, Атырау, Казахстан

СИНТЕЗ УГЛЕРОДНЫХ НАНОТРУБОК НА КАТАЛИЗАТОРЕ NI-TI

Аннотация. Углеродные нанотрубки в течение последних 30 лет, благодаря своим уникальным свойствам, представляют интерес для ученых. Их использование в качестве материала для создания гибких проводящих покрытий, суперконденсаторов, батарей и солнечных элементов является перспективным ввиду того, что они обладают превосходными механическими и электрическими свойствами, а также высокой электрохимической стабильностью. В этой статье рассматривается один из методов синтеза углеродных нанотрубок на Ni-Ti биметаллическом катализаторе на поверхности кремниевой подложки. Также изучено влияние толщины каталитического слоя и температуры синтеза на качество полученных образцов. Синтез проводился методом CVD как один из наиболее распространённых методов получения наноматериалов с большим количественным выходом конечного продукта. Полученные образцы были изучены методами сканирующей электронной микроскопии и спектроскопии комбинационного рассеяния. Обнаружено, что с ростом температуры синтеза и уменьшением толщины каталитического слоя наблюдается улучшение кристалличности структуры, уменьшение количества дефектов и рост структурной упорядоченности. Использование катализатора и адгезионного слоя металла, который являлся барьером между катализатором и подложкой, дало положительные результаты в улучшении качества синтеза углеродных нанотрубок.

Углеродная нанотрубка – это полая цилиндрическая структура диаметром от нескольких до нескольких десятков нанометров, длиной от одной до нескольких сотен микрометров и более, образованная атомами углерода и представляющая собой плоскость графена, свёрнутую в цилиндр. Впервые УНТ систематически описаны Сумио Иидзимой (Sumio Iijima, корпорация NEC), обнаружившего их в 1991 г. как побочный продукт синтеза фуллерена C60, и практически одновременно с ним – группой Л.А. Чернозатонского. Упоминания о существовании схожих по морфологии необычных форм углерода встречались и раньше, однако дальнейшего развития эти работы тогда не получили.

Углеродные нанотрубки (УНТ) обладают множеством физических и химических свойств, многие из которых уникальны. УНТ имеют очень высокую теплопроводность и прочность, а модуль упругости при растяжении во много раз выше, чем у стали. Широкий диапазон электропроводности от полупроводника до металла делает их перспективными для создания проводников и pn-переходов в наноэлектронике, для создания проводящих высокопрочных композитных материалов и функциональных добавок к полимерам. Применение углеродных нанотрубок в различных областях науки и техники является перспективной задачей. Кроме того, углеродные материалы, такие как аморфный углерод или активированный уголь, широко применяются, и их замена на УНТ в некоторых случаях даёт уникальный эффект, ограниченный только более высокой стоимостью УНТ по сравнению с другими углеродными материалами. Поэтому разработка эффективных методов синтеза УНТ очень актуальна.

CVD является методом с высоким уровнем контроля процесса, который позволяет контролировать местоположение роста и геометрические параметры углеродных трубок на любом типе подложки. Чтобы получить массив УНТ на поверхности подложки, нужен затравочный слой. В качестве затравочного слоя выступает тонкая плёнка металла, которая является катализатором для роста УНТ, в роли таких металлов выступают в основном никель, железо и кобальт. Нанесение плёнки катализатора возможно с использованием методов химического осаждения из раствора, содержащего катализатор, термического испарения, ионно-лучевого распыления или магнетронного распыления. В качестве основного вопроса в данной работе было исследование влияния наличия буферного слоя, а также температурная зависимость и толщина каталитического слоя на рост УНТ.

Ключевые слова: углеродные нанотрубки (УНТ), синтез, химическое осаждение из паровой фазы (CVD), катализатор, магнетронное распыление.

Information about authors:

Ayaganov Zh.E., Ph.D student at Al-Farabi KazNU, Almaty, Kazakhstan, E-mail: zhanibek13@gmail.com, https://orcid.org/0000-0002-5239-3147;

Gabdullin M.T., PhD, professor, senior researcher at NNLOT, Almaty, Kazakhstan, E-mail: gabdullin@physics.kz, https://orcid.org/0000-0003-4853-3642;

Batryshev D.G., PhD, vice Rector at Atyrau State University named after Kh. Dosmukhamedov, Atyrau and senior lecturer at Al-Farabi KazNU, Almaty, Kazakhstan, E-mail: batryshev@physics.kz, https://orcid.org/0000-0002-9847-1067;

Ramazanov T.S., Academician of NAS RK, Doctor of physical and mathematical sciences, professor, vice Rector for Research-Innovation Affairs at Al-Farabi KazNU, Almaty, Kazakhstan, E-mail: tlekkabul.ramazanov@kaznu.kz, https://orcid.org/0000-0001-7172-8005;

Guseinov N., master degree, engineer at NNLOT, Almaty, Kazakhstan, E-mail: solar_neo@mail.ru, https://orcid.org/0000-0002-4712-3273;

Baughman Ray, Ph.D, Director of the Alan G. MacDiarmid NanoTech Institute at the University of Texas in Dallas, USA, E-mail: ray.baughman@utdallas.edu, https://orcid.org/0000-0001-5845-5137

REFERENCES

[1] Iijima S., Ichihashi T. (1993). Single-shell carbon nanotubes of 1-nm diameter. Nature, 363:603–605. DOI:10.1038/363603a0.

[2] Kosakovskaya Y. et al. (1992). Nanofiber carbon structure [Nanovolokonnaya uglerodnaya struktura] 56:26 (in Russ.).

[3] Radushkevich LV., Lukyanovich VM. (1952). About the structure of carbon formed during the thermal decomposition of carbon monoxide at an iron contact [O strukture ugleroda, obrazuyushchegosya pri termicheskom razlozhenii okisi ugleroda na zheleznom kontakte] 26:88 (in Russ.).

[4] Oberlin A., Endo M., Koyama T. (1976). High resolution electron microscope observations of graphitized carbon fibers. Carbon, 14:133–135. DOI:10.1016/0008-6223(76)90124-x

[5] Berber S., Kwon Y.-K., Tománek D. (2000). Unusually High Thermal Conductivity of Carbon Nanotubes. Physical Review Letters, 84:4613–4616. DOI:10.1103/physrevlett.84.4613.

[6] Kim P., Shi L., Majumdar A., McEuen P. L. (2001). Thermal Transport Measurements of Individual Multiwalled Nanotubes. Physical Review Letters, 87(21). DOI:10.1103/physrevlett.87.215502.

[7] Yu M. (2000). Strength and Breaking Mechanism of Multiwalled Carbon Nanotubes Under Tensile Load. Science, 287:637–640. DOI:10.1126/science.287.5453.637.

[8] Mintmire JW., Dunlap BI., White CT. (1992). Are fullerene tubules metallic? Physical Review Letters, 68:631–634. DOI:10.1103/physrevlett.68.631.

[9] Tans SJ., Devoret MH., Dai H., Thess A., Smalley RE., Geerligs LJ., Dekker C. (1997). Individual single-wall carbon nanotubes as quantum wires. Nature, 386:474–477. DOI:10.1038/386474a0.

[10] Smagulova GT, Prikhodko NG, Zakhidov AA, Mansurov ZA. (2015). Thermocatalytic synthesis of carbon nanotubes on fe2o3-glass fiber fabrics catalysts. N E W S OF THE ACADEMY OF SCIENCES OF THE REPUBLIC OF KAZAKHSTAN, 2:29 – 34. ISSN 2224-5286.

[11] Xu F., Zhao H., Tse SD. (2007). Carbon nanotube synthesis on catalytic metal alloys in methane/air counterflow diffusion flames. Proceedings of the Combustion Institute, 31:1839–1847. DOI:10.1016/j.proci.2006.08.062.

[12] Zhang XX., Li ZQ., Wen GH., Fung KK., Chen J., Li Y. (2001). Microstructure and growth of bamboo-shaped carbon nanotubes. Chemical Physics Letters, 333:509–514. DOI:10.1016/s0009-2614(00)01431-7

[13] Poulopoulos P.; Goschew A.; Pappas SD. et al. (2014). Graphene-Assisted Growth of Nanoblocks of Single-Crystalline Epitaxial Nickel Disilicides on Si(001). Journal of Surfaces and Interfaces of Materials, 2:161-165. DOI:10.1166/jsim.2014.1039

[14] Iijima S. (1991). Helical microtubules of graphitic carbon. Nature, 354:56–58. DOI:10.1038/354056a0

[15] Nii H., Sumiyama Y., Nakagawa H., Kunishige A. (2008). Influence of Diameter on the Raman Spectra of Multi-Walled Carbon Nanotubes. Applied Physics Express, 1:064005. DOI:10.1143/apex.1.064005.

[16] Antunes EF., Lobo AO., Corat EJ., Trava-Airoldi VJ. (2007). Influence of diameter in the Raman spectra of aligned multi-walled carbon nanotubes. Carbon, 45:913–921. DOI:10.1016/j.carbon.2007.01.003.

NEWS
OF THENATIONAL ACADEMY OF SCIENCES OF THE REPUBLIC OF KAZAKHSTAN
PHYSICO-MATHEMATICAL SERIES
ISSN 1991-346X **https://doi.org/10.32014/2020.2518-1726.60**
Volume 4, Number 332 (2020), 13 – 20

E.A. Abylkasymova[1], G.I. Beysenova[1], U.P. Suiinzhanova[2]

[1]Regional Social Innovation University, Shymkent, Kazakhstan;
[2]South KazakhstanState Pedagogical University, Shymkent, Kazakhstan.
E-mail: megaelmyra@mail.ru, gulia-74-74@mail.ru, only-kh@mail.ru

WEAK CONVERGENCE OF INTEGRAL CURVATURES OF CONVEX SURFACES

Abstract. The article contains a concentrated analysis of the existing information on the main problems of the theory of convex surfaces and differential geometry "in general" and is devoted to the problems of the reconstructing convex surfaces from the information about their curvature studied by the topological methods of the functional analysis.

The class of smooth surfaces in a bounded convex domain $G \subset E^2$ is considered. The concept of the R-area of a normal image is set forth. In the class K+(G), the Monge–Ampere equation is considered.

The paper considers the integrals of transverse Minkowski measures associated with the parallel surfaces. If the surface Φ is given by the explicit equation z = f (x, y), then for the integral curvatures of this surface transferred to the plane E^2, the inequalities $\varpi_k(\Phi, G) \leq \omega_k(\partial Z_\varphi, \partial Z_\varphi)$ for k = 0, 1, 2. Of these inequalities, inequalities follow

$$\varpi_0(\Phi, G) \leq 2\pi r^2 + 4\pi r\|\varphi\|_G,\ \varpi_1(\Phi, G) \leq 2\pi^2 r + 4\pi\|\varphi\|_G,\ \varpi_2(\Phi, G) \leq 4\pi,$$

which are used in reasoning. We prove the weak convergence of the integral curvatures of the convex surfaces. The result obtained in the form of a theorem plays an important role in the proofs of the theorems on the existence of a convex hypersurface with a given combination of the integral conditional curvatures. For the first time, the conditional curvatures are taken in the most general form, as a given function of the integral conditional curvatures of the various orders. The integrand functions are the product of the continuous functions and the integral curvatures of the various orders.

Keywords: convex surface, convex surfaces in Euclidean space, Monge-Ampère equation, the cone of convex surfaces in the space of continuous functions, conditional curvature, integral curvature, restoration of surface.

1. Introduction. The existence and uniqueness of a surface with the predetermined geometrical characteristics is one of the important and urgent problems of the differential geometry "in general" and its various analytical and mechanical applications[15]. The formulation of this problem in the language of analysis leads to the boundary value problems for the elliptic or hyperbolic partial differential equations of the second order, and also, as I.Ya. Bakelman showed, to integral equations.[12],[13], [14]

The class of smooth surfaces in a bounded convex domain $G \subset E^2$ is considered. The concept of the R-area of a normal image is set forth[16]. In the class K+(G), the Monge–Ampere equation is considered.

A number of geometric problems, including the Minkowski problem of constructing a convex surface, are reduced to the simplest Monge–Ampere equations.[9] G. Minkowskiposed and solved the problem of constructing a convex surface, whose Gaussian curvature has a given normal function.

2. Setting of a problem. Integrals of transverse Minkowski measures. The papers [1], [3], [10] set forth the information from the theory of integrals of the transverse Minkowski measures for the convex bodies, and also presented in [2], [11] the concepts and properties of the integral curvatures of the various orders for the closed convex surfaces. In [4], some fundamental formulas of the theory of surfaces are considered.

Let T be a bounded convex body in the space E^3. Then $F=\partial T$ is a closed surface that homeomorphic to the sphere S^2.

Let P be the plane of support to F at the point $X_0 \in F$. We denote by Π such of the closed half-spaces E^3 with the boundary P, which contains the body T. If the origin of coordinates is placed in a point lying inside the body T, then the plane P and the half-space Π are specified analytically as follows:

$$P=\{X \in E^3 | \langle X, \nu\rangle = d\};\ \Pi = \{X \in E^3 | \langle X, \nu\rangle \le d\}, \quad (1)$$

where ν is the unit outward normal to P, X is the current radius vector of points from P or from $\Pi$and d is the distance from the origin to the plane P.

To each plane of support P to F we assign the plane P_h, having the equation

$$P_h=\{X \in E^3 | \langle X, \nu\rangle = d+ h\}, \quad (2)$$

where $h \ge 0$ is a fixed number. We denote by Π_h the half-space given by the inequality

$$\Pi_h =\{X \in E^3 | \langle X, \nu\rangle \le d+h\}. \quad (3)$$

Obviously, $P_h=\partial\Pi_h$. Denote by T_h the intersection of all half-spacesΠ_h,which are constructed along all possible support hyperplanes$P$ to F. Then T_h is a bounded convex body, and $F_h=\partial T_h$ is a closed convex surface geomeomorphic to the sphere S^2. Surfaces $F_h$are called parallel to surface F.

3. Research methods. The following formula is valid ([5], [1]):

$$V(T_h) = \sum_{k=0}^{3} C_3^k W_k(T) h^k, \quad (4)$$

where $h \ge 0$ is a fixed number, the numbers $W_k(T)$ that are factors in the coefficients of the polynomial on the right-hand side of (4) are called integrals of Minkowski transverse measures for a convex body T. Integrals of transverse Minkowski measures are the functionals on a class of the bounded convex bodies. We point out the properties of these functionals necessary for further.

1. $W_0(T)=V(T)$, $W_1(T)=\frac{1}{3}\sigma(\partial T)$.

2. For any k = 0..3, the functionals$W_k(T)$ on the class of convex bodies are non-negative, invariant with respect to motions in E^3, monotone, bounded, homogeneous degrees $(3 - k)$, continuous, and additive.

The formulation and proof of these properties are given in [5], Chapter VI, §1.

3. For convex bodies with a smooth C^2 boundary, in the sense of differential geometry, the functional Wk(T) can be represented as integrals on ∂T from elementary symmetric functions of order $(k - 1)$ of 3 principal curvatures ∂T.

For each fixed $h \ge 0$, the mapping is defined

χ_h: subset $F \to$ subset F_h,

which assigns $A_h \subset F_h$ to each set $A \subset F$ such that:

If P is the plane of support to the surface F, such that $A \cap P \ne \varnothing$, then the plane $P_h = \{X \in E^3 \mid \langle X, \nu\rangle = d+h\}$ is the plane of support to the surfaceF_h and $A_h \cap P_h \ne \varnothing$, and, on the contrary, if P_h is the plane of support to the surface F_h, then P is the plane of support to the surface F.

Obviously, χ_0 is the identity transformation.

Let F be a complete convex surface in E^3. As is known, the limit of a converging sequence of planes of support to a complete convex surface F is the plane of support to F. From this fact the following properties of the map χ_h follow:

1. χ_h translates the closed subsets into the closed subsets.
2. χ_h translates the bounded subsets into the bounded subsets.
3. χ_h translates the compact subsets into the compact subsets.
4. χ_h translates the Borel subsets into the Borel subsets.

It is known that, under the imposed conditions, the areas of the Borel subsets exist.

In [8] the formula is proved

$$\sigma(A_h) = \sum_{k=0}^{2} C_3^k \omega_k(F, A) h^k, \quad (5)$$

where $\omega_k(F,A)$ are non-negative completely additive functions on the ring of Borel sets of the surface F such that $\omega_k(F,F)=W_1(T)$.

In [5], [6], it was shown that for the convex bodies with a smooth C^2boundary of the function of the set $\omega_k(F,A)$, $k = 1,2$, there are integrals over the set A of the elementary symmetric functions of order k of the 2 principal curvatures F. Therefore, $\omega_k(F,A)$ can be considered as functions of a set associated with integrals of transverse Minkowski measures. We will call these functions the integral curvatures of order k of the convex surface F.

The following was proved in [7]: if the closed convex surfaces $F_m$converge to a closed convex surface F, then the completely additive non-negative functions of the sets $\omega_k (F_m, A_m)$ weakly converge to a completely additive non-negative function of the set $\omega_k (F, A)$.

We give a more detailed formulation of the last statement. Since the convex surface F is homeomorphic to the sphere S^2 and the convex surfaces $F_m$converge to F, not breaking its generality, we can assume that there is a closed ball contained simultaneously within all $F_m$and F. Let's transfer the origin of coordinates to the center of this ball; the values of functions do not change from this.

Let θ be an arbitrary point of the sphere S^2. We obtain that the surfaces $F_m$and F are given respectively by the equations Φ_μ: $\rho=\rho_\mu(\theta)$, Φ: $\rho=\rho(\theta)$, the convergence of F_m to F means the uniform convergence of the functions $\rho_m(\theta)$ to $\rho(\theta)$ on S^2.

Let H be an arbitrary Borel set from S^2. Denote by A and Am the Borel sets of convex hypersurfaces$F$ and F_m, which are obtained as a result of the central projection of the set H from the origin of coordinates on these surfaces. Put now

$$\varpi_k (F, H) = \omega_k (F, A),\ \varpi_k (F_m, H) = \omega_k (F_m, A_m),\ k = 0, 1, 2.$$

Obviously, $\varpi_k(F,H)$ and $\varpi_k(Fm,H)$ are completely additive nonnegative functions of sets on the sphere S^2. We will call these set functions the integral curvatures of order k for convex surfaces F and F_m transferred to the sphere S^2.

The weak convergence of the functions of the sets $\varpi_k(F_m,H)$ to $\varpi_k(F,H)$ according to [7] means that for any continuous function $f(\theta)\in C(S^2)$, the equality

$$\lim_{m\to\infty} \iint_{S^2} f(\theta)\varpi_k(F_m, dH) = \iint_{S^2} f(\theta)\varpi_k(F, dH). \tag{6}$$

As is known, see [1], [9], a necessary and sufficient condition for the weak convergence of $\omega_k(F_m,A_m)$ to $\omega_k(F,A)$, provided that F_m converges to F, is that if $H\subset S^2$ is a closed set, then

$$\overline{\lim_{m\to\infty}}\ \overline{\omega}_k(F_m, H) \le \overline{\omega}_k(F, H) \tag{7}$$

and if $H\subset S^2$ is an open set, then

$$\underline{\lim_{m\to\infty}}\ \overline{\omega}_k(F_m, H) \le \overline{\omega}_k(F, H) \tag{8}$$

The functions of the sets $\omega_k(\Phi, B)$ of convex surfaces given by explicit equations. Let $\Phi_z\in K(G)$ be the surface and let M be a convex compact subset of G. Without loss of generality, we can assume that $\Phi_z\in K^-(G)$. Then the distance $\delta M = dist(M, \partial G)$ is positive. Let denote by Φ_M the graph of the function $z_M(x, y) = z (x, y)/\delta M$.

Let h be an arbitrary real number satisfying the condition $h<h_M=inf_M z(x,y)$.

Let $T_M(\Phi, h) = conv (F_M,H(M,h))$. It's obvious that

$$\partial T_M (F, h) = F_M \cup H (M, h) \cup Z_M,$$

where Z_M is the part of the cylindrical surface with the guide ∂M, forming - segments, parallel to the Z axis, located between ∂F_M and $\partial H(M, h)$. Set

$$\omega_k(z_M, A)=\omega_k(\partial T_M(\Phi,h), A), \tag{9}$$

where $A\subset F_M$ is a Borel subset. Note that the number $\omega_k(\partial T_M(\Phi,h), A)$does not depend on the number h.

If $M \subset M_1$ are two compact convex subsets of G, then for any $h \in (-\infty, h_M)$, obviously, the equality

$$\omega_k(\Phi_M, A) = \omega_k(\Phi_M, A), \tag{10}$$

where $A \subset F_M$ is an arbitrary Borel subset. From (10) it follows that in the left-hand side of formula (9), the F_M surface can be replaced by F.

Thus, for $\Phi \in K^{-}(G)$and any Borel set $A \subset \Phi$ such that the orthogonal projection A^1 of the set A on E^2 is removed from ∂G by a positive distance, we have

$$\omega_k(\Phi, A) = \omega_k(\partial T_m(\Phi, h), A) \tag{11}$$

where $T_M(\Phi, h) = conv\ (F_M, N_M)$,

M is any compact convex subset of G such that $A_1 \subset M$,

h is any number satisfying the inequality $h < h_M = inf_M z\ (x, y)$.

Formula (10) implies an important corollary:

1) Let $M \subset G$ be a compact convex subset. Then, on the ring of Borel subsets A of the F_M surface, the integral curvatures $\omega_k(\Phi, A),\ k=0,1,2,$ represent nonnegative completely additive functions of a set of bounded variation.

2) For any Borel set $A \subset \Phi$ we set

$$\omega_k(\Phi, A) = sup_{M \subset G} \omega_k(\Phi, A \cap \Phi_M) \tag{12}$$

over all convex compact subsets of $M \subset G$. The number $\omega_k(\Phi, A)$ is always non-negative, it can also take the value $+\infty$.

3) For any $\Phi \in K(G)$, the integral curvatures $\omega_k(\Phi, A),\ k = 0,1,2$, are completely additive, non-negative functions on the ring of Borel sets F. If Φ is a bounded set in E^3, then these functions have limited variation.

For any $\Phi \in K\ (G)$ we set

$$\varpi_k(\Phi, A^1) = \omega_k(\Phi, A),\ k = 0,\ 1,\ 2, \tag{13}$$

where A is a Borel subset on Φ, and A^1 is the orthogonal projection of A onto the plane E^2. Obviously, $A^1$is a Borel subset of G. It follows directly from the definition that $\varpi_k(\Phi, B)$ are the non-negative completely additive functions on the ring of Borel subsets of G, which take finite values for sets B remote from ∂G by a positive distance.

These set functions will be called the integral curvatures of the surface Φ transferred to the plane E^2.

We consider the question of the weak convergence of these integral curvatures. We give a well-known literature definition of the weak convergence of the completely additive functions of sets defined on the Borel subsets of the domain G. It is said that the sequence of the completely additive functions of the sets $\mu_m(B)$ weakly converges to a completely additive function of the set $\mu(B)$, if for any $f \in C(G)$ with a compact support $M \subset G$, an equality holds

$$\lim_{m \to \infty} \iint_G f(x, y) \mu_m(dB) = \iint_G f(x, y) \mu(dB).$$

The following theorem is true.

4. Results of the research. Theorem 1. Let the convex surfaces $\Phi_m \in K(G)$ converge to the convex surface $\Phi \in K\ (G)$, then for all $k = 0,1,2$ the integral curvatures $\varpi_k(\Phi_m, B)$ of the hypersurfacesΦ_m, transferred to E^2, weakly converge to the integral curvature $\varpi_k(\Phi, B)$, transferred to E^2.

Proof. For definiteness, we assume that $\Phi_m \in K^{+}\ (G)$ and $\Phi \in K^{+}\ (G)$. Since Since, under parallel shifts of Φ along the Z axis, the integral curvatures $\varpi_k(\Phi, B)$ of the surface Φ transferred to E^2 do not change, without loss of generality, we can assume that all surfaces $\Phi$and Φ_m lie under the plane E^2.

Now let $f \in C(G)$ with compact support $M' \subset G$. Obviously, $dist(M', \partial G) > 0$. Therefore, one can find a compact convex set M such that $G \supset M \supset M'$. Obviously, $dist(M, \partial G)$ is also positive. We introduce the convex surfaces Φ_M and $\Phi_{M,m}$. Since they are uniformly bounded in E^3, one can find a point (x,y,h) in

E^3 such that $(x,y) \in M$, and h is a sufficiently large number, and the projections of the surfaces Φ_M and $\Phi_{M,m}$ from the points (x,y,h) on the plane E^2 are contained in some compact convex set N satisfying the condition $M \subset N \subset G$.

Obviously, $dist(M, \partial G) > 0$. Without loss of generality, we can assume that all surfaces Φ_M and $\Phi_{M,m}$ lie above the plane $z = h$.

Now suppose that the S_1^2 is the sphere centered at the point (x,y,h) of the radius 1. Without loss of generality, we can assume that S_1^2 lies under all the surfaces Φ_M and $\Phi_{M,m}$.. Let S_{1+}^2 be the open hemisphere S_1^2, the equatorial plane of which is parallel to the E^2 plane. Denote by $\pi: S_{1+}^2 \to E^2$ the central projection of S_{1+}^2 to the plane E^2. Obviously, π is a diffeomorphism.

Suppose $N' = \pi^{-1}(N)$, then N' is a convex compact subset on S_1^2, contained inside S_{1+}^2. We introduce the function on S_1^2

$$g(\theta) = \begin{cases} f(\pi(\theta)), \text{ if } \theta \in N', \\ 0, \text{ if } \theta \in S_1^2 \setminus N'. \end{cases}$$

It is easy to see that $g(\theta) \in C(S_1^2)$. By construction, this function is such that it is zero on S_1^2 outside the set $\pi^{-1}(M')$. Note that $\pi^{-1}(M') \subset \pi^{-1}(M) \subset \pi^{-1}(N)$.

We now construct the convex bodies.

$T_N(\Phi, h) = conv\,(\Phi_N, H(N, h))$, $T_N(\Phi_m, h) = conv\,(\Phi_{N,m}, H(N, h))$.

Let B be an arbitrary Borel subset of the set M. Let, further, A and A_m be the Borel subsets of surfaces Φ and Φ_m, whose orthogonal projections are the set B. Then

$\varpi_k(\Phi,B) = \omega_k(\Phi_N,A) = \omega_k(\Phi_M,A)$, $\varpi_k(\Phi_m,B) = \omega_k(\Phi_{N,m},A) = \omega_k(\Phi_{M,m},A)$,

$k = 0, 1, 2$, $m = 1, 2, \ldots$

According to the above, we also have

$$\varpi_k(\Phi,B) = \omega_k(\Phi_N,A) = \omega_k(\Phi_M,A) = \varpi_k(\partial T_N(\Phi, h), \pi^{-1}(A)),$$
$$\varpi_k(\Phi_m,B) = \omega_k(\Phi_{N,m},A_m) = \omega_k(\Phi_{M,m},A_m) = \varpi_k(\partial T_N(\Phi_m, h), \pi^{-1}(A)). \quad (14)$$

Formulas (14) establish the relations between the integral curvatures of a fixed order k of the convex surfaces Φ and Φ_m, transferred respectively to the E^2 plane and the S_1^2sphere. From these formulas and the definition of the function g, the properties of the functions f and g, and the fact that $\pi: S_{1+}^2 \to E^2$ is a diffeomorphism, we obtain

$$\iint_G \varpi_k(\Phi, dB) = \oiint_{S_1^2} g\,\varpi_k(\Phi, dH),$$
$$\iint_G \varpi_k(\Phi_m, dB) = \oiint_{S_1^2} g\,\varpi_k(\Phi_m, dH).$$

Using the weak convergence of the functions of the sets $\varpi_k(\Phi_m, dH)$ to the function of the set $\varpi_k(\Phi, dH)$, we obtain

$$\lim_{m\to\infty} \oiint_{S_1^2} g\,\varpi_k(\Phi_m, dH) = \oiint_{S_1^2} g\,\varpi_k(\Phi, dH).$$

From here we have

$$\lim_{m\to\infty} \iint_G f\varpi_k(\Phi_m, dB) = \iint_G f\varpi_k(\Phi, dB).$$

Since the continuous function f, which vanishes outside a certain compact set in G, is chosen arbitrarily, the functions of the set $\varpi_k(\Phi_m, B)$ converge weakly to the function of the set $\varpi_k(\Phi_m, B)$.The theorem is proved.

5. Conclusions. Thus, we investigated the integrals of transverse Minkowski measures associated with parallel surfaces. The weak convergence of integral curvatures of convex surfaces is proved. The result obtained in Theorem 1 is new and plays an important role in the proofs of the existence theorems for a convex hypersurface with a given combination of integral conditional curvatures.

Э.А. Абылкасымова[1], Г.И. Бейсенова[1], Ү.П. Сүйінжанова[2]

[1]Аймақтық әлеуметтік-инновациялық университеті, Шымкент, Қазақстан;
[2]Оңтүстік Қазақстан мемлекеттік педагогикалық университеті, Шымкент, Қазақстан

ДӨҢЕС БЕТТІҢ ИНТЕГРАЛ ҚИСЫҒЫНЫҢ ӘЛСІЗ ЖИНАҚТАЛУЫ

Аннотация. Мақалада дөңес бет теориясы мен «тұтастай» дифференциалды геометрияның негізгі проблемалары туралы талдау жасалған және функционалдық талдаудың топологиялық әдістері арқылы меңгерілген қисықтар туралы ақпараттарға, дөңес беттерді қалпына келтірудің мәселелері іздестірілген.

Шектелген дөңес $\mathbf{G} \subset E^2$ аймағындағы тегіс беттер класы қарастырылады. Қалыпты кескіннің R-ауданы туралы түсінік берілген. K+(G) класындағы Монж-Ампер теңдеуі қарастырылады.

Мақалада параллель беттерге қатысты Минковскийдің көлденең өлшем интегралдары қарастырылады. Егер Ф беті анық z=f(x,y) теңдеуімен берілсе, онда E2 жазықтығына берілген осы беттің интегралдық қисықтары үшін мұндағы k=0, 1, 2 болғанда мына теңсіздік $\varpi k(\Phi, G) \leq \omega k(\partial Z\varphi, \partial Z\varphi)$ ақиқат болып саналады. Бұл теңсіздіктен кейін болжау барысында қолданылатын келесі теңсіздік шығады:

$$\varpi_0(\Phi, G) \leq 2\pi r^2 + 4\pi r||\varphi||_G,\ \varpi_1(\Phi, G) \leq 2\pi^2 r + 4\pi||\varphi||_G,\ \varpi_2(\Phi, G) \leq 4\pi$$

F дөңес беті S2 сферасына гомеоморфты және Fm дөңес беттері F-ге ортақтықты жоғалтпай жинақталады, сондықтан барлық Fm және F ішінде бір мезгілде тұйық шар бар деп болжауға болады. Координатаның бастапқы мәндерін осы шардың ортасына әкелгенде, функцияның мәндері өзгермейді.

θ - S^2 сферасындағы еркін нүкте деп алайық. F_m және F беттері тиісінше мынадай теңдулермен F_m: $\rho=\rho_m(\theta)$,F: $\rho=\rho(\theta)$ беріледі. S^2 сферасындағы F_m-нің F-ке жинақталуыρ_m (θ) функциясының $\rho(\theta)$-ге біркелкі жинақталуын білдіреді.

H – S^2 сферасының еркін борель көпмүшелігі деп алайық. A және A_m борель көпмүшелігі арқылы дөңес гипербеттерінің F және F_m, H көпмүшелікті орталық жобалауы осы беттегі бастапқы координатасынан алынады. Енді k=0, 1, 2 болғанда төмендегідей формулаға келтіреміз:

$$\varpi_k(F, H) = \omega_k(F, A),\ \varpi_k(F_m, H) = \omega_k(F_m, A_m),$$

Көріп тұрғанымыздай, $\varpi_k(F,H)$ және $\varpi_k(F_m,H)$ – S^2 сферасында көпмүшеліктің толықтай аддитивтік теріс емес функциясы болып саналады. Көпмүшеліктің бұл функцияларын біз әрі қарай S^2 сферасына тасымалданған F және F_m, дөңес беттері үшін k ретіндегі интегралдық қисықтар деп айтамыз. Осы интегралдық қисықтардың әлсіз жинақталуы туралы мәселе қарастырылды. Борель ішкі көпмүшелігінің G аймағында берілген көпмүшелік функциясының толықтай аддитивті әлсіз жинақталуын анықтау туралы анықтамалар келтірілді.

μ_m(B) көпмүшелігінің толықтай аддитивті функциялар тізбегі μ(B) көпмүшелігінің толықтай аддитивті функциясымен әлсіз жинақталады деп айтылады, барлығына $f \in C(G)$ ықшамды тасымалдаушы $M \subset G$ болса, онда мынадай теңдікті ұсынады:

$$\lim_{m\to\infty} \iint_G f(x,y)\mu_m(dB) = \iint_G f(x,y)\mu(dB).$$

Келесі теореманы тұжырымдаймыз: $\Phi_m \in K(G)$ дөңес беті $\Phi \in K$ (G) дөңес бетімен жинақталатын болса, онда барлығына k=0,1,2 болғанда, E^2 -ге берілген Φ_m гипербетінің $\varpi_k(\Phi_m,B)$ интегралдық қисығы E^2-ге берілген $\varpi_k(\Phi,B)$ интегралдық қисығы арқылы әлсіз жинақталады. Дөңес беттердің интегралдық қисықтардың әлсіз жинақталуы дәлелденді.

Теорема түрінде алынған нәтиже интегралды шартты қисықтардың комбинациясы арқылы берілген дөңес гипербеттердің туралы теоремаларды дәлелдеуде мағызды рөл атқарады. Түрлі реттегі интегралды шартты қисықтардың берілген функциясы ретінде алғашқы рет оның жалпылама түрдегі шартты қисық сызықтары алынды. Ішкі интегралды функциялар үздіксіз функциялардың және түрлі ретті интегралдық қисықтардың туындысы болып саналады.

Түйін сөздер: дөңес бет, Евклид кеңістігіндегі дөңес беттер, Монж-Ампер теңдеуі, үздіксіз функциялар кеңістігіндегі дөңес беттердің конусы, шартты қисық, интегралдық қисық, бетті қалпына келтіру.

Э.А.Абылкасымова[1], Г. И. Бейсенова[1], Ү.П. Сүйінжанова[2]

[1]Региональный социально-инновационный университет, Шымкент, Казахстан;
[2]Южно-Казахстанский государственный педагогический университет, Шымкент, Казахстан

СЛАБАЯ СХОДИМОСТЬ ИНТЕГРАЛЬНОЙ КРИВИЗНЫ ВЫПУКЛЫХ ПОВЕРХНОСТЕЙ

Аннотация. Статья содержит концентрированный анализ существующей информации об основных проблемах теории выпуклых поверхностей и дифференциальной геометрии «в целом» и посвящена задачам восстановления выпуклых поверхностей по информации об их кривизне, изучаемым топологическими методами функционального анализа.

Рассматривается класс гладких поверхностей в ограниченной выпуклой области $G\subset E^2$. Излагается понятие R-площади нормального изображения. В классе$K^+(G)$ рассматривается уравнение Монжа-Ампера.

В работе рассматриваются интегралы поперечных мер Минковского, связанные с параллельными поверхностями. Если поверхность Ф задана явным уравнением z=f(x,y), то для интегральной кривизны этой поверхности, перенесенных на плоскость E^2, справедливы неравенства $\varpi_k(\Phi, G)\le\omega_k(\partial Z_\varphi, \partial Z_\varphi)$ при k=0, 1, 2.

Из этих неравенств следуют неравенства

$$\varpi_0(\Phi, G)\le 2\pi r^2+4\pi r\|\varphi\|_G,\ \varpi_1(\Phi, G)\le 2\pi^2 r+4\pi\|\varphi\|_G,\ \varpi_2(\Phi, G)\le 4\pi,$$

которые используются в рассуждениях.

Так как выпуклая поверхность F гомеоморфна сфере S^2и выпуклые поверхностиF_mсходятся к F, то не нарушая общности, можно считать, что существует замкнутый шар, содержащийся одновременно внутри всех F_m иF. Перенесем начало координат в центр этого шара, от этого значения функций не изменятся.

Пусть θ – произвольная точка сферы S^2. Получаем, что поверхности F_m иF задаются соответственно уравнениями F_m: $\rho=\rho_m(\theta)$,F: $\rho=\rho(\theta)$, сходимость F_mк F означает равномерную сходимость функций $\rho_m(\theta)$ к $\rho(\theta)$ на S^2.

Пусть H – произвольное борелевское множество из S^2. Обозначим через A и A_mборелевские множества выпуклых гиперповерхностей F иF_m, которые получаются в результате центрального проектирования множества H из начала координат на эти поверхности. Положим теперь

$$\varpi_k(F, H)=\omega_k(F, A),\ \varpi_k(F_m, H)=\omega_k(F_m, A_m),\ k=0, 1, 2.$$

Очевидно, $\varpi_k(F,H)$ и $\varpi_k(F_m,H)$ являются вполне аддитивными неотрицательными функциями множеств на сфере S^2. Эти функции множеств мы называем далее интегральными кривизнами порядка k для выпуклых поверхностей Fи F_m, перенесенных на сферу S^2.

Рассмотрен вопрос о слабой сходимости этой интегральной кривизны. Приведен известное из литературы определение слабой сходимости вполне аддитивных функций множеств, заданных на борелевских подмножествах области G.

Говорят, что последовательность вполне аддитивных функций множеств $\mu_m(B)$ слабо сходится к вполне аддитивной функции множества μ(B), если для всякой $f\in C(G)$ с компактным носителем $M\subset G$, имеет место равенство

$$\lim_{m\to\infty}\iint_G f(x,y)\mu_m(dB)=\iint_G f(x,y)\mu(dB).$$

Справедлива следующая теорема: пусть выпуклые поверхности $\Phi_m\in K(G)$ сходятся к выпуклой поверхности $\Phi\in K$ (G), тогда при всех k=0,1,2 интегральная кривизна $\varpi_k(\Phi_m,B)$ гиперповерхностей Φ_m, перенесенная на E^2, слабо сходится к интегральной кривизне $\varpi_k(\Phi,B)$, перенесенной на E^2.

Доказана слабая сходимость интегральной кривизны выпуклых поверхностей. Результат, полученный в виде теоремы, играет важную роль в доказательствах теорем существования выпуклой гиперповерхности с заданной комбинацией интегральной условной кривизны. Впервые условная кривизна взята в самом общем виде как заданная функция от интегральных условных кривизн различных порядков. Подынтегральные функции являются произведением непрерывных функций и интегральной кривизны различных порядков.

Ключевые слова: выпуклая поверхность, выпуклые поверхности в Евклидовом пространстве, уравнение Монжа-Ампера, конус выпуклых поверхностей в пространстве непрерывных функций, условная кривизна, интегральная кривизна, восстановление поверхности.

Information about authors:

Abylkasymova E.A., cand.ph.-math.sc., senior teacher of the chair "Math, physics and technique specialty",Regional Social Innovation University, megaelmyra@mail.ru, https://orcid.org/0000-0002-4416-5638;

Beysenova G.I., cand.ped.sc., dean of the faculty of "Physics-Math and Business", Regional Social Innovation University, gulia-74-74@mail.ru, https://orcid.org/0000-0003-0545-0652;

Suiinzhanova U.P., masterof Engineering of the chair of Physics, South Kazakhstan State Pedagogical University, only-kh@mail.ru, https://orcid.org/0000-0001-7267-2912

REFERENCES

[1] Hadviger G. Lectures on volume, surface area and isometry. Moscow, Science, 1966. 320 p.

[2] Buseman G. Convex surfaces. Moscow. Science, 1964. 320 p.

[3] Buseman G. Geodesic geometry. Moscow: Fismatgiz, 1962. 222 p.

[4] Bliev N.K., Myrzakul K., Rahimov F.K., Serikbaev N. S. On the geometry of Heisenberg ferromagnets. News of the National Academy of Sciences of the Republic of Kazakhstan, series physico-mathematical, 2002,No. 2, p. 10-15.

[5] Cantor B.E. Restoration of smooth surfaces from given curvature functions// Issues of differential geometry as "a whole".Leningrad, 1983. p. 155-164.

[6] Federer H. Curvature measures. Trans. Amer. Math. Soc. 93, 1959, p. 418-491.

[7] Verner A.L. About external curvature of convex surfaces in spaces of constant curvature.Izv.vuzov, 1960, No. 1, seriiamatem., p. 58-68.

[8] Krasnoselsky M.A. Positive equations of operational solutions. Moscow,Fizmatgiz, 1962. 418p.

[9] Abylkasymova E.A., Koshanov M.,Koshanova G., Taskaraev A.Monge-Ampere equation and the main challenge of differentional geometry in general. Collection of abstracts of International scientific conference "Actual issues of partial differential equations" dedicated to 60th anniversary of professor Tungatarov A.B. Astana, 2008. p. 16-17.

[10] Pogorelov A.V. External geometry of convex surfaces. Moscow, Science, 1969. 540 p.

[11]TaskaraevA., Abylkasymova E.A. Surfaces with given conditional curvatures. Collection of papers of international scientific-practical conference dedicated to the 70th anniversary of the president of Kazakhstan university of friendship, Academician Kuatbekov A.M. Shymkent, 2012. p. 449-451.

[12] Kopzhasarova A.A., Besbayev E.A., Abylkasymova E.A., Shaldanbayev A. Sh.Spectral resolutions of solution of Volterra nonlocal boundary value problems of a wave equation. News of the National Academy of Sciences of the Republic of Kazakhstan.Series of physico-mathematical sciences.2016, Volume 5, Number 309, p.203-213.http://road.issn.org/issn/2518-1726, ISSN 1991-346X (print).

[13]BakelmanI.Ya.Geometric methods for solving elliptic equations. Moscow, Science, 1964.

[14] Abylkasymova E.A. The recovery of minimal and convex surfaces from the sum of integral conditional curvatures. Studies inintegro-differential equations, 2010, 42. p.168-173, Byshkek. ISSN0130-6553

[15]AsanovaA.T., AlikhanovaB.Zh., NazarovaK.Zh. Well-posedness of a nonlocal problem with integral conditions for third order system of the partial differential equation. News of the National Academy of Sciences of the RepublicofKazakhstan.Series of physic-mathematical sciences. 2018, Volume 5, No. 321, p. 33-41, DOI:10.32014/2018.2518-1726.5

[16]AldashevS.A., MaikotovM.N. Dirichlet problem in a cylindrical area for one class of multidimensional elliptic-parabolic equations .News of the National Academy of Sciences of the Republic of Kazakhstan. Series of physic-mathematical sciences. 2019, Volume 5, No.327. p.89–97. http://doi.org/10.32014/2019.2518-1726.62

NEWS
OF THENATIONAL ACADEMY OF SCIENCES OF THE REPUBLIC OF KAZAKHSTAN
PHYSICO-MATHEMATICAL SERIES
ISSN 1991-346X **https://doi.org/10.32014/2020.2518-1726.61**
Volume 4, Number 332 (2020), 21 – 27

UDC 539.142
MRNTI 29.15.03

G. Khuukhenkhuu[*], M. Odsuren[2,*], J. Munkhsaikhan[*], A. Tursukh[*], Ch. Saikhanbayar[1], A.T. Sarsembayeva[3], M. Abyshev[3]

[*]Nuclear Research Center, National University of Mongolia, Ulaanbaatar, Mongolia;
[2]School of Engineering and Applied Sciences, National University of Mongolia, Ulaanbaatar, Mongolia;
[3]Department of Physics and Technology, Al-Farabi Kazakh National University, Almaty, Kazakhstan.
E-mail: g_khuukhenkhuu@yahoo.com; *odsuren@seas.num.edu.mn; munkhsaikhan.nrc@gmail.com; tursukh.amgalan@gmail.com; saikhanaa.ok@gmail.com; sarsembaeva.a@kaznu.kz; medeu.abishev@kaznu.kz

TRITON CLUSTERING IN (n,t) REACTIONS

Abstract. According to the traditional definition of a nucleus, protons and neutrons in the nucleus have a roughly homogeneous distribution. At the beginning of nuclear physics it was known that nuclear clustering was extremely important in determining the structure of nuclei. The discovery of alpha-decay of heavy-nuclei initiated the idea that clusters of nucleons might be preformed prior to emission. Afterwards Gamow, Gurney and Condon described the alpha particle as undergoing quantum mechanical tunneling from inside the decaying nucleus. Furthermore, an alpha particle model with bonds connecting clusters for N=Z even-even nuclei was suggested. In 1941, Margenau used a Slater determinant wave function for alpha clusters to compute an effective alpha-alpha interaction. Moreover, Morigana supposed to apply linear chains of alpha clusters for describing some states of alpha-like nuclei. Cluster structures are typically observed as excited states close to the corresponding decay threshold. The origin of this phenomenon lies in the effective nuclear interaction, but the detailed mechanism of clustering in nuclei has not yet been fully understood.

Clustering properties of nuclei would be helpful to understand both the nuclear structure and nuclear reaction mechanisms. Different kind of clusters can be in principle exist in nuclei, for example, light (two, three and four nucleons) and heavy ones. The clustering effect of nuclei has been investigated for a long time using different methods based on various theoretical approaches. However, most of these studies were devoted to the α-clustering in the α-decay, α-particle scattering, α-particle transfer and emission reactions, and molecule like α-cluster structure of light nuclei. A famous example is Be isotopes for alpha-clustering. ^{8}Be has a tight two-alpha cluster structure and the nucleus is unstable. If we consider another isotope of ^{9}Be (adding one neutron into ^{8}Be), the cluster structure is stabilized and the system is bound.

In the last years we have been studying the α-clustering in fast and slow neutrons induced (n,α) reactions using the statistical model and knock-on mechanism. In this work in the framework of the compound and direct reaction mechanisms, triton clustering factors (or probabilities) were first obtained for (n,t) reactions. In the case of compound mechanism, the statistical model based on the evaporation model and constant nuclear temperature approximation was used. For the direct reaction mechanism, the knock-on model was utilized. It was shown that the triton clustering factors obtained by the knock-on model are much larger than ones found by the statistical model. At the same time, the triton clustering factors for even-even target nuclei are on an average one order of magnitude lower than ones for odd-even nuclei.

In addition, the triton clustering factors are much lower than the α-clustering in (n,α) reactions at the same neutron energy range for medium-mass nuclei.

Keywords: compound mechanism, statistical model, evaporation model, constant nuclear temperature approximation, direct reaction, knock-on model, alpha-clustering, triton-clustering.

1. Introduction

Clustering properties of nuclei are useful for the understanding both the nuclear structure and nuclear reaction mechanisms [1-4]. Different kind of clusters can be in principle exist in nuclei, for example, light (two, three and four nucleons) and heavy ones. The clustering effect of nuclei has been investigated for a long time using different methods based on various theoretical approaches. However, most of these studies

were focused on the α-clustering in the α-decay, α-particle scattering, α-particle transfer and emission reactions, and molecule like α-cluster structure of light nuclei. The clusterization is usually described by a clustering factor which is defined as the probability of finding some cluster structure from several nucleons inside the nucleus. Consequently, this factor (or probability) should be less than or equal to one.

In the last years we have been studying the α-clustering in fast and slow neutrons induced (n,α) reactions using the compound and direct reaction mechanisms [5,6]. In this work the triton clustering in (n,t) reactions is first studied using the statistical and knock-on models.

2. Theoretical background

2.1. Statistical Model Formulae

In the framework of the statistical model based upon Bohr's assumption of a compound mechanism the (n,t) cross section can be expressed [7] as following:

$$\sigma_{(n,t)}^{stat} = \sigma_c(n)G(t). \tag{1}$$

Here:

$$\sigma_c(n) = \pi(R + \lambda\!\!\!^{-}_n)^2 \tag{2}$$

is the compound nucleus formation cross section, where $R = r_0 A^{1/3}$ is the target nucleus radius, $r_0 = 1.3 \cdot 10^{-13}$ cm and A is the target nucleus mass number;

$$\lambda\!\!\!^{-}_n = \frac{4.55 \cdot 10^{-13}}{\sqrt{E_n(MeV)}}(cm) \tag{3}$$

is the wavelength of the incident neutrons divided by 2π, where E_n is the neutron energy.

The triton decay probability of the compound nucleus is given by

$$G(t) = \frac{\Gamma_t}{\Gamma}, \tag{4}$$

where Γ_t and Γ are the triton and total level widths.

Using the detailed balancing principle and evaporation model [8] the triton width of level, Γ_t, is determined as following:

$$\Gamma_t = \frac{2S_t + 1}{\pi^2 \hbar^2 \rho_c(E_c)} M_t \int_{V_t}^{E_t^{\max}} E_t \sigma_c(E_t) \rho_y(U_t) dE_t. \tag{5}$$

Here: S_t, M_t, E_t, and V_t are the spin, mass, energy and the Coulomb potential energy for the outgoing triton, respectively; $\rho_c(E_c)$ and $\rho_y(U_t)$ are the level densities of the compound and residual nuclei, respectively; U_t is the excitation energy of the residual nuclei; The inverse reaction cross section, $\sigma_c(E_t)$, can be determined by the semi-classical formula [7]. Then, using the nuclear entropy [9] and constant temperature approximation [7], we can get from (1), (2) and (5) the following simple formula for fast neutron induced (n,t) reaction cross section:

$$\sigma_{(n,t)}^{stat} = \pi(R + \lambda\!\!\!^{-}_n)^2 \frac{2S_t + 1}{2S_n + 1} \frac{M_t}{M_n} e^{\frac{Q_{nt} - V_t}{\theta}}. \tag{6}$$

If we use Weizsäcker's formula for binding energy [10] and an approximation A>>2 for medium mass and heavy nuclei can obtain following formula for (n,t) reaction energy:

$$Q_{nt} = \gamma \frac{2Z - 1}{A^{1/3}} - 4\xi \frac{N - Z + 1}{A} + \varepsilon_t \tag{7}$$

where: γ and ξ the Weizsäcker's constants, N and Z are the neutron and proton numbers, respectively, of the target nucleus, $\varepsilon_t = 8.48$ MeV is the internal binding energy of triton.

The Coulomb potential energy of triton can be written [11] in the form:

$$V_t = 1.029\frac{(Z-1)}{A^{1/3}+3^{1/3}}(MeV). \tag{8}$$

Using the Fermi gas model for level density parameter [12], the nuclear thermodynamic temperature [7] is expressed as:

$$\Theta = \sqrt{\frac{13.5(E_n + Q_{nt})}{A}}. \tag{9}$$

So, from Eqs. (6)-(8) the (n,t) cross section can be obtained as follows:

$$\sigma_{(n,t)}^{stat} = C\pi\left(R+\lambda\!\!\!^{-}_n\right)^2 e^{-K\frac{N-Z+1}{A}}, \tag{10}$$

The parameters C and K are expressed by:

$$C = 3\exp\left\{\frac{\gamma\frac{2Z-1}{A^{1/3}} + \varepsilon_t - 1.029\frac{(Z-1)}{A^{1/3}+3^{1/3}}}{\Theta}\right\} \tag{11}$$

and

$$K = \frac{4\xi}{\Theta}. \tag{12}$$

Formulae (9)-(12) are used for calculation of the (n,t) cross sections. So, the triton clustering factor (or probability) can be, by analogy with the spectroscopic factor [13], obtained as a ratio of experimental (n,t) cross sections for 14-15 MeV neutrons to the theoretical ones which were calculated using the one-body approximation (10):

$$\phi_t = \frac{\sigma_{(n,t)}^{\exp}}{\sigma_{(n,t)}^{stat}}. \tag{13}$$

2.2. Knock-on Model Formulae

In the framework of the direct reaction mechanism and using the knock-on model, the (n,t) cross section for fast neutrons can be obtained as following:

$$\sigma(n,t) = k_t\phi_t\sigma_n^{tot}(t). \tag{14}$$

Here: k_t is the parameter of the neutron hitting the target nucleus which can be expressed by the ratio of geometric cross sections as following:

$$k_t = \frac{\pi r_t^2}{\pi(R_D^2 + r_t^2)} = \frac{3^{2/3}}{(A-3)^{2/3}+3^{2/3}}, \tag{15}$$

where r_t is the radius of the triton; R_D is the radius of the daughter nucleus and A is the mass number of the target nucleus; ϕ_t is the triton clusterization factor; $\sigma_n^{tot}(t)$ is the total neutron cross section for the triton. So, from (14) and (15) the triton clusterization factor can be got as following:

$$\phi_t = \frac{\sigma(n,t)}{\sigma_n^{tot}(t)}\frac{(A-3)^{2/3}+3^{2/3}}{3^{2/3}}. \tag{16}$$

The formula (16) is used to calculate the triton clusterization factor for (n,t) reactions.

3. Results and discussion

3.1. Triton Clustering Factors by the Statistical Model

Theoretical (n,t) cross sections calculated by the statistical model formulae (9)-(12) and experimental values taken from EXFOR data [14] are shown in figure 1.

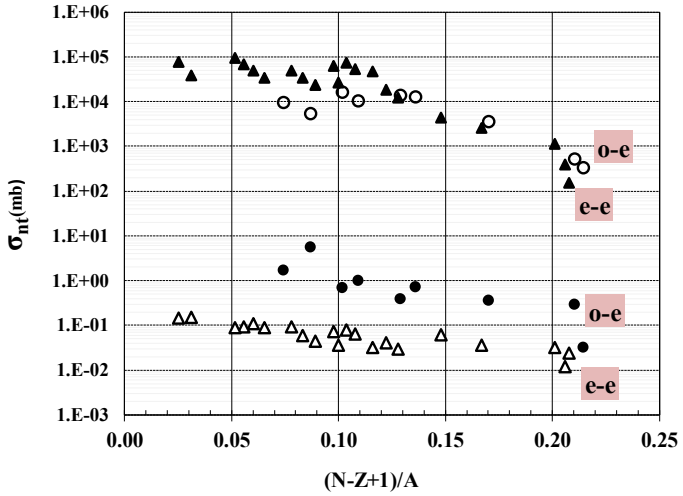

Figure 1 - Theoretical (o,▲) and experimental (●,Δ) (n,t) cross sections
for odd-even and even-even target nuclei versus the parameter (N-Z+1)/A

It is seen that the statistical model formulae give systematically overestimated values of the (n,t) cross sections. We assume that this fact is, perhaps, caused by triton clustering effect which was not considered in the theoretical formulas. So, the triton clustering factor was determined by formula (13). Results of such calculations by formula (13) are shown in figure 2 for odd-even and even-even nuclei.

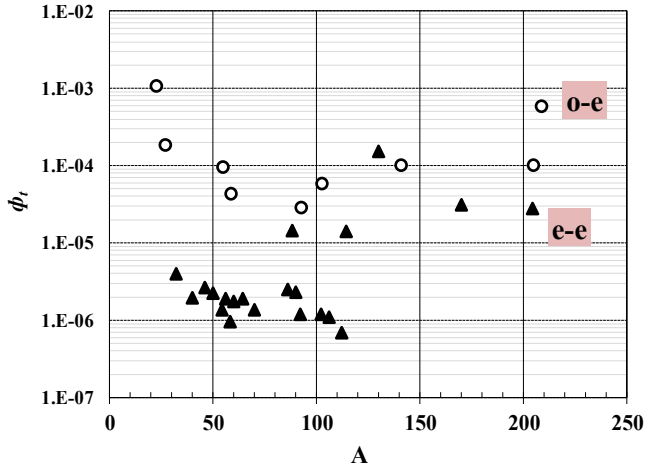

Figure 2 - The dependence of the triton clustering factors on the mass number of target nuclei:
(o-odd-even and ▲-even-even nuclei)

The figure 2 shows that the triton clustering factors for even-even nuclei on an average are around 10^2 times less than ones for odd-even nuclei. This fact is, possibly, connected with odd-even composition of the triton.

3.2. Triton Clustering Factors by the Knock-on Model

Values of the triton clustering factors depending on mass numbers for odd-even and even-even target nuclei are shown in figure 3.

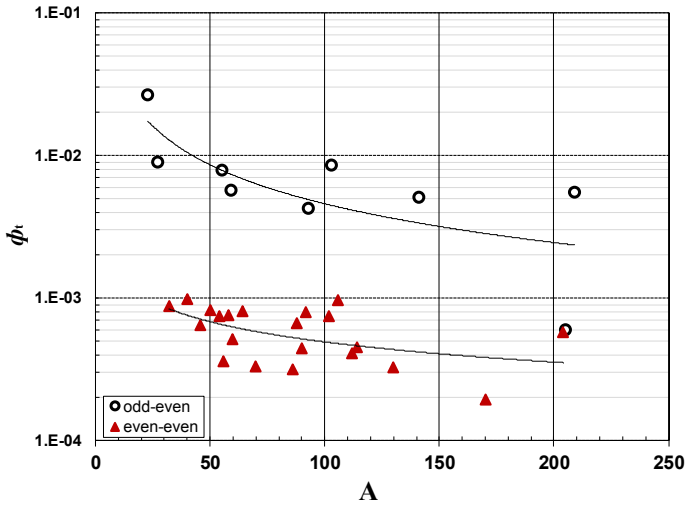

Figure 3 - The triton clustering factor versus mass number of target nuclei

It can be seen that the triton clustering factors for even-even target nuclei are on an average by one order of magnitude (~10 times) lower than ones for odd-even nuclei. This result can be, also, explained by the composition of triton which is odd-even. Figures 2 and 3 show that the clustering factors obtained by statistical model are on an average two order of magnitude (~10^2) lower than ones by knock on model. This result means that in the most case the triton cluster is, probably, performed before interaction of incident neutrons with the target nuclei. At the same time, triton clustering factors are much lower than α-clustering in (n,α) reactions ($\phi_\alpha \approx 10^{-2}$-$10^{-1}$) at the same energy range for medium mass nuclei [6]. It means that four nucleons clustering factor is more than three nucleons one. This difference of the clustering factors is, perhaps, caused by the difference of the α-particle and triton binding energy.

Acknowledgement

The present work was performed in the framework of the project "Nuclear Cluster Structure and Reaction Study" supported by the Mongolian Science and Technology Foundation (Contract: No.ShuSs-2019/06).

Г.Хуухэнхуу[1], М.Одсурэн[2,*], Ж.Мунхсайхан[1], А.Турсух[1], Ч.Сайханбаяр[1], А.Сарсембаева[3], М.Абишев[3]

[1]Ядролық физикалық зерттеу орталығы, Моңғолия ұлттық университеті, Улан-Батор, Моңғолия;
[2]Инженерлік және қолданбалы ғылымдар институты, Моңғолия ұлттық университеті, Улан-Батор, Моңғолия;
[3]Физика-техникалық факультеті, Әл-Фараби атындағы ҚазҰУ, Қазақстан

(n,t) РЕАКЦИЯСЫНДАҒЫ ТРИТОН-КЛАСТЕРЛЕУ

Аннотация. Ядроның дәстүрлі анықтамасына сәйкес ядродағы протондар мен нейтрондар шамамен біркелкі таралады. Ядролық физиканың бастапқы кезеңінде ядролардың кластерленуі ядролардың құрылымын анықтау үшін өте маңызды екені белгілі болды. Ауыр ядродағы альфа ыдырауының ашылуы нуклон кластерлерін шығарудан бұрын қалыптастыруға болатындығы туралы идеяға жол салды. Кейін Гамов, Герни және Гордон альфа бөлшегі ыдырайтын ядроның ішінен кванттық механикалық туннельден өтетіндігін сипаттады. Сонымен қатар, сиқырлы (біркелкі) N = Z ядроларына арналған кластерлерді байланыстыратын альфа-бөлшектердің моделі ұсынылды. 1941 жылы Маргенау тиімді альфа-альфа өзара әрекеттесуін есептеу үшін альфа кластерлері үшін Слейтер детерминант толқынының функциясын қолданды. Сонымен қатар, Моригана альфа тәрізді ядролардың кейбір күйлерін сипаттау үшін альфа кластерлерінің сызықты тізбегін қолдануды ұсынды. Кластерлік құрылымдар, әдетте, ыдыраудың тиісті шегіне жақын қозған күй түрінде байқалады. Бұл құбылыстың басталуы тиімді ядролық әрекеттестікке байланысты, бірақ ядролардағы кластерлердің егжей-тегжейлі механизмі әлі толық зерттелмеді.

Ядролардың кластерлік қасиеттері ядроның құрылымын да, ядролық реакция механизмдерін де түсіну үшін пайдалы болар еді. Ядролар түбегейлі түрлі кластерлерге ие болуы мүмкін, мысалы, жеңіл (екі, үш және төрт нуклон) және ауыр. Ядролардың кластерлік эффектісі әртүрлі теориялық тәсілдерге негізделген түрлі әдістерді қолдану арқылы ұзақ уақыт зерттелді. Алайда бұл зерттеулердің көпшілігі α-ыдырау кезіндегі α-кластерлерге, бөлшектердің α-шашырауына, α-бөлшектердің тасымалдануы және шығару реакцияларына және жеңіл ядролардың α-кластерінің молекулалық тәрізді құрылымына арналған болатын. Белгілі мысал ретінде альфа кластеріне арналған Be изотоптарын алсақ болады. ^{8}Be тығыз екі альфа кластерлік құрылымға ие, ал ядросы тұрақсыз болып саналады. Егер ^{9}Be изотопын қарастыратын болсақ (^{8}Be-ге бір нейтрон қосқанда), онда кластер құрылымы тұрақтанады және жүйе байланысқан болып саналады.

Соңғы жылдары статистикалық модель мен нокаут механизмін қолдана отырып, жылдам және баяу нейтрондық индукция (n, α) бар реакциялардағы α-кластерлеуді зерттедік.

Бұл жұмыста құрама ядро және тікелей реакция механизмдері аясында алғаш рет (n, t) реакциялар үшін тритонды кластерлеу факторы (немесе ықтималдығы) табылды. Құрама механизм жағдайында булану және тұрақты ядролық температураның жуықтау моделіне негізделген статистикалық модель қолданылды. Тікелей реакция механизмі үшін нокаут моделі қолданылды. Нокаут моделін қолдану арқылы алынған тритонды кластерлеу коэффициенттері статистикалық модель арқылы табылған коэффициенттерге қарағанда әлдеқайда үлкен екендігі көрсетілді. Сонымен қатар, жұп-жұп ядро нысанасы үшін тритонды кластерлеу факторы тақ-жұп ядролар үшін орташа мәнмен алғанда әлдеқайда төмен болып саналады.

Сонымен қатар, тритондардың кластерлеу факторлары орташа масса ядролары үшін нейтрон энергиясының бірдей диапазонындағы (n, α) реакциялардағы α-кластерлеуге қарағанда әлдеқайда төмен болып есептелінді.

Түйін сөздер: құрама механизм, статистикалық модель, булану моделі, тұрақты ядролық температураға жақындату, тікелей реакциялар, нокаут моделі, альфа-кластерлеу, тритонды-кластерлеу.

Г. Хуухэнхуу[1], М. Одсурэн[2,*], Ж. Мунхсайхан[1], А. Турсух[1], Ч. Сайханбаяр[1], А. Сарсембаева[3], М. Абишев[3]

[1] Центр ядерно-физических исследований, Национальный университет Монголии, Улан-Батор, Монголия;
[2] Школа инженерных и прикладных наук, Национальный университет Монголии, Улан-Батор, Монголия;
[3] Физико-технический факультет, КазНУ им.аль-Фараби, Казахстан

ТРИТОН-КЛАСТЕРИЗАЦИЯ В (n,t) РЕАКЦИЯХ

Аннотация. Согласно традиционному определению ядра, протоны и нейтроны в ядре имеют примерно однородное распределение. В начале ядерной физики было известно, что ядерная кластеризация является чрезвычайно важной для определения структуры ядер. Открытие альфа-распада тяжелых ядер положило начало идея о том, что кластеры нуклонов могут быть предварительно сформированы до испускания. Впоследствии Гамов, Герни и Кондон объяснили, что альфа-частица подвергается квантово-механическому туннелированию изнутри распадающегося ядра. Кроме того, предлагалась альфа-частичная модель для четно-четных ядер N = Z, которые состоят из связанных альфа-кластеров. В 1941 году Маргенау использовал волновую функцию детерминанта Слейтера для альфа-кластеров, чтобы вычислить эффективное альфа-альфа-взаимодействие. Более того, Моригана предполагал применять линейные цепочки альфа-кластеров для описания некоторых состояний альфа-подобных ядер. Кластерные структуры обычно наблюдаются в виде возбужденных состояний, близких к соответствующему порогу распада. Происхождение этого явления лежит в эффективном ядерном взаимодействии, но детальный механизм кластеризации в ядрах еще не полностью изучен.

Кластерные свойства ядер были бы полезны для понимания как структуры ядра, так и механизмов ядерных реакций. Разные типы кластеров могут в принципе существовать в ядре, например, легкие (двух, трех и четырех нуклонные) и тяжелые кластеры. Эффект кластеризации длительное время был исследован разными авторами, которые использовали разные методы, основанные на различных теоретических подходах. Однако большинство таких исследований было посвящено α-кластеризации в α-распаде, рассеянии α-частиц, ядерных реакиях с передачей и испускания α-частиц и молекулярно-подобной α-кластерной структуре легких ядер. Известными примерами являются изотопы Be для альфа-кластеризации. ^{8}Be имеет плотную двух альфа кластерную структуру, а данное ядро нестабильно. Если мы рассмотрим другой изотоп ^{9}Be (добавив один нейтрон в ^{8}Be), кластерная структура стабилизируется, и система будет связана.

В последние годы мы, используя статистическую модель и механизм выбивания, исследовали α-кластеризацию в (n,α) реакциях, индуцированных быстрыми и медленными нейтронами.

В данной работе в рамках механизмов компаунд-ядра и прямой реакции впервые были найдены фактор (или вероятность) тритонной кластеризации для (n,t) реакций. В случае компаунд-механизма была использована статистическая модель, основанная на модели испарения и приближении постоянной температуры ядра. Модель выбивания использовалась для механизма прямых реакций. Было показано, что факторы тритонной кластеризации, найденные с использованием модели выбивания, значительно больше, чем в случае статистической модели. В то же время, факторы тритонной кластеризации для четно-четных ядер в среднем на один порядок меньше, чем для нечетно-четных ядер. Кроме того, факторы тритонной кластеризации намного меньше, чем α-частичной кластеризации при одинаковой энергии нейтронов для ядер средных масс.

Ключевые слова: составной механизм, статистическая модель, модель испарения, аппроксимация постоянной ядерной температуры, прямые реакции, модель выбивания, альфа-кластеризация, тритонная кластеризация.

Information about authors:

Khuukhenkhuu Gonchigdorj, Professor, Head of the Nuclear Data Division, Nuclear Research Center, National University of Mongolia, E-mail: g_khuukhenkhuu@yahoo.com; https://orcid.org/0000-0002-1011-3127;

Odsuren Myagmarjav, Associate professor, School of Engineering and Applied Sciences and Nuclear Research Center, National University of Mongolia, E-mail: odsuren@seas.num.edu.mn; https://orcid.org/0000-0003-2756-4909;

Munkhsaikhan Jargalsaikhan, Researcher, Nuclear Research Center, National University of Mongolia, E-mail: munkhsaikhan.nrc@gmail.com; https://orcid.org/0000-0002-3895-6177;

Tursukh Amgalan, Researcher, Nuclear Research Center, National University of Mongolia, E-mail: tursukh.amgalan@gmail.com; https://orcid.org/0000-0002-6885-3398;

Saikhanbayar Chinzorig, Researcher, Nuclear Research Center, National University of Mongolia, E-mail: saikhanaa.ok@gmail.com; https://orcid.org/0000-0002-2909-2362;

Sarsembayeva Aiganym, PhD, Senior lecturer, Department of Theoretical and Nuclear Physics, Al-Farabi Kazakh National University, E-mail: sarsembaeva.a@kaznu.kz; https://orcid.org/0000-0002-3003-0038;

Abyshev Medeu, Associate Professor, Head of the Department of Theoretical And Nuclear Physics, Al-Farabi Kazakh National University, E-mail: Medeu.Abishev@Kaznu.Kz; http://orcid.org/0000-0003-3602-6934

REFERENCES

[1] Hodgson P.E., Alpha-clustering in Nuclei, In book: “The Uncertainty Principle and Foundations of Quantum Mechanics”. Editors: W.C.Price and S.S.Chissick, Chapter 23, New York, John Wiley, 1977, p.485.

[2] Clusters in Nuclei, Editor: Christion Beck, vol.1, (2010), vol.2, (2012) and vol.3, (2014), Springer-Verlag, Berlin Heidelberg.

[3] Wildermuth K. and Tang Y.C. A Unified Theory of the Nucleus, Academic Press, Inc. New York, 1977.

[4] Odsuren M., Sarsembayeva A.T., Khuukhenkhuu G., Davaa S., Kato K., Usukhbayar B. Newsof the National Academy of Sciences of the Republic of Kazakhstan, Series Physico-Mathematical, 2 (324), (2019), p.5

[5] Khuukhenkhuu G., Odsuren M., Gledenov Yu.M., Munkhsaikhan J., Davaa S., Saikhanbayar Ch., Sansarbayar E. and Sedysheva M.V. Acta Physica Polonica, vol.49B, No 23, 2018, p. 325.

[6] Batchimeg B., Khuukhenkhuu G., Odsuren M., Munkhsaikhan J., Saikhanbayar Ch., Gledenov Yu.M., Sansarbayar E., Sedysheva M.V. and Guohui Zhang Proceedings of the XXVI International Seminar on Interaction of Neutrons with Nuclei, (ISINN-26, May 28-June 1, 2018, Xi’an, China), 2019, JINR, Dubna, p.55.

[7] Blatt J.M. and Weisskopf V.F. Theoretical Nuclear Physics, John Wiley and Sons, New York, 1952.

[8] Weisskopf V.F. and Ewing D.H. Phys. Rev., v.57, No.6, 1940, p.472.

[9] Landau L.D. and Smorodinsky Ya. Lectures on Nuclear Theory, Translated from Russian, Plenum Press, Inc., New York, 1959.

[10] C.F.von.Weizsäcker, Z. Phys., v.96A, No.7-8, 1935, p.431.

[11] Gardner D.G. and Rosenblum S. Nucl. Phys., v.96A, No.1, 1967, p.121.

[12] Bohr A. and Mottelson B.R. Nuclear Structure, W.A. Benjamin Inc., New York, Amsterdam, 1969.

[13] Scherk L. and Vogt E.W. Can. Jour. Phys., v.46, No.9, 1968, p.1119.

[14] http:/www-nds.iaea.org/exfor/exfor.htm

NEWS
OF THENATIONAL ACADEMY OF SCIENCES OF THE REPUBLIC OF KAZAKHSTAN
PHYSICO-MATHEMATICAL SERIES
ISSN 1991-346X **https://doi.org/10.32014/2020.2518-1726.62**
Volume 4, Number 332 (2020), 28 – 34

UDC 004.032.26
IRSTI 28.23.37

Marat Nurtas[1], Zh. Baishemirov [2,3],
V. Tsay[1], M. Tastanov[1], Zh. Zhanabekov[1]

[1]International Information Technologies University, Almaty, Kazakhstan;
[2]Abai Kazakh National Pedagogical University, Almaty, Kazakhstan;
[3]RSE Institute of Information and Computational Technology CS MES RK, Almaty, Kazakhstan.
E-mail: maratnurtas@gmail.com; zbai.kz@gmail.com;
tsay.victor96@gmail.com; tychty4@gmail.com; zzhanabekov@gmail.com

APPLYING NEURAL NETWORK FOR PREDICTING CARDIOVASCULAR DISEASE RISK

Abstract. This article concerns the problem of the prevalence of cardiovascular disease in economically developed countries. The purpose of this article is to create a neural network to determine the risk of cardiovascular disease based on the individual characteristics of the patient. In order to predict the risk of cardiovascular disease a neural network has been developed. The model was built in the Python programming language using the open-source library for building neural networks Keras. Data containing patient information for model building were taken from Kaggle.com. The accuracy of the neural network is 82%. With the help of neural network it will be possible to analyze the changes and the development of diseases in the future by changing the patient's input parameters, for instance, age, increase in blood pressure and etc. Also it would be possible to change the predictive diagnosis for the better if follow the parameters such as refusal from addictions, regular sleep, a healthy lifestyle and proper nutrition.

Key worlds: Neural network, cardiovascular system diseases, predicting models, supervised learning, activation function, Keras.

Introduction. Cardiovascular system diseases, in particular chronic heart failure, cardiac ischemia and arterial hypertension are a public health problem in economically developed countries. One of the obvious and main reasons is the complexity of the initial diagnosis and the reluctance of people to visit clinics and hospitals when the first symptoms appear. A fast pace of life, poor nutrition, a sedentary lifestyle, addictions, and a lack of proper sleep all negatively affect the cardiovascular system. According to World Health Organization in 2016, more than 17.9 million people died from coronary heart disease, which amounted to 31% of all deaths[1]. Given the prevalence of cardiovascular diseases in developed countries, there is an urgent need to create a tool for the diagnosis of cardiovascular disease in the early stages of development. A neural network can be one of solutions to the problem due to its accessibility and ease of use.

The first attempts to create diagnostic neural networks date back to the 40-50s of the XX century, after the publication of the fundamental works of W. McCallock, W. Pitts and F. Rosenblatt, who laid the theoretical foundations of neural networks[2].

The list of medical spheres where neural networks have begun to be applied for diagnosing diseases are very long, and it is increasing from year to year. The accessibility of the neural networks courses, electronic patient records, a large number of articles about implementing of neural networks, the ability to create neural networks on ordinary laptops contributes to the development and application of neural networks not only in medicine, but also in other areas of human activities[3].

Neural networks largely borrow their structure and principles of work from the cerebral cortex. Like the brain, they learn from life examples, extract and encode this knowledge in the form of synoptic neural connections. After training and testing, neural networks become mathematical models. This means that you can experiment with them, solve practical problems, predict behavior in the subject area (predicting the development of the disease), and diagnose the state of the subject area[4].

The selection of input parameters with high information value, in other words parameters that affect the result of the model, is of great importance. The choice of parameters that have significant impact on the diagnosis of cardiovascular disease is not obvious. Therefore, as the input parameters for the neural network, all provided parameters should be selected that characterize the patient and are able to influence the result. On the other hand, in order to create a neural network accessible for mass use, the most accessible data were used, which did not require complex analyzes in hospitals.

Neural network. A neural network is a mathematical model and its software embodiment, which operates on the principle of a biological neural network, where each neuron is connected to another neuron from the previous layer. Each neuron receives and sends signals to other neurons, which provides a connection between them by synapses.

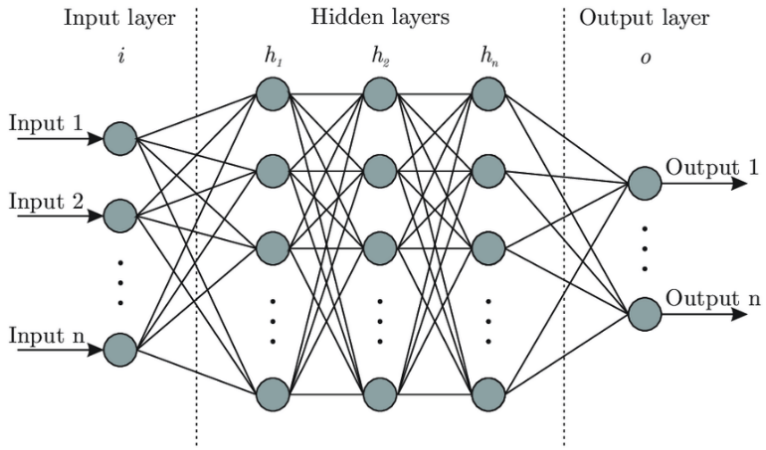

Figure 1 – General structure of neural network

A neuron is a computing unit that receives information, performs simple calculations on it, and passes the changed information on. Neurons are mainly divided into 3 groups: input, hidden and output as shown in Figure 1. There is also a displacement neuron and a contextual neuron. In the case when the number of neurons is large, the term layer is used. Each neuron has input and output data. In the case of an input neuron, income data is equivalent to output. In other cases, the income data is a summary of data from all previous layers. Further, this input information is normalized using the activation function, usually written *f(x)*. Neurons operate with numbers in the range of [0,1] or [-1,1]. Therefore, it is necessary to carry out the normalization process.

A synapse is a connection between two neurons that has a weight, usually denoted by *w*. Due to this weight, the input information changes during transmission from one neuron to another. The higher the weight of one neuron, the more significant the information transmitted to the next neuron will be. Thanks to these scales, the input information is processed and turned into a result. During the initialization of the neural network, weights are randomly distributed.

The activation function is a way to normalize input data, in other words, if you have a large number at the input, going through the activation function, this number will be reduced in the required range. The most commonly used activation functions are: linear, sigmoid (logistic) and hyperbolic tangent. The linear function (1) is used in cases where it is necessary to transmit information without changes or to test a neural network. The sigmoid (2), also called the logistic function, takes values in the range [0,1] and is the most common activation function. It makes sense to use hyperbolic tangent (3) when the values can be negative and positive. It has a range of [-1.1]. Using hyperbolic tangent, when the values are only positive, will adversely affect the accuracy of the neural network.

$$f(x) = x \tag{1}$$

$$f(x) = \frac{1}{(1+e^{-x})} \tag{2}$$

$$f(x) = \frac{(e^{2x}-1)}{(e^{2x}+1)} \tag{3}$$

Neural network training is divided into two large clusters: supervised learning and unsupervised learning. Supervised learning is a method of building a neural network, in which the results of observations from dataset, which is used for training the model, are already known initially and the neural network learns to correctly determine the future results using examples. Supervised learning is used for problems such as regression and classification. In unsupervised learning, the result of observation in the dataset is not initially known. Most often, this approach is used when it is necessary to group data by certain parameters or to create a recommendation system.

Model building. For building any predicting model. As the dataset on which the neural network was built, the file heart.csv[5] was used. The file contains information about 303 patients and 14 significant variables, among which:

1) age;
2) sex;
3) cp: chest pain type (value 1: typical angina, value 2: atypical angina, value 3: non-anginal pain, value 4: asymptomatic);
4) trestbps: resting blood pressure (in mm Hg on admission to the hospital);
5) chol: serum cholestoral (in mg/dl);
6) fbs: fasting blood sugar > 120 mg/dl (1 = true; 0 = false);
7) restecg: resting electrocardiographic result (value 0: normal, value 1: having ST-T wave abnormality [T wave inversions and/or ST elevation or depression of > 0.05 mV], value 2: showing probable or definite left ventricular hypertrophy by Estes' criteria);
8) thalach: maximum heart rate achieved;
9) exang: exercise induced angina (1 = yes; 0 = no);
10) oldpeak = ST depression induced by exercise relative to rest;
11) slope: the slope of the peak exercise ST segment (value 1: upsloping, value 2: flat, value 3: downsloping);
12) ca: number of major vessels (0-3) colored by fluoroscopy;
13) thal: 3 = normal; 6 = fixed defect; 7 = reversible defect;
14) num: diagnosis of heart disease or angiographic disease status (value 0: < 50% diameter narrowing, value 1: > 50% diameter narrowing).

```
In [3]: data.head(10)
```

Out[3]:

	age	sex	cp	trestbps	chol	fbs	restecg	thalach	exang	oldpeak	slope	ca	thal	target
0	63	1	3	145	233	1	0	150	0	2.3	0	0	1	1
1	37	1	2	130	250	0	1	187	0	3.5	0	0	2	1
2	41	0	1	130	204	0	0	172	0	1.4	2	0	2	1
3	56	1	1	120	236	0	1	178	0	0.8	2	0	2	1
4	57	0	0	120	354	0	1	163	1	0.6	2	0	2	1
5	57	1	0	140	192	0	1	148	0	0.4	1	0	1	1
6	56	0	1	140	294	0	0	153	0	1.3	1	0	2	1
7	44	1	1	120	263	0	1	173	0	0.0	2	0	3	1
8	52	1	2	172	199	1	1	162	0	0.5	2	0	3	1
9	57	1	2	150	168	0	1	174	0	1.6	2	0	2	1

Figure 2 – Dataset for predicting cardiovascular disease risk

```
In [5]: data.corr()
```

Out[5]:

	age	sex	cp	trestbps	chol	fbs	restecg	thalach	exang	oldpeak	slope	ca	thal	target
age	1.000000	-0.098447	-0.068653	0.279351	0.213678	0.121308	-0.116211	-0.398522	0.096801	0.210013	-0.168814	0.276326	0.068001	-0.225439
sex	-0.098447	1.000000	-0.049353	-0.056769	-0.197912	0.045032	-0.058196	-0.044020	0.141664	0.096093	-0.030711	0.118261	0.210041	-0.280937
cp	-0.068653	-0.049353	1.000000	0.047608	-0.076904	0.094444	0.044421	0.295762	-0.394280	-0.149230	0.119717	-0.181053	-0.161736	0.433798
trestbps	0.279351	-0.056769	0.047608	1.000000	0.123174	0.177531	-0.114103	-0.046698	0.067616	0.193216	-0.121475	0.101389	0.062210	-0.144931
chol	0.213678	-0.197912	-0.076904	0.123174	1.000000	0.013294	-0.151040	-0.009940	0.067023	0.053952	-0.004038	0.070511	0.098803	-0.085239
fbs	0.121308	0.045032	0.094444	0.177531	0.013294	1.000000	-0.084189	-0.008567	0.025665	0.005747	-0.059894	0.137979	-0.032019	-0.028046
restecg	-0.116211	-0.058196	0.044421	-0.114103	-0.151040	-0.084189	1.000000	0.044123	-0.070733	-0.058770	0.093045	-0.072042	-0.011981	0.137230
thalach	-0.398522	-0.044020	0.295762	-0.046698	-0.009940	-0.008567	0.044123	1.000000	-0.378812	-0.344187	0.386784	-0.213177	-0.096439	0.421741
exang	0.096801	0.141664	-0.394280	0.067616	0.067023	0.025665	-0.070733	-0.378812	1.000000	0.288223	-0.257748	0.115739	0.206754	-0.436757
oldpeak	0.210013	0.096093	-0.149230	0.193216	0.053952	0.005747	-0.058770	-0.344187	0.288223	1.000000	-0.577537	0.222682	0.210244	-0.430696
slope	-0.168814	-0.030711	0.119717	-0.121475	-0.004038	-0.059894	0.093045	0.386784	-0.257748	-0.577537	1.000000	-0.080155	-0.104764	0.345877
ca	0.276326	0.118261	-0.181053	0.101389	0.070511	0.137979	-0.072042	-0.213177	0.115739	0.222682	-0.080155	1.000000	0.151832	-0.391724
thal	0.068001	0.210041	-0.161736	0.062210	0.098803	-0.032019	-0.011981	-0.096439	0.206754	0.210244	-0.104764	0.151832	1.000000	-0.344029
target	-0.225439	-0.280937	0.433798	-0.144931	-0.085239	-0.028046	0.137230	0.421741	-0.436757	-0.430696	0.345877	-0.391724	-0.344029	1.000000

Figure 3 – Correlation matrix of the dataset

The model was built with open-source neural network library Keras written in Python[6]. Keras is designed for building deep neural networks. It is user-friendly and modular library, which includes blocks such as layers, optimizers, activation functions, objectives and host of tools to work with image and text data. Keras supports standard, convolutional and recurrent neural networks.

Results. The neural network, after training and optimization, was tested on data that was not involved in the learning process of the model. As a result, the neural network has an accuracy of 82% and a standard deviation of 0.026. The most valuable variables were chest pain type, maximum heart rate achieved, exercise induced angina, ST depression induced by exercise relative to rest and number of major vessels (0-3) colored by fluoroscopy.

```
variance = accuracies.std()
162/162 [==============================] - 0s 56us/step - loss: 0.2412 - accuracy: 0.8951
Epoch 9992/10000
162/162 [==============================] - 0s 56us/step - loss: 0.2394 - accuracy: 0.8889
Epoch 9993/10000
162/162 [==============================] - 0s 43us/step - loss: 0.2358 - accuracy: 0.8889
Epoch 9994/10000
162/162 [==============================] - 0s 56us/step - loss: 0.2457 - accuracy: 0.8704
Epoch 9995/10000
162/162 [==============================] - 0s 49us/step - loss: 0.2373 - accuracy: 0.8827
Epoch 9996/10000
162/162 [==============================] - 0s 43us/step - loss: 0.2423 - accuracy: 0.8827
Epoch 9997/10000
162/162 [==============================] - 0s 49us/step - loss: 0.2463 - accuracy: 0.9012
Epoch 9998/10000
162/162 [==============================] - 0s 43us/step - loss: 0.2510 - accuracy: 0.9012
Epoch 9999/10000
162/162 [==============================] - 0s 49us/step - loss: 0.2430 - accuracy: 0.8704
Epoch 10000/10000
162/162 [==============================] - 0s 86us/step - loss: 0.2369 - accuracy: 0.8765
80/80 [==============================] - 0s 313us/step

In [8]: print("Accuracy mean: "+ str(mean))
        print("Accuracy variance: "+ str(variance))

Accuracy mean: 0.8221707940101624
Accuracy variance: 0.026507396106117874
```

Figure 4 – Results of the neural network model and part of training algorithm

Conclusion. A neural network has been developed to predict the risk of cardiovascular disease. The standard deviation was 0.026, which allows us to state that the model is stable and can be used to identify patterns in this area of medicine, including those pattern that are not explicit. Such patterns can be revealed by experiments. By changing the patient's input parameters, for example, age, increase in blood pressure, it will be possible to analyze changes and the development of diseases in the future. You can try to improve the predictive diagnosis of the patient by changing the input parameters. Refusal from

addictions, a healthy lifestyle, proper nutrition, physical activity - all these parameters can change the predictive diagnosis for the better. By observing changes in input parameters and predicted results, it is possible to identify the dependence, on the basis of which you can develop an individual patient treatment plan.

Although the neural network has high predictive power, it is still the primary diagnosis of cardiovascular disease. And more accurate and complete analysis requires visiting the hospital.

Марат Нуртас[1], Ж.Д. Байшемиров [2,3], В. Цай [1],
М. Тастанов [1], Ж. Жанабеков [1]

[1]Халықаралық ақпараттық технологиялар университеті, Алматы, Қазақстан,
[2]Абай атындағы Қазақ ұлттық педагогикалық университеті, Алматы, Қазақстан,
[3]Ақпараттық және есептеуіш технологиялар институты, Алматы, Қазақстан

ЖҮРЕК-ҚАН ТАМЫРЛАРЫ АУРУЛАРЫНЫҢ ҚАУПІН БОЛЖАУ ҮШІН НЕЙРОНДЫҚ ЖЕЛІНІ ПАЙДАЛАНУ

Аннотация. Бұл мақалада экономикалық дамыған елдерде жүрек-қан тамырлары ауруларының таралуы туралы айтылады. Осы мақаланың мақсаты пациенттің жеке ерекшеліктеріне негізделген, жүрек-қан тамырлары ауруларының қаупін анықтау үшін нейрондық желі құру болып табылады. Модель Python-да жазылған Keras нейрондық желілік кітапхананың көмегімен жасалды. Керас терең нейрондық желілерді құруға арналған. Бұл пайдаланушыға ыңғайлы және модульді кітапхана, оның құрамына қабаттар, оптимизаторлар, активтендіру функциялары, мақсаттар, кескіндермен және мәтіндік деректермен жұмыс істеуге арналған құралдар жиынтығы кіреді. Керас стандартты, үйірткілі және рекурентті нейрондық желілерді қолдайды. Үлгіні құру үшін қажет пациенттер туралы мәліметтер Kaggle.com сайтынан алынды. Нейрондық желінің дәлдігі 82% құрайды.

Жүрек-қантамыр жүйесінің аурулары, атап айтқанда созылмалы жүрек жетіспеушілігі, жүрек ишемиясы және артериялық гипертензия, экономикалық дамыған елдерде қоғамдық денсаулық сақтау мәселесі болып табылады. Бұл жағдайдың басты және анықталған себептерінің бірі - алғашқы диагноздың күрделілігі және де алғашқы белгілер пайда болған кезде адамдардың емханалар мен ауруханаларға барғысы келмеуі. Өмірдің жылдам қарқыны, дұрыс тамақтанбау, отырықшы өмір салты, жаман әдеттер және дұрыс ұйқының болмауы жүрек-қантамыр жүйесіне кері әсерін тигізеді.

Дүниежүзілік денсаулық сақтау ұйымының мәліметтері бойынша, 2016 жылы жүректің ишемиялық ауруынан 17,9 миллионнан астам адам қайтыс болды, бұл барлық өлімнің 31% құрады [1]. Дамыған елдерде жүрек-қантамыр ауруларының кең таралуын ескере отырып, дамудың алғашқы кезеңдерінде жүрек-қантамыр ауруларының диагнозын анықтайтын құрал қажет. Өзінің қол жетімділігі мен қолданылуының қарапайымдылығына байланысты нейрондық желі осы мәселені шешудің бір жолы болуы мүмкін. Жүрек-қантамыр ауруларының қаупін болжауға арналған нейрондық желі әзірленді. Желінің стандартты ауытқуы 0.026 құрады, бұл модельдің тұрақтылығын және медицинаның осы саласындағы, оның ішінде анықталмайтын модельдерді анықтау үшін пайдаланылуы мүмкін екендігін пайымдауға мүмкіндік береді. Мұндай заңдылықтарды тәжірибелер арқылы анықтауға болады. Оқыту мен оңтайландырудан кейін нейрондық желі модельдік оқыту процесіне қатыспайтын мәліметтер негізінде тексерілді. Ең құнды ауыспалыларға кеудедегі ауырсыну түрлері, максималды жүрек соғуы, физикалық белсенділіктен туындаған стенокардия, демалыспен салыстырғанда физикалық белсенділіктің нәтижесінде пайда болған ST депрессиясы және флюороскопиямен боялған ірі тамырлардың саны (0-3) кірді.

Пациенттің енгізу параметрлерін, мысалы, жасын, қан қысымының жоғарылауын өзгерту, болашақта аурулардың өзгеруі мен дамуын талдауға мүмкіндік береді. Пациенттің енгізу параметрлерін өзгерту арқылы оның болжамды диагнозын жақсартуға мүмкін болады.

Жаман әдеттерден бас тарту, салауатты өмір салты, дұрыс тамақтану, физикалық белсенділік сияқты параметрлер болжамды диагнозды жақсы жаққа өзгерте алады. Енгізу параметрлерінің өзгеруін және болжамды нәтижелерді байқау арқылы тәуелділікті анықтауға болады, соның негізінде пациенттің жеке емдеу жоспарын жасауға болады.

Түйін сөздер: нейрондық желі, жүрек-тамыр жүйесі аурулары, болжау модельдері, бақыланатын оқыту, активация функциясы, Keras.

Марат Нуртас[1], Ж.Д. Байшемиров [2,3], В. Цай [1],
М. Тастанов [1], Ж. Жанабеков [1]

[1]Международный университет информационных технологий, Алматы, Казахстан;
[2]Казахский национальный педагогический университет имени Абая, Алматы, Казахстан;
[3]Институт информационных и вычислительных технологий КН МОН РК, Алматы, Казахстан

ПРИМЕНЕНИЕ НЕЙРОННОЙ СЕТИ ДЛЯ ПРОГНОЗИРОВАНИЯ РИСКА СЕРДЕЧНО-СОСУДИСТЫХ ЗАБОЛЕВАНИЙ

Аннотация. Данная статья касается проблемы распространения сердечно-сосудистых заболеваний в экономически развитых странах. Цель этой статьи заключается в создании нейронной сети для определения риска сердечно-сосудистых заболеваний на основе индивидуальных характеристик пациента. Модель была построена с открытым исходным кодом нейронной сетевой библиотеки Keras, написанной на Python. Keras разработан для построения глубоких нейронных сетей. Это удобная для пользователя и модульная библиотека, которая включает такие блоки, как слои, оптимизаторы, функции активации, цели и набор инструментов для работы с изображением и текстовыми данными. Keras поддерживает стандартные, сверточные и рекуррентные нейронные сети. Данные, содержащие информацию о пациенте для построения модели, были взяты с сайта Kaggle.com. Точность нейронной сети составляет 82%.

Заболевания сердечно-сосудистой системы, в частности хроническая сердечная недостаточность, ишемия сердца и артериальная гипертония являются проблемой общественного здравоохранения в экономически развитых странах. Одной из очевидных и основных причин является сложность первоначального диагноза и нежелание людей посещать клиники и больницы, когда появляются первые симптомы. Быстрый темп жизни, плохое питание, сидячий образ жизни, вредные привычки и отсутствие надлежащего сна негативно влияют на сердечно-сосудистую систему.

По данным Всемирной организации здравоохранения в 2016 году, от ишемической болезни сердца умерло более 17,9 миллиона человек, что составило 31% от всех смертей [1]. Учитывая распространенность сердечно-сосудистых заболеваний в развитых странах, существует острая необходимость в создании инструмента для диагностики сердечно-сосудистых заболеваний на ранних этапах развития. Нейронная сеть может быть одним из решений проблемы из-за ее доступности и простоты использования. Нейронная сеть была разработана для прогнозирования риска сердечно-сосудистых заболеваний. Стандартное отклонение составило 0,026, что позволяет нам утверждать, что модель стабильна и может быть использована для идентификации закономерностей в этой области медицины, включая те, которые не являются явными. Такие закономерности могут быть выявлены в ходе экспериментов. Нейронная сеть после обучения и оптимизации была протестирована на основе данных, которые не были задействованы в процессе обучения модели. Наиболее ценными переменными были типы боли в груди, максимальная частота сердечных сокращений, стенокардия, вызванная физической нагрузкой, депрессия ST, вызванная физической нагрузкой, по сравнению с отдыхом, и количество крупных сосудов (0-3), окрашенных с помощью флюороскопии.

Изменение входных параметров пациента, например, возраст, повышение кровяного давления, позволит анализировать изменения и развитие заболеваний в будущем. Можно попытаться улучшить прогнозную диагностику пациента, изменив входные параметры.

Отказ от вредных привычек, здоровый образ жизни, правильное питание, физическая активность – все эти параметры могут изменить прогнозирующий диагноз в лучшую сторону. Наблюдая изменения входных параметров и прогнозируемых результатов, можно определить зависимость, на основе которой можно разработать индивидуальный план лечения пациента.

Ключевые слова: нейронная сеть, заболевания сердечно-сосудистой системы, модели прогнозирования, контролируемое обучение, функция активации, Keras.

Information about authors:

Nurtas Marat, PhD, Associate Professor of Department of Mathematical and Computer Modeling, International Information Technologies University; maratnurtas@gmail.com, https://orcid.org/0000-0003-4351-0185;

Baishemirov Zh.D., PhD, Associate Professor of Abai Kazakh National Pedagogical University, Senior Research Officer of RSE Institute of Information and Computational Technology CS MES RK; zbai.kz@gmail.com, https://orcid.org/0000-0002-4812-4104;

Tsay V., master student, Department of Mathematical and Computer Modeling, [1]International Information Technologies University; tsay.victor96@gmail.com, https://orcid.org/0000-0002-6073-2030;

Tastanov M., Master Student of Department of Mathematical and Computer Modeling, International Information Technologies University; tychty4@gmail.com, https://orcid.org/0000-0002-1802-6394;

Zhanabekov Zh., Master Student of Department of Mathematical and Computer Modeling, International Information Technologies University; zzhanabekov@gmail.com, https://orcid.org/0000-0001-5984-7132;

REFERENCES

[1] World Health Organization, "Cardiovascular diseases (CVDs)", available at https://www.who.int/en/news-room/fact-sheets/detail/cardiovascular-diseases-(cvds) (accessed 5 March 2020).

[2] Yasnitsky, L.N., Dumler, A.A., Poleshchuk, A.N., Bogdanov, K.V., Cherepanov, F.M. (2011), "Neuronetwork system of cardiovascular diseases express-diagnosis", *Perm Medical Journal*, Vol. XXVIII № 4, pp. 77-86.

[3] Kim, J.K., Sanggil K. (2017), "Neural Network-Based Coronary Heart Disease Risk Prediction Using Feature Correlation Analysis", *Journal of healthcare engineering*, vol. 2017: 2780501. doi:10.1155/2017/2780501

[4] Mazakov T. Zh., Jomartova Sh. A., Wojcik Waldemar, Ziyatbekova G. Z., Amirkhanov B. S., Zholmagambetova B. R. "Universal complex of psychophysiological testing", *News of the National Academy of sciences of the Republic of Kazakhstan,* Volume 2, Number 330 (2020), 14 – 22. https://doi.org/10.32014/2020.2518-1726.10

[5] Kaggle, Heart Disease UCI, available at https://www.kaggle.com/ronitf/heart-disease-uci (accessed 25 March 2020)

[6] Wikipedia, "Keras", available at https://en.wikipedia.org/wiki/Keras (accessed 4 April 2020).

NEWS
OF THENATIONAL ACADEMY OF SCIENCES OF THE REPUBLIC OF KAZAKHSTAN
PHYSICO-MATHEMATICAL SERIES
ISSN 1991-346X **https://doi.org/10.32014/2020.2518-1726.63**
Volume 4, Number 332 (2020), 35 – 41

UDC 523.985
MRNTI 41.21.05; 41.21.19

A.T. Sarsembayeva[1], M. Odsuren[2], F.B. Belisarova[1], A.T. Sarsembay[3], M.E. Abyshev[1]

[1]Department of Physics and Technology, Al-Farabi Kazakh National University, Almaty, Kazakhstan;
[2]School of Engineering and Applied Sciences National University of Mongolia, Ulaanbaatar, Mongolia;
[3]School-Lyceum №250 named after T.Komekbayev, Karmakchi area, Kyzylorda region, Kazakhstan.
E-mail: sarsembaeva.a@kaznu.kz; odsuren@seas.num.edu.mn; farida.belisarova@kaznu.kz;
cronus87_87@mail.ru; medeu.abishev@kaznu.kz

SOLAR ACTIVITY MONITORING FOR THE PERIOD MARCH 20-25, 2019

Abstract. During a large solar flare, the flux of hard electromagnetic radiation from the sun increases many times. In the ultraviolet (UV), X-ray and gamma rays that are invisible to us, our Sun becomes “brighter than a thousand suns”. Radiation reaches the Earth’s orbit eight minutes after the solar flare. In a few tens of minutes, flow of charged particles arrive, accelerated to gigantic energies, and after two or three days - huge clouds of solar plasma. The huge interest in solar flares is not accidental. Large flares have a strong effect on near-Earth outer space. Particle and radiation flows are dangerous for astronauts. In addition, they can damage the electronic devices of spacecraft, disrupt their work. UV and X-rays from a flash suddenly increase ionization in the upper atmosphere of the Earth, in the ionosphere. This can lead to radio communications disruptions, malfunctions of the radio navigation devices of ships and aircraft, radar systems, and long power lines.

The source of flare energy is a magnetic field in the atmosphere of the Sun. It determines the morphology and energy of the active region where the flare will occur. Here, the field energy is much larger than the thermal and kinetic energy of the plasma. During a solar flare, the excess field energy is rapidly converted to particle energy and plasma changes. The physical process that provides this transformation is called magnetic reconnection.

In this paper was monitored solar flares registered in the period 20-25 March 2019. We measure physical parameters of 2 flares, such as the temporal scale, size, and magnetic flux density, and find that the sizes of flares tend to be distributed more broadly as the GOES class becomes weaker and that there is a lower limit of magnetic flux density that depends on the GOES class. We also made a brief analysis of solar flares registered in these days, also has shown the duration of time and peak of solar flares in Universal time.

We have identified several physical quantities of solar flares and estimated reconnection rate of solar flares. To determine the physical parameters we used images taken with the AIA instrument on board SDO satellite at wavelengths 131 Å, 174 Å, 193 Å, 211 Å, 335 Å, 1600 Å, 1700 Å, 4500 Å, SXT - pictures, HMI Magnetogram, SOLIS Chromospheric Magnetogram, GOES XRT-data. We estimate reconnection inflow velocity, coronal Alfven velocity, and reconnection rate using the observed values. The inflow velocities are distributed from a few km s^{-1} to several tens of km s^{-1}, and the Alfven velocities in the corona are in the range from 10^3 to 10^4 km s^{-1}. Hence, the reconnection rate is 10^{-3}. We find that the reconnection rate in a flare tends to decrease as the GOES class of the flare increases.

Keywords: solar flares, X-rays, reconnection rate.

Introduction. Solar flares can be classified according to their brightness in the x-ray wavelengths. There are three categories: X-class flares are big; they are major events that can trigger radio blackouts around the whole world and long-lasting radiation storms in the upper atmosphere. M-class flares are medium-sized; they generally cause brief radio blackouts that affect Earth's polar regions. Minor radiation storms sometimes follow an M-class flare. Compared to X- and M-class events, C-class flares are small with few noticeable consequences here on Earth [1-4].

Monitoring of solar flares in a real time is carried out by the Geostationary Operational Environmental Satellite or GOES [5]. Data on the electrons, protons, and X-rays were taken from satellites GOES 13, GOES 14 and GOES 15 [5-6].

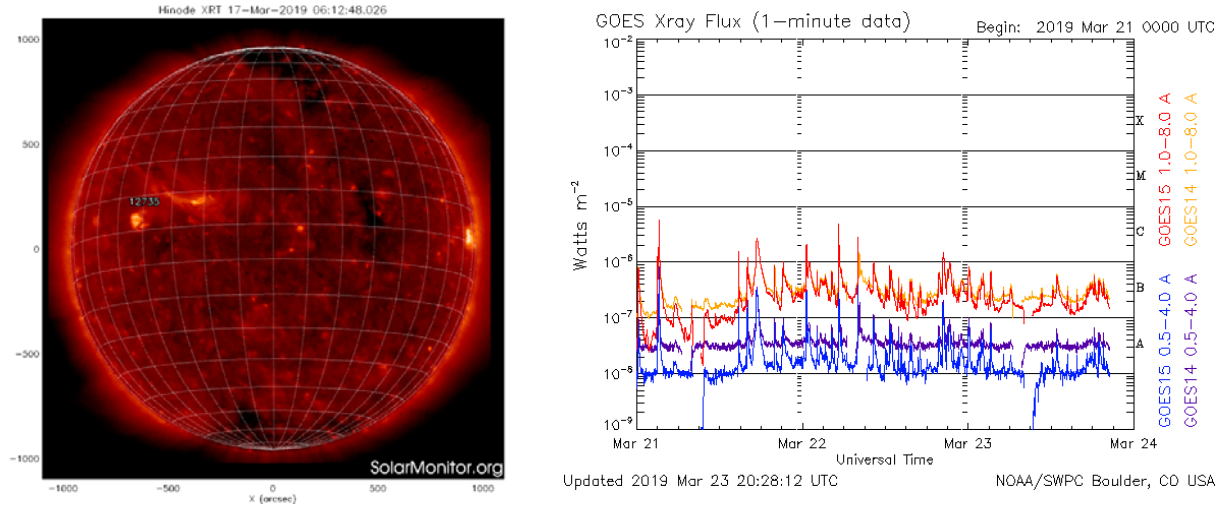

Figure 1 - Active area 12735 (XRT Hinode) and the total X-ray flux obtained in GOES 13 and GOES 15 [5]

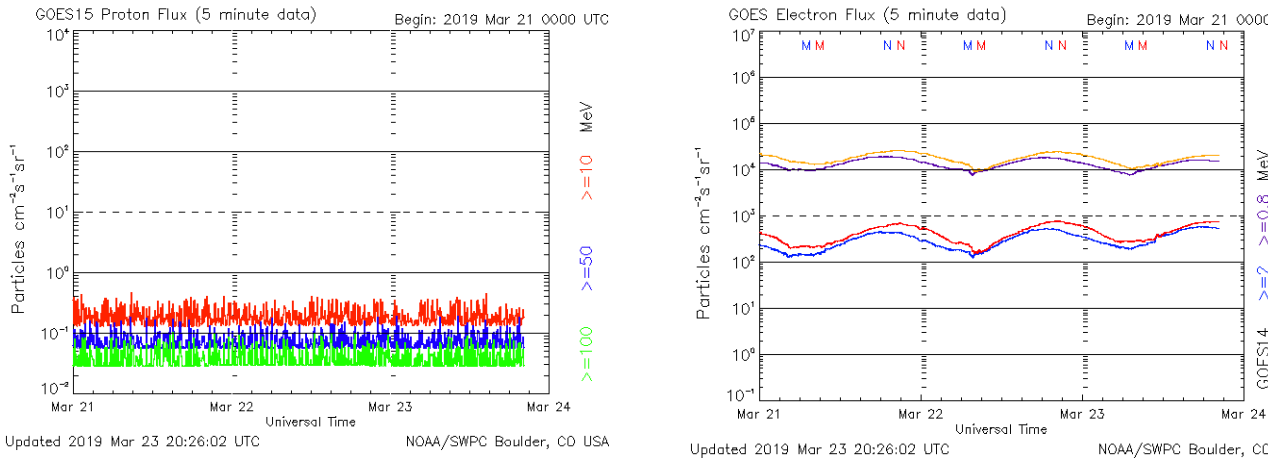

Figure 2 - Total proton and electron flux obtained in GOES 13 and GOES 15 [5]

On March 20, 2019, on the Sun, 1 class C and 8 class B flares were registered. In total, 2 classes are distinguished in the scale of solar flares: A, B, C, M and X, each subsequent of which exceeds the previous power by 10-100 times. The event, more accurately estimated as B1.1, occurred at night and observed for about 3 minutes with a maximum at 00:20 UT [6].

On March 21, at 00:04 UT recorded the first flare of class B8.0 with a duration of 9 minutes from the highs of 00:13 UT on the Sun. In total, 7 solar flares of class B and 5 solar flares of class C were registered.

On 22 March midnight, there was an eruption of class C2.1 at 00:27 UT and was observed for about 7 minutes with a maximum of 00:34 UT. In total, 17 flares of class B and 6 flares of class C were registered.

On March 23 around 01:16 on World time there was a fairly strong release of solar matter into space. The solar flare is estimated as B3.2 and its maximum was observed at 01:31 on world time. In total, 19 solar flares of class B were registered.

On March 24, 2019, around 02:28 GMT, another solar flare of class B8.6 was registered and was observed for about 5 minutes with a maximum at 02:33 UT. In total, 6 flares of class B were registered.

On March 25, at 06:07, the first M class flare B1.5 was registered. The event occurred in the active area of 12736 and was observed for about 8 minutes with a maximum at 06:15 UT. In total, 7 flares of class B were registered.

Table 1 - Solar flares registered in the period from 20 to 25 March 2019 [6]

Date	X-ray class	Start time (hhmm)	Maximim time (hhmm)	End time (hhmm)
1	2	3	4	5
20/03/19	B1.1	00:17	00:20	00:22
	B6.1	07:07	07:14	07:16
	C4.8	10:35	11:18	11:34
	B4.4	12:19	12:25	12:28
	B1.0	13:06	13:09	13:14
	B1.0	13:40	13:43	13:49
	B2.1	14:23	14:32	14:48
	B3.2	17:36	17:59	18:12
	B1.8	21:19	21:24	21:32
21/03/19	B8.0	00:04	00:13	00:19
	C1.2	02:52	03:00	03:04
	C5.6	03:08	03:12	03:15
	B1.6	07:56	07:59	08:01
	B1.4	09:45	10:12	10:22
	B1.1	11:17	11:21	11:31
	C1.5	14:40	14:44	14:47
	B2.2	15:42	15:45	15:47
	C1.2	15:58	16:01	16:03
	C2.6	17:13	17:21	17:39
	B8.8	19:54	19:59	20:02
	B9.9	20:54	21:13	21:19
22/03/19	C2.1	00:27	00:34	00:38
	B6.7	02:00	02:06	02:08
	B6.5	04:11	04:15	04:20
	C4.8	05:05	05:14	05:17
	C2.6	07:54	08:01	08:04
	C1.3	08:13	08:19	08:22
	C1.0	10:14	10:19	10:25
	B3.5	11:54	11:58	12:04
	B3.7	12:10	12:13	12:15
	B8.5	12:31	12:39	12:42
	B7.0	12:46	12:54	12:57
	B4.9	13:48	13:52	13:55
	B3.5	14:13	14:18	14:21
	B2.1	14:41	14:44	14:46
	B4.4	15:24	15:34	15:55
	B2.3	16:38	16:42	16:46
	B3.6	16:55	17:03	17:07
	B6.3	19:29	19:47	19:56
	C1.4	20:16	20:23	20:33
	B9.7	20:52	21:19	21:31
	B9.8	21:11	21:19	21:26
	B3.2	22:35	22:39	22:42
	B8.1	23:57	00:04	00:15
23/03/19	B3.2	01:16	01:31	01:43
	B5.0	01:50	01:53	02:01
	B6.1	02:07	02:12	02:14
	B2.5	02:57	03:02	03:05
	B6.6	03:10	03:17	03:23
	B3.0	05:06	05:09	05:11
	B3.4	06:02	06:10	06:16
	B2.7	10:33	10:40	10:44
	B3.1	12:10	12:16	12:22
	B5.7	12:41	12:49	13:01
	B3.0	14:18	14:22	14:24
	B5.7	18:14	18:17	18:20
	B4.5	18:49	18:53	18:55
	B4.5	18:57	19:00	19:15
	B2.1	20:48	20:51	20:54
	B8.9	21:09	21:20	21:27
	B5.3	22:04	22:11	22:19
	B8.0	22:36	22:39	22:41
	B9.9	23:30	23:59	00:17

Continuation of the table

1	2	3	4	5
24/03/19	B8.6	02:28	02:33	02:51
	B4.8	04:35	04:39	04:44
	B4.3	07:13	07:20	07:27
	B1.8	08:03	09:22	09:33
	B2.6	14:32	14:37	14:43
	B9.6	19:16	19:31	19:40
25/03/19	B1.5	06:07	06:15	06:27
	B2.2	06:52	07:23	07:27
	B1.3	09:42	09:47	09:53
	B1.7	11:29	11:34	11:44
	B3.6	13:08	14:10	14:35
	B4.1	18:03	18:11	18:25
	B3.4	21:26	21:48	22:23

Data analysis. In the energy release process in solar flares, magnetic reconnection is generally considered to play a key role. The reconnection rate is an important quantity, because it puts critical restrictions on the reconnection model. To evaluate the reconnection rate in nondimensional form, $M_A \equiv \frac{V_{in}}{V_A}$, we must estimate the Alfven velocity in the inflow region: $V_A = \frac{B_{cor}}{(4\pi\rho)^{1/2}}$. Hence, if we measure the coronal density ρ, the spatial scale of the flare L, the magnetic flux density in the corona B_{cor}, and the timescale of flares τ_{flare}, we can calculate inflow velocity V_{in}, Alfven velocity V_A, and reconnection rate M_A [7].

Monitoring of solar flares in real time is performed by the Geostationary Operational Surveillance Satellite GOES. Electron, proton and X-ray fluxes are tracked by the satellites GOES 11, GOES 13 and GOES 15.

In figure 1 shown the images obtained on the board of Hinode satellite in XRT. To determine the length of the loops, we used SXT images. From the SXT data, we get values for the length of the loops.

In figure 2 shows the total flux of X-rays and an electron, which was registered on March 21-24, 2019.

Results. Using the method described in [7-9], we analyzed solar flare that have been registered on March 21-22, 2019. Examined the dependence of the reconnection rate from GOES class of solar flares. The temperature were obtained in SunPY using the methods of White et al. [10-11] who used the CHIANTI atomic physics database to model the response of the ratio of the short (0.5-4 angstrom) to long (1-8 angstrom) channels of the XRSs onboard various GOES satellites [12-13]. Table 2 summarizes the parameters of the flares obtained in this work. Figure 3 shows the dependence of the reconnection rate from timescale.

Table 2 - Parameters of the flares

Parameter	2019 Mar 21 19:54 B8.8 Flare	2019 Mar 22 05:05 C4.8 Flare
$\tau\,(s)$	300	540
$L\,(10^9\ cm)$	7.25×10^9	6.525×10^9
$T\,(10^6\ K)$	10	16
$V_{in}(cm\ s^{-1})$	6.04×10^6	3.02×10^6
$V_A(cm\ s^{-1})$	6.76×10^8	8.56×10^8
M_A	8.93×10^{-3}	3.52×10^{-3}
$E_{flare}/\tau\ (ergs\ s^{-1})$	7.29×10^{29}	4.72×10^{29}
$\lvert dE_{mag}/dt \rvert\ (ergs\ s^{-1})$	4.86×10^{29}	3.14×10^{29}

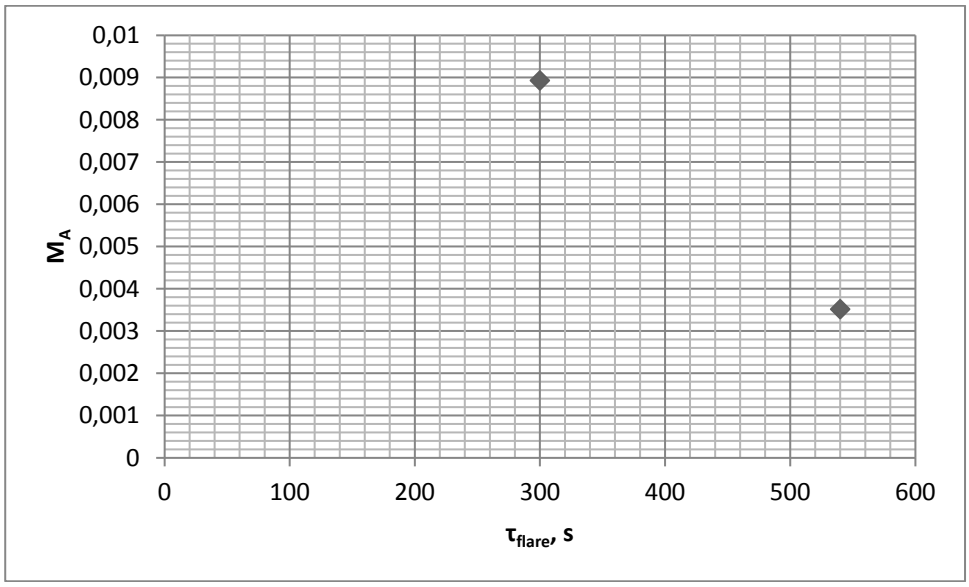

Figure 3 - Reconnection rate M_A plotted against timescale

Conclusion. During the period from 20 to 25 March 2019, 64 B class flares and 12 C class flares were registered. The solar flares are recorded by a network of space observatories: telescopes on the board of American SDO observatory, LASCO coronagraphs (European SOHO station), and by both STEREO satellites (USA), which are now at a giant distance of hundreds of millions of kilometers from our planet.

The values of reconnection rate is distributed in the range 10^{-3}. Here, the value of the reconnection rate decreases as the GOES class increases. The value of the reconnection rate obtained in this study is within 1 order of magnitude from the predicted maximum value of the Petschek model [14].

А.Т. Сарсембаева[1], М. Одсурен[2], Ф.Б. Белисарова[1], А.Т. Сарсембай[3], М.Е. Абишев[1]

[1]Физика-техникалық факультеті, Әл-Фараби атындағы ҚазҰУ, Казақстан;
[2]Инженерлік және қолданбалы ғылымдар институты, Моңғолия Ұлттық Университеті, Улан-Батор;
[3]Т. Көмекбаев атындағы №250 мектеп-лицейі, Қармақшы ауданы, Қызылорда облысы, Қазақстан

2019 ЖЫЛДЫҢ 20-25 НАУРЫЗ АРАЛЫҒЫНДАҒЫ КҮН ЖАРҚЫЛЫНЫҢ БАҚЫЛАУЫ

Аннотация. Күн жарқылы кезінде күн сәулесінен қатты электромагниттік сәулелену ағыны бірнеше есе артады. Бізге көрінбейтін ультракүлгін (УК), рентген және гамма-сәулелерде біздің Күн «мың күннен де артық жарқырайды». Радиация Жер орбитасына сегіз минут өткен соң жетеді. Бірнеше ондаған минут ішінде зарядталған бөлшектердің ағындары пайда болады, олар үлкен энергияға айналады, ал екі-үш күннен кейін - күн плазмасындағы үлкен бұлттар келіп жетеді. Күн жарқылына деген үлкен қызығушылық кездейсоқ емес. Үлкен Күн жарқылы Жердің жақын кеңістігіне қатты әсер етеді. Бөлшек және радиациялық ағындар ғарышкерлер үшін қауіпті. Сонымен қатар, олар ғарыш аппараттарының электрондық құрылғыларына нұқсан келтіріп, жұмысын істен шығаруы мүмкін. Күн жарқылынан ультракүлгін және рентген сәулелері кенеттен жердің жоғарғы атмосферасында, ионосферада иондануды күшейтеді. Бұл радио байланысының үзілуіне, кемелер мен әуе кемелерінің, радиолокациялық жүйелер мен электр желілерінің навигациялық құрылғыларының ақауларына әкелуі мүмкін.

Күн жарқылының энергиясының көзі - күн атмосферасындағы магнит өрісі. Ол Күн жарқылы болатын белсенді аймақтың морфологиясы мен энергиясын анықтайды. Мұнда өріс энергиясы плазманың жылу және кинетикалық энергиясынан әлдеқайда үлкен. Күн жарқылы кезінде артық өріс энергиясы бөлшектердің энергиясына тез айналады және плазманың өзгерісіне алып келеді. Бұл түрленуді қамтамасыз ететін физикалық процессті магниттік қайта ұштасу деп атайды.

Осы мақалада 2019 жылдың 20-25 наурыз аралығында тіркелген күн жарқылдарының бақылауы жүргізілді. Бұл мақалада екі күн жарқылының физикалық параметрлерін өлшедік, ол негізінен уақыт шкаласы, күн жарқылының өзіндік өлшемін және магнит ағынының тығыздығын, және GOES класы әлсірей

бастаған сайын күн жарқылының өзіндік өлшемдері кеңірек таралуға бейім болатындығын анықтадық, және бұл жерде GOES класына тәуелді магнит ағынының тығыздығының төменгі шегі болатыны анықталды. Біз сондай-ақ 20-25 наурыз аралығында тіркелген күн жарқылының қысқаша талдауын жүргіздік, сонымен қатар күн жарқылының уақыт шкаласының ұзақтылығы және Бүкіл әлемдік уақытта көрсетілген максимумы анықталды.

Біз күн жарқылдарының бірнеше физикалық мәндері мен қайта ұштасу жылдамдығын есептеп талқыладық. Физикалық параметрлерді анықтау үшін SDO спутникінің бортында AIA инструментінің 131 Å, 174 Å, 193 Å, 211 Å, 335 Å, 1600 Å, 1700 Å, 4500 Å толқын ұзындығында алынған және SXT суреті, HMI Magnetogram, SOLIS Chromospheric Magnetogram, GOES XRT- деректері пайдаланылды. Байқау нәтижесінде алынған мәндерді қолдана отырып, біз магниттік қайта ұштасудың түсу жылдамдығын, короналық Альфвен жылдамдығын және магниттік қайта ұштасуды есептедік. Ағынның түсу жылдамдығы бірнеше км $с^{-1}$-ден бірнеше ондаған км-ге $с^{-1}$-ге дейін таралған, ал коронадағы Альфвен жылдамдығы 10^3-тен 10^4 км $с^{-1}$ диапазон аралығын құрайды. Сонымен, магнитті қайта ұштасу жылдамдығы 10^{-3} мәнін құрайды. Күн жарқылындағы магнитті қайта ұштасу жылдамдығы төмендеген сайын GOES класы жоғарылайтыны анықталды.

Түйін **сөздер**: күн жарқылы, рентген сәулесі, қайта ұштасу жылдамдығы.

А.Т. Сарсембаева[1], М. Одсурен[2], Ф.Б. Белисарова, А.Т. Сарсембай, М.Е. Абишев

[1]Физико-технический факультет, КазНУ им.аль-Фараби, Казақстан;
[2]Школа инженерных и прикладных наук, Национальный университет Монголии, Улан-Батор;
[3]Школа-лицей №250 им. Т. Комекбаева, Кармакчинский район, Кызылординская область, Казахстан

МОНИТОРИНГ СОЛНЕЧНЫХ ВСПЫШЕК В ПЕРИОД 20-25 МАРТА 2019 ГОДА

Аннотация. Во время большой вспышки поток жесткого электромагнитного излучения Солнца возрастает во много раз. В невидимых для нас ультрафиолетовых (УФ), рентгеновских и гамма-лучах наше Солнце становится "ярче тысячи солнц". Излучение достигает орбиты Земли через восемь минут после начала вспышки. Через несколько десятков минут приходят потоки заряженных частиц, ускоренных до гигантских энергий, а через двое-трое суток - огромные облака солнечной плазмы. Огромный интерес к вспышкам на Солнце не случаен. Большие вспышки оказывают сильное воздействие на околоземное космическое пространство. Потоки частиц и излучения опасны для космонавтов. Кроме того, они могут повредить электронные приборы космических аппаратов, нарушить их работу. УФ- и рентгеновские лучи от вспышки внезапно увеличивают ионизацию в верхних слоях атмосферы Земли, в ионосфере. Это может приводить к нарушениям радиосвязи, сбоям в работе радионавигационных приборов кораблей и самолетов, радиолокационных систем, длинных линий электроснабжения.

Источник энергии вспышки - магнитное поле в атмосфере Солнца. Оно определяет морфологию и энергетику той активной области, где произойдет вспышка. Здесь энергия поля много больше, чем тепловая и кинетическая энергия плазмы. Во время вспышки происходит быстрое превращение избыточной энергии поля в энергию частиц и изменения плазмы. Физический процесс, обеспечивающий такое превращение, называется магнитным пересоединением.

В этой статье был проведен мониторинг солнечных вспышек зарегистрированных в период 20-25 марта 2019 года. Мы измерили физические параметры двух вспышек, в основном шкалу времени, характерный размер вспышек и плотность магнитного потока, и обнаружили, что характерные размеры вспышек имеют тенденцию распределяться более широко, поскольку класс GOES становится слабее и здесь существует нижний предел плотности магнитного потока, которая зависит от класса GOES. Мы также сделали краткий анализ солнечных вспышек зарегистрированные в эти дни, а также показана продолжительность времени вспышки и ее максимум по Всемирному времени.

Мы определили несколько физических величин вспышек и оценили скорость пересоединения солнечных вспышек. Для определения физических параметров мы использовали снимки, полученные с инструмента AIA на борту спутника SDO на длинах волн 131 Å, 174 Å, 193 Å, 211 Å, 335 Å, 1600 Å, 1700 Å, 4500 Å, SXT - снимки, HMI Magnetogram, SOLIS Chromospheric Magnetogram, GOES XRT-данные. Используя наблюдаемые значения, мы оценили скорость притока магнитного пересоединения, корональную альфвеновскую скорость и магнитное пересоединение. Скорости притока распределяются от нескольких км $с^{-1}$ до нескольких десятков км $с^{-1}$, а альфвеновские скорости в короне находятся в диапазоне от 10^3 до 10^4 км $с^{-1}$. Следовательно, магнитное пересоединение составляет 10^{-3}. Мы находим, что скорость магнитного пересоединения в вспышке имеет тенденцию уменьшаться с увеличением класса GOES.

Ключевые слова: солнечная вспышка, рентгеновское излучение, скорость пересоединения.

Information about authors:

Sarsembayeva Aiganym - PhD, Senior lecturer, Department of Theoretical and Nuclear Physics, Al-Farabi Kazakh National University, Email: sarsembaeva.a@kaznu.kz; https://orcid.org/0000-0002-3003-0038;

Odsuren Myagmarjav - Associate professor, School of Engineering and Applied Sciences and Nuclear Research Center, National University of Mongolia, Email: odsuren@seas.num.edu.mn; https://orcid.org/0000-0003-2756-4909;

Belisarova Farida - Associate professor, Department of Theoretical and Nuclear Physics, Al-Farabi Kazakh National University, Email: farida.belisarova@kaznu.kz; https://orcid.org/0000-0003-0531-3818;

Sarsembay Akmaral - B.Sc., High school teacher, School-Lyceum No250 named after T.Komekbayev, Email: cronus87_87@mail.ru; https://orcid.org/0000-0002-1066-8755;

Abyshev Medeu - Associate professor, Head of the Department of Theoretical and Nuclear Physics, Al-Farabi Kazakh National University, Email: medeu.abishev@kaznu.kz; http://orcid.org/0000-0003-3602-6934

REFERENCES

[1] Sweet P.A. Electromagnetic Phenomena in Cosmical Physics. Cambridge: Cambridge Univ. Press, 1958. P.123.

[2] Parker E.N. Sweet's mechanism for merging magnetic fields in conducting fluids // J. Geophys. Res. 1957. Vol.62. P.509-520.

[3] Parker E.N. The solar flare phenomenon and theory of reconnection and annihilation of magnetic fields // Astrophys. J. Supp. 1963. Vol.8. P.177-211.

[4] Garcia, H. A.: 2004, Space Weather 2, S06003.

[5] http://www.ngdc.noaa.gov/stp/satellite/goes/

[6] ftp://ftp.ngdc.noaa.gov/STP/space-weather/solar-data/solar-features/solar-flares/x-rays/goes/

[7] Isobe H., Takasaki H., Shibata K. Measurement of the Energy Release Rate and the Reconnection Rate in Solar Flares // ApJ. 2005. Vol. 632. P.1184.

[8] A.T. Sarsembayeva. Definition of reconnection rate of solar flares registered in 2011-2012 years. Adv. Studies Theor. Phys., Vol.6, 2012, no.28, 1405-1408.

[9] Sarsembayeva A.T., et al. 26 January, 2019 solar flares diagnostics based on the soft x-ray emission measures. NEWS of the National Academy of Sciences of the Republic of Kazakhstan. Series of Physical and Mathematical. №2, 2019. P.41-46. https://doi.org/10.32014/2019.2518-1726.10

[10] Feldman, U. and Widing, K. G.: 2003, Space Sci Rev. 107, 665.

[11] White, S. M., Thomas, R. J., & Schwartz, R. A. 2005, Sol. Phys., 227, 231.

[12] The Sunpy Community et al. 2015, Comput. Sci. Disc., 8, 014009.

[13] Sarsembayeva A.T., et al. May 5, 2015 solar flare data analysis in SUNPY. NEWS of the National Academy of Sciences of the Republic of Kazakhstan. Series of Physical and Mathematical. №2, 2019. P.37-41. https://doi.org/10.32014/2019.2518-1726.9

[14] Petschek H.E. Magnetic field annihilation // Physics of Solar Flares / ed. by W.N. Hess. NASA SP-50. Washington: DC, 1964. P.425-439.

NEWS
OF THENATIONAL ACADEMY OF SCIENCES OF THE REPUBLIC OF KAZAKHSTAN
PHYSICO-MATHEMATICAL SERIES
ISSN 1991-346X **https://doi.org/10.32014/2020.2518-1726.64**
Volume 4, Number 332 (2020), 42 – 51

UDK 004.89
MRNTI 28.23.37

O. Mamyrbayev[1], D. Oralbekova[2]

[1]Institute of Information and Computational Technologies, Kazakhstan, Almaty;
[2]Satbayev University, Kazakhstan, Almaty.
E-mail: dinaoral@mail.ru

MODERN TRENDS IN THE DEVELOPMENT OF SPEECH RECOGNITION SYSTEMS

Abstract. This article presents the main ideas, advantages and disadvantages of models based on hidden Markov models (HMMs) - a Gaussian mixture models (GMM), end-to-end models and indicates that the end-to-end model is a developing area in the field of speech recognition. A review of studies that conducted in this subject area shows that end-to-end speech recognition systems can achieve results comparable to the results of standard systems using hidden Markov models, but using a simpler configuration and faster operation of the recognition system both in training and in decoding. An analytical review of the varieties of end-to-end systems for automatic speech recognition is considered, namely, models based on the connection time classification (CTC), attention-based mechanism and conditional random fields (CRF), and theoretical comparisons are made. Ultimately, their respective advantages and disadvantages and the possible future development of these systems are indicated.

Key words: automatic speech recognition, hidden Markov models, end-to-end, neural networks, CTC.

1. Introduction

Automatic speech recognition (ASR) is now widely used in our daily life. ASR can help people with disabilities interact with society. ASR is used in such areas as the automated user interface, mobile device management, information services and access control interfaces [1].

The purpose of ASR is identify the sequence of acoustic input $X = \{x_1, \cdots, x_T\}$ of length T as a sequence of words $W= \{w_1, \cdots, w_N\}$ of length N. The task of ASR is to find the most probable sequence of words W from given X. This can be represented as follows [2]:

$$W = \underset{W \in \gamma^*}{\operatorname{argmax}} * p(W \mid X). \quad (1)$$

Therefore, the main work of ASR is to create a model that can accurately calculate the posterior distribution p(W|X).

In the task of recognizing continuous and long speech, a model based on the Hidden Markov Model (HMM) was one of the best-known method. Even today, the best speech performance still comes from the HMM-based model combined with deep learning methods (hybrid models). At the same time, deep learning methods also simulated the emergence of an alternative, which is an end-to-end (E2E) model. This model, compared with HMM, uses one model to match directly sound to words. It replaces the design process with a learning process and does not require special knowledge in this area. Therefore, it is easier to create and train the E2E model. According to these advantages, the E2E model is quickly attracted much attention as a powerful method in the field of continuous speech recognition.

This article provides a detailed overview of the E2E model, as well as a brief comparison between the HMM-based model and the E2E model, an analysis of the various paradigms of E2E models and a comparison of their advantages and disadvantages. First, consider the main methods of speech recognition.

2. The main methods of speech recognition

2.1 Speech Processing Methods

Currently, there are several basic approaches for ASR.

The standard process for automatic speech recognition consists of the following steps:

– Feature extraction from the input signal.
– Acoustic modeling.
– Language modeling.
– Decoding sequence.

The most important parts of a speech recognition system are feature extraction methods and recognition methods. Feature extraction is a process that extracts a small amount of data from a signal [4]. At the beginning, the original signal is converted into feature vectors, based on which classification will then be performed. This step includes the following steps:

– conversion of the signal into digital form;
– the use of various filters to suppress noise;
– highlighting the boundaries of speech;
– extraction of signal features [5].

The most popular extraction features methods are the Mel Frequency Cepstral Coefficients (MFCC) and the linear prediction cepstral coefficients (PLP). MFCC is an audio function extraction method that extracts the speaker's specific parameters from speech [6]. MFCCs are extracted from speech signals through cepstral analysis. The input signal is first formed and processed in the form of a window, then the Fourier transform is taken and the value of the resulting spectrum is deformed according to the Mel scale [7].

By using the obtained feature vectors, it is necessary to determine which sound or sequence of words was in the original signal. Widespread methods of automatic speech recognition (ASR) are hidden Markov models (HMM) and neural networks (NN) [5].

2.2 Standard Speech Recognition System. HMM-based model

For a long time, the HMM-based model was the main model for continuous speech recognition with a large dictionary with better recognition results. In general, an HMM-based model can be divided into three parts; each of them is independent of each other and plays a different role: acoustic, pronunciation and language model. The acoustic signal of speech is modeled by a small set of acoustic units, which can be considered as elementary sounds of the language. The traditionally chosen unit is a phoneme, so the word is formed by combining them [8]. The pronunciation model, which is usually created by professional human linguists, is used to achieve a correspondence between phonemes (or sub-phonemes) and graphemes. The language model maps a sequence of characters into free final transcription [9].

The HMM mechanism was used in all of these three parts. However, an HMM-based model emphasized the use of HMM in an acoustic model. In this HMM, sound was observation, and feature was a latent state. For an HMM that had a set of states {1, ⋯, J}, the HMM-based model used the Bayesian theorem and introduced the sequence of states HMM S = {$s_t \in$ {1, ⋯, J} | t = 1, ⋯, T} and expanded p(L | X).

$$
\begin{aligned}
\underset{L \in \gamma^*}{argmax}\, p(L|X) &= \underset{L \in \gamma^*}{argmax}\, \frac{p(L,X)}{P(X)} \\
&= \underset{L \in \gamma^*}{argmax}\, p(L,X) \\
&= \underset{L \in \gamma^*}{argmax} \sum_S p(P,L,X) \\
&= \underset{L \in \gamma^*}{argmax} \sum_S p(X|S,L)\, p(S,L) \\
&= \underset{L \in \gamma^*}{argmax} \sum_S p(X|S,L)\, p(S|L)\, p(L)
\end{aligned} \tag{2}
$$

According to the conditionally independent hypothesis, we can approximate p (X | S, L) ≈p (X | S), therefore

$$\underset{L \in \gamma^*}{argmax}\ p(L|X) \approx \underset{L \in \gamma^*}{argmax}\ \sum_S p(X|S)\ p(S|L)\ p(L) \quad (3)$$

p (X | S), p (S | L), and p (L) in equation (3) correspond to the acoustic model, pronunciation model, and language model, respectively.

– The acoustic model P (X | S) indicates the probability of observing X from a hidden sequence S. According to the rule of the chain of probabilities and the hypothesis of independence of observations in HMM (observations at any time depend only on the latent state at that time), P (X | S) can be laid out in the following form:

$$p(X|S) = \prod_{t=1}^{T} p(x_t|x_1, \ldots, x_{t-1}, S) \approx \prod_{t=1}^{T} p(x_t|s_t) \propto \prod_{t=1}^{T} \frac{p(s_t|x_t)}{p(s_t)} \quad (4)$$

In the acoustic model p (x_t | s_t) is the probability of observation, which is usually represented by the Gaussian Mixture Model (GMM). The distribution of the posterior probability of the latent state p (s_t | x_t) can be calculated using the method of deep neural networks (DNN). These two different calculations of P (X | S) lead to two different models, namely HMM-GMM and HMM-DNN. Over time, the HMM-GMM model has been a common framework for speech recognition. With the development of deep learning technology, DNN is being introduced into speech recognition for acoustic modeling. The role of DNN is to calculate the posterior probability of the state of the HMM, which can be converted into probability, replacing the usual probability of observing GMM [10]. Thus, the HMM-GMM model turns into an HMM-DNN, which achieves better results than the HMM-GMM, and becomes a modern ASR model.

In an HMM-based model, different modules use different technologies and play different roles. HMM is mainly used for dynamic time warping at the frame level. GMM and DNN are used to calculate the probability of emission of latent HMM states. The building process and the mode of operation of the model based on HMM determines whether they encounter the following difficulties in practical use [11]:

– The training process is complex and difficult for global optimization. An HMM-based model often uses different training methods and data sets to train different modules. Each module is independently optimized using its own target optimization functions, which usually differ from the true criteria for evaluating the performance of continuous speech recognition. Thus, the optimality of each module does not necessarily mean global optimality.

– Conditionally independent assumptions. To simplify model building and training, an HMM-based model uses assumptions about conditional independence within HMM and between different modules.

2.3 End-to-end ASR models

End-to-end (E2E) automatic speech recognition is a new paradigm in the field of speech recognition based on a neural network, which offers many advantages. Traditional “hybrid” ASR systems, which consist of an acoustic model, a language model, and a pronunciation model, require separate training for these components, each of which can be complex. For example, training an acoustic model is a multi-stage process of training a model and aligning the time between a sequence of acoustic characteristics of speech and a sequence of labels at the output. The E2E ASR, by contrast, is a single integrated approach with a much simpler learning pipeline with models that work with low audio frame rates. This reduces training time, decoding time and allows joint optimization with subsequent processing, such as understanding of a natural language.

However, modern E2E ASR systems also have some limitations:

Firstly, E2E ASR systems require more training data than ASR hybrid systems to achieve a similar word error rate (WER). This is because E2E ASR systems tend to exceed training data when they are limited.

Secondly, Connectionist Temporal Classification (CTC), a popular version of the E2E ASR, is not amenable to ‘student-teacher’ training, which is useful for deploying high-precision ASR systems with time-out limits [12].

The end-to-end model can be divided into three different categories depending on their smooth alignment implementations: CTC, attention-Based Models, the model, based on Conditional Random Fields (CRF).

2.3.1 End-to-end model based on Connectionist Temporal Classification

Although the HMM-DNN hybrid model still has the most up-to-date results, the role of DNN is limited. It is mainly used to model the probability of an a posteriori state of the latent state of HMM, presenting only local information. The temporary domain function is still modeled by HMM. By trying to simulate objects in the time domain using RNN or convolutional neural networks (CNN) instead of HMM, he encounters the problem of data alignment. The loss functions of both RNN and CNN (Convolutional Neural Networks) are determined at each point in the sequence, therefore, to provide training opportunities, need to know the alignment relationship between the output RNN sequence and the target sequence [13].

The CTC process can be thought of as including two subprocesses: calculating the probability of a path and aggregating a path. In these two subprocesses, the most important is the introduction of a new blank label ("-", which means no output) and an intermediate path to the concept.

By solving these two problems, CTC can use a single network structure to map the input sequence directly to the label sequence and implement end-to-end speech recognition.

For a given input sequence $X = \{ x_1, \cdots, x_T \}$ of length T, the encoder encodes it into a sequence of signs $F = \{ f_1, \cdots, f_T \}$ of length T for any t, f_t - this is a vector whose dimension is greater than the number of elements in the dictionary γ, i.e., $f_t \in R^{|\gamma|+1}$.

CTC acts on the sequence of signs $F = \{ f_1, \cdots, f_T\}$. Through the softmax operation, CTC transforms it into a probability distribution sequence $Y = \{ y_1, \cdots, y_T\}$, $yt = \{ y^1_t, \cdots, y_t^{|\gamma+1|}\}$, where y^i_t indicates the probability that the output signal at time step t is the label i, $y_t^{|\gamma+1|}$ indicates the probability of outputting an empty label at time step t.

Let $\gamma' = \gamma \cup \{b\}$, γ'^T denote the set of all sequences of length T defined in the dictionary γ′. In combination with the definition of y^k_t, we can conclude that for a given input sequence X, the conditional probability distribution of any sequence π in the set γ'^T is calculated as equation (5):

$$p(\pi|X) = \prod_{t=1}^{T} y_t^{\pi t}, \forall \pi \in \gamma'^T \quad (5)$$

where π_t represents the label at position t of the sequence π. An element in γ'^T is a path and is represented as π.

After the calculation process described above, the input sequence $\{x_1, \cdots, x_T\}$ is mapped onto a path π of the same length, and the conditional probability π can also be calculated in accordance with equation (5). In this mapping process, each input x_t frame is mapped to a specific label π_t. This might be thought that mapping an input sequence to a path is actually a tightly coordinated process.

From the process of calculating equation (5), we can see that there is a very important assumption, which is an assumption of independence: the elements in the output sequence are independent of each other. Any time step whose label is selected as the output does not affect the distribution of marks at other time steps. On the contrary, in the coding process, the value of y^k_t is influenced by the speech context information in both historical and future directions. That is, CTC uses conditional independence conditions in language models, but not in acoustic models. Therefore, the encoder obtained by training CTC is essentially and completely an acoustic model that is not capable of modeling the language.

Let $\gamma \leq T$ denote the set of all label sequences defined in the dictionary γ whose length is less than or equal to T, and path aggregation is defined as a function of the map O: $L'T \mapsto L \leq T$. It maps paths in γ'^T (that is, a path) to a real label sequence in $\gamma^{\leq T}$. Aggregation of O paths mainly consists of two operations:

1. The union of the same adjacent labels. If consecutive identical marks appear in the path, combine them and leave only one of them. For example, for two different paths "d-oo-t-" and "d-o-tt-", they are aggregated in accordance with the above principles to obtain the same result: "d-o-t-".

2. Removing the empty "-" mark in the path. Since the "-" label indicates no output, it should be deleted when the final label sequence is generated. The above sequence "d-o-t-" after aggregation in accordance with this principle becomes the final sequence "dot".

In addition to obtaining a sequence of labels corresponding to these paths, aggregation is also aimed at calculating the probability of a sequence of labels. We use O^{-1} (L) to represent the set of all paths in γ'^T corresponding to the sequence of labels L, then, obviously, given the input sequence X, the probability p (L | X) for L can be calculated as in equation (6):

$$p(L|X) = \sum_{\pi \in O^{-1}(L)} p(\pi|X) \quad (6)$$

Obviously, the calculation of the probability L is differentiable. Therefore, after obtaining the probability of the label for training the model, it can be used the back propagation method of the error.

However, there is still difficulty in calculating equation (6). Although p (π | X) is easy to calculate, it is difficult to determine which and how many paths from γ^T are included in O^{-1} (L). Consequently, this equation is not actually used to calculate p (L | X). Its operational method of calculation is the forward and reverse algorithm.

The advent of CTC technology greatly simplifies the design and training of continuous speech recognition models. No longer required experience to create various dictionaries; this eliminates the need for data alignment, allowing us to use any number of layers, any network structure to build an end-to-end model that maps sound directly to text [14].

One of the great benefits of CTC is that it eliminates the need to align data segmentation, so deep learning techniques such as CNN and RNN can play an increasingly important role. Network models with different structure and depth were introduced in the end-to-end ASR and achieved better results.

2.3.2 Attention-Based Model

An alternative approach to the end-to-end mapping between speech and tag sequences is to use an encoder-decoder architecture based on the attention mechanism [15]. This architecture has two separate subnets. One of them is the encoder subnet, which converts the sequence of acoustic features into a sequential representation of the length T. Based on this encoded information, the decoder subnet predicts a sequence of labels whose length L is usually less than the input length. The decoder uses only the relevant portion of coded sequential representations to predict the label at each time step using the attention mechanism.

The encoder is implemented as a multilayer bidirectional recurrent neural network (RNN), such as Long short-term memory (LSTM), and the decoder usually consists of a 1st level unidirectional RNN, followed by the output layer softmax. The structure of the attention-based model is shown in figure 1 [16].

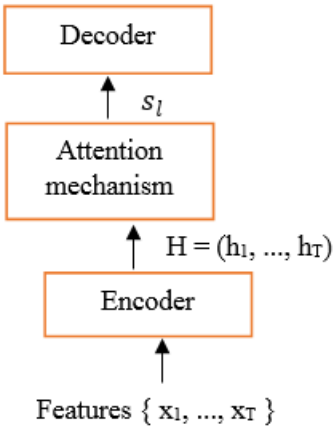

Figure 1 - Attention Mechanism Model

The attention-based model is formulated as follows. The encoder converts X into intermediate representation vectors H = (h_1, ..., h_T). At the next stage of decryption, activation of the latent state (memory) of the RNN-based decoder at the l-th time step is calculated as:

$$s_l = Recurrency(s_{l-1}, g_l, y_{l-1}) \quad (7)$$

where g_l and y_{l-1} denote a "glimpse" at the l-th time step and the predicted mark at the previous step. The glimpse g_l is a weighted sum of the encoder output sequence as

$$g_l = \sum_l \alpha_{l,t} h_t \quad (8)$$

where $\alpha_{l,t}$ – weight of attention h_t and calculated as

$$e_{l,t} = Score(s_{l-1}, h_t, \alpha_{l-1}) \quad (9)$$

$$\alpha_{l,t} = \frac{\exp(e_{l,t})}{\sum_{t'=1}^{T} \exp(e_{l,t})} \quad (10)$$

The encoder-decoder method that use the attention mechanism does not require preliminary data segmentation. With attention, it can implicitly learn the soft alignment of input and output sequences, which solves a big problem for speech recognition [17].

The encoder plays the role of an acoustic model, which is the same as in CTC models, RNN converters, and even hybrid HMM-DNN models. Thus, he faces the same problems as they, and their solutions are the same. However, when the encoder is combined with attention, new problems arise [18].

A serious problem caused by the combination of encoder and attention is delay. Since attention is paid to the entire sequence of coding results, it is necessary to wait until the encoding process is fully completed before it can start working, so the time spent on the encoding process will increase the model delay. In addition, an encoder that does not reduce the length of the sequence will have a sequence of encoding results that is much longer than the target label sequence (for the input speech sequence is much longer than for transcription) [19]. This leads to two problems: on the one hand, a longer sequence of encoding results means more attention, thereby increasing the delay; on the other hand, since speech is much more than transcription, the sequence generated by the encoding process without sub-sampling that will bring a lot of redundant information to the attention mechanism.

Similar to the development trend in models based on CTC and RNN converters, to improve the encoding capabilities, the encoder in attention-based models is also becoming more and more complex. The most obvious moment is reflected in its depth. The early encoder was mainly in three layers and gradually developed to six layers. As the network structure becomes more complex and its depth deepens, the model effect is constantly improving. In [20], a 15-layer network of encoders was built by using network on the network, packet normalization, residual network, convolutional LSTM, and ultimately achieved a WER of 10.53% without using a dictionary or language model.

2.3.3 Conditional Random Field Model

Conditional Random Fields (CRF) model allows to combine local information to predict the global probabilistic model for sequences. This model was first proposed in [21] for speech recognition.

In this method, X is a random variable for the data sequences that is labeled, and Y is a random variable for the corresponding label sequences. All Y_i components from Y are located in the alphabet of the final label Y. Random variables X and Y are distributed together, but in the discriminatory structure they must build a conditional model p (Y | X) from pair observations and sequences of labels. Let G = (V, E) be a graph, and $Y = (Y_v)_{v \in V}$, so that Y is indexed by the vertices of G. Then (X, Y) is a conditional random field in the case where the condition on X is random variables Y_v obey the Markov property with respect to the graph: p (Y_v | X, Y_w, w ≠v) = p (Y_v | X, Y_w, w ~ v), where w ~ v means that w and v are neighbors in G. The structure of the model on CRF-based is presented in figure 2.

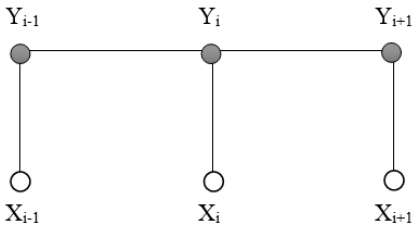

Figure 2 - Graphical representation of a CRF model

The most common application is the linear chain CRF model. This model is most often used to solve the problems of marking and segmentation of sequences [22].

A similar method for CRF is the MEMM algorithm (maximum-entropy Markov model), which is also a discriminative probabilistic model. The main difference between CRF and MEMM is the absence of a label bias problem (label bias is a situation where states with fewer transitions take precedence, since a single probability distribution and normalization are built) [23].

According to [24], [25] studies, after using CRF, better results were obtained than MEMM or HMM without using a language model.

3. Conclusion

The considered methods for constructing end-to-end models are superior the HMM-GMM model, but its performance is still worse or comparable to the HMM-DNN model, which also uses methods of deep learning. In order to take an advantage of the end-to-end model, there should be at least improved in the following aspects:

– CTC-based models are monotonous and support stream decoding, so they are suitable for low-latency online scenarios. However, their recognition efficiency is limited. The main disadvantage of the CRF-based model is the computational complexity of the training sample analysis, which makes it difficult to constantly update the model when new training data arrives. Models based on the attention mechanism can effectively improve recognition characteristics, but they are not monotonous and have a long delay. Although methods exist such as 'a window' to reduce attention delay, they can reduce recognition performance to some extent. Therefore, reducing latency while ensuring performance is an important research problem for the end-to-end model.

– The HMM-based model uses additional language models to provide a wealth of language training, while all linguistic training of the end-to-end model is obtained only from transcriptions of training data, the scope of which is very limited. This leads to great difficulties when working with scenes with great linguistic diversity. Therefore, the E2E model should improve the study of linguistic training while maintaining the integral structure. This article was prepared based on the project: IRN AP05131207 Development of technology for multilingual automatic speech recognition using deep neural networks.

О.Ж. Мамырбаев[1], Д.О. Оралбекова[2]

[1]Ақпараттық және есептеуіш технологиялар институты, Алматы, Қазақстан;
[2]Satbayev University, Алматы, Қазақстан

СӨЙЛЕУДІ ТАНУ ЖҮЙЕСІНІҢ ДАМУЫНДАҒЫ ҚАЗІРГІ ТЕНДЕНЦИЯЛАР

Аннотация. Бұл мақалада жасырын Марков модельдеріне (HMMs) негізделген модельдердің негізгі идеялары, артықшылықтары мен кемшіліктері - Gaussian үлестірімдері (GMM) және интегралдық жүйелер (end-to-end) гибриді ұсынылған, сонымен қатар интегралды модель сөйлеуді тану саласында дамып келе жатқан жаңа саланың бірі болып табылады.

Кіріккен сөйлеуді тану проблемасында жасырын Марков моделіне (HMM) негізделген модель әрдайым басты технология болып келді және кең қолданылды. Тіпті қазіргі уақытта сөйлеуді тану бойынша ең жақсы көрсеткіш HMM-ге негізделген (терең оқыту әдістерімен біріктірілген). Көптеген өнеркәсіптік орналастырулар HMM-ге негізделген.

Сонымен бірге терең оқыту әдістері интегралды модель болып табылатын баламаның пайда болуына түрткі болды. HMM негізіндегі модельмен салыстырғанда дыбысты таңбаларға немесе сөздерге тікелей сәйкестендіру үшін біріктірілген модель бір модельді қолданады. Ол өңдеу процесін оқыту үрдісімен алмастырады және осы салада арнайы оқытуды қажет етпейді, сондықтан интегралды модельді құру және оқыту оңайырақ. Осы артықшылықтардың арқасында интегралды модель тез арада сөйлеуді тану саласындағы танымал зерттеу аймағына айналып отыр.

Көптеген интегралды сөйлеуді тану модельдеріне келесі бөліктер кіреді: сөйлеу енгізу тізбегін мүмкіндіктер тізбегімен салыстыратын кодер; объектілер тізбегі мен тіл арасындағы теңестіруді жүзеге асыратын түзету; түпнұсқалық сәйкестендіру нәтижесін ашатын декодер. Тағы айта кететін жайт, бұл бөлу әрдайым бола бермейді, өйткені интегралдық құрылымның өзі толық құрылым болып табылады және инженерлік модульдік жүйеге ұқсастығы бойынша жұмысты қай бөлігі орындайтынын анықтау өте қиын.

Бірнеше модульден тұратын HMM моделінен айырмашылығы, интегралды модель акустикалық сигналдардың тікелей көрсетілуін іске асыратын терең желілер модулін алмастырады. Сонымен қатар, нәтиже шығарған кезде кейінгі өңдеуді қажет етпейді.

HMM негізделген модельмен салыстырғанда, жоғарыдағы айырмашылықтар интегралды модельге келесі сипаттамаларды береді:

– бірлескен жаттығулар үшін бірнеше модульдер бір желіге біріктірілген. Бірнеше модульді біріктірудің артықшылығы - әр түрлі аралық жағдайының (қалпының) айырмашылығы арасындағы көрсетілуін жүзеге асыру үшін көп модуль жасаудың қажеттігі жоқ. Бірлескен оқыту интегралды модельге жаһандық

оңтайландыру мақсаты ретінде қорытынды бағалау критерийлері үшін өте маңызды функцияны қолдануға мүмкіндік береді, осылайша тиімді нәтижелерге қол жеткізуге мүмкіндік береді.

– акустикалық сигнатурасы мәтіндік нәтижесінің тізбегіне тікелей сәйкестендіріледі және нақты транскрипцияға қол жеткізу немесе тану сипаттамаларын жақсарту үшін одан әрі өңдеуді қажет етпейді, ал HMM модельдерінде айтылым үшін ішкі оқыту бар.

Интегралды модельдің осы артықшылықтары сөйлеуді тану модельдерінің құрылысы мен жаттығуын айтарлықтай жеңілдетеді.

Интегралды модельді олардың жұмсақ теңестірілуіне байланысты үш санатқа бөлуге болады:

- CTC негізінде: CTC алдымен барлық ықтимал теңестірулерді тізімдейді, содан кейін осы қатты туралауларды біріктіріп жұмсақ теңестіруге қол жеткізеді. CTC шығыс белгілері қатаң туралауды тізімдеген кезде бір-бірінен тәуелсіз болады деп болжайды.

- назар аудару механизміне негізделген: бұл әдіс кіріс деректері мен шығыс белгілері арасындағы тегістеу ақпаратын тікелей есептеу үшін назар аудару механизмін қолданады.

- CRF шартты кездейсоқ өрістеріне негізделген модель ғаламдық ықтималды модельді тізбектей болжау үшін жергілікті ақпаратты біріктіруге мүмкіндік береді.

Осылайша, сөйлеуді автоматты түрде тануға арналған интегралды жүйелердің түрлеріне аналитикалық шолу және теориялық салыстырулар жасалды. Соңында, олардың тиісті артықшылықтары мен кемшіліктері және осы жүйелердің болашақта дамуы мүмкін перспективасы көрсетілген. HMM моделі мен интегралды модель туралы қысқаша салыстырамыз. Сайып келгенде, олардың тиісті артықшылықтары мен кемшіліктері және осы жүйелердің болашақта дамуы мүмкін екендігі көрсетілген.

Түйін сөздер: сөйлеуді автоматты түрде тану, жасырын Марков модельдері, end-to-end; нейрондық желілер, CTC.

О.Ж. Мамырбаев[1], Д.О. Оралбекова[2]

[1]Институт информационных и вычислительных технологий, Казахстан, Алматы;
[2]Satbayev University, Казахстан, Алматы

СОВРЕМЕННЫЕ ТЕНДЕНЦИИ РАЗВИТИЯ СИСТЕМ РАСПОЗНАВАНИЯ РЕЧИ

Аннотация. В данной статье представлены основные идеи, преимущества и недостатки моделей, на основе скрытых марковских моделей (HMM) - смеси гауссовских распределений (GMM) и интегральных систем (end-to-end), а также указано, что интегральная модель является развивающим направлением в области распознавания речи.

В задаче распознавания слитной речи широко использовалась модель на основе скрытой модели Маркова (HMM) и всегда была одной из основных технологий в этой области. Даже сегодня лучшая производительность распознавания речи по-прежнему исходит от модели на основе HMM (в сочетании с методами глубокого обучения). Большинство промышленно развернутых систем основаны на HMM.

В то же время, методы глубокого обучения также стимулировали появление альтернативы, которая является интегральной моделью. По сравнению с моделью, основанной на HMM, в интегральной модели используется одна модель для непосредственного сопоставления звука с символами или словами. Он заменяет процесс проектирования процессом обучения и не требует специальных знаний в этой области, поэтому интегральную модель проще создавать и обучать. Благодаря этим преимуществам интегральная модель быстро становится популярным направлением исследований в области распознавания речи.

Большинство интегральных моделей распознавания речи включают в себя следующие части: кодер, который отображает последовательность ввода речи в последовательность признаков; выравниватель, который реализует выравнивание между последовательностью объектов и языком; декодер, который декодирует окончательный результат идентификации. Необходимо отметить, что это разделение не всегда существует, потому что интегральная структура сама по себе является законченной структурой, и обычно очень трудно определить, какая часть выполняет какую подзадачу по аналогии с инженерной модульной системой.

В отличие от модели на основе HMM, которая состоит из нескольких модулей, интегральная модель заменяет несколько модулей глубокой сетью, реализуя прямое отображение акустических сигналов в последовательности меток без тщательно продуманных промежуточных состояний. Кроме того, нет необходимости выполнять последующую обработку на выходе.

По сравнению с моделью на основе HMM вышеуказанные различия дают интегральной модели следующие преимущества:

– несколько модулей объединены в одну сеть для совместного обучения. Преимущество объединения нескольких модулей состоит в том, что нет необходимости разрабатывать много модулей для реализации

отображения между различными промежуточными состояниями. Совместное обучение позволяет интегральной модели использовать функцию, которая очень важна для окончательных критериев оценки, в качестве цели глобальной оптимизации, тем самым добиваясь глобально оптимальных результатов.

– он напрямую отображает входную последовательность акустической сигнатуры в последовательность текстового результата и не требует дальнейшей обработки для достижения истинной транскрипции или для улучшения характеристик распознавания, тогда как в моделях на основе HMM обычно есть внутреннее представление для произношения.

Эти преимущества интегральной модели позволяют значительно упростить построение и обучение моделей распознавания речи.

Интегральная модель может быть разделена на три различные категории в зависимости от их реализаций гладкого выравнивания:

– на основе CTC: CTC сначала перечисляет все возможные грубые выравнивания, затем он достигает гладкого выравнивания путем объединения этих грубых выравниваний. CTC предполагает, что выходные метки не зависят друг от друга при перечислении таких выравниваний.

– основанная на механизме внимания: этот метод использует механизм внимания, чтобы непосредственно вычислить информацию гладкого выравнивания между входными данными и выходной меткой.

– модель, на основе условных случайных полей (Conditional Random Fields, CRF), позволяет комбинировать локальную информацию для прогнозирования глобальной вероятностной модели по последовательностям.

Таким образом, в статье приведен аналитический обзор разновидностей интегральных систем автоматического распознавания речи, и делаются теоретические сравнения. Кратко сравниваются модели на основе HMM и интегральная модель, тщательно анализируются различные парадигмы интегральных технологий и сравниваются их преимущества и недостатки. В конечном итоге указываются возможное будущее развитие этих систем.

Ключевые слова: автоматическое распознавание речи, скрытые марковские модели, end-to-end; нейронные сети, CTC.

Information about authors:

Mamyrbayev Orken, ass. Professor, PhD-doctor of information systems, Institute of Information and Computational Technologies, morkenj@mail.ru, https://orcid.org/0000-0001-8318-3794;

Oralbekova Dina Orymbayevna, PhD-student, Satbayev University, dinaoral@mail.ru, https://orcid.org/0000-0003-4975-6493

REFERENCES

[1] Kazachkin A. E. **(2019)** Speech recognition methods, modern speech technology [Metody raspoznavanija rechi, sovremennye rechevye tehnologii] // Young scientist. №39. pages 6-8. URL https://moluch.ru/archive/277/62675/ (accessed: 28.01.2020)]. (In Russian).

[2] Ronzhin A.L., Karpov A.A., Li I.V. **(2006)** Voice and multimodal interfaces [Rechevoj i mnogomodal'nyj interfejsy] // M.: Science. Page 173] (In Russian).

[3] Gusev M.N. **(2013)** Speech Recognition System: basic models and algorithms **[**Sistema raspoznavanija rechi: osnovnye modeli i algoritmy] / M.N. Gusev, V.M. Degtjarev. SPb.: Sign, page 128 c.] (In Russian).

[4] Ibrahim M. El-Henawy, Walid I. Khedr, Osama M. ELkomy, Al-Zahraa M.I. AbdallaЮ **(2014)** Recognition of phonetic Arabic figures via wavelet based Mel Frequency Cepstrum using HMMs, HBRC Journal, Volume 10, Issue 1, 2014, Pages 49-54, ISSN 1687-4048. DOI:10.1016/j.hbrcj.2013.09.003 (in Eng).

[5] Vorob'eva S. A. **(2016)** Speech Recognition Methods [Metody raspoznavanija rechi] // Young scientist. №26. pages 136-141. URL https://moluch.ru/archive/130/36213/ (accessed: 28.01.2020). (In Russian).

[6] Sirko Molau, Michael Pitz, Ralf Schluter and Hermann Ney. **(2001)** "Computing Mel frequency Cepstral Coefficients on the power spectrum." IEEE Transactions on Audio, Speech and Language Processing. DOI: 10.1109/ICASSP.2001.940770 (in Eng).

[7] Bezoui Mouaz, Beni Hssane Abderrahim, Elmoutaouakkil Abdelmajid. **(2019)** Speech Recognition of Moroccan Dialect Using Hidden Markov Models, Procedia Computer Science, Volume 151, Pages 985-991, ISSN 1877-0509. DOI:10.11591/ijai.v8.i1.pp7-13 (in Eng).

[8] Rabiner L-R., Juang B-H. **(1993)** Fundamentals of Speech Recognition, Prentice-Hall. Englewood Cliffs, N.J.: PTR Prentice Hall, 1993. (in Eng).

[9] Rao, K.; Sak, H.; Prabhavalkar, R. **(2017)** Exploring architectures, data and units for streaming end-to-end speech recognition with RNN-transducer. In Proceedings of the 2017 IEEE Automatic Speech Recognition and Understanding Workshop (ASRU), Okinawa, Japan; pp. 193–199.]. (in Eng).

[10] Lu, L.; Zhang, X.; Cho, K.; Renals, S. **(2015)** A study of the recurrent neural network encoder-decoder for large vocabulary speech recognition. In Proceedings of the Sixteenth Annual Conference of the International Speech Communication Association, Dresden, Germany; pp. 3249–3253. (in Eng).

[11] Rahhal Errattahi, Asmaa El Hannani, Hassan Ouahmane. **(2018)** Automatic Speech Recognition Errors Detection and Correction: A Review, Procedia Computer Science, Volume 128, Pages 32-37, ISSN 1877-0509, DOI: 10.1016/j.procs.2018.03.005 (in Eng).

[12] Mamyrbayev O., Alimhan K., Zhumazhanov B., Turdalykyzy T., Gusmanova F. **(2020)** End-to-End Speech Recognition in Agglutinative Languages. In: Nguyen N., Jearanaitanakij K., Selamat A., Trawiński B., Chittayasothorn S. (eds) Intelligent Information and Database Systems. ACIIDS 2020. Lecture Notes in Computer Science, vol 12034. Springer, Cham. DOI: 10.1007/978-3-030-42058-1_33 (in Eng).

[13] O Mamyrbayev, A Toleu, G Tolegen, N Mekebayev. **(2020)** Neural architectures for gender detection and speaker identification. Cogent Engineering 7 (1), 1727168. (in Eng).

[14] O Mamyrbayev, N Mekebayev, M Turdalyuly, N Oshanova, TI Medeni. **(2019)** Voice Identification Using Classification Algorithms. Intelligent System and Computing. DOI: 10.5772/intechopen.88239 (in Eng).

[15] Ueno, Sei & Inaguma, Hirofumi & Mimura, Masato & Kawahara, Tatsuya. **(2018)** Acoustic-to-Word Attention-Based Model Complemented with Character-Level CTC-Based Model. 5804-5808. 10.1109/ICASSP.2018.8462576.]. DOI: 10.1109/ICASSP.2018.8462576 (in Eng).

[16] Prabhavalkar, R.; Rao, K.; Sainath, T.N.; Li, B.; Johnson, L.; Jaitly, N. **(2017)** A comparison of sequence-to-sequence models for speech recognition. In Proceedings of the Interspeech, Stockholm, Sweden; pp. 939–943. (in Eng).

[17] M.N. Kalimoldayev, O.Z. Mamyrbayev, A.S. Kydyrbekova, N.O. Mekebayev. **(2019)** Voice verification and identification using i-vector representation. International Journal of Mathematics and Physics 10 (1), 66-74. DOI: 10.26577/ijmph-2019-i1-9 (in Eng).

[18] Wang, Dong & Wang, Xiaodong & Lv, Shaohe. **(2019)** An Overview of End-to-End Automatic Speech Recognition. Symmetry. 11. 1018. 10.3390/sym11081018. DOI:10.3390/sym11081018 (in Eng).

[19] O.Zh.Mamyrbayev, M.Turdalyuly, N.O.Mekebaev, A.S.Kydyrbekova. **(2019)** "Automatic Recognition of the Speech Using Digital Neural Networks", ACIIDS, Indonesia, Proceedings , Part II. (in Eng).

[20] Bahdanau, D.; Chorowski, J.; Serdyuk, D.; Brakel, P.; Bengio, Y. **(2016)** End-to-end attention-based large vocabulary speech recognition. In Proceedings of the 2016 IEEE International Conference on Acoustics, Speech and Signal Processing (ICASSP), Shanghai, China; pp. 4945–4949.] DOI: 10.1109/ICASSP.2016.7472618 (in Eng).

[21] J. Lafferty, A. McCallum, and F. Pereira. **(2001)** "Conditional random fields: Probabilistic models for segmenting and labeling sequence data" in Proceedings of the International Conference on Machine Learning (ICML'01), Williamstown, MA, USA, pp. 282–289. (in Eng).

[22] E. Fosler-Lussier, Y. He, P. Jyothi, and R. Prabhavalkar. **(2013)** "Conditional random fields in speech, audio, and language processing" Proceedings of the IEEE, vol. 101, no. 5, pp. 1054–1075. DOI: 10.1109/JPROC.2013.2248112 (in Eng).

[23] N. M. Markovnikov, I. S. Kipjatkova. **(2018)** Analytical review of end-to-end speech recognition systems [Analiticheskij obzor integral'nyh sistem raspoznavanija rechi], SPIIRAN, 58, pages 77–110 (In Russian).

[24] Hifny Y., Renals S. **(2009)** Speech recognition using augmented conditional random fields // IEEE Transactions on Audio, Speech, and Language Processing, vol. 17. no. 2, pp. 354–365. (in Eng).

[25] H. Tang et al.**(2017)** "End-to-End Neural Segmental Models for Speech Recognition," in IEEE Journal of Selected Topics in Signal Processing, vol. 11, no. 8, pp. 1254-1264. DOI: 10.1109/JSTSP.2017.2752462 (in Eng).

NEWS
OF THENATIONAL ACADEMY OF SCIENCES OF THE REPUBLIC OF KAZAKHSTAN
PHYSICO-MATHEMATICAL SERIES
ISSN 1991-346X **https://doi.org/10.32014/2020.2518-1726.65**
Volume 4, Number 332 (2020), 52 – 60

UDC 004.032.26
IRSTI 28.23.37

Marat Nurtas [1], Zh. Baishemirov[2,3], V. Tsay[1], M. Tastanov[1], Zh. Zhanabekov[1]

[1]International Information Technologies University, Almaty, Kazakhstan;
[2]Abai Kazakh National Pedagogical University, Almaty, Kazakhstan;
[3]RSE Institute of Information and Computational Technology CS MES RK, Almaty, Kazakhstan.
E-mail: maratnurtas@gmail.com; zbai.kz@gmail.com;
tsay.victor96@gmail.com; tychty4@gmail.com; zzhanabekov@gmail.com

CONVOLUTIONAL NEURAL NETWORKS AS A METHOD TO SOLVE ESTIMATION PROBLEM OF ACOUSTIC WAVE PROPAGATION IN POROELASTIC MEDIA

Abstract. This article concerns the problem of the acoustic wave propagation in the 3 layered half-space. The first and third layers are assumed to be solid, whereas the second is assumed to be poroelastic. This article considers results of finding acoustic wave propagation with regard to its depth and time (further called solution to the forward problem) [1-4] and tries to estimate the initial physical properties of aforementioned three layers. The aim of this article is to create a convolutional neural network that estimates said properties, namely speed of sound in each layer and porosity of the second layer. Model was built using "PyTorch", open-source machine learning library. In order to evaluate the initial coefficients of acoustic wave propagation the convolutional neural networks were used. During the procedure, 3 convolutional hidden layers and 2 fully connected linear hidden layers were used. The data for data characterization was simulated by iteratively solving forward problem of acoustic wave propagation described by Stokes equation and continuity equation with given initial values of the acoustic model.

Key worlds: Neural network, Convolutional neural network, acoustic wave propagation, predicting models, supervised learning, activation function, PyTorch.

Introduction. Researching acoustic wave propagation, is one of overlying problems of geological exploration [6]. The prominent problems in the aforementioned area is the problem of acoustic wave propagation in poroelastic medium, the problem related to the discovery of oil and water reserves underground. In practice however the solution of the problem requires extensive reliance on regularization of data, and thorough and expensive measurements that sometimes are hard to provide due to various circumstances.

The relevance of the utilization of deep learning algorithms is defined by the fact that deep learning algorithms provide solution that is more robust and do not require extensive data regularization.

The aim of this article is to explore possibilities of building a neural network capable of estimating solutions to problem of acoustic wave propagation in poroelastic medium.

Specification of the problem. Consider 3 layered half-space that consists of: $\Omega_2 = \{x \in R : 0 < x < H_1\}$ which is a first layer, $\Omega_1 = \{x \in R : H_1 < x < H_2\}$ and $\Omega_2 = \{x \in R : x > H_2\}$, and let 0-point be a surface of the first layer.

Let L (within dataset it is denoted as H) be the depth of the portion of half-space under consideration, while r denotes the time frame of the experiment, their respective values during experiment is going to be equal to 1000 meters and timeframe of the experiment in question is going to be equal to 1.5 seconds. The acoustic wave is sent at the surface at x = 0, y=0.

The mathematical model is at the edges of the layers of the half-space could be described via Stokes equation and continuity equation as follows in terms of acoustic pressure p on the whole layer Ω, as described by [1]:

$$\left(\frac{m}{\tilde{c}_f^2}+\frac{(1-m)}{\tilde{c}_s^2}\right)\frac{\partial p}{\partial t}+divv=0 \tag{1}$$

$$\left(m\tilde{\rho}_f+(1-m)\tilde{\rho}_s\right)\frac{\partial v}{\partial t}=-\nabla\left(p+\frac{mv_0}{\tilde{c}_f^2}\frac{\partial p}{\partial t}\right)$$

Where m represents porosity of the second layer, p shows the acoustic pressure,

$$c^2=\frac{1}{\frac{m}{\tilde{c}_f^2}+\frac{(1-m)}{\tilde{c}_s^2}}$$

is an average speed of wave propagation in the considered area of half-space.

That could be brought to the form:

$$\rho\frac{\partial^2 p}{\partial t^2}=div\left(c^2\nabla\left(p+\frac{mv_0}{\tilde{c}_f^2}\frac{\partial p}{\partial t}\right)\right) \tag{2}$$

With initial conditions:

$$p(x,0)=0,\quad x\in\Omega \tag{3}$$

$$\frac{\partial p}{\partial t}(x,0)=0,\quad x\in\Omega$$

and boundary condition:

$$p(0,t)=p_0(t),t>0 \tag{4}$$

to solve the above problem, we don't need a second boundary condition, so we don't need to set a second boundary condition.

At this point it is possible to apply Fourier Transformation so that our mathematical model stable, thus making the equation dependent on ω (angular frequency) and the depth of underground length:

$$\frac{d^2P}{dx^2}+\frac{\rho\omega^2}{c^2(1-i\omega\frac{mv_0}{\tilde{c}_f^2})}P=0 \tag{5}$$

Applying continuity conditions and continuous differentiability conditions on the equation (5) near layer boundaries yields a system of linear algebraic equations (6-9) [5]:

$$[P_1-i\omega\frac{mv_0}{\tilde{c}_f^2}P_1]_{H_1-0}=[P_2-i\omega\frac{mv_0}{\tilde{c}_f^2}P_2]_{H_1+0} \tag{6}$$

$$\left[c^2\frac{d}{dx}\left(P_1-i\omega\frac{mv_0}{\tilde{c}_f^2}P_1\right)\right]_{H_1-0}=\left[c^2\frac{d}{dx}\left(P_2-i\omega\frac{mv_0}{\tilde{c}_f^2}P_2\right)\right]_{H_1+0} \tag{7}$$

$$\left[P_2-i\omega\frac{mv_0}{\tilde{c}_f^2}P_2\right]_{H_2-0}=\left[P_3-i\omega\frac{mv_0}{\tilde{c}_f^2}P_3\right]_{H_2+0} \tag{8}$$

$$\left[c^2\frac{d}{dx}\left(P_2-i\omega\frac{mv_0}{\tilde{c}_f^2}P_2\right)\right]_{H_2-0}=\left[c^2\frac{d}{dx}\left(P_3-i\omega\frac{mv_0}{\tilde{c}_f^2}P_3\right)\right]_{H_2+0} \tag{9}$$

Which in turn could be solved [5]:

$$e^{\frac{i\omega\sqrt{\rho}}{c_1}H_1} + A_2 e^{-\frac{i\omega\sqrt{\rho}}{c_1}H_1} = \left(B_1 e^{\frac{i\omega\sqrt{\rho}}{c_2\sqrt{1-\frac{mv_0}{c_f^2}i\omega}}H_1} + B_2 e^{\frac{i\omega\sqrt{\rho}}{c_2\sqrt{1-\frac{mv_0}{c_f^2}i\omega}}H_1} \right)\left(1 - i\omega\frac{mv_0}{\tilde{c}_f^2}\right) \quad (10)$$

$$c_1^2\left(\frac{i\omega\sqrt{\rho}}{c_1}e^{\frac{i\omega\sqrt{\rho}}{c_1}H_1} - A_2\frac{i\omega\sqrt{\rho}}{c_1}e^{\frac{i\omega\sqrt{\rho}}{c_1}H_1}\right) = c_2^2\left(B_1\frac{i\omega\sqrt{\rho}}{c_2\sqrt{1-\frac{mv_0}{c_f^2}i\omega}}e^{\frac{i\omega\sqrt{\rho}}{c_2\sqrt{1-\frac{mv_0}{\tau_f^2}i\omega}}H_1} - B_2\frac{i\omega\sqrt{\rho}}{c_2\sqrt{1-\frac{mv_0}{c_f^2}i\omega}}e^{-\frac{i\omega\sqrt{\rho}}{c_2\sqrt{1-\frac{mv_0}{\tau_f^2}i\omega}}H_1}\right)_1 \quad (11)$$

$$\left(B_1 e^{\frac{i\omega\sqrt{\rho}}{c_2\sqrt{1-\frac{mv_0}{c_f^2}i\omega}}H_1} + B_2 e^{\frac{i\omega\sqrt{\rho}}{c_2\sqrt{1-\frac{mv_0}{c_f^2}i\omega}}H_1}\right)\left(1 - i\omega\frac{mv_0}{\tilde{c}_f^2}\right) = D_1 e^{\frac{i\omega\sqrt{\rho}}{c_3}H_2} \quad (12)$$

$$c_2^2\left(B_1\frac{i\omega\sqrt{\rho}}{c_2\sqrt{1-\frac{mv_0}{c_f^2}i\omega}}e^{\frac{i\omega\sqrt{\rho}}{c_2\sqrt{1-\frac{mv_0}{\tau_f^2}i\omega}}H_1} - B_2\frac{i\omega\sqrt{\rho}}{c_2\sqrt{1-\frac{mv_0}{c_f^2}i\omega}}e^{-\frac{i\omega\sqrt{\rho}}{c_2\sqrt{1-\frac{mv_0}{\tau_f^2}i\omega}}H_1}\right)\left(1 - i\omega\frac{mv_0}{\tilde{c}_f^2}\right) = c_3^2\left(D_1\frac{i\omega\sqrt{\rho}}{c_3}e^{\frac{i\omega\sqrt{\rho}}{c_3}H_2}\right) \quad (13)$$

Iteratively solving (10)-(13) will find the values of acoustic wave pressure dependent on angular velocity (ω) and depth of the half-space (x). By applying inverse Fourier transformation [7] on those values we obtain the values of acoustic wave propagation (acoustic pressure) dependent on time (t) and depth of the half-space (x). These values were calculated using MatLAB and stored in the form of text file with comma separated complex numbers [2].

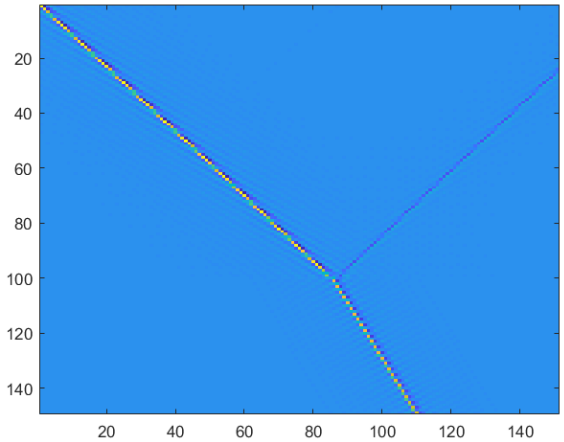

Figure 1 – Values of acoustic pressure at given time (horizontal axis) and depth (vertical axis).
1 pixel in time ≈ 0.01 seconds, while 1 pixel in depth ≈ 20 meters

Neural Network architecture. Convolutional neural network (CNN) is a method of modeling data analysis with statistical tools, loosely based around the idea of how neurons and synapses work. The structure of neural networks consists of 3 layers [8]:

a) Input layer;
b) Hidden layer;
c) Output layer.

On their turn each layer consists of neurons that work as a simple function, taking data, via connections referred to as synapses from neurons in the previous layer, making calculations to it and then passing the results to the neurons in the next layer.

The input layer works as a primary data input part of our model. It accepts data, sometimes referred as a training data that forms conditions of the problem. Once the data is inputted the neurons in input layer start sending signals to the first hidden layer.

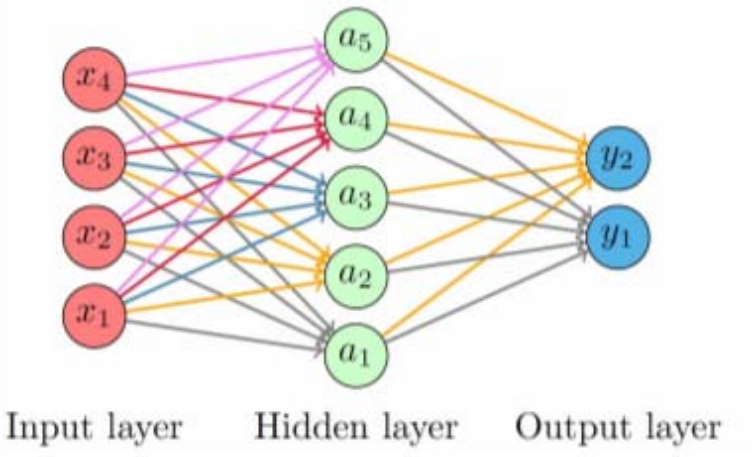

Figure 2 – the general model of machine learning algorithm [3, 15]

The hidden layer is where most calculations happen in the following way [3, 8, 15]:

$$A = \sigma(w^{(1)} \cdot X + b^{(1)}), Y = \sigma(w^{(2)} \cdot A + b^{(2)}) \tag{14}$$

$$\Theta_\theta(X) = \sigma(w^{(2)}(\sigma(w^{(1)} \cdot X + b^{(1)})) + b^{(2)}) \tag{15}$$

$$f(\theta) = f(\theta; \{X_\ell\}, \{Y_\ell\}) = \frac{1}{N_{nn}} \sum_{\ell=1}^{N_{nn}} (\Theta_\theta(X_\ell) - Y_\ell)^2 \tag{16}$$

where $X = (x_1, \dots, x_4)^T$, $Y = (y_1, y_2)^T$, $A = (a_1, \dots, a_5)^T$, w and b representing weights and biases of our model.

The activation function is a way to model the cell firing procedure and to standardize data sent from one layer to the other.

Convolutional neural network works on the idea of convolutions. The data given to us with in the form the matrix get convolved and pooled from one layer to another, with the idea of finding patterns in each receptive field.

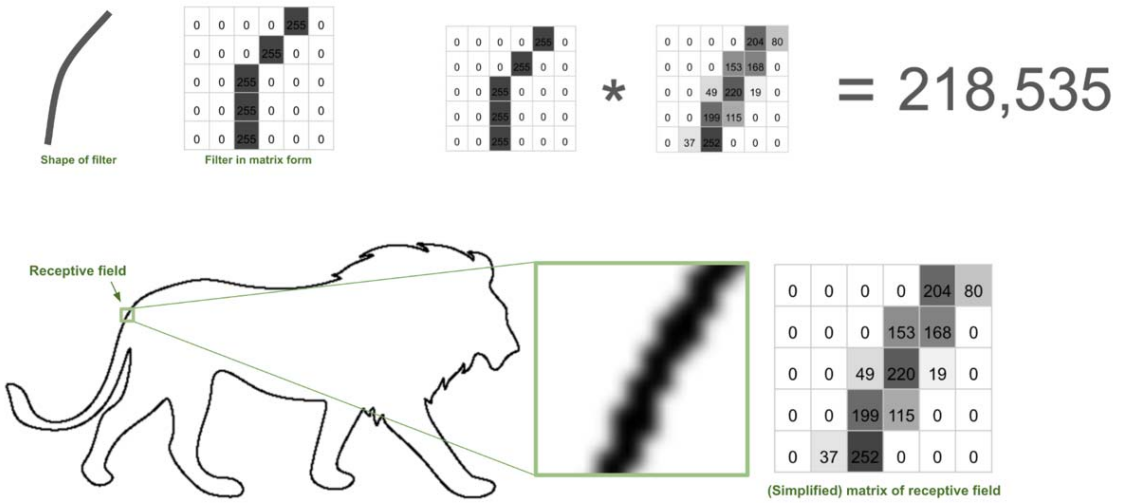

Figure 3 --Example of convolutions and pooling for CNN [14]

Creation of neural network. For the purpose of building a deep learning model it is necessary to specify input and output datasets. In this case the input is a set of text files that describe acoustic pressure at various depths over time, whereas the output are values characterizing the layers of the half-space under consideration, including [5]-[6]:

1) speed of acoustic wave propagation at the first layer;
2) speed of acoustic wave propagation at the second layer;
3) speed of acoustic wave propagation at the third layer;
4) porosity of the second layer;

There is a variety of other coefficients that influence the acoustic wave propagation, including depth and viscosity of the layers. For the purposes of this experiment those values were taken as constant, simulating conditions where it is necessary to find out what is a content of porous media in the second layer, often met in more practical applications.

The number of datasets is equal to 3600, with a data sets being given in 149x151 2 dimensional arrays.

Figure 2 – Dataset of acoustic pressure

The model was created with open-source deep learning library PyTorch. Convolutional neural networks were used for the purposes of estimating initial coefficients of acoustic wave propagation. There were 3 convolutional hidden layers and 2 fully connected linear hidden layers utilized during the procedure. The sigmoid function was used for activation.

Results. During training procedure, the neural network shows clear decrease in standard deviation over the number of batches:

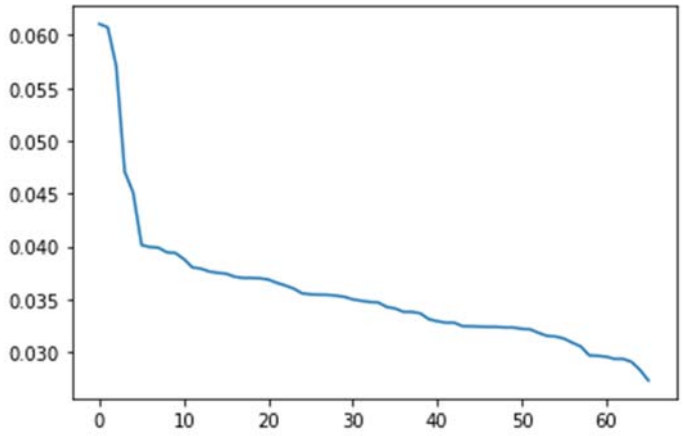

Figure 4 – Standard deviation over the number of batches

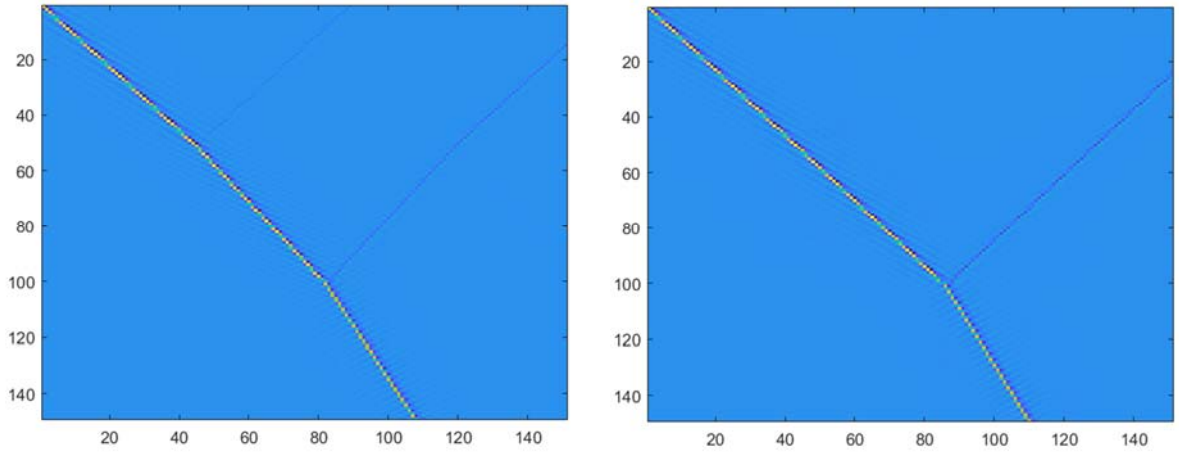

Figure 5 – Comparison of expected (left) solution created by forward model
and predicted (right) values created by applying results from deep learning algorithm

Conclusion. All in all, the experiment shows that it is possible to create a deep learning algorithms that estimates the solution of the acoustic wave propagation in poroelastic media. The deep learning neural network was successfully developed with standard deviation of 0.03 over the course of last batches, showing the convergence of neural network model, which gives an alternative to analytical solution to the problem given in [1]-[2]. After training neural network model can provide characterization of the physical properties of the layers based only on data of acoustic wave propagation over time and depth. Experiments display successful results in potential of deep learning in building seismic-acoustic wave propagation model and thus also successful in estimating solution to the problem via neural networks. This opens up a lot of opportunities with regard to making seismic-acoustic problems solving algorithm in geophysics that is robust to data regularization.

One of the ways of future developments that are possible in this area is generation of deep learning neural networks for more thorough and sophisticated wave propagation models such us inverse seismic-acoustic problems and then try to industrial application of trained network in real world conditions.

Марат Нуртас[1], Ж.Д. Байшемиров [2,3], В. Цай[1], М. Тастанов[1], Ж. Жанабеков[1]

[1]Халықаралық ақпараттық технологиялар университеті, Алматы, Қазақстан;
[2]Абай атындағы Қазақ ұлттық педагогикалық университеті, Алматы, Қазақстан;
[3]Ақпараттық және есептеуіш технологиялар институты, Алматы, Қазақстан

КОНВОЛЮЦИЯЛЫҚ (ЖИНАҚТАЛАТЫН) НЕЙРОНДЫҚ ЖЕЛІЛЕР АКУСТИКАЛЫҚ ТОЛҚЫНДАРДЫҢ ТАРАЛУ МӘСЕЛЕСІН ШЕШУДІҢ ӘДІСІ РЕТІНДЕ

Аннотация. Бұл мақала үш қабатты жартылай кеңістікте акустикалық толқынның таралу мәселесіне арналған. Бірінші және үшінші қабаттар үздіксіз қатқыл қабаттар, ал екінші қабат кеуектік қатқыл деп болжанады. Бұл мақалада акустикалық толқынның таралуын оның тереңдігі мен уақытын ескере отырып анықтау нәтижелері қарастырылады [1-4], сонымен қатар жоғарыда аталған үш қабаттың бастапқы физикалық қасиеттерін нейрондық желінің арқылы есептеуге тырысады.

Мақала мақсаты – бірнеше дербес жағдайды есепке ала отырып, осы қасиеттерді, атап айтқанда әр қабаттағы дыбыс жылдамдығын және екінші қабаттың кеуектігін есептейтін конвульсиялық (жинақталатын) нейрондық желі құру. Модель PyTorch, ашық оқу машиналарын оқыту кітапханасы арқылы жасалған. Акустикалық толқындардың таралу коэффициенттерін бағалау үшін үйірткілі нейрондық желілер пайдаланылды. Үйірткілі нейрондық желі – нейрондар мен синапстардың жұмысы туралы еркін негізделген статистикалық құралдарды қолдану арқылы мәліметтерді талдаудың модельдеу әдісі болып саналады. Нейрондық желілердің құрылымы 3 қабаттан тұрады: кіріс қабаты, жасырын қабат және шығу қабаты. Өз кезегінде, әрбір қабат қарапайым функция ретінде жұмыс істейтін нейрондардан тұрады. Алдыңғы қабаттағы нейрондардан синапстар деп аталатын қосылыстар арқылы мәліметтерді жинап, сол арқылы есептеу жүргізеді де, нәтижелерін келесі қабаттағы нейрондарға өткізеді. Кіріс қабаты модельдік деректерді енгізудің негізгі бөлігі ретінде жұмыс істейді. Ол кейде мәселенің жағдайын құрайтын оқыту мәліметтері деп аталатын деректерді алады. Деректерді енгізгеннен кейін кіріс қабатындағы нейрондар бірінші жасырын қабатқа сигнал жібере бастайды. Бұл жағдайда 3 үйірткілі жасырын қабаттар және 2 толық жалғанған сызықты жасырын қабаттар қолданылды. Активтеу үшін сигма тәрізді функция қолданылды. Мәліметтерді сипаттауға арналған мәліметтер сұйықтықтарға арналған Стокс теңдеуі және үзіліссіздік теңдеуінің көмегімен сипатталған акустикалық толқынның таралуының тікелей есебін итеративті шешу арқылы модельденді, акустикалық модельдің бастапқы мәндері берілген [5] - [6].

Акустикалық толқынның таралуын зерттеу геологиялық барлаудың негізгі міндеттерінің бірі болып саналады [6]. Бұл саладағы негізгі мәселелер – кеуекті-серпімді ортадағы акустикалық толқындардың таралуы, жер астындағы мұнай мен су қорларының ашылуына байланысты мәселе болып есептеледі. Алайда іс жүзінде бұл мәселені шешу деректерді жүйелеудің кең қолданылуын талап етеді, сонымен қатар, кейде әртүрлі жағдайларға байланысты елестетуге қиын мұқият және қымбат өлшемдерді қажет етеді.

Тәжірибе кеуекті-серпімді ортадағы акустикалық толқынның таралу шешімін бағалайтын терең оқыту алгоритмдерін құруға болатындығын көрсетеді. Терең оқытылған нейрондық желі [1]-[2]-да келтірілген мәселенің аналитикалық шешіміне балама ұсынатын, нейрондық желі моделінің жақындасқандығын көрсете отырып, соңғы партиялар бойынша 0,03 стандартты ауытқу негізінде сәтті дамытылды. Оқытудан кейін нейрондық желі моделі тек акустикалық толқынның таралуы туралы мәліметтер негізінде қабаттардың физикалық қасиеттерінің сипаттамасын бере алады.

Эксперименттер сейсмикалық-акустикалық толқындардың таралу моделін құруда терең оқытудың үздік нәтижелерін көрсетеді, сонымен қатар нейрондық желілерді қолдана отырып, есепті шешуді сәтті іске асырады. Бұл геофизикадағы сейсмостакустикалық, деректерді реттеуге тұрақты есептерді шешудің алгоритмін құруға мүмкіндік береді.

Бұл салада ықтимал болашақ даму әдістерінің бірі – толқынның таралуының неғұрлым мұқият және күрделі модельдерін терең оқытатын нейрондық желілерді құру, мысалы, кері сейсмикалық акустикалық мәселелер, содан кейін нақты жағдайда оқытылған желіні индустрияландыру әрекеті.

Түйін сөздер: нейрондық желі, конволюциялық нейрондық желі, акустикалық толқындардың таралуы, болжау модельдері, бақыланатын оқыту, активтендіру функциясы, PyTorch.

Марат Нуртас[1], Ж.Д. Байшемиров[2,3], В. Цай[1], М. Тастанов[1], Ж. Жанабеков[1]

[1]Международный университет информационных технологий, Алматы, Казахстан;
[2]Казахский национальный педагогический университет имени Абая, Алматы, Казахстан;
[3]Институт информационных и вычислительных технологий КН МОН РК, Алматы, Казахстан

СВЕРТОЧНЫЕ НЕЙРОННЫЕ СЕТИ КАК МЕТОД РЕШЕНИЯ ЗАДАЧИ РАСПРОСТРАНЕНИЯ АКУСТИЧЕСКИХ ВОЛН В ПОРОУПРУГИХ СРЕДАХ

Аннотация. Данная статья посвящена задаче распространения акустической волны в трехслойном полупространстве. Предполагается, что первый и третий слои являются сплошными, а второй – пороэластичными. В данной статье рассматриваются результаты определения распространения акустической волны с учетом ее глубины и времени [1-4], а также пытается рассчитать начальные физические свойства вышеупомянутых трех слоев.

Целью данной статьи является создание свёрточной нейронной сети, которая рассчитывает указанные свойства, а именно скорость звука в каждом слое и пористость второго слоя. Модель была построена с использованием PyTorch, библиотеки машинного обучения с открытым исходным кодом. Для оценки начальных коэффициентов распространения акустических волн использовались сверточные нейронные сети. Сверточная нейронная сеть – это метод моделирования анализа данных с помощью статистических инструментов, свободно основанный на идее работы нейронов и синапсов. Структура нейронных сетей состоит из 3 слоев: входной слой, скрытый слой и выходной слой. В свою очередь, каждый слой состоит из нейронов, которые работают как простая функция, собирая данные через соединения, называемые синапсами из нейронов в предыдущем слое, делая с ним вычисления и затем передавая результаты нейронам в следующем слое. Входной слой работает как первичная часть ввода данных нашей модели. Он принимает данные, иногда называемые данными обучения, которые формируют условия проблемы. После ввода данных нейроны во входном слое начинают посылать сигналы первому скрытому слою. При этом использовались 3 сверточных скрытых слоя и 2 полностью связанных линейных скрытых слоя. Сигмовидная функция была использована для активации. Данные для характеристики данных моделировались путем итеративного решения прямой задачи распространения акустической волны, описываемой уравнением Стокса и уравнением неразрывности, с заданными начальными значениями акустической модели [5]-[6].

Исследование распространения акустической волны является одной из основных задач геологической разведки [6]. Основными проблемами в этой области является проблема распространения акустических волн в пористо-упругой среде, проблема, связанная с обнаружением запасов нефти и воды под землей. Однако на практике решение этой проблемы требует широкого использования регуляризации данных, а также тщательных и дорогостоящих измерений, которые иногда трудно представить в силу различных обстоятельств.

Эксперимент показывает, что можно создать алгоритмы глубокого обучения, оценивающие решение распространения акустической волны в пористо-упругих средах. Нейронная сеть с глубоким обучением была успешно разработана со стандартным отклонением 0,03 в течение последних партий, демонстрируя сходимость модели нейронной сети, которая дает альтернативу аналитическому решению проблемы, приведенной в [1]-[2]. После обучения модель нейронной сети может обеспечить характеристику физических свойств слоев на основе только данных распространения акустической волны по времени и глубине.

Эксперименты показывают успешные результаты в потенциале глубокого обучения в построении модели распространения сейсмоакустических волн и, таким образом, также успешны в оценке решения проблемы с помощью нейронных сетей. Это открывает много возможностей для создания алгоритма решения сейсмоакустических задач в геофизике, который устойчив к регуляризации данных.

Одним из способов будущих разработок, которые возможны в этой области, является создание нейронных сетей глубокого обучения для более тщательных и сложных моделей распространения волн, таких как обратные сейсмическиеакустические проблемы и затем попытка промышленного применения обученной сети в реальных условиях.

Ключевые слова: нейронная сеть, сверточная нейронная сеть, распространение акустических волн, модели прогнозирования, контролируемое обучение, функция активации, PyTorch.

Information about authors:

Nurtas Marat, PhD, Associate Professor of Department of Mathematical and Computer Modeling, International Information Technologies University; maratnurtas@gmail.com, https://orcid.org/0000-0003-4351-0185;

Baishemirov Zh.D., PhD, Associate Professor of Abai Kazakh National Pedagogical University, Senior Research Officer of RSE Institute of Information and Computational Technology CS MES RK; zbai.kz@gmail.com, https://orcid.org/0000-0002-4812-4104;

Tsay V., master student, Department of Mathematical and Computer Modeling, [1]International Information Technologies University; tsay.victor96@gmail.com, https://orcid.org/0000-0002-6073-2030;

Tastanov M., Master Student of Department of Mathematical and Computer Modeling, International Information Technologies University; tychty4@gmail.com, https://orcid.org/0000-0002-1802-6394;

Zhanabekov Zh., Master Student of Department of Mathematical and Computer Modeling, International Information Technologies University; zzhanabekov@gmail.com, https://orcid.org/0000-0001-5984-7132

REFERENCES

[1] Meirmanov A., Nurtas M., (2016) "Mathematical models of seismic in composite media: elastic and poro-elastic components", Electronic Journal of differential equations, Vol. 2016, No. 184, pp. 1–22. USA.

[2] Meirmanov A., Nurtas M., (2016) "Seismic in composite media: elastic and poroelastic components", Siberian Electronic Mathematical Reports, Novosibirsk, Russia.

[3] M. Nurtas, Zh. D. Baishemirov, (2019) "Investigation of the temperature regime of the territory of the semipalatinsk polygon and description of the mathematical model and its numerical solution", News of the National Academy of sciences of the Republic of Kazakhstan, Vol 4, Number 326, 110-121. https://doi.org/10.32014/2019.2518-1726.49

[4] A. Meirmanov, M. Nurtas, (2015) "Inverse problems of acoustics of poroelastic media: constructing approximate solutions", Herald of the Kazakh-British Technical University. pp 77 – 87.

[5] Marat N., (2015) "Direct and inverse problems of acoustic equation in poroelastic medium", Herald of the Kazakh-British Technical University, pp 16 – 23.

[6] A. Meirmanov, (2013) Mathematical models for poroelastic flow, Atlantis Press.

[7] A. Fichtner, (2011) Full Seismic Waveform Modelling and Inversion, Advances in Geophysical and Environmental Mechanics and Mathematics, Springer- Verlag Berlin Heidelberg.

[8] Budum N., (2017) Fundamentals of Deep Learning.

[9] Justin Sirignano, Konstantinos Spiliopoulos, (2018) "DGM: A deep learning algorithm for solving partial differential equations".

[10] S. Asmussen and P. Glynn, (2007) "Stochastic Simulation: Algorithms and Analysis", Springer.

[11] Fangshu Yang, Jianwei Ma, (2019) "Deep-learning inversion: a next generation seismic velocity-model building method".

[12] M. Heidari1, M. Garshasbi, (2015) "Using Artificial Neural Networks in Solving Heat Conduction Problems", International Journal of Operations Research Vol. 12, No. 1, pp.016-020.

[13] Jens Berg, Kaj Nystrom, (2018), "Neural network augmented inverse problems for PDEs", Department of Mathematics, Uppsala University S-751 06 Uppsala, Sweden.

[14] Stureborg, R., (2020). Conv Nets For Dummies: A Bottom-Up Approach. [online] Medium. Available at: <https://towardsdatascience.com/> [Accessed 10 April 2020].

[15] Timo L¨ahivaaraa, Leo K¨arkk¨ainenb, Janne M.J. Huttunenb, and Jan S. Hesthavenc, 2020. Deep convolutional neural networks for estimating porous [online] Available at: <https://www.researchgate.net/publication/320075165_Deep_convolutional_neural_networks_for_estimating_porous_material_parameters_with_ultrasound_tomography> [Accessed 23 Apr. 2020].

NEWS
OF THENATIONAL ACADEMY OF SCIENCES OF THE REPUBLIC OF KAZAKHSTAN
PHYSICO-MATHEMATICAL SERIES
ISSN 1991-346X **https://doi.org/10.32014/2020.2518-1726.66**
Volume 4, Number 332 (2020), 61 – 67

УДК 004.89-004.31
МРНТИ 28.23.33

Y.T. Kozhagulov, D.M. Zhexebay, S.A. Sarmanbetov, A.A. Sagatbayeva, D. Zholdas

Al-Farabi Kazakh National University, Almaty, Kazakhstan.
Email: kaznu.kz@gmail.com, zhexebay92@gmail.com, sarmanbetov.sanzhar@gmail.com, sagalua95@gmail.com, dauletzholdas@mail.ru

COMPARATIVE ANALYSIS OF OBJECT DETECTION PROCESSING SPEED ON THE BASIS OF NEUROPROCESSORS AND NEUROACCELERATORS

Abstract. This paper is devoted to a comparative analysis of neural network models based on neuroprocessors. The following neural network models were selected: MobileNetSSD v1, SSD MobileNet v2. As a research task, the authors determined an attempt to compare several platforms that differ in size, computational capabilities and cost: Coral Dev Board, NVIDIA Jetson Nano, Coral USB Accelerator, Neural Compute Stick 2, Raspberry Pi 4. Local data processing offers a number of advantages compared to downloading calculations to a remote server or data center. Firstly, downloading data to remote servers takes a lot of time, as well as additional costs for infrastructure with energy, financial and computer equipment. It also requires high bandwidth and reliability, as data transfer may not be completed in case of a bad signal. Secondly, data transfer can lead to security and privacy issues. Finally, local processing can reduce the amount of data transferred to the cloud, which allows to performing tasks of a higher level.

The aim of this paper is a comparative analysis of platforms for object recognition tasks (object detection) with MobileNetSSD v1 / v2 models. For training, a cloud service based on the Jupyter Notebook, which gives access to incredibly fast GPUs and TPUs was used. The paper addresses the topic of determining small objects using the example of car detection.

Based on the study of platforms and models, it was found that the MobileNetSSD v1 model is effective for NVIDIA Jetson Nano by NVIDIA (61FPS), but in turn, the MobileNet v2 SSD model is less efficient (11FPS). Google's Coral Dev Board is more productive than other devices (47.8FPS and 63FPS). Raspberry Pi 4 (0.8FPS and 1.4FPS) turned out to be less effective. Among neuroprocessors, Neural Compute Stick 2 (9FPS and 7.1FPS) showed poor performance.

Key words: convolutional neural network, neuroaccelerators, neuroprocessor, object detection, deep learning.

1. Introduction

In modern conditions, the tasks of intelligent image processing are relevant, so the question arises of choosing a hardware platform with minimal power consumption, small size and high computing power [1-3]. There are a number of neural network models for object detection: Single Shot Detector (SSD), Faster Region-based Convolutional Neural Networks (R-CNN) and Region based Fully Convolutional Networks (R-FCN) [4]. These models, combined with various models such as VGG, Resnet101 and Mobilenet, determine the optimal combination of performance and speed. The combination of Faster R-CNN with Resnet-101 provides the best accuracy for object definition with 33.7% average accuracy and 396 ms of time in the GPU. The SSD-MobileNet model provides 19% and 40 ms in the GPU.

Other studies are aimed at improving the available models. For example, in [5], the performance of the traditional Faster R-CNN method is optimized by connecting blocks to the Fast R-CNN model, this new network is called RF-RCNN. The traditional Faster R-CNN method has an accuracy of about 61%, and with RF-RCNN this value improves to 75%.

The paper [6] describes the analysis in terms of the power and computational capabilities of the CNN-based model for an object detection system. The implementation uses a platform for embedded devices with support for a graphics processor (GPU), and the results are compared with a traditional platform based on a personal computer (PC).

In [7], the Movidius Neural Computer Stick is used to implement real-time object detection systems on the Raspberry Pi 3B. The results show that Movidius reaches 3.5 FPS. In most cases, detection models are used in modern computers with a GPU, the reason is that models such as Faster R-CNN, R-FCN or GoogleLenet require high processing, which cannot be satisfied with the built-in device. The most suitable deployment model with embedded devices and additional graphics processing elements is SSD-Mobilnet, which is strictly designed for devices with low performance. And also, the MobileNet SSD is an advanced convolution network architecture (model) that allows for fast recognition [8-9]. MobileNet SSDs are 20 times faster than their peers. The aim of this work is a comparative analysis of the computing capabilities of neuroprocessors and neuroaccelerators such as Coral Dev Board, NVIDIA Jetson Nano, Coral USB Accelerator, Movidus Neural Compute.

2. Hardware testing platforms

Platform NVIDIA Jetson Nano single-board computer for computing in the field of Artificial Intelligence (AI). A small computer with CUDA-X AI library support delivers 472 gigaflops to run modern AI workloads. The solution expands the capabilities of developers in terms of creating IoT applications, including for entry-level DVRs, home robots and smart gateways with analytical capabilities.

Figure 1 - NVIDIA Jetson Nano

Table 1 - NVIDIA Jetson Nano Features

Parameter	Value
CPU	Quad-core ARM A57 @ 1.43 GHz
GPU	128-core Maxwell
RAM	4 GB 64-bit LPDDR4 25.6 GB/s
Cost	100$

Intel® Neural Compute Stick 2 is a plug-and-play development kit for AI. The module can work without connecting to cloud technologies and allows you to create prototypes using inexpensive end devices such as Raspberry Pi4, etc.

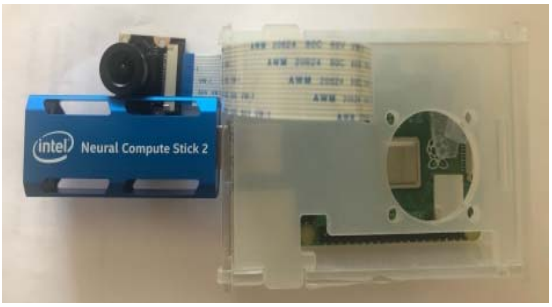

Figure 2 - Intel® Neural Compute Stick 2+Rb Pi4

Table 2 - Intel® Neural Compute Stick 2 Specifications

Parameter	Value
VPU	Intel Movidius Myriad X
Power supply	USB 3.0 Type-A
Sizes	72,5 x 27 x 14 mm
Cost	100$

Coral USB Accelerator is a specialized ASIC developed by Google, which is considered a lightweight version of the TPU (Tensor Processing Unit) provided as part of cloud services for training neural networks.

Coral USB Accelerator supports two different operating modes: at standard frequency and maximum frequency. At maximum frequency, output performance grows in two.

Figure 3 - Coral USB Accelerator+Rb Pi4

Table 3 - Coral USB Accelerator Specifications

Parameter	Value
ML accelerator	Google Edge TPU coprocessor
Connector	USB 3.0 Type-C* (data/power)
Sizes	65 mm x 30 mm
Cost	75 $

Coral Dev Board is a single-board computer that is ideal for quickly performing machine learning (ML) operations in a small form factor (technical product standard). You can use Dev Board to prototype your embedded system and then scale it to production using the integrated Coral System-on-Module (SoM) system in combination with custom PCB hardware.

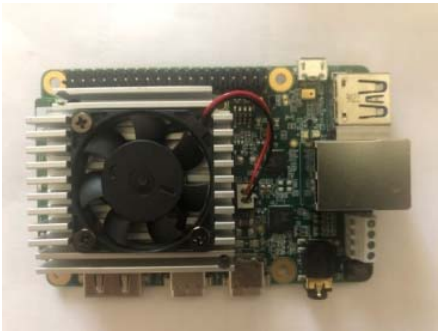

Figure 4 - Coral Dev Board

Table 4 - Coral Dev Board Specifications

Parameter	Value
CPU	NXP i.MX 8M SoC (quad Cortex-A53, Cortex-M4F)
GPU	Integrated GC7000 Lite Graphics
ML accelerator	Google Edge TPU coprocessor
RAM	1 GB LPDDR4
Flash memory	8 GB eMMC
Sizes	48mm x 40mm x 5mm
Cost	150 $

The Raspberry Pi 4 is a single-board computer the size of a bank card, originally developed as a budget system for teaching computer science, but later gaining wider application and fame.

Figure 5 - Raspberry Pi 4

Table 5 - Raspberry Pi 4 Specifications

Parameter	Value
SoC	Quad core Cortex-A72 (ARM v8) 64-bit SoC @ 1.5GHz
GPU	VideoCore VI c OpenGL ES
Sizes	88 x 58 mm.
Cost	35$

3. The results of a comparative analysis of neuroprocessors

The following neural network models were selected as objects for testing: MobileNetSSD v1, SSD MobileNet v2. Models are trained on common objects in the Common Objects in Context (COCO) database of a data set. For training, we used a cloud service based on the Jupyter Notebook, which gives access to incredibly fast GPUs and TPUs.

Graph 1 below shows the results of a study on the processing speed of data on single-board platforms.

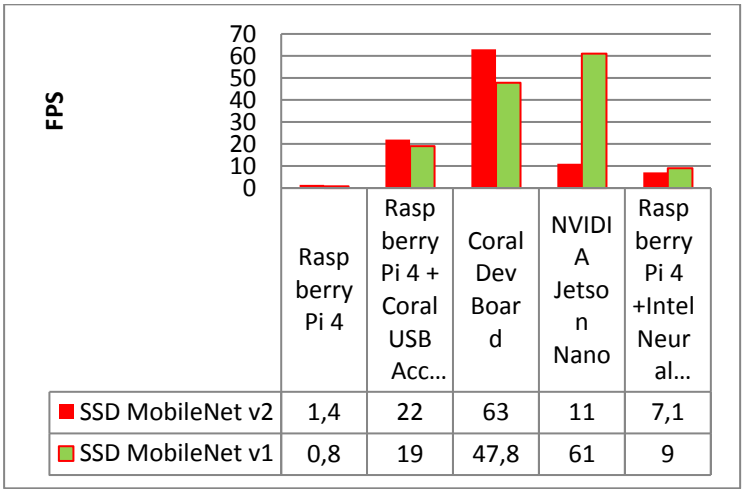

Graph 1 - The result of testing platforms in FPS (the number of frames per second)

The diagram shows that the MobileNetSSD v1 model is an order of magnitude faster with the NVIDIA Jetson Nano (61FPS). The results obtained were tested for the task of recognizing the flow of cars in real time (Figure 6).

Figure 6 - Test result of MobileNet v1 / v2 SSD models in FPS (frames per second) trained using the COCO dataset

Based on the result (Figure 6), it can be seen that the detector missed small cars. The solution to this problem is to increase the resolution of input images. Vehicles that are far away are not a problem for the model. As the approach getting closer, models will be able to recognize their presence. The second problem that may encounter is that the models do not distinguish between the "front" and "frontal" type of vehicle. These incorrect classifications are partly due to the fact that the front and rear parts of vehicles have many visually similar characteristics. Despite this, MobileNet SSDs achieve high recognition accuracy.

4. Conclusion

The results of this paper show that the MobileNetSSD v1 model is effective for NVIDIA Jetson Nano from NVIDIA (61FPS), however, this device for the MobileNet v2 SSD model showed a low performance (11FPS) compared to other devices. Google's Coral Dev Board is more productive than NVIDIA Jetson Nano, whose results for neural network models are 47.8FPS and 63FPS, respectively. The Raspberry Pi 4 (0.8FPS and 1.4FPS) turned out to be not effective, since the platform does not have a built-in neuroprocessor and a neuro accelerator. Among neuroprocessors, Neural Compute Stick 2 (9FPS and 7.1FPS) showed poor performance.

Е.Т. Кожагулов, Д.М. Жексебай, С.А. Сарманбетов, А.А. Сағатбаева, Д. Жолдас

әл-Фараби атындағы Қазақ Ұлттық Университеті, Алматы, Казахстан

НЕЙРОПРОЦЕССОРЛАР МЕН НЕЙРОЖЫЛДАМДАТҚЫШТАРДЫҢ БАЗАСЫНДА ОБЪЕКТІЛЕРДІ АНЫҚТАУ ЖЫЛДАМДЫҒЫН САЛЫСТЫРМАЛЫ ТАЛДАУ

Аннотация. Ақпараттық технологияға деген сұраныстың артуы нейрондық желілер мен алгоритмдердің дамуына әкелді. Соңғы жылдары зерттеушілердің қызығушылығын арттырған машиналық оқыту алгоритмдері, соның ішінде, нейрондық желілер басты назарға ілігіп отыр. Нейрондық желі алгоритмдеріне кескінді өңдеу, мәтіндік тілді өңдеу, мәліметтерді талдау және т.б. жатады, нейрондық желі көптеген салаларда жоғары нәтижелерге қол жеткізеді. Бұл жетістіктер зерттеушілерді адам өмірінің барлық салаларында нейрондық алгоритмдерді қолдануға шабыттандырады. Бүгінгі таңда зияткерлік бейнені өңдеу міндеттері өзекті болып отыр.

Жұмыс нейропроцессорлар негізінде нейрондық желі моделдерін салыстырмалы түрде талдауға арналған. Зерттеуге нейрондық желінің келесі моделдері таңдалды: MobileNetSSD v1, SSD MobileNet v2.

Жұмыстық мақсаты MobileNetSSD v1/v2 модельдері мен объектілерді анықтауға арналған алаңдарды салыстырмалы түрде талдау. Моделдер жалпы нысандардағы Common Objects in Context (COCO) базасында оқытылды. Оқыту үшін біз Jupyter Notebook-ке негізделген қызметті қолдандық, ол GPU мен TPU-ға жылдам қол жеткізуге мүмкіндік береді. Жұмыс автомобильдерді анықтау мысалын қолдана отырып, кішкентай заттарды анықтауда қарастырылған.

Көзделген мақсатқа қол жеткізу үшін келесі міндеттер қойылды:

Coral Dev Board, NVIDIA Jetson Nano, Coral USB Accelerator, Neural Compute Stick 2, Raspberry Pi 4 платформаларын салыстыру. Бір платалы процессорлар - бұл қол жетімді бағамен машиналық оқытудың озық үлгілерін орналастыруға мүмкіндік беретін керемет құралдар болып табылады. Jetson Nano - бұл толық функционалдығы бар кішкентай Linux компьютері, оны бағдарламалық жасақтаманы қолдану тұрғысынан икемді етеді. Ол TensorFlow, Caffe, PyTorch, Keras және MXNet сияқты машиналарды оқытудың барлық орталарымен жұмыс істей алады. Салыстыру үшін, Coral Dev Board, Coral USB Accelerator, Neural Compute Stick 2, Raspberry Pi - Jetson Nano сияқты фреймворктарды қолдану тұрғысынан икемді емес, өйткені аппараттық архитектурасына сәйкес келетін арнайы форматтағы модельдерді ғана қолдана алады. Сонымен жоғарыда атылып кеткен платформалар өздерінің шектеулі мүмкіндіктеріне қарамастан оларды машиналық оқытуда пайдалануда тиімді ететін бірнеше факторлар бар. Шағын қуатты тұтыну арқасында кірістірілген жүйелер деректерді жинау орнында өңдеуге мүмкіндік береді, мысалы ретінде IoT құрылғысын, роботтарды, автономды автомобиль немесе дрондарды жатқызсақ болады. Жергілікті деректерді өңдеу қашықтағы серверге немесе деректерді өңдеу орталығына есептеулерді жүктеумен салыстырғанда бірқатар артықшылықтарды береді. Біріншіден деректерді қашықтағы серверлерге жүктеу үлкен кідірістер алады, сонымен қатар энергетикалық, қаржылық және есептеу техникаларымен инфраструктураға қосымша шығындар алып келеді. Сондай-ақ, бұл жоғары өткізу қабілеттілігі мен сенімділікті қажет етеді, өйткені нашар сигнал болған жағдайда деректерді жіберу аяқталмай қалуы мүмкін. Екіншіден, деректерді жіберу қауіпсіздік пен құпиялылық мәселелеріне алып келуі мүмкін. Соңында, жергілікті өңдеу бұлтқа берілетін деректер көлемін азайтуы мүмкін, бұл оған жоғары деңгейдегі тапсырмаларды орындауға мүмкіндік береді.

Олардың есептеу қабілеттері мен құны бойынша ерекшеліктерін бірнеше платформаларды салыстыра отырып анықтау;

Платформалар мен модельдерді зерттеу негізінде NVIDIA Jetson Nano NVIDIA-ден (61FPS) үшін MobileNetSSD v1 моделі тиімді екені анықталды, бірақ SSD MobileNet v2 моделі MobileNetSSD v1 моделімен салыстырғанда тімділігі төмен. Google Coral Dev Board басқа құрылғыларға қарағанда тиімді (47,8FPS және 63FPS). Ал Raspberry Pi 4 (0,8FPS и 1,4FPS) тіимділігі төмен. Сонымен қатар Neural Compute Stick 2 (9FPS и 7,1FPS) моделдері нейропроцессорлардың арасында төменгі көрсеткіштер көрсетті.

Түйін сөздер: жинақталған нейрондық желі, нейроүдеткіштер, нейропроцессор, объектіні анықтау, тереңдетіп оқыту.

Е.Т. Кожагулов, Д.М. Жексебай, С.А. Сарманбетов, А.А. Сағатбаева, Д. Жолдас

Казахский национальный университет имени аль-Фараби, Алматы, Казахстан.

СРАВНИТЕЛЬНЫЙ АНАЛИЗ СКОРОСТИ ОБРАБОТКИ ОБНАРУЖЕНИЯ ОБЪЕКТОВ НА БАЗЕ НЕЙРОПРОЦЕССОРОВ И НЕЙРОУСКОРИТЕЛЕЙ

Аннотация. Быстрый рост данных, внедрение нейронных сетей и появление различных технологий, ускоряющих процесс обучения, привели к разработке нейропроцессоров и нейроускорителей. В последние годы алгоритмы машинного обучения привлекают большое внимание исследователей, это связано с необходимостью обработки большого массива данных. Алгоритмы нейронной сети включают обработку изображений, обработку естественного языка, анализ данных и т. д. достигает высоких результатов во многих областях. Эти достижения вдохновили исследователей на применение алгоритмов нейронных сетей в сложных областях человеческой жизни, требующей использование нетрадиционных алгоритмов аналитических вычислений. На сегоднящний день задачи интеллектуальной обработки изображений актуальны.

Работа посвящена сравнительному анализу нейросетевых моделей на базе нейропроцессоров. Были выбраны следующие нейросетевые модели: MobileNetSSD v1, SSD MobileNet v2. В качестве исследовательской задачи авторами была определена попытка сравненить несколько платформ, которые отличаются по размеру, вычислительным возможностям и стоимости: Coral Dev Board, NVIDIA Jetson Nano, Coral USB Accelerator, Neural Compute Stick 2, Raspberry Pi 4. Из-за низкого энергопотребления встроенные системы позволяют обрабатывать данные в точке сбора, например, устройства IoT, роботы, автономные транспортные средства или дроны. Локальная обработка данных предлагает ряд преимуществ по сравнению с загрузкой вычислений на удаленный сервер или в центр обработки данных. Во-первых, загрузка данных на удаленные серверы занимает много времени, а также дополнительные расходы на инфраструктуру с энергетическим, финансовым и компьютерным оборудованием. Это также требует высокой пропускной способности и надежности, поскольку передача данных может быть не завершена в случае плохого сигнала. Во-вторых, передача данных может привести к проблемам безопасности и конфиденциальности. Наконец,

локальная обработка может уменьшить объем данных, передаваемых в облако, что позволяет выполнять задачи более высокого уровня. Одноплатные процессоры являются отличными инструментами, которые позволяют развертывать передовые модели машинного обучения по доступной цене. Jetson Nano - это небольшой полнофункциональный компьютер Linux, который делает его гибким в плане использования программного обеспечения. Он может работать со всеми средами машинного обучения, такими как TensorFlow, Caffe, PyTorch, Keras и MXNet. Для сравнения, он является негибким с точки зрения использования таких платформ, как Coral Dev Board, Coral USB Accelerator, Neural Compute Stick 2, Raspberry Pi -Jetson Nano, поскольку может использовать модели только в специальных форматах, соответствующих аппаратной архитектуре.

Целью работы является сравнительный анализ платформ для задач распознавания объектов (object detection) с моделями MobileNetSSD v1/v2. В сатье модели обучены на общие объекты в базе Common Objects in Context (COCO) набора данных. Для обучения использовалась облачный сервис на основе Jupyter Notebook, которая дает доступ к невероятно быстрым GPU и TPU. В работе затрагивается тема определения маленьких объектов на примере детектирования автомобилей.

На основе изучения платформ и моделей установлено ,что модель MobileNetSSD v1 эффективна для NVIDIA Jetson Nano от NVIDIA (61FPS), но в свою очередь модель SSD MobileNet v2 менее эффективна (11FPS). Coral Dev Board от Google является более производительнее чем другие устройства (47,8FPS и 63FPS). Менее эффективным оказался Raspberry Pi 4 (0,8FPS и 1,4FPS). Среди нейропроцессоров низкую производительность показал Neural Compute Stick 2 (9FPS и 7,1FPS).

Ключевые слова: сверточная нейронная сеть, нейроускорители, нейропроцессор, обнаружение объектов, глубокое обучение.

Information about authors:

Kozhagulov YE., Lead researcher, PhD, Lecturer of Department of Physics and Technology, Al-Farabi Kazakh National University, Almaty, Kazakhstan, kazgu.kz@gmail.com ,https://orcid.org/0000-0001-5714-832X;

Zhexebay D., PhD candidate, zhexebay92@gmail.com, https://orcid.org/0000-0002-3974-0896;

Sarmanbetov S., Master of Natural Sciences,sarmanbetov.sanzhar@gmail.com, https://orcid.org/0000-0003-1749-2163;

Sagatbayeva A., Master of Engineering and Technology,sagalua95@gmail.com, https://orcid.org/0000-0002-8601-8900;

Zholdas D., Student,dauletzholdas@mail.ru, https://orcid.org/0000-0001-5183-8354;

REFERENCES

[1] Barthélemy J., Verstaevel N., Forehead H., Perez P. Edge-computing video analytics for real-time traffic monitoring in a smart city //Sensors. 2019. Vol. 19, №. 9. P. 2048.

[2] Zhong Q., Li C., Zhang Y., Xie D., Yang S., Pu S. Cascade region proposal and global context for deep object detection //Neurocomputing. 2019.

[3] Antonini M., Vu T.H., Min C., Montanari A., Mathur A., Kawsar F. Resource Characterisation of Personal-Scale Sensing Models on Edge Accelerators //Proceedings of the First International Workshop on Challenges in Artificial Intelligence and Machine Learning for Internet of Things. 2019. P. 49-55.

[4] Nikhil Yadav U. B., “Comparative study of object detection algorithms,” in International Research Journal of Engineering and Technology (IRJET), May 2017, pp. 586–591.

[5] M. Roh and J. Lee, “Refining faster-rcnn for accurate object detection,” in 2017 Fifteenth IAPR International Conference on Machine Vision Applications (MVA), May 2017, pp. 514–517.

[6] Z. Chen, T. Ellis, and S. A. Velastin, “Vehicle detection, tracking and classification in urban traffic,” in 2012 15th International IEEE Conference on Intelligent Transportation Systems, Sept 2012, pp. 951– 956.

[7] R. H. Pea-Gonzlez and M. A. Nuo-Maganda, “Computer vision based real-time vehicle tracking and classification system,” in 2014 IEEE 57th International Midwest Symposium on Circuits and Systems (MWSCAS), Aug 2014, pp. 679–682.

[8] Nicholas D Lane. 2019. EmBench: Quantifying Performance Variations of Deep.

Neural Networks across Modern Commodity Devices. In The 3rd InternationalWorkshop on Deep Learning for Mobile Systems and Applications. ACM, 1–6.

[9] Saisakul Chernbumroong, Shuang Cang, Anthony Atkins, and Hongnian Yu. 2013. Elderly activities recognition and classification for applications in assisted living. Expert Systems with Applications 40, 5 (2013).

NEWS
OF THENATIONAL ACADEMY OF SCIENCES OF THE REPUBLIC OF KAZAKHSTAN
PHYSICO-MATHEMATICAL SERIES
ISSN 1991-346X **https://doi.org/10.32014/2020.2518-1726.67**
Volume 4, Number 332 (2020), 68 – 76

IRSTI 29.05.23; 29.05.29; 29.05.41
UDK 539.1
ISSN 1991-346X

D.M. Zazulin[1,2], S.E. Kemelzhanova[1], I. Satyshev[3], O. Ormantaev[1]

[1] al-Farabi Kazakh National University, Physics and Technology Department Almaty, Kazakhstan;
[2] Institute of Nuclear Physics, Almaty, Kazakhstan;
[3]Almaty Institute of Nuclear Physics, Almaty, Kazakhstan.
E-mail: denis_zazulin@mail.ru

APPLICATION OF GEOMETROTHERMODYNAMICS TO THE TWO-DIMENSIONAL SYSTEMS: IDEAL BOSE-GAS AND SYSTEM WITH STRONG INTERACTION

Abstract. In the framework of the method of geometrothermodynamics, in present work, we studied the properties of equilibrium manifolds of the following thermodynamic systems: a two-dimensional Bose gas, a Berezinsky-Kosterlitz-Thouless system. The results are invariant under the Legendre transformations, i.e. independent of the choice of thermodynamic potential. For the systems under consideration, the corresponding metrics and scalar curvatures are calculated, and their properties are also described. Research of two-dimensional quantum thermodynamic systems is becoming more urgent. It is sufficiently to mention that such systems are related to, for example, topological insulators, graphene, systems with quantum Hall effect, etc. Two-dimensional quantum systems may have a statistical distribution different from distributions of Fermi-Dirac and Bose-Einstein. Geometric approaches in research of these thermodynamic systems certainly open the new perspective.

In this paper the thermodynamic properties of two-dimensional Bose-Gas and Berezinsky-Kosterlitz-Thouless system have been studied with the help of geometrothermodynamics. The main objective was to reproduce the Bose-Einstein condensation for the first system and find possible new phase transitions for the second.

In order to study the above mentioned thermodynamic systems, we have consequently calculated the covariant metric tensors of corresponding equilibrium manifolds and their determinants, then counter-variant metric tensors, Christoffel symbols, curvature tensors and corresponding scalar curvatures. Using the thermodynamic potential, we obtained (using the Matlab system) the corresponding geometric values in a wide range of temperature and area.

Explicit formulas were also obtained for each geometric quantity but due to their bulkiness we do not present them in this paper. Examples of calculated scalar curvatures for a certain range of parameters T and S are shown in the figures. The figures also show that despite the significantly different behavior of the curvatures depending on the parameters T and S, both metrics lead to the same General result regarding the location of singularities for the corresponding curvatures.

Next, we used geometric thermodynamics for the system of the Berezinsky-Kosterlitz-Thoules. This is a two-dimensional system of Bose particles with a strong interaction (strong in the sense that topological defects - point vortices-contribute to the thermodynamics of the system) with a complex, not fully studied system of phase transitions. An ideal two-dimensional Bose gas with a finite number of particles and a Berezinsky-Kosterlitz-Thoules system are considered. As thermodynamic potentials for these thermodynamic systems, the chemical potential depending on temperature and area and the Free energy depending on the temperature and size of the system were taken, respectively. The paper also presents 3-dimensional drawings that clearly show at which values of thermodynamic variables scalar curvatures tend to infinity or to zero, which indicates possible phase transitions and possible compensation of interactions by quantum effects, respectively. It is shown that both variants of metrics for an ideal two-dimensional Bose gas lead to the same arrangement of lines, where scalar curvatures become singular. This arrangement of lines is consistent with the region where the phase transition occurs - Bose condensation in a two-dimensional Bose gas. It is also shown that for large values of temperature and area parameters, the curvature is close to zero and this corresponds to a classical ideal two-dimensional gas. When considering the Berezinsky-Kosterlitz-taules system, possible new phase transitions were discovered by the method of geometric

thermodynamics. The metric calculation leads to a possible phase transition located below the Berezinsky-Kosterlitz-Taules transition, and the calculation leads to a possible phase transition located above.

Keywords: geometrothermodynamics, Legendre transformations, metric tensor, scalar curvature, two-dimensional Bose gas, Berezinsky-Kosterlitz-Thouless system.

1. Introduction. Interactions in thermodynamic systems in geometrothermodynamics (GTD) developed by H. Quevedo (described in detail by him and his co-authors, for example, in papers [1-8]) are determined using the scalar curvature of equilibrium manifolds. This curvature, in turn, is invariant relatively to Legendre transformations. In thermodynamics, the physical properties of the system also do not depend on the choice of thermodynamic potentials using which this system is described. Transition from one set of thermodynamic potentials to another is carried out with the help of Legendre transformations, and in this sense the thermodynamics is invariant relatively to Legendre transformations. In GTD, for example, as it is shown in [1], the ideal gas, which particles do not interact with each other, corresponds to manifold with zero curvature. In the case of interacting systems with nontrivial structure of phase transitions, the curvature, as shown in [2-5], reproduces the behavior of the system near the points where phase transitions occur. So, for example, near the phase transitions in gases of Van der Waals, Bose - Einstein, etc., the scalar curvature of the corresponding equilibrium manifolds tends to infinity, i.e. becomes singular. This circumstance can be used for searching unknown phase transitions in insufficiently studied thermodynamic systems. Research of two-dimensional quantum thermodynamic systems is becoming more urgent. It is sufficiently to mention that such systems are related to, for example, topological insulators, graphene, systems with quantum Hall effect, etc. Two-dimensional quantum systems may have a statistical distribution different from distributions of Fermi-Dirac and Bose-Einstein. Geometric approaches in research of these thermodynamic systems certainly open the new perspectives. In this paper the thermodynamic properties of two-dimensional Bose-Gas and Berezinsky-Kosterlitz-Thouless (BKT) system have been studied with the help of GTD. The main objective was to reproduce the Bose-Einstein condensation for the first system and find possible new phase transitions for the second.

2. Formalism of GTD method. In order to study the above mentioned thermodynamic systems, we have consequently calculated the covariant metric tensors of corresponding equilibrium manifolds and their determinants, then counter-variant metric tensors, Christoffel symbols, curvature tensors and corresponding scalar curvatures.

For calculating metrics and corresponding metric tensors we used the following formulas [1]:

$$dl^2 = E_a \frac{\partial \Phi}{\partial E^a} \delta_{ab} \frac{\partial^2 \Phi}{\partial E^b \partial E^c} dE^a E^c \tag{1}$$

$$dl^2 = E_a \frac{\partial \Phi}{\partial E^a} \eta_{ab} \frac{\partial^2 \Phi}{\partial E^b \partial E^c} dE^a E^c \tag{2}$$

where l^2 - square of thermodynamic length, $\Phi \equiv \Phi(E^a)$ – thermodynamic potential, which obviously depends on other thermodynamic potentials - E^a (a = 1,….,n), n – number of thermodynamic potentials, from which Φ depends $\delta_{a,b} = diag(1,1,....,1)$ and $\eta_{a,b} = diag(1,-1,....,-1)$. Both relations (1) and (2) are invariant with respect to Legendre transformations [1].

The expression for the curvature tensor has the general form:

$$R_{abcd} = \frac{1}{2}\left(\frac{\partial^2 g_{ad}}{\partial E^b \partial E^c} + \frac{\partial^2 g_{bc}}{\partial E^a \partial E^d} - \frac{\partial^2 g_{ac}}{\partial E^b \partial E^d} - \frac{\partial^2 g_{bd}}{\partial E^a \partial E^c} \right) + g_{np}\left(\Gamma^n_{bc}\Gamma^p_{ad} - \Gamma^n_{bd}\Gamma^p_{ac} \right) \tag{3}$$

where $g^{nm}(g_{ad})$ – metric tensor, $\Gamma^n_{bc} = \frac{1}{2} g^{nm}\left(\frac{\partial g_{mb}}{\partial E^c} + \frac{\partial g_{mc}}{\partial E^b} - \frac{\partial g_{bc}}{\partial E^m} \right)$ – Christoffel symbols. Further, the scalar curvature is calculated by formula: $R = g^{ac} g^{bd} R_{abcd}$.

Since in the future we deal with systems which depend only on two thermodynamic potentials, the expression for scalar curvature is simplified to:

$$R = \frac{2P_{1212}}{\det(g)}, \tag{4}$$

where det(g) – determinant of two-dimensional metric tensor.

3. Two-dimensional ideal Bose gas. First consider the well-known system - two-dimensional ideal Bose-gas particles with mass *m*. As a thermodynamic potential we take the chemical potential μ, which depends on temperature T and area S (two-dimensional volume) with a fixed number of particles N (see for example [9]):

$$\mu(T,S) = T\ln\left(1 - e^{-\frac{2\pi\hbar^2 N}{SmT}}\right) \tag{5}$$

To simplify the formula, let's assume a constant $\frac{2\pi\hbar^2 N}{m}$ is equal to one and rewrite the expression (5) in the form:

$$\mu(T,S) = T\ln\left(1 - e^{-\frac{1}{ST}}\right) \tag{6}$$

Figure 1 shows a graph (6) for certain range of parameters T and S. Using (1 - 4) and thermodynamic potential (6) we have obtained (using the Matlab system) corresponding geometric values in a wide range of temperature and area. For each geometric value we have also obtained explicit formulas, but due to their extensionality we do not show them in this paper. Examples of calculated scalar curvatures for certain range of parameters T and S are shown in Figures 2a and 2b for metrics (1) and (2) respectively.

From calculations and figure 2a and (2b) it can be seen, that curvature tends to plus (minus) infinities when approaching zero of temperature at finite value of parameter of the area, that is just corresponds to Bose condensation for two-dimensional Bose-gas (see for example [10]). Also from these calculations and figure 2a and (2b) it is seen, that the curvature tends to plus (minus) infinities when approaching infinity of density at finite value of temperature. At large values of parameters T and S the curvatures are close to zero and it corresponds to classical ideal gas.

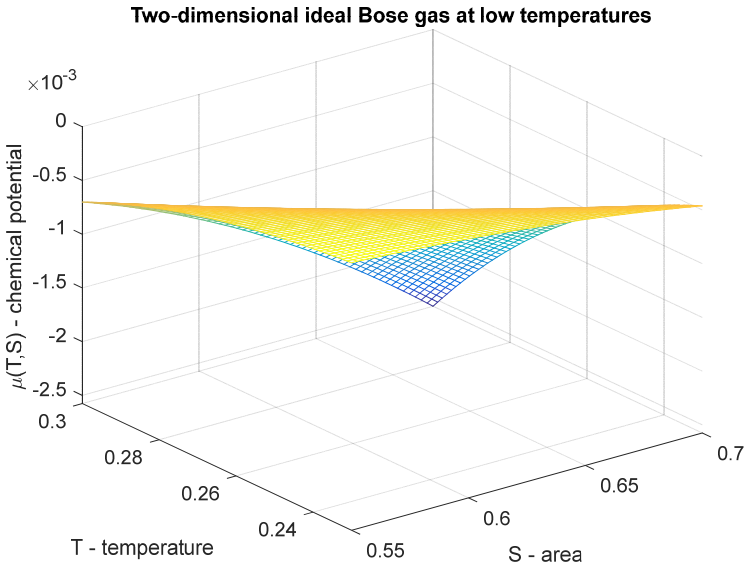

Figure 1: Chemical potential (6) depending on the temperature and area of two-dimensional ideal Bose-gas at low temperatures [9]

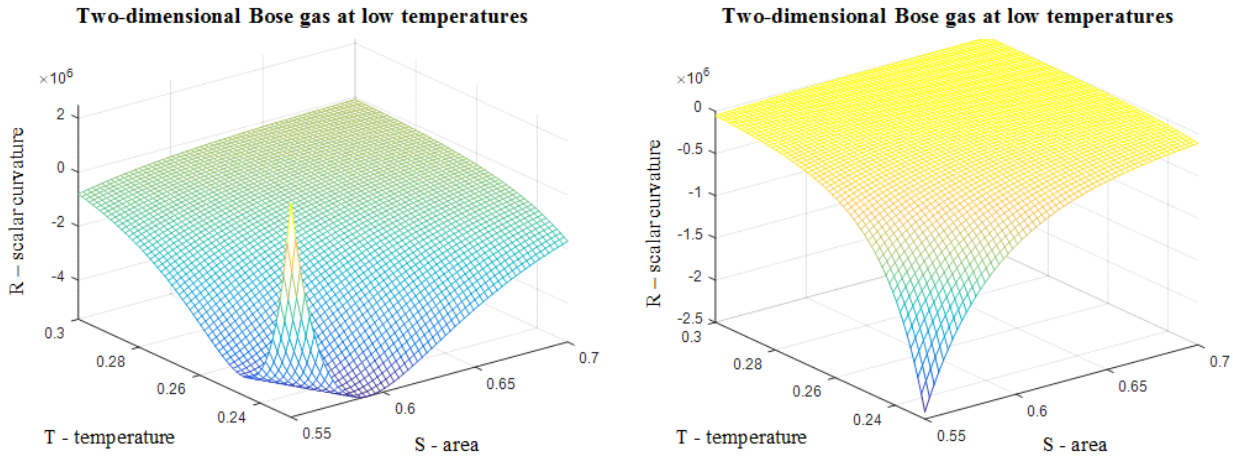

A b

Figure 2 - Dependence of scalar curvature on temperature and area: a) metrics calculated using formula (1), b) metrics calculated using formula (2).

Figures 2a and 2b also show that despite the significantly different behavior of the curvatures depending on the T and S parameters, both metrics (1) and (2) lead to one common result related to the location of singularities for the corresponding curvatures.

4. BKT system. Then we applied GTD to BKT system (see for example [11-15]). This is a two-dimensional Bose system of particles with strong interaction (strong in the sense that the contribution to the thermodynamics of the system is made by topological defects - point vortices) with a complicated, not fully understood system of phase transitions [16-20]. Consider free energy as a thermodynamic potential [20]:

$$F(T,L)=\left(J\pi-2k_BT\right)\ln\left(\frac{L}{a}\right) \tag{7}$$

where T – temperature, L – system size, a – vortices size, k_B - Boltzmann constant, J – certain constant. Formula (7) makes sense at $L > a$, and near the BKT transition at $T=T_c=\frac{J\pi}{2k_B}$ when the appearance of a free vortex becomes energetically favorable. At lower temperatures in the system there is a vortex - anti vortex bound pair and the phase transition is interpreted as a process of dissociation of this pair.

To simplify the following calculations, we assume $J\pi=k_B=a=1$. Then

$$F(T,L)=(1-2T)\ln(L) \tag{8}$$

Figure 3 shows the graph (8) for certain range of parameters T and L. Applying the formula (1) to expression for metrics (8) we obtain the metric tensor:

$$g(T,L)=\begin{bmatrix} 0 & \frac{2(T+T\ln(L)-0.5)}{L} \\ \frac{2(T+T\ln(L)-0.5)}{L} & -\frac{(2T-1)^2}{L^2} \end{bmatrix} \tag{9}$$

Determinat of this tensor:

$$\det(g)=-\frac{4(T+T\ln(L)-0.5)^2}{L^2} \tag{10}$$

and the scalar curvature (4):

$$R = \frac{L^2\left(\frac{4(\ln(L)+1)}{L^2} - \frac{12}{L^2} + \frac{(\ln(L)+1)(\frac{8T-4}{L^2} - \frac{T+T\ln(L)-0.5}{L^2} + \frac{T}{L^2})}{4(T+T\ln(L)-0.5)}\right)}{4(T+T\ln(L)-0.5)^2} \quad (11)$$

Applying the formula for the metrics (2) to the expression (6), we obtain:

$$g_1(T,L) = \begin{bmatrix} 0 & \frac{2(T\ln(L)-T+0.5)}{L} \\ \frac{2(T\ln(L)-T+0.5)}{L} & \frac{(2T-1)^2}{L^2} \end{bmatrix} \quad (12)$$

Determinant of this tensor:

$$\det(g_1) = -\frac{4(T\ln(L)-T+0.5)^2}{L^2} \quad (13)$$

And scalar curvature:

$$R_1 = \frac{L^2\left(\frac{4(\ln(L)-1)}{L^2} + \frac{4}{L^2} - \frac{(\ln(L)-1)(\frac{8T-4}{L^2} - \frac{T-T\ln(L)-0.5}{L^2} - \frac{T}{L^2})}{4(T+T\ln(L)-0.5)}\right)}{4(T\ln(L)-T+0.5)^2} \quad (14)$$

Examples of calculated scalar curvatures for a certain range of parameters T and L are shown in the figures 4a and 4b for the metrics (1) and (2), respectively.

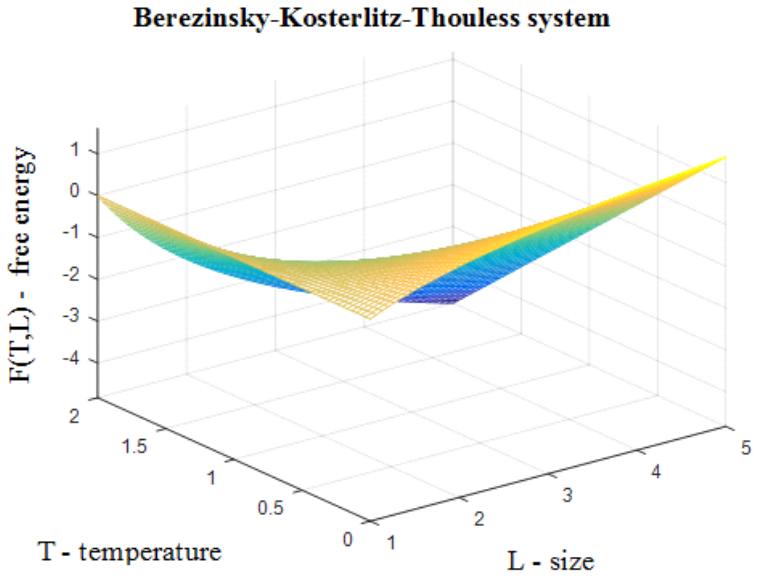

Figure 3 - Free energy (8) depending on temperature and system size [20]

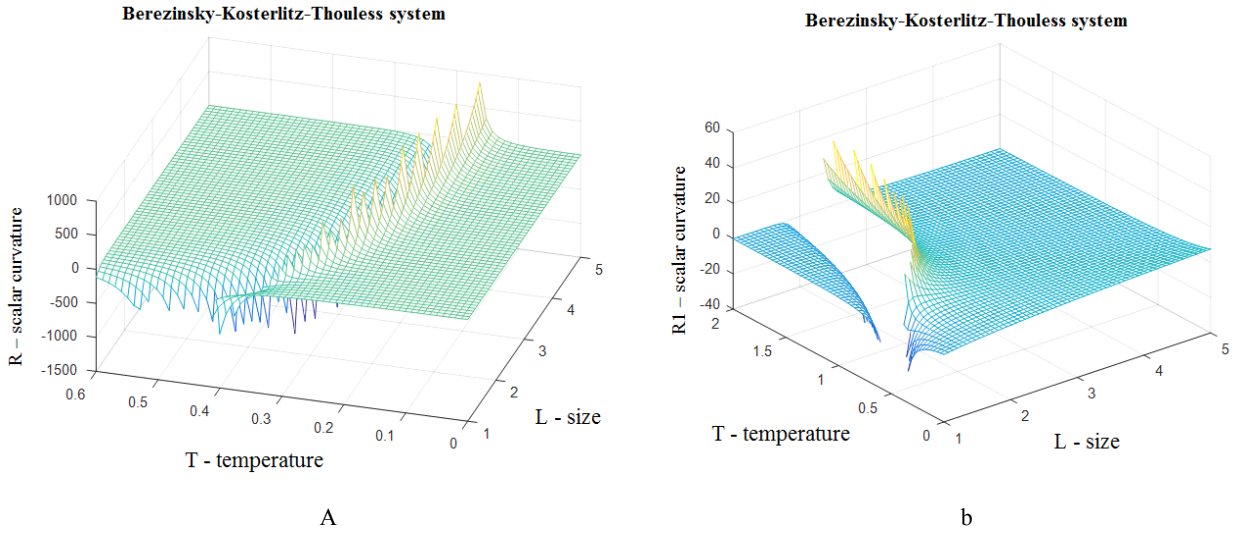

A b

Figure 4 - Dependence of the scalar curvature on temperature and size of the system:
a) metrics calculated by formula (1), b) metrics calculated by formula (2)

Formulas (11) and (14), as well as Figures 4a and 4b show that the scalar curvatures for metrics (1) and (2) become singular at $T_1(L) = \frac{1}{2(1+\ln(L))}$ and $T_2(L) = \frac{1}{2(1-\ln(L))}$ respectively. At these values of T and L parameters, GTD predicts possible phase transitions. Moreover, if using the metrics (1), then the phase transition is located below the BKT transition (in given units $T_c = \frac{1}{2}$), and if using (2), then above. At larger values of parameter T the curvatures, and thus the intensity of the interaction between the particles of the system (both for metrics (1) and for (2)) are close to zero.

5. Conclusion. Using GTD method in this work, the metric tensors and scalar curvatures are calculated for equilibrium manifolds of two-dimensional quantum systems.

The ideal two-dimensional Bose-gas with a finite number of particles and BKT system are considered. Chemical potential depending on temperature and area and the free energy depending on temperature and size of the system were taken as thermodynamic potentials for these thermodynamic systems, respectively.

The paper also presents 3-dimensional figures which clearly show at which values of thermodynamic variables the scalar curvatures tend to infinity or to zero that indicates possible phase transitions and possible compensation of interactions by quantum effects.

It is shown that both versions of metrics (1) and (2) for an ideal two-dimensional Bose-gas lead to the same location of the lines where the scalar curvatures become singular. This location of the lines consistents with the region in which the phase transition occurs (the Bose condensation in the two-dimensional ideal Bose gas). It is also shown that for large values of the temperature and area the curvatures are close to zero and this corresponds to the classical ideal two-dimensional gas.

When considering BKT system using GTD method, possible new phase transitions (calculations based on metrics (1) and (2)) have been found. Calculation by metrics (1) leads to a possible phase transition located below the BKT transition, while calculation by metrics (2) leads to a possible phase transition located above. For large values of the temperature the curvatures, and hence the interactions between particles of the system (both for metric (1) and for (2)) are small.

Д.М. Зазулин[1,2], С.Е. Кемелжанова[1], И. Сатышев[3], О. Ормантаев[1]

[1] Әл-Фараби атындағы ҚазҰУ, Алматы, Қазақстан;
[2] Ядролық физика институты, Алматы, Қазақстан;
[3]Алматы ядролық физика институты, Алматы, Қазақстан

ГЕОМЕТРОТЕРМОДИНАМИКАНЫ ЕКІӨЛШЕМДІ ЖҮЙЕГЕ ҚОЛДАНУ: ИДЕАЛДЫ БОЗЕ ГАЗ ЖӘНЕ КҮШТІ ӨЗАРА ӘСЕРЛЕСУ ЖҮЙЕСІ

Аннотация. Жұмыста Березин-Костерлиц-Таулес жүйесі мен екіөлшемді идеалды Бозе-газ термодинамикалық жүйесі бойынша тепе-теңдіктің көптүрлілік қасиеті геометротермодинамика әдісі арқылы зерттелді. Термодинамикалық потенциалды есепке алмай Лежандр түрлендіруіне қатысты инвариантты нәтижелер алынды. Қарастырып отырған жүйелерге сәйкес өлшемдер мен скалярлық қисықтық есептелді және қасиеттері сипатталды.

Екіөлшемді кванттық термодинамикалық жүйелерді зерттеу қазіргі кезде өзекті саналады. Мұндай жүйелерге мысалы, топологиялық оқшаулағыш, графен, Холлдың кванттық эффектісі бар жүйелер және т.б. жүйелер жатады. Бозе-Эйнштейн және Ферми Дирак үлестірулерінен өзгеше екіөлшемді кванттық жүйеде статистикалық үлестіру болуы мүмкін. Осы термодинамикалық жүйелерді геометротермодинамика әдісі арқылы зерттеу барысында жаңа нәтижелер алынды.

Зерттеу барысында геометротермодинамиканы қолдана отырып, екіөлшемді идеалды Бозе газының және Березин-Костерлиц-Таулес жүйесінің термодинамикалық қасиеттерін қарастырдық. Зерттеу барысында негізгі мақсатымыз – бірінші кезеңге қатысты Бозе-Эйнштейн конденсациясын көбейту және екінші кезеңге сәйкес ықтимал жаңа фазалық ауысуды іздестіру. Жоғарыда аталған термодинамикалық жүйелерді зерттеу үшін сәйкес тепе-теңдіктің көптүрлілігіне қатысты ковариантты метрикалық тензорды, детерминанттарды, Кристофел символын, қисықтық тензоры және сәйкес скалярлық қисықтықты есептедік.

Термодинамикалық потенциалды пайдаланып, температура мен ауданның кең аумағына сәйкес геометриялық шамаларды Matlab жүйесін қолдана отырып қарастырдық. Әрбір геометриялық шамалар үшін нақты формулалар алынды. T және S параметрлерінің белгілі бір диапазонына есептелген скалярлық қисықтардың мысалы суретте көрсетілді. Суреттен T және S параметрлеріне байланысты қисықтардың әртүрлі болуына қарамастан екі метрикаға сәйкес қисықтарға арналған сингулярлардың орналасуына қатысты жалпы ортақ нәтиже беретінін көруге болады.

Арықарай Березин-Костерлиц-Таулес жүйесіне геометротермодинамика әдісін қолдандық. Бұл екіөлшемді жүйе Бозе жүйесіне қатысты күшті әрекеттесетін бөлшектерді қарастырады. Осы жүйедегі фазалық ауысулар толық зерттелмеген. Сондықтан бұл жерде бөлшектердің соңғы саны және БКТ жүйесі бар идеалды екіөлшемді Бозе – газ қарастырылған. Термодинамикалық жүйенің термодинамикалық потенциалы болғандықтан, сәйкесінше жүйенің өлшемі және температураға тәуелділігі, еркіндік энергиясы, аудан мен температураға тәуелділігі, химиялық потенциалы есептелді.

Сондай-ақ үшөлшемді сызбалар берілген, олар термодинамикалық айнымалылардың қандай шамалары шексіздікке немесе нөлге ұмтылатындығын көрсетеді, бұл фазалардың ауысуы мен кванттық әсер арқылы өзара әрекеттесудің ықтималдығын көрсетеді. Идеалды екіөлшемді Бозе газына арналған метриканың екі нұсқасы да скалярық қисықтың сингуляр болып бір сызықтың бойында орналасқаны көрсетілген. Бұл орналасқан сызықтар екіөлшемді Бозе газындағы фазалық ауысулар жүретін аймаққа сәйкес келеді. Сонымен қатар, температура мен ауданның үлкен мәні нөлге ұмтылатындықтан классикалық идеалды екіөлшемді газға сәйкес келеді.

Березин-Костерлиц Таулес жүйесіне геометротермодинамика әдісін қолдану барысында жаңа фазалық ауысу анықталды. Метрика бойынша есептегенде ықтимал фазалық ауысу Березин-Костерлиц-Таулес ауысуынан төмен орналасқан фазалық көшуге, ал есептеу барысында жоғарыда орналасқан ықтимал фазалық ауысуға әкеледі.

Түйін сөздер: геометротермодинамика, Лежандр түрлендіруі, метрикалық тензор, скалярлық қисық, екіөлшемді Бозе-газ, Березин-Костерлиц-Таулес жүйесі.

Д.М. Зазулин[1,2], С.Е. Кемелжанова[1], И. Сатышев[3], О. Ормантаев[1]

[1] КазНУ им. аль-Фараби, Алматы, Казахстан;
[2] Институт Ядерной Физики, Алматы, Казахстан;
[3]Алматинский институт ядерной физики, Алматы, Казахстан

ПРИМЕНЕНИЕ ГЕОМЕТРОТЕРМОДИНАМИКИ К ДВУМЕРНЫМ СИСТЕМАМ: ИДЕАЛЬНОМУ БОЗЕ-ГАЗУ И СИСТЕМЕ С СИЛЬНЫМ ВЗАИМОДЕЙСТВИЕМ

Аннотация. Методом геометротермодинамики в настоящей работе исследованы свойства равновесных многообразий следующих термодинамических систем: двумерного идеального Бозе-газа и системы Березинского-Костерлица-Таулеса. Получены результаты, инвариантные относительно преобразований Лежандра, т.е. независимые от выбора термодинамического потенциала. Для рассматриваемых систем рассчитаны соответствующие метрики и скалярные кривизны, а также описаны их свойства.

Изучение двумерных квантовых термодинамических систем в настоящее время является актуальным. Достаточно упомянуть, что к таким системам относятся, например, топологические изоляторы, графен, системы с квантовым эффектом Холла и т.д. Двумерные квантовые системы могут иметь статистическое распределение, отличное от распределений Ферми-Дирака и Бозе-Эйнштейна. Геометрические подходы в изучении этих термодинамических систем, безусловно, открывают новые перспективы.

В настоящей работе с помощью геометротермодинамики было проведено исследование термодинамических свойств идеального двумерного Бозе-газа и системы Березинского-Костерлица-Таулеса. Основной целью было воспроизведение конденсации Бозе-Эйнштейна для первой системы и поиск возможных новых фазовых переходов для второй.

Для изучения вышеназванных термодинамических систем мы вычисляли последовательно ковариантные метрические тензоры соответствующих равновесных многообразий, их детерминанты, далее контравариантные метрические тензоры, символы Кристофеля, тензоры кривизны и соответствующие скалярные кривизны.

Используя термодинамический потенциал, нами были получены (с помощью системы Matlab) соответствующие геометрические величины в широком диапазоне температуры и площади. Для каждой геометрической величины также были получены явные формулы, но ввиду громоздкости в настоящей работе мы их не приводим. Примеры вычисленных скалярных кривизн для некоторого диапазона параметров T и S показаны на рисунках. Из рисунков также видно, что несмотря на существенно различное поведение кривизн в зависимости от параметров T и S обе метрики приводят к одному общему результату относительно расположения сингулярностей для соответствующих кривизн.

Далее мы применили геометротермодинамики для системы Березинского-Костерлица-Таулеса. Это двумерная система Бозе – частиц с сильным взаимодействием (сильным в том смысле что вклад в термодинамику системы вносят топологические дефекты - точечные вихри) со сложной, до конца не изученой системой фазовых переходов. Рассмотрены идеальный двумерный Бозе-газ с конечным числом частиц и система БКТ. В качестве термодинамических потенциалов для этих термодинамических систем брались, соответственно, химический потенциал, зависящий от температуры и площади и свободная энергия, зависящая от температуры и размера системы.

В работе также приведены 3-мерные рисунки, на которых хорошо видно, при каких значениях термодинамических переменных скалярные кривизны стремятся к бесконечности или к нулю, что указывает на возможные фазовые переходы и на возможную компенсацию взаимодействий квантовыми эффектами соответственно.

Показано, что оба варианта метрик для идеального двумерного Бозе-газа приводят к одному и тому же расположению линий, где скалярные кривизны становятся сингулярными. Это расположение линий согласуется с областью, в которой происходит фазовый переход - Бозе конденсация в двумерном Бозе-газе. Также показано, что при больших значениях параметров температуры и площади кривизны близки к нулю и это соответствует классическому идеальному двумерному газу.

При рассмотрении системы Березинского-Костерлица-Таулеса методом геометротермодинамики были обнаружены возможные новые фазовые переходы. Расчет по метрике приводит к возможному фазовому переходу расположенному ниже перехода Березинского-Костерлица-Таулеса, а расчет приводит к возможному фазовому переходу расположенному выше.

Ключевые слова: геометротермодинамика, преобразования Лежандра, метрический тензор, скалярная кривизна, двумерный Бозе-газ, система Березинского-Костерлица-Таулеса.

Information about authors:

Zazulin D.M., Candidate of physical and mathematical Science, associate Professor, Department of Nuclear and Theoretical Physics, al-Farabi Kazakh National University, Almaty, Kazakhstan, denis_zazulin@mail.ru, https://orcid.org/0000-0003-2115-6226;

Kemelzhanova S.E., second year doctoral student, Department of Nuclear and Theoretical Physics, al-Farabi Kazakh National University, Almaty, Kazakhstan, kemelzhanova.sandugash@gmail.com, https://orcid.org/0000-0002-5469-3960

Satyshev I., master, Department of Nuclear and Theoretical Physics, al-Farabi Kazakh National University, Almaty, Kazakhstan, satyshevi@gmail.com, https://orcid.org/0000-0002-9121-8173;

Ormantaev O., first year master, Department of Nuclear and Theoretical Physics, ai-Farabi Kazakh National University, Almaty, Kazakhstan, ormantaev.orken@gmail.com https://orcid.org/0000-0001-7819-0551,

Information about the reviewer:

Abishev Medeu Erzhanovish – corresponding members of NAS RK, Professor of physical and mathematical Science, associate Professor, Department of Nuclear and Theoretical Physics, al-Farabi Kazakh National University, Almaty, Kazakhstan, abishevme@gmail.com;

Zhaugasheva Saule Amanbaevna - Candidate of physical and mathematical Science, associate Professor, Department of Nuclear and Theoretical Physics, al-Farabi Kazakh National University, Almaty, Kazakhstan, zhaugashevas@gmail.com.

REFERENCES

[1] Quevedo H. (2007) Geometrothermodynamics, J. Math. Phys. 48, 013506, DOI: https://doi.org/10.1063/1.2409524

[2] Quevedo H., Sanchez A., Taj S., Vazquez A. (2011) Phase transitions in Geometrothermodynamics, Gen. Rel. Grav. 43, 1153, arXiv:1010.5599

[3] Quevedo H., Sasha A. Zaldivar (2015) A geometrothermodynamic approach to ideal quantum gases and Bose-Einstein condensates, arXiv:1512.08755v3

[4] Quevedo H., Ramirez A. (2012) A geometric approach to the thermodynamics of the van der Waals system, arXiv:1205.3544

[5] Bravetti, D., Momeni R., Myrzakulov R. and Quevedo H. (2013) Geometrothermodynamics of higher dimensional black holes, arXiv:1211.7134

[6] Quevedo H., Sánchez A.,Vázquez A. (2015) Relativistic like structure of classical thermodynamics. Gen. Rel. Grav. 47, 4, P.36. DOI: 10.1007/s10714-015-1881-9

[7] Quevedo H., Nettel F., Cesar S. Lopez-Monsalvo, Bravetti A. (2014) Representation invariant Geometrothermodynamics: applications to ordinary thermodynamic systems. J.Geom.Phys. 81, P.1. DOI: 10.1006/j.geomphys.2014.03.001

[8] Vazquez A., Quevedo H., Sanchez A. (2010) Thermodynamic systems as extremal hypersurfaces. J. Geom. Phys. 60, P.1942. DOI: 10.1006/j.geomphys.2010.08.001

[9] Горелкин В.Н. (2010) Лекции по статистической физике, https://mipt.ru/education/chair/theoretical_physics/php

[10] Lifshitz E.M., Pitaevskii L.P. (2013) Statistical Physics: Theory of the Condensed State, Part 2, Volume 9, ISSN 978-0750626361

[11] Berezinskii V.L. (1971) Destruction of long-range order in one-dimensional and two-dimensional systems having a continuous symmetry group I. Classical systems. JETP 32, 3, P.493.

[12] Berezinskii V.L. (1972) Destruction of long-range order in one-dimensional and two-dimensional systems possessing a continuous symmetry group. II. Quantum systems. JETP 34, 3, P. 1144-1156.

[13] Kosterlitz J.M., Thouless D.J. (1973) Ordering, metastability and phase transitions in two-dimensional systems, J.Phys. C6, P.1181. DOI: 10.1088/0022-3719/6/7/010

[14] Kosterlitz J.M. (1974) The critical properties of the two-dimensional xy model. J. of Phys. C: Solid State Physics, 7, 6, P.1046. DOI: 10.1088/0022-3719/7/6/005

[15] Kosterlitz J.M. (2016) Kosterlitz-Thouless physics: a review of key issues Rep. Prog. Phys. 79, 026001. DOI: 10.1088/0034-4885/79/2/026001

[16] Hebard A.F. and Paalanen M.A. (1984) Pair-breaking model for disorder in two-dimensional superconductors, Phys. Rev. B 30, P.4063. https://doi.org/10.1103/PhysRevB.30.4063

[17] Marković N., Christiansen C., Goldman A.M. Thickness-magnetic field phase diagram at the superconductor-insulator transition in 2d, Phys. Rev. Lett. 81, 23, P.5217. https://doi.org/10.1103/PhysRevLett.81.5217

[18] Fisher M.P.A. (1990) Quantum phase transitions in disordered two-dimensional superconductors Phys. Rev. Lett. 65, P.923. https://doi.org/10.1103/PhysRevLett.65.923

[19] Hebard A.F. and Paalanen M.A. (1990) Magnetic-field-tuned superconductor-insulator transition in two-dimensional films, Phys. Rev. Lett. 65, P.927. https://doi.org/10.1103/PhysRevLett.65.927

[20] Ryzhov V.N., Tareyeva E.E., Fomin Yu.D., Tsiok E.N. (2017) Berezinskii-Kosterlitz-Thouless transition and two-dimensional melting Phys. Usp. 60, P.857. https:// doi.org/10.3367/UFNr.2017.06.038161

NEWS
OF THENATIONAL ACADEMY OF SCIENCES OF THE REPUBLIC OF KAZAKHSTAN
PHYSICO-MATHEMATICAL SERIES
ISSN 1991-346X **https://doi.org/10.32014/2020.2518-1726.68**
Volume 4, Number 332 (2020), 77 – 85

UDC 539.142
MRNTI 29.15.03

M. Odsuren[1]*, A. Sarsembayeva[2], G. Khuukhenkhuu[1], S. Davaa[1], A. Zolbayar[1], B. Usukhbayar[1], A. Tursukh[1], K. Katō[3], M. Abyshev[2]

[1]School of Engineering and Applied Sciences and Nuclear Research Center, National University of Mongolia, Ulaanbaatar, Mongolia;
[2]Department of Physics and Technology, Al-Farabi Kazakh National University, Almaty, Kazakhstan;
[3]Nuclear Reaction Data Centre, Faculty of Science, Hokkaido University, Sapporo, Japan.
E-mail: *odsuren@seas.num.edu.mn; sarsembaeva.a@kaznu.kz; g_khuukhenkhuu@yahoo.com; ts.suren.davaa@gmail.com; zolo.011263@gmail.com; usuhbayar_batsaihan@yahoo.com; tursukh.amgalan@gmail.com; kato-iku@gd6.so-net.ne.jp; medeu.abishev@kaznu.kz

INVESTIGATION OF VIRTUAL STATE OF ^{8}Be+n SYSTEM USING THE COMPLEX SCALING METHOD

Abstract. Nuclear states observed around threshold energies provide us with interesting problems associated with the nuclear cluster structure. Most of them are also interesting astrophysically from the viewpoint of nucleosynthesis.

The first excited $1/2^+$ state in ^{9}Be has been observed as a sharp peak above the ^{8}Be+n threshold energy in the photo-disintegration cross section of $\gamma+^{9}\text{Be}->\alpha+\alpha+n$. Since the size of the peak has a strong influence on the reaction rate of the ^{9}Be synthesis, new experimental data have been investigated. Recently, we performed calculations using an α+α+n three-cluster model together with the complex scaling method (CSM), which well reproduces the recently-observed photo-disintegration cross section. The results indicate that the virtual-state character of the $1/2^+$ state plays an important role in formation of the peak structure appearing in the cross section observed above the ^{8}Be+n threshold. From these results, we discuss that the first excited $1/2^+$ state in ^{9}Be is a ^{8}Be+*n* virtual state but not resonant one. However, the virtual state cannot be directly obtained as an isolated pole solution in the CSM, because the scaling angle in the CSM cannot be increased over the position of the virtual state pole on the negative imaginary axis of the complex momentum plane.

In our previous work, the cross section form of the photodisintegration and the phase shift behavior of a virtual state assuming a simple two-body model are discussed. In the CSM, the virtual state cannot be obtained as an isolated solution, but the continuum solutions are considered to include the effect of the virtual state. There is no previous study that the CSM can be applied successfully to virtual state. Applying the CSM to the simple schematic potential model, we have shown that the sharp peak of the photodisintegration cross section calculated just above the threshold which does not correspond to a usual Breit-Wigner type pole. A new approach for the CSM to describe the virtual state was proposed, and we discussed the pole position of the virtual state using the continuum level density (CLD), the scattering phase shift, and scattering length calculated in the CSM. The next problem is how to distinguish a virtual state from a resonant state and how to see the difference in the observed photo-disintegration cross sections.

The purpose of this work is to investigate the reliability of the virtual state solutions in the CSM as comparing with the solutions of the Jost function method. To investigate the structure of the virtual state, we calculate the energy eigenvalues, phase shifts and photodisintegration cross section of the two-body model with a two-range Gaussian potential by changing the strength of the attractive potential.

Keywords: Complex scaling method, continuum level density, phase shift.

Introduction. It is a long-standing problem to determine its resonance energy and width of the first excited $1/2^+$ state of ^{9}Be, which is closely connected with the problem to clarify whether it is a resonant state or not. Recently, we studied the $1/2^+$ unbound state of ^{9}Be and the photodisintegration cross section

applying the complex scaling method (CSM) [1-2] to the *α*+*α*+*n* three-cluster model [3]. The results indicate that there is no sharp resonant state corresponding to the distinguished peak observed just above the ^{8}Be+n threshold in the photodisintegration cross section of ^{9}Be. However, the recent experimental cross section data [4, 5] can be well explained by the *α*+*α*+*n* calculation. From these results, we concluded that the first excited $1/2^{+}$ state in ^{9}Be is a ^{8}Be+n virtual state but not resonant one.

The purpose of this work is to investigate the reliability of the virtual state solutions in the CSM as comparing with the solutions of the Jost function method. To investigate the structure of the virtual state, we calculate the energy eigenvalues, phase shifts and photodisintegration cross section of the two-body model with a two-range Gaussian potential by changing the strength of the attractive potential.

Complex scaled two-body model. To understand the characterization of the virtual state [7-9], we investigate the simple two-body model corresponding to the ^{8}Be+n structure in ^{9}Be. In this model, both clusters are assumed to have no-spin and the relative motion between clusters is described by the following Schrödinger equation:

$$H\Psi^{\nu}_{J^{\pi}} = E_{\nu}\Psi^{\nu}_{J^{\pi}} . \tag{1}$$

Where J^{π} is the spin and parity, and ν is the state index. The Hamiltonian is given as

$$H = -\frac{\hbar^2}{2\mu}\nabla^2 + V(r) . \tag{2}$$

Where we assume a simple Gaussian potential

$$V(r) = -V_1 \exp(-ar^2) , \tag{3}$$

where a = 0.16 fm^{-2}. For simplicity, we put $\frac{\hbar^2}{\mu} = 1$ (MeV fm^2).

In this study we use the CSM, in the CSM the relative coordinate r is transformed as

$$U(\theta): \quad r \to re^{i\theta} , \tag{4}$$

Where $U(\theta)$ is a complex scaling operator given by a scaling parameter θ. Applying this trans formation to Eq.(1), we obtain the complex-scaled Schrödinger equation:

$$H^{\theta}\Psi^{\nu}_{J^{\pi}}(\theta) = E^{\theta}_{\nu}\Psi^{\nu}_{J^{\pi}}(\theta) . \tag{5}$$

The complex-scaled Hamiltonian H^{θ} and wave function $\Psi^{\nu}_{J^{\pi}}(\theta)$ are defined as $U(\theta)HU(\theta)^{-1}$ and $U(\theta)\Psi^{\nu}_{J^{\pi}}$, respectively, and see Ref. [10] for detail.

Applying the L^2 basis function method, the wave function is expanded as

$$\Psi^{\nu}_{J^{\pi}}(\theta) = \sum_{n=1}^{N} c_n^{J^{\pi}\nu}(\theta)\phi_n(r) , \tag{6}$$

Where $\{\phi_n(r)\}$ is an appropriate basis function set. The expansion coefficients $c_n^{J^{\pi}\nu}(\theta)$ and the complex energy eigenvalues E^{θ}_{ν} are obtained by solving the complex-eigenvalue problem.

The scattering phase shifts $\delta^{J^{\pi}}(E)$ for the Hamiltonian Eq.(2) can be calculated using the solutions of the complex scaled Schrödinger Eq.(5) with and without interaction.

From Eq. (12) in Ref. [11-14], we have

$$\delta^{J^\pi}(E) = N_b\pi + \sum_{r=1}^{N_r^\theta}\left\{-\cot^{-1}\left(\frac{E-E_r^{res}}{\Gamma_r/2}\right)\right\} + \sum_{c=1}^{N_c^\theta}\left\{-\cot^{-1}\left(\frac{E-\varepsilon_c^r}{\varepsilon_c^i}\right)\right\} - \sum_{k=1}^{N}\left\{-\cot^{-1}\left(\frac{E-\varepsilon_k^{0r}}{\varepsilon_k^{0i}}\right)\right\}, \quad (7)$$

where the eigenvalues E_ν^θ are classified into N_b bound states, N_r^θ resonant states and N_c^θ continuum states for a given θ; $N = N_b + N_r^\theta + N_c^\theta$. The N eigenvalues of the free Hamiltonian given by the only kinetic energy operator are expressed as $\varepsilon_k^{0r} - i\varepsilon_k^{0i}$ $(k = 1,\ldots,M)$.

The photodisintegration cross section due to the electric dipole transition from the ground state $J_{gs}^\pi = 1^-$ to the continuum $J_f^\pi = 0^+$ states is expressed as

$$\sigma_{E1}(E_\gamma) = \frac{16\pi^2}{9}\cdot\left(\frac{E_\gamma}{\hbar c}\right)\frac{dB(E1,E_\gamma)}{dE_\gamma}, \quad (8)$$

where the transition strength is calculated by using the solutions of the CSM

$$\frac{dB(E1,E_\gamma)}{dE_\gamma} = -\frac{1}{\pi}\frac{1}{2J_{gs}+1}\mathrm{Im}\left[\sum_{\nu=1}^{N}\left\langle\tilde{\Psi}_{J_{gs}^\pi}^{gs}(\theta)\right\| \hat{O}^{\theta+}(E1) \left\|\Psi_{J_f^\pi}^{\nu}(\theta)\right\rangle \times\frac{1}{E-E_\nu^\theta}\left\langle\tilde{\Psi}_{J_f^\pi}^{\nu}(\theta)\right\| \hat{O}^{\theta}(E1) \left\|\Psi_{J_{gs}^\pi}^{gs}(\theta)\right\rangle\right]. \quad (9)$$

Numerical results. To understand the characterization of a virtual state, we investigate a simple two-body potential model for the ^{8}Be+n system in the CSM. The potential strength V_1 in Eq.(3) is taken to reproduce one bound state of s-and p-waves. The energy levels of $J^\pi = 0^+$ and 1^- obtained by solving the complex-scaled Schrödinger equation which are presented schematically in figure 1. The potential strength V_1 is taken to reproduce one bound 0^+state of s-waves. In this model, this 0^+ solution is assumed as the Pauli forbidden state, because this model simulates ^{8}Be(0^+)+n. Hence the 1^- solution describes the ground state, and there is no 0^+ bound state.

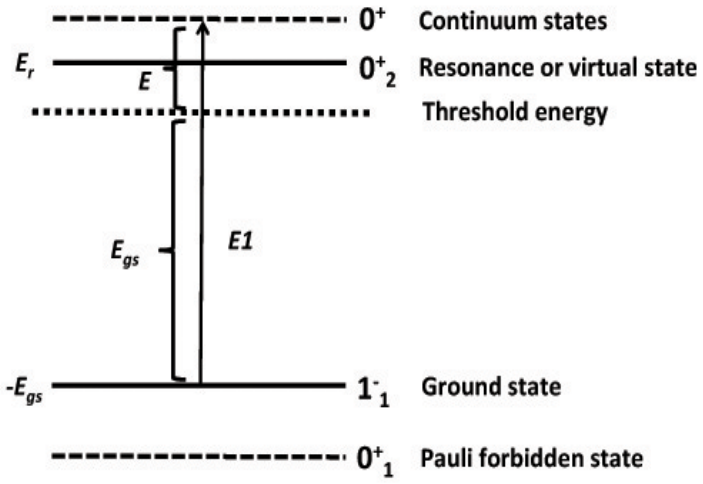

Figure 1 - Schematic diagram of the energy spectrum

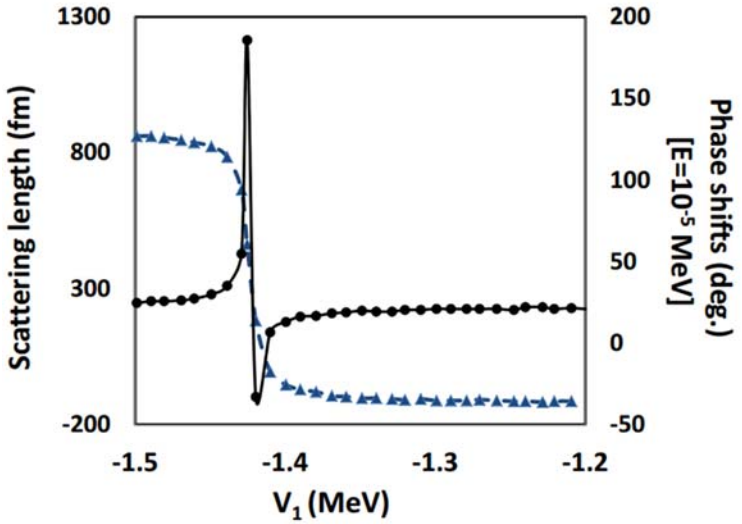

Figure 2 - The scattering length and phase shifts

In this work, we first apply different method ideally the Jost function method [8] for analyzing the virtual state to the simple schematic potential and two-body model. The Jost function method is applicable not only to study resonant states but also bound and scattering states. Using the Jost function method, poles of the *S*-matrix for a virtual state can be obtained without the complex rotation in the same way as bound states. The Jost function method is applied to calculate scattering phase shifts and scattering length at different strengths between $V_1 = -1.5$ MeV and -1.2 MeV. In figure 2, we show the calculated scattering length and scattering phase shifts applying the Jost function method. The blue with filled triangle and black with filled circle lines show the phase shifts and scattering length, respectively. From the scattering length we find that an increase at the strength $V_1 = -1.43$ MeV and sudden decrease at the strength $V_1 = -1.42$ MeV. It can be seen from figure 2, the scattering length shows an extreme sensitivity to the choice of the potential strength V_1. This result indicates the existence of the virtual state at the strength $V_1 = -1.42$ MeV which is consistent with our previous results in Ref. [6].

Next we consider the different case when there exists the resonance state to see how the resonance state contributes to the photodisintegration cross section. It is needed to perform calculation using both types of potentials (with and without a repulsion term). As a purely attractive potential we choose the potential Eq.(3) and with a repulsive term of the potential we employ as following

$$V(r) = -V_1 \exp(-ar^2) + V_2 \exp(-\gamma r^2), \tag{10}$$

Where $\gamma = 0.04$ fm^{-2}. We adjusted the strength of the potential for second term of Eq.(10) so that the resonant state generates when the V_2 switch on.

To investigate the structure of the obtained state, we calculate the energy eigenvalues of the system by changing the strength of the repulsive potential V_2 in Eq.(10), which is shown in figure 3. In the present calculation, when the strength of the repulsive potential $V_2 = 0.7$ MeV, the resonance pole suddenly appears just below the threshold. This resonance pole with a narrow decay width moves smoothly to the bound state region as the repulsive potential becomes zero, and we finally obtain the bound state with the region of $V_2 = 0.6$ MeV. On the other hand, we consider the pole trajectory in the opposite case of the repulsive potential with $V_2 = 0.7$ MeV. If the resonance exists, the pole with a narrow decay width should appear above the threshold as the analytical continuation from the resonance pole. However, we found that no resonances appear above the threshold for $V_2 > 0.7$ MeV of the repulsive potential.

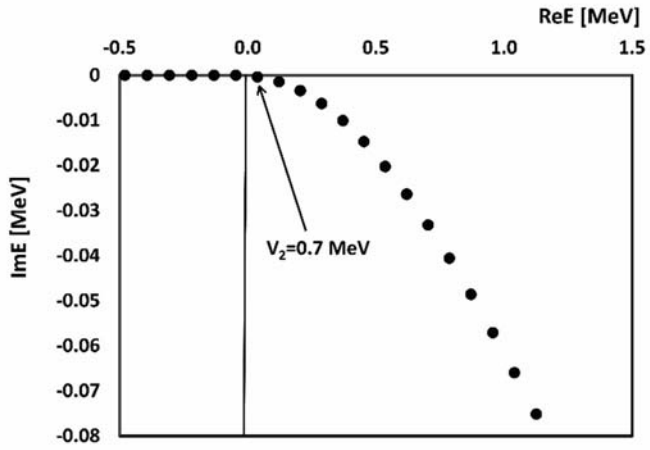

Figure 3 - Pole trajectory of the state in a complex energy plane by changing the repulsive potential

We consider the different case when there exists the resonance state to see how the resonance state contributes to the phase shifts. By using the repulsive potential with $V_2 = 0.7$ MeV, the resonance state is obtained with the energy and decay width being 0.038 and 6.58×10^{-4} MeV, respectively.

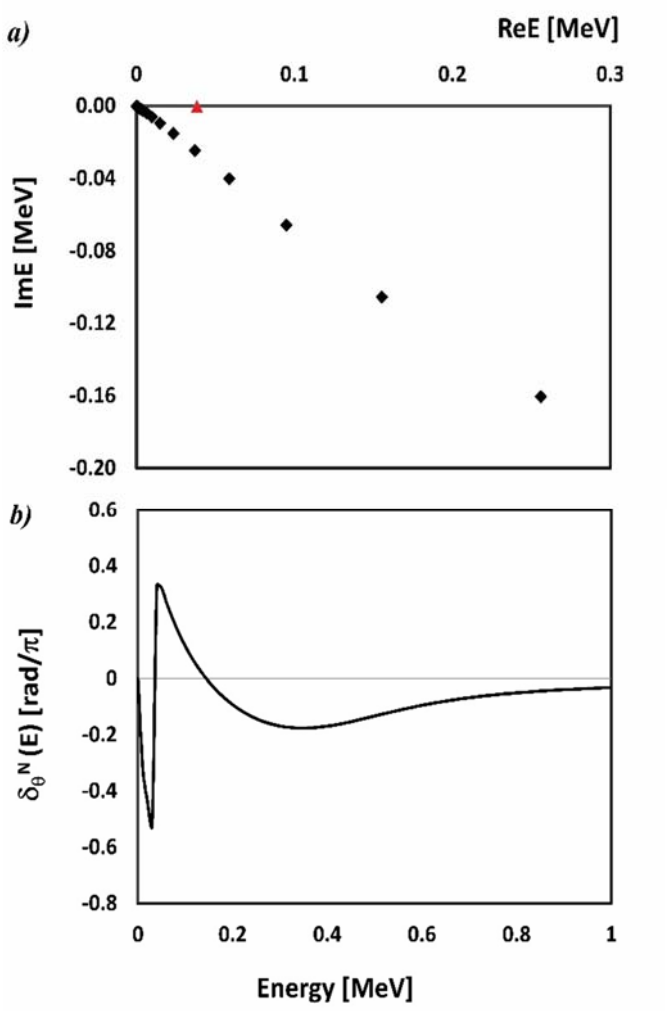

Figure 4 - Upper panel: Energy eigenvalues on the complex energy plane at V_1=-1.42 MeV and V_2=0.7 MeV. Bottom panel: Phase shifts at V_1=-1.42 MeV and V_2=0.7 MeV

In figure 4*a*) we show the distribution of eigenvalues in the complex energy plane calculated at the strengths $V_1 = -1.42$ MeV and $V_2 = 0.7$ MeV in Eq.(10). It can be seen from figure 4*a*), the segregated pole is obtained near the zero energy imaginary part which means a narrow resonance state is calculated and it is presented as a red triangle and continuum states are displayed by black diamonds. We can calculate the scattering phase shift using the eigenvalue solutions of $H(\theta)$ and $H(\theta)$ in the CSM [10], where $H_0(\theta)$ is the free-Hamiltonian without potentials. In figure 4*b*) the scattering phase shift is given which is calculated at the strengths $V_1 = -1.42$ MeV and $V_2 = 0.7$ MeV in Eq.(10). It is found that the effect of the narrow resonance state to the calculated phase shift is remarkable.

We investigate $E1$ transition from the 1^- ground state to the excited 0^+ unbound state including the 0_2^+ state. From the $E1$ transition we can calculate photodisintegration cross section using Eq.(9). In the present calculation, when the strength of the repulsive potential $V_2 = 0.7$ MeV, the resonance pole appears just below the threshold. In figure 5, we show the photodisintegration cross section, which shows a sharp peak at the resonance energy. It can be seen from the calculated photodisintegration cross section, we obtain the peak with a usual Breit-Wigner type pole and the peak shape of the calculated photodisintegration cross section is much different from figure 4 in Ref.[6] for the virtual state. This trend is much different from that figure 4 in Ref. [6]. Comparing with Fig. 4 in Ref.[6], we can understand how the shape of the photodisintegration cross section deviates from the Breit-Wigner type form for virtual state. As was discussed by Fano [15], deviation from the Breit-Wigner form can be investigated by calculating the interference between resonance and continuum terms.

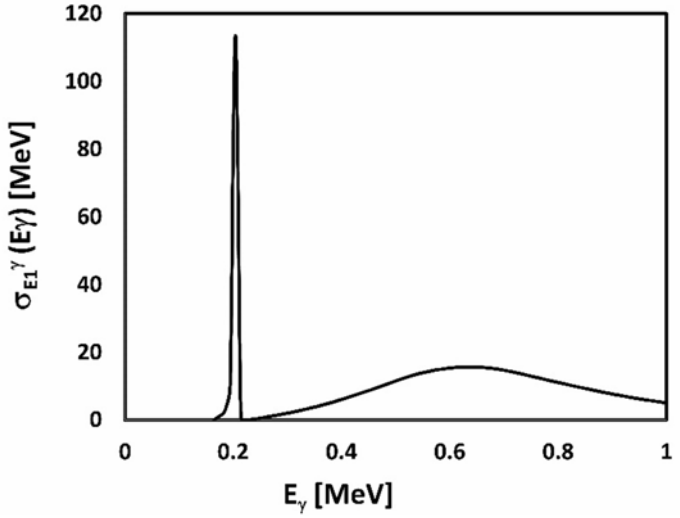

Figure 5 - Photodisintegration cross section at V_1=-1.42 MeV and V_2=0.7 MeV

Discussion and summary. We investigate the character of the virtual state using the CSM and the Jost function method. In both methods, the virtual state is obtained $V_1 = -1.42$ MeV. The pole trajectory of the resonance state is calculated at different repulsive potential strengths.

In the present calculation, we do not investigate the decomposed photodisintegration cross section in detail. It would be important to understand the structure of the resonance states and the virtual states, and the detailed analysis will be performed in a forth coming paper.

Acknowledgements

This work was supported by funds provided by the National University of Mongolia for Asia Research Center project (ARC2020-2021 P2019-3710). The numerical calculation was supported by the MINATO cluster computing system at the Nuclear Research Center, National University of Mongolia.

**М. Одсурэн[1]*, А.Т. Сарсембаева[2], Г. Хуухэнхуу[1], С.Даваа[1],
А. Золбаяр[1], Б.Усухбаяр[1], А. Турсух[1], К. Като[3], М.Е. Абишев[2]**

[1]Инженерлік және қолданбалы ғылымдар институты, Ядролық зерттеулер орталығы,
Моңғолия Ұлттық Университеті, Улан-Батор;
[2]Физика-техникалық факультеті, Әл-Фараби атындағы ҚазҰУ, Казақстан;
[3]Ядролық реакция деректер орталығы, Ғылым факультеті, Хоккайдо университеті, Саппоро, Жапония

^{8}Be + n ЖҮЙЕСІН КЕШЕНДІ МАСШТАБТАУ ӘДІСІ АРҚЫЛЫ ВИРТУАЛДЫ КҮЙІН ЗЕРТТЕУ

Аннотация. Табалдырық энергиялардың айналасында байқалған ядролық күйлер бізге ядролық кластер құрылымымен байланысты қызықты сұрақтар мен мәселелерді көтереді. Олардың көпшілігі нуклеосинтез тұрғысынан қарастырғанда астрофизикалық қызығушылық тудырады.

^{9}Be-дегі алғашқы қозған $1/2^{+}$ күйі γ + ^{9}Be-> α + α + n-дің фото-ыдырау қимасындағы ^{8}Be + n реакциясының табалдырық энергиясынан жоғары айқын шың ретінде байқалды. Шыңның өлшемі ^{9}Be синтезінің реакция жылдамдығына қатты әсер ететіндіктен, жаңа тәжірибелік мәліметтер зерттелді. Жақында біз үш өлшемді α + α + n моделін қолдана отырып, кешенді масштабтау әдісі (КМӘ) қолдандық, ол жақында байқалған фото-ыдырау қимасына жақсы сәйкес келеді. Нәтижелер $1/2^{+}$ күйінің виртуалды күйінің сипаттамасы ^{8}Be + n шегінен жоғары көлденең қимада пайда болатын шың құрылымын қалыптастыруда маңызды рөл атқаратынын көрсетеді. Осы нәтижелерге сүйене отырып, ^{9} Be-дегі алғашқы қозған $1/2^{+}$ күйі ^{8}Be + *n* виртуалды күйі екенін талқылаймыз, бірақ ол резонанс тудырмайды. Алайда виртуалды күйді кешенді масштабтау әдісінде (КМӘ) оқшауланған полюстің шешімі ретінде алу мүмкін емес, өйткені кешенді масштабтау әдісіндегі масштабтау бұрышы күрделі импульстік жазықтықтың виртуалды осіне қатысты виртуалды күй полюсінің орнына көбейтілмейді.

Біздің алдыңғы жұмысымызда фотодисинтеграцияның көлденең қимасы және виртуалды күйдің фазалық беталысы қарапайым екі денелі модельдің болжамы негізінде қарастырылды. Кешенді масштабтау әдісінде (КМӘ) виртуалды күйді оқшауланған шешім ретінде алу мүмкін емес, бірақ континуумдық шешімдер виртуалды күйдің әсерін қамтиды деп есептеледі. Кешенді масштабтау әдісін (КМӘ) виртуалды күйге сәтті қолдануға болатындығы туралы зерттеулер кездеспейді. Схемалық потенциалдың қарапайым моделіне кешенді масштабтау әдісін қолдана отырып, біз шекті деңгейден жоғары есептелген фотодиинтеграция қимасының шыңы Брейт-Вигнер типті полюсте сәйкес келмейтінін көрсеттік.

Виртуалды күйді сипаттау үшін кешенді масштабтау әдісінде жаңа тәсіл ұсынылды, біз виртуалды күйдің полюсті жағдайын үзіліссіз деңгейдің тығыздығын (ҮДТ), шашырау фазалық ығысуын және кешенді масштабтау әдісінде (КМӘ) есептелген шашырау ұзындығын қолдана отырып талқыладық. Келесі мәселе виртуалды күйді резонанстық күйден қалай ажыратуға және байқалған фото-ыдыраудың көлденең қималарындағы айырмашылықты көру жолдары болып саналады.

Жұмыстың мақсаты – Йост функциясы әдісінің шешімімен салыстырғанда кешенді масштабтау әдісіндегі (КМӘ) виртуалды күй шешімінің сенімділігін зерттеу. Виртуалды күйдің құрылымын зерттеу үшін алдымен тартылыс потенциалының күшін өзгерту арқылы екі диапазонды Гаусс потенциалы бар екі денелі моделіндегі энергияның меншікті мәндерін, фазалық жылжуын және фотодисинтеграция көлденең қимасын есептейміз.

Түйін сөздер: кешенді масштабтау әдісі, үзіліссіз деңгейінің тығыздығы, фазалық ығысу.

**М. Одсурэн[1]*, А.Т. Сарсембаева[2], Г. Хуухэнхуу[1], С.Даваа[1],
А. Золбаяр[1], Б.Усухбаяр[1], А. Турсух[1], К. Като[3],М.Е. Абишев[2]**

[1]Школа инженерных и прикладных наук и Центр ядерно-физических исследований,
Национальный университет Монголии, Улан-Батор;
[2]Физико-технический факультет, КазНУ им.аль-Фараби, Казахстан;
[3]Центр данных по ядерным реакциям, Факультет науки, Университет Хоккайдо, Саппоро, Япония

ИССЛЕДОВАНИЕ ВИРТУАЛЬНОГО СОСТОЯНИЯ СИСТЕМЫ ^{8}Be + n С ИСПОЛЬЗОВАНИЕМ МЕТОДА КОМПЛЕКСНОГО МАСШТАБИРОВАНИЯ

Аннотация. Ядерные состояния, наблюдаемые вокруг пороговых энергий, предоставляют нам весьма интересные вопросы и задачи, связанные со структурой ядерного кластера. Большинство из них также имеет астрофизический интерес с точки зрения нуклеосинтеза.

Первое возбужденное состояние $1/2^+$ в ^{9}Be наблюдалось в виде резкого пика выше пороговой энергии ^{8}Be + n в сечении фоторасщепления γ + ^{9}Be-> α + α + n. Новые экспериментальные данные были исследованы, поскольку размер пика сильно влияет на скорость реакции синтеза ^{9}Be. Недавно мы провели расчеты с использованием трехкластерной модели α + α + n вместе с методом комплексного масштабирования (МКМ), который хорошо воспроизводит недавно наблюдаемое сечение фоторасщепления. Результаты показывают, что характер виртуального состояния $1/2^+$ играет важную роль в формировании структуры пика, появляющейся в поперечном сечении, наблюдаемом выше порога 8Be + n. Исходя из этих результатов, мы обсуждаем, что первое возбужденное состояние $1/2^+$ в ^{9}Be является виртуальным состоянием ^{8}Be + n, но не является резонансным. Однако виртуальное состояние не может быть непосредственно получено как решение с изолированным полюсом в МКМ, потому что угол масштабирования в методе комплексного масштабирования (МКМ) не может быть увеличен по положению полюса виртуального состояния на отрицательной мнимой оси плоскости комплексного импульса.

В нашей предыдущей работе было рассмотрено сечение фоторасщепления и фазовое поведение виртуального состояния в предположении простой модели двух тел. В методе комплексного масштабирования (МКМ) виртуальное состояние не может быть получено как изолированное решение, но считается, что континуальные решения включают в себя влияние виртуального состояния. Нет предыдущих исследований, что метод комплексного масштабирования (МКМ) может быть успешно применен к виртуальному состоянию. Применяя метод комплексного масштабирования (МКМ) к простой модели схематического потенциала, мы показали, что резкий пик сечения фоторасщепления, рассчитанный чуть выше порога, который не соответствует обычному полюсу типа Брейта-Вигнера.

Был предложен новый подход для метода комплексного масштабирования (МКМ) для описания виртуального состояния, и мы обсудили положение полюса виртуального состояния, используя плотность уровня континуума (ПУК), фазовый сдвиг рассеяния и длину рассеяния, вычисленные методом комплексного масштабирования (МКМ). Следующая проблема состоит в том, как отличить виртуальное состояние от резонансного и как увидеть разницу в наблюдаемых сечениях фото-распада.

Целью данной работы является исследование надежности решений виртуального состояния в методе комплексного масштабирования (МКМ), сравнивая их с решениями метода функции Йоста. Для того чтобы исследовать структуру виртуального состояния, мы в самом начале вычисляем собственные значения энергии, затем определяем фазовые сдвиги, а также путем изменения напряженности потенциала сил притяжения находим поперечное сечение фоторасщепления модели двух тел с двух диапазонным гауссовым потенциалом.

Ключевые слова: метод комплексного масштабирования, плотность уровня континуума, фазовый сдвиг.

Information about authors:

Odsuren Myagmarjav - Associate professor, School of Engineering and Applied Sciences and Nuclear Research Center, National University of Mongolia, Email: odsuren@seas.num.edu.mn; https://orcid.org/0000-0003-2756-4909;

Sarsembayeva Aiganym - PhD, Senior lecturer, Department of Theoretical and Nuclear Physics, Al-Farabi Kazakh National University, Email: sarsembaeva.a@kaznu.kz; https://orcid.org/0000-0002-3003-0038;

Khuukhenkhuu Gonchigdorj - Professor, School of Engineering and Applied Sciences and Nuclear Research Center, National University of Mongolia, Email: g_khuukhenkhuu@yahoo.com; https://orcid.org/0000-0002-1011-3127;

Suren Davaa - Professor, School of Engineering and Applied Sciences and Nuclear Research Center, National University of Mongolia, Email: ts.suren.davaa@gmail.com; https://orcid.org/0000-0002-5047-6248;

Zolbayar Ankhbayar - Researcher, School of Engineering and Applied Sciences and Nuclear Research Center, National University of Mongolia, Email: zolo.011263@gmail.com; https://orcid.org/0000-0001-6873-1078;

Usuhbayar Batsaihan - Researcher, School of Engineering and Applied Sciences and Nuclear Research Center, National University of Mongolia, Email: usuhbayar_batsaihan@yahoo.com; https://orcid.org/0000-0002-9160-5202;

Tursukh Amgalan - Researcher, School of Engineering and Applied Sciences and Nuclear Research Center, National University of Mongolia, Email: tursukh.amgalan@gmail.com; https://orcid.org/0000-0002-6885-3398;

Kato Kiyoshi - Professor, Nuclear Reaction Data Centre, Faculty of Science, Hokkaido University, Email: kato-iku@gd6.so-net.ne.jp; https://orcid.org/0000-0002-1272-5629;

Abyshev Medeu - Associate Professor, Head of the Department Of Theoretical And Nuclear Physics, Al-Farabi Kazakh National University, Email: Medeu.Abishev@Kaznu.Kz; http://Orcid.Org/0000-0003-3602-6934.

REFERENCES

[1] Ho Y. K. Phys. Rep. 99, 1 (1983).

[2] Aguilar J., Combes J. M. Comm. Math. Phys. 22 (1971) 269, E. Balslev, J.M. Combes, Comm. Math.Phys. 22 (1971) 280.

[3] Odsuren M., Kikuchi Y., Myo T., Aikawa M., Kato K. Phys. Rev. C 92, 014322 (2015).

[4] Arnold C. W., Clegg T. B., Iliadis C., Karwowski H. J., Rich G. C., Tompkins J. R., Howell C. R. Phys. Rev. C 85, 044605, (2012).

[5] Utsunomiya H., Katayama S., Gheorghe I., Imai S., Yamaguchi H., Kahl D., Sakaguchi Y., Shima T., Takahisa K., Miyamoto S. Phys. Rev. C 92, 064323, (2015).

[6] Odsuren M., Kikuchi Y., Myo T., Khuukhenkhuu G., Masui H., Kato K. Phys. Rev. C95, 064305, (2017)

[7] Ma S. T. Rev. Mod. Phys. 25, 853 (1953).

[8] Descouvemont P. Nucl. Phys. A626, 647 (1997).

[9] Masui H., Aoyama S., Myo T., Kato K., Ikeda K. Nucl.Phys. A673, 207 (2000).

[10] Myo T., Kikuchi Y., Masui H., Kato K. Prog. Part. Nucl.Phys. 79, 1 (2014).

[11] Odsuren M., Kato K., Aikawa M., Myo T. Phys. Rev. C89, 034322 (2014).

[12] Odsuren M., Kikuchi Y., Myo T., Masui H., Katō K. Phys. Rev. C 99, 034312 (2019).

[13] Odsuren M., Khuukhenkhuu G., Katō K. Acta Physica Polonica B 50(3), 549 (2019).

[14] Odsuren M., Sarsembayeva A.T., Khuukhenkhuu G., Davaa S., Kato K., Usukhbayar B. News of the National Academy of Sciences of the Republic of Kazakhstan, Series Physico-Mathematical, 2 (324), (2019), p.5. https://doi.org/10.32014/2019.2518-1726.6

[15] U. Fano, Phys. Rev. 124, 1866 (1961).

NEWS
OF THENATIONAL ACADEMY OF SCIENCES OF THE REPUBLIC OF KAZAKHSTAN
PHYSICO-MATHEMATICAL SERIES
ISSN 1991-346X **https://doi.org/10.32014/2020.2518-1726.69**
Volume 4, Number 332 (2020), 86 – 94

UDK 539.141/.142
IRSTI 29.15.03; 29.15.19

N. Kalzhigitov[1], N. Zh. Takibayev[1],V.S. Vasilevsky[2],
M. Akzhigitova[1], V.O. Kurmangaliyeva[1]

[1]Al-Farabi Kazakh National University, Almaty, Kazakhstan;
[2]Bogolyubov Institute for Theoretical Physics, Kiev, Ukraine
knurto@mail.ru, venera_baggi@mail.ru, kzo1994@mail.ru

A MICROSCOPIC TWO-CLUSTER MODEL OF PROCESSES IN ^{6}Li

Abstract. Structure of bound and resonance states and dynamics of different processes in ^{6}Li are investigated within a microscopic two-cluster model. The model is an algebraic version of the resonating group method which correctly treats the Pauli principle and makes use of the oscillator basis to expand a wave function of a two-cluster system. Within this model the nucleus ^{6}Li is considered as two-cluster $\alpha + d$ system. Dynamics of the two-cluster system is totally governed by a semi-realistic nucleon-nucleon potential. We study interaction of ^{6}Li with electrons and photons. Form factors of elastic scattering of electron are determined for two nucleon-nucleon potentials. We also study the density distribution of protons and neutrons in ^{6}Li. We demonstrate that the model used correctly reproduces form factors for the ground state of ^{6}Li. Our results are compatible with results of other microscopic models. The capture reaction $\alpha + d = {}^6\text{Li} + \gamma$ are investigated in detail. The astrophysical S-factor of the reaction is obtained at low-energy region.

Keywords: cluster model, light nuclei, capture reaction, density distribution.

1. Introduction. In this paper we consider in more detail the structure of ^{6}Li. We will consider the processes initiated by the interaction of ^{6}Li with electrons and photons. Interaction of electrons with ^{6}Li will be represented by a form factor of the electrons elastic scattering from the ^{6}Li ground state. Interaction of photons with ^{6}Li will be represented by a cross section of the ^{6}Li photodisintegration $\gamma + {}^6\text{Li} = \alpha + d$, or by a cross section and the astrophysical S-factor of the radiative capture reaction $\alpha + d = {}^6\text{Li} + \gamma$. It is well known that the radiative capture reaction $\alpha + d = {}^6\text{Li} + \gamma$ is very important for the astrophysical applications.

To achieve these goals we apply a two-cluster microscopic model. This model is so-called the algebraic version of the resonating group method formulated in Refs. [1], [2]. The main peculiarity of the algebraic version is that it employs a full set of oscillator functions to describe the relative motion of the interacting clusters in bound and continuous spectrum states. In Ref. [3], which includes many important details of formulation and implementations of the algebraic version of the resonating group, this model was applied to study the lightest nuclei of the p-shell represented by the dominant two-cluster configuration. It was shown that this model reproduces the main features of the nucleus ^{5}He, ^{5}Li, ^{6}Li, ^{7}Li, ^{7}Be and ^{8}Be. In the present paper we concentrate our attention on some interesting features of ^{6}Li which have not been considered in Ref. [3].

2. Two-cluster model. The total wave function describing the state of two-cluster systems within the resonating group method can be represented as:

$$\Psi_J = \hat{A}\{[\,\varphi_1(A_1)\,\varphi_2(A_2)]_s\psi^J_{LS}(\,\vec{q})\}, \qquad (1)$$

where $\varphi_1(A_1)$ is a wave function describing the internal motion of A_1 nucleons which comprise the first cluster, $\varphi_2(A_2)$ is a wave function describing the internal motion of A_2 nucleons which comprise the second cluster. Both functions depend on the spatial, spin and isospin coordinates of individual nucleons.

And both functions are antisymmetric with respect to a permutation of any pair of nucleons. It is assumed within the resonating group method that these functions are known. There are some simple methods how to construct such functions. Contrary to the functions $\varphi_1(A_1)$ and $\varphi_2(A_2)$, the wave function $\psi_{LS}^J(\vec{q})$ which describes the relative motion of two clusters is unknown and has to be determined by solving dynamical equations of the resonating group method. This function is a function of the Jacobi vector $\vec{q}$, which determines the distance between clusters.

Within the algebraic version of the resonating group method, the wave function $\psi_{LS}^J(q)$ is decomposed into an infinite series of the three-dimension harmonic oscillator wave functions $\psi_n(q, r_0)$:

$$\psi_{LS}^J(q) = \sum_{n=n_0}^{\infty} \mathrm{C}_{nL}\, \psi_{nL}(q, r_0), \tag{2}$$

where C_{nL} is the expansion coefficient, q is the modulus of the vector $\vec{q}$. The explicit form of the oscillator functions $\psi_n(q, r_0)$ can be found in Ref. [3]. As oscillator functions form a complete set of orthonormal functions, then any wave function of a two-cluster system can be expanded over these functions. In the framework of the algebraic version of the resonating group method, the wave function (1) of two-cluster system, by taking into account Eq. (2), can be represented as a generalized Fourier series

$$\Psi_J = \sum_{n=n_0}^{\infty} \mathrm{C}_{nL}\, \Psi_{nL}, \tag{3}$$

it also yields the dynamical equations for the expansion coefficients as a set of the linear algebraic equations

$$\sum_{m=n_0}^{\infty} [\langle \bar{n}L \,|\hat{\mathrm{H}}|\, \bar{m}L\rangle - \mathrm{E}\cdot\delta_{n,m}]\, \bar{\mathrm{C}}_{mL} = 0, \tag{4}$$

where $\hat{\mathrm{H}}$ is the many-particle Hamiltonian of the nucleus, E is the total energy of the nuclear system, and

$$\psi_{nL} = A\{\varphi_1(A_1)\, \varphi_2(A_2)\psi_{nL}(q, b)Y_{LM}(\vec{\boldsymbol{q}})\} \tag{5}$$

is the many-particle, cluster oscillator function.

To construct matrix elements of Hamiltonian and other operators of physical importance we employ the technique of the generating functions [4]. The generating functions of two-cluster system is the Slater determinant constructed from single-particle Brink orbitals. A single-particle Brink orbital is connected with Gaussian functions:

$$\phi(\boldsymbol{r}_i, \boldsymbol{R}_j) = \exp\left\{-\left(\boldsymbol{r}_i - \boldsymbol{R}_j\right)^2 / (2b^2)\right\}, \tag{6}$$

where $\boldsymbol{r}_i$ is a coordinate of the ith nucleon (i = 1, 2, …, A) and $\boldsymbol{R}_j$ (j = 1, 2) is a generator parameter representing center of mass of jth cluster. After elimination of a wave function of the center of mass motion, we obtain the translationally invariant generating function of A nucleons system. We denote this function as $\boldsymbol{\Phi(R)}$, where $\boldsymbol{R}$ is the generator coordinate associated with relative position of clusters in the space and equals

$$\boldsymbol{R} = \sqrt{\frac{A_1 A_2}{A_1 + A_2}}\,[\boldsymbol{R}_1 - \boldsymbol{R}_2]. \tag{7}$$

By using properties of the determinant functions, we can easy calculate the kernel of the Hamiltonian (or the generating matrix elements of the Hamiltonian)

$$\langle \boldsymbol{R} \,|\hat{H}|\, \widetilde{\boldsymbol{R}}\rangle = \langle \boldsymbol{\Phi}(\boldsymbol{R}) \,|\hat{\mathrm{H}}|\, \boldsymbol{\Phi}(\widetilde{\boldsymbol{R}})\rangle, \tag{8}$$

the norm kernel

$$\langle \boldsymbol{R}|\widetilde{\boldsymbol{R}}\rangle = \langle \boldsymbol{\Phi}(\boldsymbol{R})|\boldsymbol{\Phi}(\widetilde{\boldsymbol{R}})\rangle \tag{9}$$

and the generating matrix elements of other operators.

The important feature of the generating function $\boldsymbol{\Phi}(\boldsymbol{R})$, as was shown in Ref. [4], is that it generates an infinite set of cluster oscillator functions (5)

$$\boldsymbol{\Phi}(\boldsymbol{R}) = \sum_{n=0}^{\infty} \sum_{L,M} a_{nL} R^{2n+L} Y_{LM}(\widehat{\boldsymbol{R}}) \psi_{nL}\,. \tag{10}$$

To extract the necessary cluster oscillator function ψ_{nL} from the generating function we use the following procedure

$$\psi_{nL} = \frac{1}{a_{nL}} \frac{1}{(2n+L)!} \left(\frac{d}{dR}\right)^{2n+L} \int d\widehat{\boldsymbol{R}} Y^*_{LM}(\widehat{\boldsymbol{R}}) \boldsymbol{\Phi}(\boldsymbol{R})|_{R=0}. \quad (11)$$

Thus we need to integrate over the unit vector $\widehat{\boldsymbol{R}}$ with the weight $Y^*_{LM}(\widehat{\boldsymbol{R}})$ and then differentiate $2n + L$ times with respect to R. After differentiation we have to put $R = 0$. Such a projecting procedure can be applied directly to the matrix elements of the kernel of the Hamiltonian

$$\langle nL \,|\hat{\mathrm{H}}|\, mL\rangle = \frac{1}{a_{nL}} \frac{1}{(2n+L)!} \left(\frac{d}{dR}\right)^{2n+L} \int d\widehat{\boldsymbol{R}} Y^*_{LM}(\widehat{\boldsymbol{R}}) \quad (12)$$

$$\times \frac{1}{a_{mL}} \frac{1}{(2m+L)!} \left(\frac{d}{d\tilde{R}}\right)^{2m+L} \int d\widehat{\tilde{\boldsymbol{R}}} Y^*_{LM}\left(\widehat{\tilde{\boldsymbol{R}}}\right) \langle \boldsymbol{R} \,|\hat{H}|\, \tilde{\boldsymbol{R}}\rangle|_{R=\tilde{R}=0}\,.$$

We use this procedure to construct matrix elements of proton and neutron form factors and operator of electromagnetic transitions, which we need to calculating cross sections of the capture reactions or photodisintegration reactions.

3. Definition of form factor and density distribution. The proton and neutron form factors are determined as the matrix elements

$$F_p(q) = \langle \psi_{EJ^\pi} | \widehat{F_p} | \psi_{EJ^\pi} \rangle, \quad (13)$$

$$F_n(q) = \langle \psi_{EJ^\pi} | \widehat{F_n} | \psi_{EJ^\pi} \rangle, \quad (14)$$

calculated with a wave function ψ_{EJ^π} describing a bound states of a nucleus. Here the operators $\widehat{F_p}$ and $\widehat{F_n}$ are

$$\widehat{F_p} = \frac{1}{2} \sum_{i=1}^{A} (1 + \widehat{\tau_{iz}}) \exp\{i(\mathrm{q}r_i)\}\,, \quad (15)$$

$$\widehat{F_n} = \frac{1}{2} \sum_{i=1}^{A} (1 - \widehat{\tau_{iz}}) \exp\{i(\mathrm{q}r_i)\}\,, \quad (16)$$

and the operators $\frac{1}{2}(1 + \widehat{\tau_{iz}})$ and $\frac{1}{2}(1 - \widehat{\tau_{iz}})$ are projection operators on proton and neutron state, respectively.

The proton and neutron density distribution are determined as

$$D_p(r) = \left\langle \psi_{EJ^\pi} \middle| \tfrac{1}{2} \textstyle\sum_{i=1}^{A} (1 + \widehat{\tau_{iz}})\, \delta(r - r_i) \middle| \psi_{EJ^\pi} \right\rangle, \quad (17)$$

$$D_n(r) = \left\langle \psi_{EJ^\pi} \middle| \tfrac{1}{2} \textstyle\sum_{i=1}^{A} (1 - \widehat{\tau_{iz}})\, \delta(r - r_i) \middle| \psi_{EJ^\pi} \right\rangle, \quad (18)$$

To calculate $F_p(q)$, $F_n(q)$, $D_p(r)$ and $D_n(r)$, one needs to perform in Eqs. (13), (14), (17) and (18) integrations over all spatial, spin and isospin coordinates.

For numerical calculations of properties of the ^{6}Li nucleus, we selected two nucleon-nucleon potentials: the Minnesota potential (MP) [5] and the modified Hasegawa-Nagata [6, 7] potential (MHNP). This is done in order to study the dependence of calculated quantities of ^{6}Li on the shape of selected nucleon-nucleon potentials.

Here, we are not going to discuss the wave function of the ground state of ^{6}Li as it was discussed in Ref. [3]. And we will not present wave functions or phase shifts of the elastic scattering of deuterons from an alpha particle as they were presented in Ref. [3]. It is necessary to note that phase shifts of the elastic α + d scattering and the parameters of resonance state are in a good agreement with the experimental data.

4. Form factor and density distribution. Within the two-cluster model used, the total isospin T = 0 for ^{6}Li, thus the neutron form factor coincides with the proton form factor. This can be deduced from the definitions of the proton and neutron form factors Eqs. (13) and (14). And this is why the proton, neutron and mass density distributions are also identical. Thus we display only the proton form factor and proton density distribution. The proton density distributions D(r) obtained with MP and MHNP are display in figure 1. There is a substantial difference in the proton density distributions for these potential at small distances r. The proton density distribution in the ground 1^+ state of ^{6}Li calculated with MP and MHNP. The proton form factor F(q) for elastic scattering of electrons from the 1^+ ground state of ^{6}Li are shown in figure 2. As we can see, the first minimum of the form factor are in the same point of the transferred momentum q for both potentials. As it is well known the range of small values of q associated with the root-mean-square radius of ^{6}Li, which has approximately the same value for MP and MHNP [8, 9].

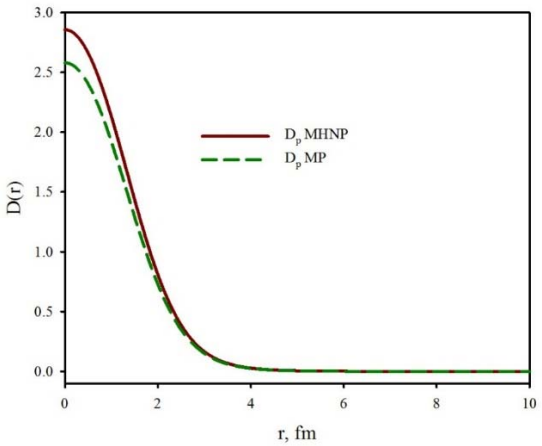

Figure 1 – The proton density distribution in the ground 1^+ state of ^{6}Li calculated with the MP and MHNP

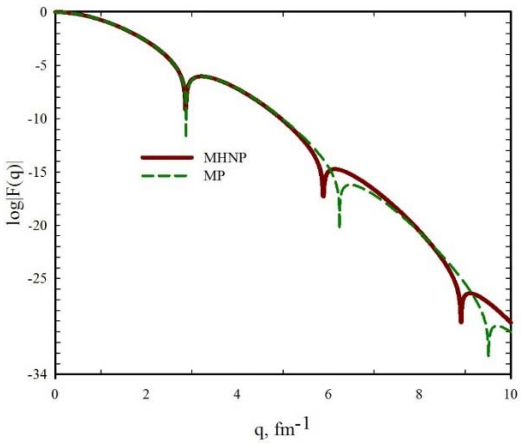

Figure 2 – The proton form factor F(q) from the ^{6}Li ground state. Results are obtained with MP and MHNP

5. The capture reaction α + d = ^{6}Li + γ. The cross section and astrophysical S factor of the reaction α + d = ^{6}Li + γ are calculated by employing the quadrupole transitions only. It has been repeatedly shown that the quadrupole transitions from continuous spectrum states to the ground state of ^{6}Li dominates in the low energy region. Having calculated wave functions of the ground state of ^{6}Li and continuous spectrum states in the channel α + d, we then easily calculated the quadrupole transitions and cross section of the capture reaction. The explicit formula for calculating the cross section of the capture reaction can be found, for example, in Ref. [10, 11]. It is worthwhile noticing that the quadrupole transitions connect the ground 1^+ state with three states of the continuous spectrum, namely, $J^\pi = 3^+$, $J^\pi = 2^+$ and $J^\pi = 1^+$. Within the present model, the total spin S is a good quantum number and S=1. Thus, the total orbital momentum L is also a good quantum number. For the ground state L = 0, and for the scattering states $J^\pi = 3^+$, $J^\pi = 2^+$ and $J^\pi = 1^+$ the total orbital momentum L = 2. The spin-orbit interaction splits the state with the total orbital momentum L = 2 on three states with the total angular momentum $J^\pi = 3^+$, $J^\pi = 2^+$ and $J^\pi = 1^+$. As the total isospin of ^{6}Li T=0, then the dipole transitions are forbidden in the long-wave approximation. It is well-known, that the dipole transition operator in the long-wave approximation contains only the isovector part, thus the dipole transitions are allowed for the nuclei with total isospin T ≥ ½.

In table 1 we show the energy and width of the $J^\pi = 3^+$, $J^\pi = 2^+$ and $J^\pi = 1^+$. These resonance states, as we can see later, play an important role in the capture reaction. It was shown in Ref. [3] that these resonance states have a great impact on the cross section of the elastic α + d scattering. The energy E of the resonance states are measured from the α + d threshold. Results of our calculation with the MP and the MHNP are compared with the experimental data [12-14]. There is a fairly good agreement between the theoretical and experimental data. As we can see, the MHNP provides more correct description of the 3^+, 2^+ and 1^+ resonance state, than the MP.

Table 1 - Experimental and theoretical values of the parameters of resonance states of ^{6}Li

Potential	L; J^π	E (MeV)	Γ (MeV)
MHNP	2; 1^+	4.100	2.357
	2; 2^+	3.063	1.013
	2; 3^+	0.763	0.019
MP	2; 1^+	5.174	6.33
	2; 2^+	4.288	3.005
	2; 3^+	0.848	0.028
Experimental data [12, 13]	2; 1^+	4.176±0.050	1.5±0.2
	2; 2^+	2.838 ±0.022	1.30 ± 1.00
	2; 3^+	0.712 ±0.002	0.024 ± 0.002

As was indicated above, all resonances in the ^{6}Li nucleus mentioned in Table 1 have the total orbital momentum L = 2, which indicates the presence of a centrifugal barrier in these states. The effective barrier in the α + d channels is complemented also by the Coulomb barrier. The spin-orbital forces increase the effective attraction between clusters in the 3^+ state and thus generates a very narrow resonance at low energies. At this energy range, the width of the barrier is large which difficult to penetrate. This stipulates the appearance of a very narrow (long-lived) resonance state. In the 1^+ state, the spin-orbital forces, contrary to the 3^+ state, reduce the interaction of the alpha particle and the deuteron and push the resonance state to a relatively larger energy, where the effective barrier is small. The spin-orbit forces have small effect on the 2^+state, as the consequence the resonance width is less than in the 1^+ state, but larger than in the 3^+ state.

In figures 3 and 4 we display the partial and the total astrophysical S factors of the reaction α + d = ^{6}Li + γ as a function of the energy E of relative motion of clusters alpha-particle and deuteron. One can immediately notice a peak below the energy E = 1 MeV. This peak is associated with the narrow 3^+ resonance state. The contribution to the partial and total S factors of wider 2^+ and 1^+ resonance states is not so prominent. By comparing Fig. 3 and Fig. 4, we see explicitly how the astrophysical S factor of the capture reaction α + d = ^{6}Li + γ depends on the shape of the nucleon-nucleon potentials used in our calculations. It is important to note, that the transition from the 3^+ continuous spectrum states to the ground state dominates at the low energy range 0 ≤ E < 1 MeV. At the higher energies, the transition from the 2^+ continuous spectrum states to the ground state is more prominent than the other transitions.

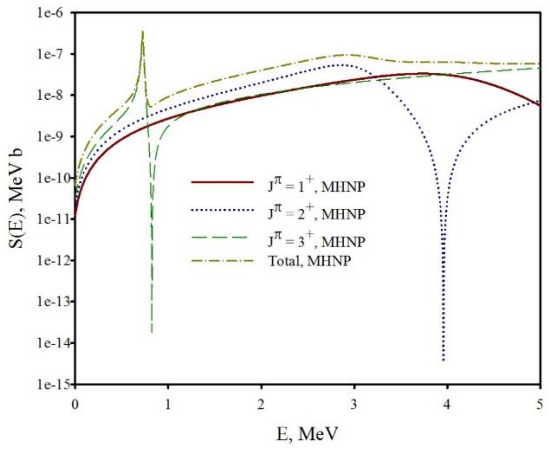

Figure 3 – The astrophysical S-factors generated by the quadrupole transitions. Results are obtained with the modified Hasegawa-Nagata potential

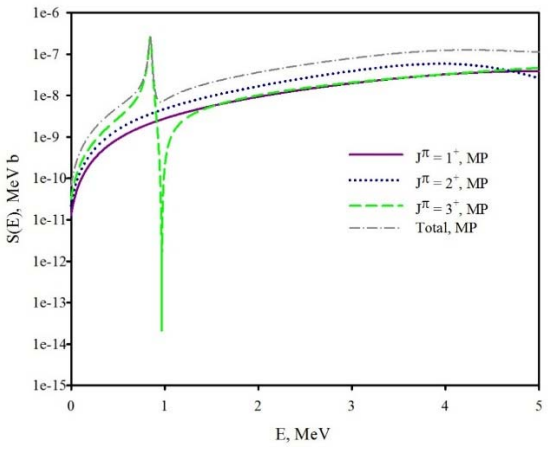

Figure 4 – The astrophysical S-factors of reaction α + d = ^{6}Li + γ generated by the quadrupole transitions. Results are obtained with the potential of Minnesota

The astrophysical S factor of the capture reaction α + d = ^{6}Li + γ obtained by the theoretical or experimental methods usually is approximated by the three terms expression:

$$S(E) = S_0 + S_1E + S_2E^2 \,. \qquad (19)$$

For this aim we selected the energy interval $0 \leq E \leq 0.2$ MeV. In Table 2 we display parameters of the three terms fit to the calculated astrophysical S-factor of the capture reactions α + d = ^{6}Li + γ. In the table we show partial astrophysical *S*-factors $S\,(E; J_i^\pi \Rightarrow J_f^\pi)$ and the total *S*-factor

$$S_T(E) = \sum_{J_i^\pi} S\big(E;\, J_i^\pi \Rightarrow J_f^\pi\big), \tag{20}$$

In our calculations this sum involves three partial astrophysical *S*-factors.

Table 2 - Parameters of three-term fitting of the calculated astrophysical *S*-factor of the reaction α + d = ^{6}Li + γ.

Potential	Transition	S_0	S_1	S_2
MHNP	$3^+ \Rightarrow 1^+$	3.092×10^{-11}	10.923×10^{-10}	7.455×10^{-9}
	$2^+ \Rightarrow 1^+$	2.035×10^{-11}	7.878×10^{-10}	4.370×10^{-9}
	$1^+ \Rightarrow 1^+$	1.214×10^{-11}	4.716×10^{-10}	2.593×10^{-9}
	Total	6.341×10^{-11}	23.517×10^{-10}	14.418×10^{-9}

The total astrophysical S factor obtained in our model is in a fairly good agreement with the available experimental data and is also compatible with results of other theoretical two- and three-cluster models.

6. Conclusions. We have applied a two-cluster microscopic model to study structure of the nucleus ^{6}Li. This nucleus was represented as a two-cluster configuration α + d, which determines the main properties of ^{6}Li at the low energy region. Two well-known nucleon-nucleon potentials were employed to study properties of ^{6}Li and their dependence on the shape of the potentials. The present model correctly reproduced the main features of bound and scattering states in ^{6}Li.

We have calculated the form factor of the elastic scattering of electron from the ground state of ^{6}Li. It was shown that at region of the small values of the transferred momentum q the form factor F(q) slightly depends on the shape of the nucleon-nucleon potentials, however for large values of the momentum q the shape of the potentials has the large impact on the form factor. As for the proton density distribution D(r), the shape of the nucleon-nucleon potentials has noticeable impact at the region of small distances r.

We have also studied the dynamics of the capture reaction α + d = ^{6}Li + γ at small energy region which is of a great importance for the different astrophysical applications. We have calculated the partial and total astrophysical S factor S(E) of the reaction. We have demonstrated how the low-lying resonance states 3^+, 2^+ and 1^+ contribute to astrophysical S factor of the capture reaction. It was shown that our model provides a satisfactory description of the S factor in the range of energy $0 \leq E \leq 1$ MeV.

Acknowledgment. One of the authors (V.S. Vasilevsky.) is grateful to the members of the sub-department of theoretical and nuclear physics from the Physical and Technical Department, Al-Farabi Kazakh National University, Almaty, Republic of Kazakhstan, for hospitality and inspiring discussions during his stay at al-Farabi Kazakh National University.

This work was supported in part by the Program of Fundamental Research of the Physics and Astronomy Department of the National Academy of Sciences of Ukraine (Project No. 0117U000239) and by the Ministry of Education and Science of the Republic of Kazakhstan, Research Grant IRN:AP 05132476.

Н. Калжигитов[1], Н.Ж. Такибаев[1], В.С. Василевский[2], Э.М. Ақжігітова[1], В.О. Құрманғалиева[1]

[1]Әл-Фараби атындағы Қазақ ұлттық университеті, Алматы, Қазақстан;
[2]Боголюбов атындағы теориялық физика институты, Киев, Украина

^{6}LI-ДЕГІ МИКРОСКОПИЯЛЫҚ ЕКІКЛАСТЕРЛІК ҮДЕРІС ҮЛГІСІ

Аннотация. Жұмыста байланысқан және резонансты күйлердің құрылымы, сонымен бірге ^{6}Li-дегі әртүрлі үдеріс динамикасы микроскопиялық екікластерлік үлгі аясында зерттелген. Бұл тәсілдің негізі abinitio және екікластерлік жүйенің толқындық функцияларын осцилляторлық негізде жіктеу үшін қолданатын резонансты топ әдісінің алгебралық нұсқасы (РТӘАН). ^{6}Li мәселесін қарастыру бастапқы нуклеосинтез кезеңінде ^{6}Li шығуының негізгі реакциясы саналатын радиациялық қарпу реакциясы тұрғысынан туындайды. Осы мәселеге екі көзқарасты қолдану өте қажет, өйткені ^{6}Li радиациялық қарпу

реакциясында алты өзара әрекеттесетін нуклондар бар, олар сәйкесінше алты дене қатысатын күрделі есепті тудырады. РТӘАН құралдары бұл мәселені екі дене есебіне: альфа-бөлшек α және сутегі изотопы дейтерий *d*-ге азайта алады. Паули принципін және антисимметризацияны ескермей, өзара әрекеттесетін кластерлердің толқындық функциясын гармоникалық осциллятор функциясының базистер жиынтығы бойынша жіктеуге мүмкіндік береді. Бұл өз кезегінде есептеуді едәуір жеңілдетуге және жұмыс соңында тәжірибелік мәліметтер негізінде сәйкес нәтижелерге қол жеткізуге мүмкіндік берді.

Зерттеліп жатқан жүйе динамикасы толығымен нуклон-нуклондық потенциалымен анықталды. Нәтижесінде ядролық әсерлесуді сипаттау үшін екі нуклон-нуклондық потенциал қолданылды: модификацияланған Хасегава-Нагата потенциалы (МХНП) және Миннесота потенциалы. Модификацияланған Хасегава-Нагата потенциалы жұп нуклон-нуклондық әсерлесу үшін алыс арақашықтықтарда тартылысты және жақын арақашықтықтарда тебілісті жақсы шығарды. Бұл потенциал көптеген жағдайда, атап айтқанда, жеңіл ядролардың энергияның кең диапазонында шашырау мәліметтерін сипаттауда, электромагниттік қасиеттердің және жеңіл ядроларының қатысуы арқылы өтетін үдерістерді сипаттау үшін қолданды. Миннесота потенциалы спин-орбиталық компоненті бар үш гаусс функциясымен анықталады.

Жұмыстың негізгі мақсаты – эксперименталды түрде резонансты күйлері бақыланған, астрофизикалық 5 МэВ энергияға жақын төменгі энергиялы интервалда ^{6}Li жеңіл ядро реакцияларындағы ядролық күштердің әсері мен табиғатын зерттеу. Жасалған жұмыстың мақсаты осындай резонанстық күйді теориялық есептеу.

Кластерлік үлгінің артықшылығы, зерттеліп жатқан бөлшектер, олардың құрылымы кейбір жағдайларда назардан тыс қалуы мүмкін нуклондардың ядролық уақытының конгломерациялары өлшемі түрінде ұсынылды. Сонымен қатар, зерттелген ядролар бірқатар қызықты сипаттамаларға ие болды. Радиациялық қарпу реакциясындағы ^{6}Li ядросында ұзақ толқындардың жақындауына байланысты дипольдік ауысуы мүмкін болмады, сондықтан тек квадруполдық ауысуы үшін зерттеулер жүргізілді.

Шредингер теңдеулерін шешуде қолданылатын шекаралық шарттарды енгізіп, осцилляторлық функциялардың базистері бойынша кластерлік қозғалыспен салыстырмалы түрдегі толқындық функцияларды алгебралық формада жіктеуге күрделі интегралды-дифференциалдық есептеулерді келтіріп, жеңіл ядролардың байланысқан және квазибайланысқан күйлерін есептеу үшін резонансты топтар әдісінің алгебралық нұсқасы қолданылды. Оның әртүрлі нуклон-нуклондық потенциалын қолдану арқылы астрофизикалық S-факторлары мен шашырау фазалары туралы мәліметтер алынды, олар кейіннен өңделді

Резонансты топтар әдісінің алгебралық нұсқасын қолдану арқылы алынған S-факторлар түріндегі теориялық нәтижелер тәжірибелік мәліметтермен салыстырылды, содан кейін әдіс пен эксперимент нәтижелері жақсы сәйкесті.

^{6}Li ядросын екікластерлік жүйе ретінде қарастыру кезінде туындайтын негізгі мәселенің бірі – ядроның электрондар мен фотондар әрекеттесуін зерттеу. Нәтижесінде екі нуклон-нуклондық потенциал үшін серпімді электронды шашыраудың форм-факторлары анықталды. Сондай-ақ, ядроның құрылымын зерттеу үшін ^{6}Li-дегі протондар мен нейтрондардың тығыздығының таралуын зерттеу қажет болды.

Резонанстық топтар әдісінің алгебралық нұсқасын қолдана отырып, жүргізілген есептеулер нәтижесінде электронның серпімді шашырау форма коэффициенті ^{6}Li ядросының негізгі күйі үшін есептелді. Осының салдарынан, берілген q импульстің аз шамасы аймағында F (q) форм-фактор нуклон-нуклондық потенциалынан әлсіз тәуелді екендігі, алайда q импульсінің үлкен мәнінде потенциалдың формасы форм-факторына көбірек әсер ете бастады. Протон тығыздығының D (r) таралуы нуклон-нуклондық потенциалдарының r арақашықтық аз болғанда аймақта айтарлықтай әсер ететінін көрсетті. Алынған ақпарат зерттеліп жатқан ядроның ішкі құрылымын қарастырып қана қоймай, сонымен бірге зерттеу деректерінде қолданылатын нуклон-нуклондық потенциалының табиғаты мен сипаттамалары туралы ақпарат берді.

Түйін сөздер: кластерлік үлгі, жеңіл ядролар, қарпу реакциясы, таралу тығыздығы.

Н. Калжигитов[1], Н. Ж. Такибаев[1], В. С. Василевский[2], Э. М. Акжигитова[1], В.О. Курмангалиева[1]

[1]Казахский национальный университет имени аль-Фараби, Алматы, Казахстан;
[2]Институт Теоретической Физики имени Боголюбова, Киев, Украина

МИКРОСКОПИЧЕСКАЯ ДВУКЛАСТЕРНАЯ МОДЕЛЬ ПРОЦЕССОВ В ^{6}Li

Аннотация. Структура связанных и резонансных состояний, а также динамика различных процессов в ^{6}Li были исследованы в данной работе в рамках микроскопической двухкластерной модели. Основой данного подхода являются ab initio и алгебраическая версия метода резонирующих групп (АВМРГ), что использует осцилляторную основу для разложения волновой функции двухкластерной системы. Рассмотрение проблемы ^{6}Li происходит с позиции реакции радиационного захвата, которая является основной реакцией происхождения ^{6}Li в период первичного нуклеосинтеза. Использование этих двух подходов к данной задаче крайне необходимы, так как в реакции радиационного захвата ^{6}Li присутствует

шесть взаимодействующих между собой нуклонов, что создаёт весьма сложную задачу с участием шести тел. Инструменты АВМРГ позволяют сократить данную задачу до рассмотрения двух тел: альфа частицы α и изотопа водорода дейтерия *d*. Не пренебрегая принципом запрета Паули и антисимметризацией, данный подход позволяет разложить волновую функцию взаимодействующих кластеров по набору базисов функций гармонического осциллятора. Это в свою очередь позволило в значительной степени упростить расчеты и получить результаты, которые по окончанию работы были сопоставлены с экспериментальными данными.

Динамика же исследуемой системы полностью определялась полуреалистичным нуклон-нуклонным потенциалом. Вследствии этого для описания ядерного взаимодействия использовались два нуклон-нуклонных потенциала: модифицированный потенциал Хасегавы-Нагаты (МПХН) и потенциал Миннесоты. Модифицированный потенциал Хасегавы-Нагаты для парного нуклон-нуклонного взаимодействия хорошо воспроизводил притяжение на больших расстояниях и отталкивание на малых расстояниях. Применялся данный потенциал во многих случаях, в частности для описания данных по рассеянию легких ядер в широком диапазоне энергий, электромагнитных свойств и процессов с участием легких ядер. Потенциал Миннесоты в свою очередь определяется тремя гауссовыми функциями с присутствием спин-орбитальной компоненты.

Основой задачи данной работы было исследование характера и влияния ядерных сил в реакциях легких ядер ^{6}Li, при которых в интервале низких энергий близкому к астрофизическим энергиям до 5 МэВ, экспериментально наблюдались резонансные состояния. Целью же проделанной работы был теоретический расчет такого резонансного состояния.

Преимуществом кластерной модели являлось то, что исследуемые частицы представлялись в виде довольно устойчивых по меркам ядерного времени нуклонных конгломераций, внутренней структурой которых в некоторых случаях можно было пренебречь. К тому же исследуемые ядра обладали рядом интересных характеристик. Так ядро ^{6}Li в реакции радиационного захвата из-за длинноволнового приближения не могло иметь дипольный переход, в связи с чем исследования проводились лишь для квадрупольного перехода.

Алгебраическая версия метода резонирующих групп использовалась для расчетов, связанных и квазисвязанных состояний в легких ядрах, приводя сложные интегрально-дифференциальные вычисления к алгебраической форме методом разложения волновой функции относительного движения кластеров по базисам осцилляторных функций и, вводя граничные условия, по которым будет решаться уравнение Шредингера. Его решение с использованием различных нуклон-нуклонных потенциалов дало данные по астрофизическим S-факторам и фазам рассеяния, которые в последствии были обработаны.

Теоретические результаты в виде S-факторов, полученных путем расчетов с использованием алгебраической версии метода резонирующих групп сравнивались с экспериментальными данными, после чего было получено хорошее соответствие результатов метода с экспериментом.

Одной из основных задач возникающей при рассмотрении ядра ^{6}Li как двух-кластерной системы является изучение взаимодействия данного ядра с электронами и фотонами. Вследствие этого были определены форм-факторы упругого рассеяния электрона для двух нуклон-нуклонных потенциалов. Также для исследования структуры ядра нужно было изучить распределение плотности протонов и нейтронов в ^{6}Li.

В результате проводимых расчетов с использованием алгебраической версии метода резонирующих групп форм-фактор упругого рассеяния электрона вычислен из основного состояния ядра ^{6}Li. Вследствие этого было показано, что в области малых значений переданного импульса q форм-фактор F(q) слабо зависел от формы нуклон-нуклонных потенциалов, однако при больших значениях импульса q форма потенциалов стала иметь большее влияние на форм-фактор. Распределение плотности протонов D(r) показало, что форма нуклон-нуклонных потенциалов оказывает заметное влияние в области, когда расстояние r было мало.

Полученная информация позволила не только рассмотреть внутреннюю структуру исследуемого ядра, но также дала сведения о природе и характеристиках, используемых в данных исследования нуклон-нуклонных потенциалах.

Ключевые слова: кластерная модель, легкие ядра, реакция захвата, плотность распределения.

Information about authors:

Kalzhigitov N.K., PhD student, al-Farabi Kazakh National University, Almaty, Kazakhstan, knurto@mail.ru, https://orcid.org/0000-0002-2598-3176;

Takibayev N.Zh., d.ph.-m.sc., professor, academic of NAS RK, al-Farabi Kazakh National University, Almaty, Kazakhstan, takibayev@gmail.com, https://orcid.org/0000-0002-2604-6838;

Vasilevsky V.S. professor, Bogolyubov Institute for Theoretical Physics, Kiev, Ukraine, vsvasilevsky@gmail.com, https://orcid.org/0000-0003-0417-5978;

Akzhigitova E.M., PhD student, al-Farabi Kazakh National University, Almaty, Kazakhstan, kzo1994@mail.ru, https://orcid.org/0000-0002-8544-1248;

Kurmangalieva V.O., c.ph.-m.sc., docent, al-Farabi Kazakh National University, Almaty, Kazakhstan, venera_bagg@mail.ru, https://orcid.org/0000-0001-8046-8508

REFERENCES

[1] Filippov GF, Okhrimenko I. (1981) Use of an oscillator basis for solving continuum problems, Sov. J. Nucl. Phys., 32: 480-484 (in Russ.).

[2] Filippov GF. (1981) On taking into account correct asymptotic behavior in oscillator-basis expansions, Sov. J. Nucl. Phys., 33: 488-489 (in Russ.).

[3] Vasilevsky VS, Kato K, Kurmangaliyeva V, Duisenbay AD, Kalzhigitov N, Takibayev N (2017) Investigation of discrete and continuous spectrum states in two-cluster system. Sapporo, Japan: Hokkaido University.

[4] Filippov GF, Vasilevsky VS, Chopovsky LL. (1985) Solution of problems in the microscopic theory of the nucleus using the technique of generalized coherent states, Sov. J. Part. Nucl., 16: 153-177 (in Russ.).

[5] Thompson DR, LeMere M, Tang YC. (1977) Systematic investigation of scattering problems with the resonating-group method, Nucl. Phys., A286, no. 1: 53-66. DOI: 10.1016/0375-9474(77)90007-0 (in Eng.).

[6] Hasegawa A, Nagata S. (1971) Ground state of ^{6}Li, Prog. Theor. Phys., vol. 45: 1786-1807. DOI: 10.1143/PTP.45.1786 (in Eng.).

[7] Tanabe F, Tohsaki A, Tamagaki R. (1975) αα scattering at intermediate energies, Prog. Theor. Phys., vol. 53: 677-691. DOI: 10.1143/PTP.53.677 (in Eng.).

[8] Vasilevsky VS, Nesterov AV, Arickx F, Broeckhove J. (2001) Algebraic model for scattering in three-s-cluster systems. I. Theoretical background, Phys. Rev. C, vol. 63: 034606-034622. DOI: 10.1103/PhysRevC.63.034606 (in Eng.).

[9] Vasilevsky VS, Kato K, Takibayev N. (2017) Formation and decay of resonance states in ^{9}Be and ^{9}B nuclei: Microscopic three-cluster model investigations, Phys. Rev. C, vol. 96: 034322 (1-16). DOI: 10.1103/PhysRevC.96.034322 (in Eng.).

[10] Vasilevsky VS, Kato K, Takibayev N. (2018) Systematic investigation of the Hoyle-analog states in light nuclei, Phys. Rev. C, vol. 98: 024325. DOI: 10.1103/PhysRevC.98.024325 (in Eng.).

[11] Duisenbay AD, Takibayev N, Vasilevsky VS, Kurmangaliyeva VO, Akzhigitova EM. (2019) Form factors and density distributions of protons and neutrons in Li-7 and Be-7, News of the national academy of sciences of the republic of Kazakhstan-series physico-mathematical, vol. 3: 71-76. DOI: 10.32014/2019.2518-1726.26 (in Eng.).

[12] Duisenbay AD, Kalzhigitov N, Katō K, Kurmangaliyeva VO, Takibayev N, Vasilevsky VS. (2020) Effects of the Coulomb interaction on parameters of resonance states in mirror three-cluster nuclei. Nucl. Phys. A, vol 996: 121692 (1-30). DOI:10.1016/j.nuclphysa.2020.121692 (in Eng.).

[13] Tilley DR, Cheves CM, Godwin JL, Hale GM, Hofmann HM, Kelley JH, Sheu CG, Weller HR. (2002) Energy levels of light nuclei A=5, 6, 7. Nuclear Physics A, vol. 708: 3-163. DOI: 10.1016/S0375-9474(02)00597-3 (in Eng.).

[14] Robertson RGH, Dyer P, Warner RA. (1981) Observation of the Capture Reaction ^{2}H(α, γ)^{6}Li and Its Role in Production of ^{6}Li in the Big Bang, Phys. Rev. Lett, vol. 47:1867-1870. DOI:10.1103/PhysRevLett.47.1867 (in Eng.).

NEWS
OF THENATIONAL ACADEMY OF SCIENCES OF THE REPUBLIC OF KAZAKHSTAN
PHYSICO-MATHEMATICAL SERIES
ISSN 1991-346X **https://doi.org/10.32014/2020.2518-1726.70**
Volume 4, Number 332 (2020), 95 – 102

UDK 517.518.87
MRNTI 27.41

M.D. Ramazanov[1], Zh.K. Kaidassov[2], Zh.S. Tutkusheva[3]

[1]Institute of Mathematics with Computing Centre, Ufa, Russian;
[2]Aqtobe Regional Zhubanov State University.
E-mail: Ramazanovmd@yandex.ru; jet-k@mail.ru; zhailan_k@mail.ru

STUDYING THE EFFECTIVENESS OF A NEW ALGORITHM WITH A DEFINING FUNCTION FOR FINDING THE GLOBAL MINIMUM OF A SMOOTH FUNCTION

Abstract. This article presents a new algorithm with a defining function to find the global minimum of multi-extreme functions of two variables. The stages of the new algorithm are described in detail.

Computational experiments were performed on three different test assignments. We have found the global minima of the test functions. A convex function was given as the first example. In the second example, a non-convex function that has a global minimum inside a parabolic strongly elongated surface has been analyzed. In the third example, a function with a large number of local minima has been analyzed. These functions are different in complexity, but our algorithm determines the global minimum of different functions in the same amount of time.

A determining function is formed depending on the function considered so that the algorithm to function. If a function is two variables, then the defining function will contain a double integral. Such integrals were calculated using Sobolev's cubature formulas with a regular boundary layer. Computer programs were used to calculate cubature formulas. The calculation algorithm has been implemented using Microsoft Visual Studio in C++.

As a result of the computational experiment, the values and coordinates of the global minima of the test functions have been found. A comparative analysis of the reference values and those found was made using the new algorithm.

Key words: multidimensional optimization, global optimization algorithm, Sobolev's cubature formulas, De Jong function, Rosenbrock function, Rastrigin function.

Recently, the relevance of optimization problems has been growing very rapidly and successfully. The range of optimization tasks has significantly expanded. There is a need to solve optimization problems in almost all Sciences. Many methods for finding the minimum of the function have been suggested [1-4]. Each method has its advantages and disadvantages. The task becomes more difficult if you need to find a global minimum for a function with a large number of local minima.

We have built a new algorithm for finding the global minimum. The algorithm for a function of a single variable has been analyzed [5] and tested.

Now let's describe the proposed algorithm for a function of two variables.

Let be a smooth function of two variables $z = f(x, y)$. The domain of the function $a \le x \le b$, $a \le y \le b$. It is necessary to find the value and coordinates of the global minimum $z = f(x, y)$.

The algorithm works by means of a defining function:

$$g(\alpha) = \int_a^b \int_a^b [|f(x,y) - \alpha| - (f(x,y) - \alpha)]^m dxdy \ , \qquad (1)$$

where the integration area on the plane xOy is a square $[a;b]_x \times [a;b]_y$. This integral defines the first touch of the global minimum of a function $z = f(x, y)$ with a plane $z = \alpha$, so the function (1) was called the defining function.

Let's start with the value of the global minimum point. Let's denote it $\hat{\alpha} = glob \min f(\hat{x}, \hat{y})$. To do this, it is necessary to select the value α and put it into the defining function and calculate the value of the integral.

If $f(x, y) \geq \alpha$, then the module as a defining function is expanded with a positive sign and is obtained $g(\alpha) = 0$. This means that the plane $z = \alpha$ passes below the function graph or touches the bottom. In further we select a value α greater than it was before.

If $f(x, y) < \alpha$, then the module in the defining function is expanded with a negative sign and is obtained $g(\alpha) > 0$. This means that the plane $z = \alpha$ passes above the function graph or intersects, so we select a value α less than it was before.

Continue to choose α until, $|\alpha_n - \alpha_{n+1}| \leq \varepsilon$ where $g(\alpha_n) = 0$ and $g(\alpha_{n+1}) > 0$. After a certain number of iterations, we will get close to the value of the global minimum up to the desired accuracy. The global minimum lies on the segment $\hat{\alpha} \in [\alpha_n; \alpha_{n+1}]$.

In searching for the coordinates of the global minimum, it is necessary that the defining function takes a positive number $g(\hat{\alpha}) > 0$. Therefore, the approximate value of the global minimum takes the right end of the segment $[a_n, a_{n+1}]$, $g(\alpha_{n+1}) > 0$.

$$\alpha_{n+1} \approx \hat{\alpha} = glob \min f(\hat{x}, \hat{y}) \tag{2}$$

We found the value of the global minimum (2) with ε - precision.

Let's start searching for the coordinates of the global minimum point $\hat{x}$ and $\hat{y}$, where $\hat{x} \in [a; b]$ and $\hat{y} \in [a; b]$. We look for the coordinates of the point in the square $[a; b]_x \times [a; b]_y$. Divide the given square into four equal parts. We get four squares $[a; x_1]_x \times [a; y_1]_y$, $[a; x_1]_x \times [y_1; b]_y$, $[x_1; b]_x \times [a; y_1]_y$ and $[x_1; b]_x \times [y_1; b]_y$ by dividing the sides in half $x_1 = \frac{b+a}{2}$ and $y_1 = \frac{b+a}{2}$. We modify the defining function for each of the obtained regions(1).

$$g_{[a;x_1]_x \times [a;y_1]_y}(\hat{\alpha}) = \int_a^{y_1} \int_a^{x_1} [|f(x, y) - \hat{\alpha}| - (f(x, y) - \hat{\alpha})]^m \, dxdy \, , \ldots\ldots \tag{3}$$

$$g_{[x_1;b]_x \times [y_1;b]_y}(\hat{\alpha}) = \int_{y_1}^{b} \int_{x_1}^{b} [|f(x, y) - \hat{\alpha}| - (f(x, y) - \hat{\alpha})]^m \, dxdy$$

The found value of the global minimum (2)were used in the modified functions (3). At least one of these four integrals must be positive. We continue to search for the point of the global minimum in the part where the modified integral will take a positive number. We divide the selected part into four more squares and build four more integrals for them in the same way. This iteration continues until $|x_m - x_{m+1}| \leq \varepsilon$ and $|y_l - y_{l+1}| \leq \varepsilon$ where $g_{[x_m; x_{m+1}] \times [y_l; y_{l+1}]}(\hat{\alpha}) > 0$. The coordinates of the global minimum point are equal to $\hat{x} = \frac{x_{m+1} + x_m}{2}$ and $\hat{y} = \frac{y_{l+1} + y_l}{2}$.

The accuracy of the value and coordinates of the global minimum is set by us. In our examples, the values and coordinates of the global minimum are calculated with precision $\varepsilon = 10^{-6}$.

To calculate a two-dimensional complex integral, we used Sobolev's cubature formulas with a regular boundary layer [6-8], as multidimensional integrals are well approached by Sobolev's formulas.

The proposed algorithm for the minimization problem has been implemented in C++ in the Microsoft Visual Studio 2017 development environment [9].

In this article, we will test the new algorithm for accuracy and efficiency. Optimization methods are tested for accuracy and efficiency by means of test functions that have well-known exact extremes. To test our algorithm three well-known functions were chosen [11-12].

De Jong's Function. It is sometimes called a spherical function. It is one of the simplest test tasks used for testing the optimization algorithm [13]. The function is defined by the following formula:

$$f(x, y) = x^2 + y^2 \ ,$$

where the scope of the function definition is $-5.12 < x < 5.12$, $-5.12 < y < 5.12$. The function is continuous and convex and has one global minimum: $f(x, y) = 0$, $x = 0$, $y = 0$. There are no local minimums. The graph of the function in space is shown in figure 1.

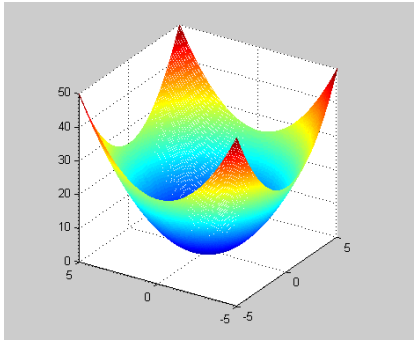

Figure 1-Graph of the De Jong' function of two variables

Rosenbrock Function. It is also called the "banana function". Finding the global minimum for this function is considered a non-trivial task [14-15]. The function has a slowly decreasing large plateau. The global minimum is located inside a long, narrow, parabolic flat valley. It is difficult to find a global minimum under these conditions,. The function has the following definition:

$$f(x; y) = 100(y - x^2)^2 + (1 - x)^2 \ ,$$

where the function definition area is: $-2.048 < x < 2.048$, $-2.048 < y < 2.048$ and has one global minimum: $f(x, y) = 0$, $x = 0$, $y = 0$. There are no local minimums. The graph of the function in space is shown in figure 2.

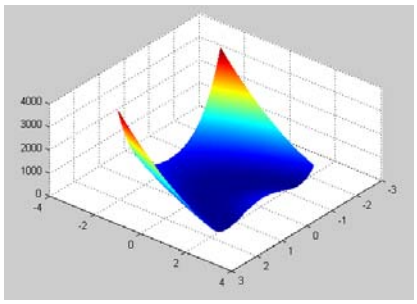

Figure 2 - Graph of the Rosenbrock function of two variables

The Rastrigin function is a non-convex and multi-extreme function [16]. Finding the global minimum of such a function is a difficult task because of the large number of local minima. For this reason, the Rastrigin function is used to test the effectiveness of optimization algorithms. The function is defined by the following formula:

$$f(x, y) = 20 + x^2 + y^2 - 10\cos(2\pi x) - 10\cos(2\pi y) \ ,$$

where the region of definition of the coordinates is $-5.12 < x < 5.12$ and $-5.12 < y < 5.12$ and has one global minimum: $f(x, y) = 0$, $x = 0$, $y = 0$. There are many local minimums. The graph of the function in space is shown in Figure 3.

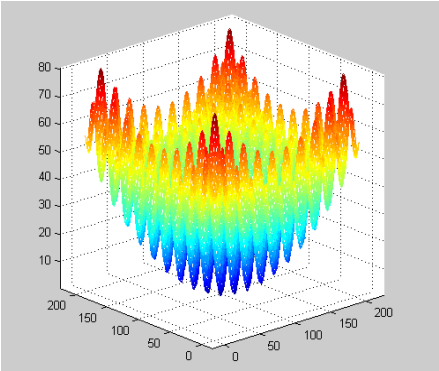

Figure 3 - Graph of the Rastrigin function of two variables

We will show how to search for the global minimum of the last example on the basis of the algorithm proposed above. It is more difficult to solve this example by using the gradient method than convex functions. The algorithm proposed above will easily calculate the value and coordinates of the global minimum.

First let's build a defining function for the Rastrigin function:

$$g(\alpha) = \int_{-5.12}^{5.12}\int_{-5.12}^{5.12}[\left|20 + x^2 + y^2 - 10\cos(2\pi x) - 10\cos(2\pi y) - \alpha\right| -$$

$$-(20 + x^2 + y^2 - 10\cos(2\pi x) - 10\cos(2\pi y) - \alpha)]^6\, dxdy$$

Search $\hat{\alpha}$ for the value of the global minimum point using the function $g(\alpha)$. The initial value α is randomly selected. If the function value area is set, you can start from it. If the function value area is not specified, then start searching with $\alpha = 0$. At $\alpha = 0$, it turns out $g(0) = 0$. Then the plane $z = \alpha$ passes below the graph of the specified function or touches at the point of the global minimum. Table 1 below shows a computational search $\hat{\alpha}$ experiment.

Table 1- step-by-step search $\hat{\alpha}$

	Select a value α	Calculate the value of the defining function	The location of the plane $z = \alpha$	We need to find the definition of an interval belonging to α
1	$\alpha = 0$	$g(0) = 0$	$z = 0$ the plane passes below the graph or touches the function graph at the global minimum point	We need to find the global minimum value is greater than 0, $\alpha \in [0;+\infty)$
2	$\alpha = 5$	$g(5) > 0$	$z = 5$ the plane passes above or intersects the function graph	We need to find the global minimum value is less than 5, $\alpha \in [0;5)$
3	$\alpha = 2{,}5$	$g(2.5) > 0$	$z = 2.5$ the plane passes above or intersects the function graph	We need to find the global minimum value is less than $2.5, \alpha \in [0;2.5)$
4	$\alpha = 1.25$	$g(1.25) > 0$	$z = 1.25$ the plane passes above or intersects the function graph	We need to find the global minimum value is less than 1.25, $\alpha \in [0;1.25)$
	….	…	…	…
	$\alpha = 0.000001$	$g(0.000001) > 0$	$z = 0.000001$ the plane passes above or intersects the function graph	The accuracy has been achieved $\alpha \in [0;0.000001)$

We stop the computational experiment when we reach the desired accuracy. In our examples, the accuracy for the value of the global minimum point $\varepsilon \le 10^{-6}$ is taken. We took the right end $\hat{\alpha} = 0{,}000001$ of the segment $\alpha \in [0;0.000001)$ as the value of the global minimum, because in searching for the coordinates of the global minimum point, the defining function must give a positive number.

Let's start searching for the coordinates of the global minimum point $\hat{x}$ and $\hat{y}$, where $\hat{x} \in [-5.12;5.12]$ and $\hat{y} \in [-5.12;5.12]$. We are looking for the coordinates of the point in the square $[-5.12;5.12]_x \times [-5.12;5.12]_y$. Divide the given square into four equal parts.

Dividing the sides in half $x_1 = \frac{5.12 + (-5.12)}{2} = 0$ and $y_1 = \frac{5.12 + (-5.12)}{2} = 0$, we get four squares $[-5.12;0]_x \times [-5.12;0]_y$, $[-5.12;0]_x \times [0;5.12]_y$, $[0;5.12]_x \times [-5.12;0]_y$ and $[0;5.12]_x \times [0;5.12]_y$. We will start calculating modified defining functions for the obtained regions.

$$g_{[-5.12;0]_x \times [-5.12;0]_y}(\hat{\alpha}) \equiv \int_{-5.12}^{0} \int_{-5.12}^{0} [\left|20 + x^2 + y^2 - 10\cos(2\pi x) - 10\cos(2\pi y) - \hat{\alpha}\right| -$$
$$- (20 + x^2 + y^2 - 10\cos(2\pi x) - 10\cos(2\pi y) - \hat{\alpha})]^6 \, dxdy$$

The integral for the first part gives a positive number. The integrals over the other parts can not be seen. We continue to search for the global minimum point in the square $[-5.12;0]_x \times [-5.12;0]_y$. We divide the selected part into four more squares and build four more integrals for them in the same way. table 1 below shows the search for global minimum coordinates.

Table 2-step-by-step search for global minimum coordinates

The definition area under consideration	Value of defining functions	Actions
$[-5.12;5.12]_x \times [-5.12;5.12]_y$.	$g_{[-5.12;5.12]_x \times [-5.12;5.12]_y}(\hat{\alpha}) > 0$	Divide the definition area into four equal parts
$[-5.12;0]_x \times [-5.12;0]_y$	$g_{[-5.12;0]_x \times [-5.12;0]_y}(\hat{\alpha}) > 0$	Divide the definition area into four equal parts
$[-5.12;-2.56]_x \times [-5.12;-2.56]_y$	$g_{[-5.12;-2.56]_x \times [-5.12;-2.56]_y}(\hat{\alpha}) = 0$	Do not consider this part, move to the next square
$[-5.12;-2.56]_x \times [-2.56;0]_y$	$g_{[-5.12;-2.56]_x \times [-2.56;0]_y}(\hat{\alpha}) = 0$	Do not consider this part, move to the next square
$[-2.56;0]_x \times [-2.56;0]_y$	$g_{[-5.12;0]_x \times [-2.56;0]_y}(\hat{\alpha}) > 0$	Divide the definition area into four equal parts
…	…	...
$[-0.000001;0]_x \times [-0.000001;0]_y$	$g_{[-0.000001;0]_x \times [-0.000001;0]_y}(\hat{\alpha}) > 0$	Stop searching for coordinates. The desired accuracy has been achieved.

This iteration continues until we reach the desired accuracy $\varepsilon \le 10^{-6}$. The coordinates of the global minimum point are $\hat{x} \approx \frac{0 + (-0.000001)}{2} \approx -0.0000005$ and $\hat{y} \approx \frac{0 + (-0.000001)}{2} \approx -0.0000005$. We found the global minimum: $f(x, y) \approx 0$, $x \approx 0$, $y \approx 0$. They match the reference values.

All test cases have been solved with accuracy $\varepsilon \le 10^{-6}$ and the answers received match the reference values.

The proposed algorithm does not do any extra work. First of all, it finds the value of the global minimum. And only then searches for the coordinates of this point. This will take less time and make your computer work easier.

М.Д. Рамазанов[1], Ж.Қ. Қайдасов[2], Ж.С.Туткушева[2]

[1]Математика институты, Уфа, Ресей;
[2]Қ. Жұбанов атындағы АӨМУ, Ақтөбе, Қазақстан;

ТЕГІС ФУНКЦИЯНЫҢ ГЛОБАЛЬДЫ МИНИМУМЫН ІЗДЕУДЕ ЖАҢА АЛГОРИТМНІҢ ТИІМДІЛІГІН ЗЕРТТЕУ

Аннотация. Соңғы уақытта оңтайландыру есептерінің өзектілігі өте қарқынды және табысты өсуде. Оңтайландыру есептерін қолдану аясы айтарлықтай кеңейді. Оңтайландыру есептерін шешу қажеттілігі барлық ғылымдарда бар. Функцияның локальды минимумын табудың көптеген әдістері ұсынылды. Бірақ функцияның глобальды минимумын табу міндеті аз зерттелген. Әр әдістің өзінің артықшылықтары мен кемшіліктері бар. Локальды минимумдары көп функцияның глобальды минимумын табу қажет болса, есеп қиындай түседі.

Бұл мақалада екі айнымалысы бар локальды минимумдары көп функцияның глобальды минимумын іздеу үшін жаңа алгоритм ұсынылған. Мұнда жаңа алгоритмнің жұмыс кезеңдері егжей-тегжейлі жазылған.

Ұсынылған әдіс басқа әдістерден ерекшеленеді, бұл жерде іздеуді глобальды минимум нүктесінің мәнін, яғна деңгейін анықтаудан бастаймыз. Глобальды минимум нүктесінің мәнін және координаталарын есептеу үшін жаңа анықтаушы функция құрылды. Анықтаушы функцияның көмегімен берілген функцияның глобальды минимум нүктесіне жанама жазықтықты табамыз. Глобальды минимум нүктесінің мәнін анықтағаннан кейін оның координаттары есептелді.

Мақалада квадратта анықталған функциялар карастырылған. Глобальды минимум координаттарын табу үшін анықталу облысын төрт тең квадратқа бөлу керек. Бұдан әрі осы квадраттардың қайсысында глобальды минимум бар екенің анықтаймыз. Таңдалған квадрат тағы төрт тең квадратқа бөлінеді. Бізге қажетті дәлдікке дейін квадратты бөлу жалғасады. Олар өзгерген анықтаушы функцияның көмегімен анықталады. Біз "жаңа" квадратты қарастырғанда, анықтаушы функция да интегралдау аймағы өзгертеді.

Бұл алгоритм есептеулер санын айтарлықтай азайтады, олай болса есептеу уақыты қысқарады.

Глобальды оңтайландыру алгоритмдерінің жылдамдығы мен дәлдігін бағалау үшін тесттік функциялар қолданылды. Үш түрлі тесттік функциялар алынды. Бірінші мысал ретінде дөңес функция келтірілді. Екінші мысалда параболалық қатты созылған беттің ішінде глобальды минимумы бар дөңес емес функция қарастырылды. Үшінші мысалда локальды минимумдары өте көп функцияның глобальды минимумы ізделді. Осы функциялармен есептеу эксперименттері жүргізілді. Барлық есептеулер $\varepsilon \le 10^{-6}$ дәлдігімен орындалды. Біз тесттік функциялардың глобальды минимумдарының мәндерін және координаттарын жаңа алгоритмнің көмегімен тауып, эталондық мәндермен салыстырдық. Есептелген мәндер эталондық мәндерге сәйкес келді. Бұл тесттік функциялар күрделілігіне қарай әр түрлі, бірақ ұсынылған алгоритм бірдей уақыт ішінде әр түрлі функциялардың глобальды минимумын анықтайды.

Анықтаушы функция қарастырылатын функцияға және оның анықтау облысына байланысты. Егер екі айнымалысы бар функция берілген болса, онда анықтаушы функция қос интегралды болады, оның интегралдау аймағы анықтау облысына сәйкес келеді. Берілген облыс бойынша еселі интегралды жуықтап есептеу үшін тұрақты шекаралық қабаты бар Соболев кубатуралық формулаларын пайдалану қолайлы. Бір өлшемді квадратураларды есептеудегі маңызды қасиеттерін Соболевтің көп өлшемді кубатуралық формулаларында да сақталады. Олар кеңістіктің кең класстары үшін колдонылады.

Кубатуралық формулаларды есептеу компьютер бағдарламалары арқылы жүзеге асырылады. Біз C++ бағдарламалау тілін таңдадық. Себебі C++ бағдарламалау тілінің қолдану аясы өте кең және күрделі есептерді іске асыру мүмкіндігі жоғары. Есептеу алгоритмі C++ тілінде Microsoft Visual Studio бағдарламасының көмегімен іске асырылды.

Түйін сөздер: көп өлшемді оңтайландыру, глобальды оңтайландыру алгоритмі, Соболев кубатуралық формулалары, Де Джонг функциясы, Розенброк функциясы, Растригин функциясы.

М.Д. Рамазанов[1], Ж.К. Кайдасов[2], Ж.С. Туткушева[2]

[1]Уфимский Институт Математики, Уфа, РФ;
[2]Актюбинский региональный государственный университет
имени К.Жубанова, Актобе, Казахстан;

ИССЛЕДОВАНИЕ ЭФФЕКТИВНОСТИ НОВОГО АЛГОРИТМА С ОПРЕДЕЛЯЮЩЕЙ ФУНКЦИЕЙ В ПОИСКЕ ГЛОБАЛЬНОГО МИНИМУМА ГЛАДКОЙ ФУНКЦИИ

Аннотация. В последнее время актуальность задач оптимизации растет очень интенсивно и успешно. Круг задач оптимизации существенно расширился. Потребность решить оптимизационные задачи есть практически во всех науках. Предложены много методов нахождения локального минимума функции. Меньше изучена задача нахождения глобального минимума функции. У каждого метода есть свои достоинства и недостатки. Задача становится сложнее, если нужно найти глобальный минимум у функции с большим количеством локальных минимумов.

В данной статье представлен новый алгоритм для поиска глобального минимума многоэкстремальных гладких функций двух переменных. Здесь детально расписаны все этапы работы нового алгоритма.

Предложенный метод отличается от других методов тем, что здесь поиск начинается со значения, то есть определяем уровень точки глобального минимума. Для вычисления значений и координат глобального минимума построена новая определяющая функция. С помощью определяющей функции мы находим касательную плоскость к графику заданной функции в точке глобального минимума. После определения значения точки глобального минимума, вычисляются координаты точки глобального минимума.

В статье рассмотрены функции определенные в квадрате, чтобы найти координаты глобального минимума, область определения делим на четыре равные квадраты. Дальше определяем, в каком из этих квадратов лежит найденное значение глобального минимума. Выбранный квадрат делим еще на четыре равные квадраты. И так продолжается до нужной нам точности. Они определяются с помощью видоизмененной определяющей функции. У определяющей функции будет меняться область интегрирования, каждый раз, когда мы рассматриваем «новый» квадрат.

Такой алгоритм значительно уменьшает количество вычислений – это значит, сокращается время вычислений.

Для оценки скорости и точности алгоритмов глобальной оптимизации применяются тестовые функции. Подобраны три различные тестовые задачи. В качестве первого примера приведена выпуклая функция, где локальный минимум совпадает с глобальным минимумом. Во втором примере разобрана невыпуклая функция, которая имеет глобальный минимум внутри параболической сильно вытянутой поверхности. В третьем примере разобрана функция с большим количеством локальных минимумов. Проведены вычислительные эксперименты с данными функциями. Мы нашли значения и координаты глобальных минимумов тестовых функций с помощью нового алгоритма и сравнили с эталонными значениями. Все вычисления сделаны с точностью $\varepsilon \le 10^{-6}$. Вычисленные значения и координаты точек глобальных минимумов совпадают с эталонными значениями. Эти функции разные по сложности, но предложенный алгоритм определяет глобальный минимум различных функций за одинаковое количество времени.

Определяющая функция зависит от рассматриваемой функции и от ее области определения. Если заданная функция двух переменных, то определяющая функция будет содержать двойной интеграл, где область интегрирования совпадает с областью определения. Для приближенного вычисления кратных интегралов по заданной области предлагается использовать кубатурные формулы Соболева с регулярным пограничным слоем. Многомерные кубатурные формулы Соболева сохраняют достоинства одномерных квадратур. Они оптимальны для широкого класса пространств.

Вычисления кубатурных формул реализованы с помощью компьютерных программ. Мы выбрали язык программирования C++ потому, что язык C++ имеет очень широкое применение и возможность реализовать сложные задачи. Алгоритм вычисления реализован с помощью программы Microsoft Visual Studio на языке C++.

Ключевые слова: многомерная оптимизация, алгоритм глобальной оптимизации, кубатурные формулы Соболева, функция Де Джонга, функция Розенброка, функция Растригина.

Information about authors:

Ramazanov Marat Davidovich - Institute of Mathematics with Computing Centre, Ufa Federal Research Centre of the Russian Academy of Science, Doctor of physical and mathematical sciences, Professor of Mathematics, Ramazanovmd@yandex.ru, https://orcid.org/0000-0002-9374-5997;

Kaidassov Zhetkerbay - Aqtobe Regional Zhubanov State University, Candidate of Physical and Mathematical Sciences, Associate Professor, jet-k@mail.ru, https://orcid.org/0000-0002-3746-6117;

Tutkusheva Zhailan Salavatovna – Aqtobe Regional Zhubanov State University, PhD Student, zhailan_k@mail.ru, https://orcid.org/0000-0003-3611-9620.

REFERENCES

[1] Kochegurova E.A. Optimization theory and methods, Tomsk: Tomsk Polytechnic University, (2011), 150. (in Russian)

[2] Yang X.-S., Deb S., Engineering optimization by cuckoo search. Int. J. Math. Modelling Num. Optimisation, (2010). Vol. 1, № 4, 330-343.

[3] Panteleev A.V., Letova T.A., Optimization methods in examples and problems, M.: Higher school, (2005), 544. (in Russian).

[4] CHernoruckij I.G. Optimization methods in management theory, SPb.: Peter, (2004), 256. (in Russian).

[5] Tutkusheva Zh.S. Determining the coordinates of the global minimum of an arbitrary smooth function // Modern innovations: Journal. Moscow(2019). No 4(32), 5-7. (in Russian).

[6] Sobolev S.L. Vaskevich V.L Cubature formula, Novosibirsk: Sobolev Institute of mathematics, (1996), 484. (in Russian).

[7] Ramazanov M.D. New algorithm for asymptotically optimal lattice cubature formulas // Ufa mathematical journal, (2009), 178. (in Russian).

[8] Ramazanov, M.D. Theory of lattice cubature formulas with a bounded boundary layer // Ufa mathematical journal, (2010), Vol. 2, No 3. 63-82. (in Russian).

[9] Kul'tin. N. Visual C++ in tasks and examples. - 2nd ed. - Petersburg: BHV-Petersburg, (2015), 268. (in Russian).

[10] Sidorina T. L. "Tutorial Microsoft Visual Studio C++ and MFC" BHV-Petersburg, (2009), 848. (in Russian).

[11] Sergienko A.B. Test functions for global optimization. Krasnoyarsk, (2012), 112. (in Russian).

[12] Yuret D. De Jong's test suite, (1997), http://www2.denizyuret.com/pub/ aitr1569/node19.html.

[13] Rosenbrock function. http://en.wikipedia.org/wiki/Rosenbrock_function.

[14] Rosenbrock H.H., An automatic method for finding the greatest or least value of a function». - The Computer Journal 3, (1960), 175–184.

[15] Rastrigin function. http://en.wikipedia.org/wiki/Rastrigin_function

NEWS
OF THENATIONAL ACADEMY OF SCIENCES OF THE REPUBLIC OF KAZAKHSTAN
PHYSICO-MATHEMATICAL SERIES
ISSN 1991-346X **https://doi.org/10.32014/2020.2518-1726.71**
Volume 4, Number 332 (2020), 103 – 113

UDC 517.929.4
MRNTI 27.29.17, 27.29.23

K.B. Bapaev[1], G.K. Vassilina[1,2], S.S. Slamzhanova[3]

[1]Institute of Mathematics and Mathematical Modeling, Almaty, Kazakhstan;
[2]Almaty University of Energy and Communications, Almaty, Kazakhstan;
[3]Zhetysu State University named after I. Zhansugurov, Taldykorgan, Kazakhstan.
E-mail: bapaev41@bk.ru, v_gulmira@mail.ru, beksultan.82e@mail.ru

ON COMPRESSIBILITY AREA OF UNSTABLE DIFFERENCE-DYNAMIC SYSTEMS AND DETERMINATED CHAOS

Abstract. In this paper saddle-point bifurcation is studied. It is shown that as a result of bifurcation or collision of stable and unstable points, they leave the area. In other words, they go into chaos, i.e. in a state of disorder. Here the normalization method is used to identify the bifurcation point. Unstable in the sense of Lyapunov difference-dynamic systems are considered.

In the first part of the paper, the transformation of linear systems in instability case is given. A linear system with a diagonal matrix is considered. It is shown that in a neighborhood of zero this system is not reduced to a special form with the help of non-degenerate transformations. It is proved that for non-degenerate transformations the trajectories of a system of a special form from a neighborhood of the origin cannot be displayed in the trajectory of solutions of a given linear system. Thus, the topology of the neighborhood of the zero point of a system of a special form does not transform into the topology of a given system in a neighborhood of zero. The causes of the contradiction obtained by applying this method are shown.

In the second part, analytic difference-dynamical systems and analytic homeomorphisms are considered. Also compressive difference-dynamical systems are investigated. The concept of ω-compressing difference-dynamical systems is given. It is shown to which system the ω-compressing difference-dynamical systems are isomorphic.

Key Words: difference-dynamic system**,** bifurcation, stability, homeomorphism, chaos.

Introduction. The word "chaos" comes from the Greek. Initially, it meant an infinite space that existed before the appearance of everything else. Later, the Romans interpreted chaos as the original raw formless mass, into which the creator brought order and harmony. In the modern sense, chaos means a state of disorder and an irregularity of physical processes, which is called hydrodynamic and plasma turbulence.

The theory of turbulence, it would seem, should be completely based on classical macroscopic equations: Navier-Stokes equations, equations of gas dynamics, etc. However, it is not yet possible to derive the main characteristics of turbulent motion from macroscopic equations and we have to resort to additional considerations.

Until recently, the Landau hypothesis reigned supreme in the theory of the appearance of turbulence [1,2]. This theory he expressed in 1944. Similar considerations were put forward by Hopf [3] in 1948.

Landau's theory connects the emergence of turbulence with instability. This is certainly true, but how Landau's theory does this will require substantial refinement. Landau's theory indicates only one of the possible variants of the appearance of turbulence and, apparently, is far from the most important. The modern theory of bifurcations offers many other ways [3-10].

These are new ways of randomization and stochatization of fluid motion, different from those indicated by Landau.

According to Landau, the occurrence of turbulence occurs as a result of a sequential series of stability loss by the equilibrium state, by the periodic motion, by the bipolar motion and etc., as a result of which the motion becomes multi-periodic:

$$V(t) = f(w_0 t, w_1 t, \ldots, w_n t),$$

here $w_0, w_1, \ldots, w_n$ are the frequencies. The function $f(\phi_1, \phi_2, \ldots, \phi_n)$ as a function of variables $\phi_1, \phi_2, \ldots, \phi_n$ is periodic for each of them with the period 2π. Ruelle and Tuckens [10] drew attention to the fact that the path indicated by Landau is not common, that the common possibility is the formation of a strange attractor [7]. But how a strange attractor arises, they have not investigated.

Statements by Yu.I. Neymark [11] on turbulence is the result of his study of homoclinic structures discovered by A. Poincare [12].

In the description of turbulence, against the background of chaos theory, one result stands out in a special way. This is a period doubling cascade discovered by the Los Alamos physicist Mitchell Feigenbaum [6,7].

One interesting aspect of the cascade of period doubling or fork-shaped bifurcation (Feigenbaum scenario) is that when you notice it during an experiment, you will not confuse it with anything else. In addition, it is known that chaos exists beyond the cascade. Therefore, the observation of the Feigenbaum cascade in hydrodynamics is particularly convincing evidence that modes must yield to chaos.

In this paper, we study bifurcation of the "saddle point" type. And the result of a collision (bifurcation) of stable and unstable fixed points is showed, as a result of which both disappear (leave the region) i.e. this point go into chaos. The use of the normalization method to identify the bifurcation point is used for the first time for difference-dynamic systems unstable in the sense of Lyapunov [13-15].

I Transformation of linear systems in instability case

Inability to make a special appearance. Consider the linear system

$$x_{n+1} = Ax_n, \ \left(x_n = x_n^1, \ldots, x_n^m \in R^m\right).$$

Without loss of generality, we can consider diagonal matrix A and restrict ourselves to the equation for one component:

$$x_{n+1} = \lambda x_n, x_n \in R^1, \quad |\lambda| > 1. \tag{1.1}$$

Using analytic mappings in a neighborhood of point $x = 0$ [4]

$$x = y + \sum_{k=2}^{\infty} a_k y^2 \equiv \varphi(y); \quad y = x + \sum_{k=2} \alpha_k x^k \equiv \varphi^{-1}(x) \tag{1.2}$$

we transform (1.1) to the following form

$$y_{n+1} = \lambda y_n - a y_n^2. \tag{1.3}$$

We calculate the coefficients α_k of the inverse transformation $\varphi^{-1}(x)$:

$$y = \sum_0^{\infty} y^x a_k + \alpha_2 \left(\sum_0^{\infty} y^x a_k \right)^2 + \alpha_3 \left(\sum_0^{\infty} y^x a_k \right)^3 + \ldots = y + (a_2 + \alpha_2) y^2 +$$

$$+ (a_3 + 2a_2\alpha_2 + \alpha_3) y^3 + \left(a_4 + 3a_2\alpha_3 + \alpha_2 (a_2^2 + 2a_3) + \alpha_4\right) y^4 + \ldots;$$

$$\alpha_2 = -a_2; \alpha_3 = 2a_2^2 - a_3; \alpha_4 = -a_4 - a_2(a_2^2 + 2a_3) + 3a_2(a_3 - 2a_2^2)_m, \ldots$$

From (1.3) we find $(a_2 \equiv a)$

$$y_{n+1} = \lambda y_n - a\lambda(\lambda - 1) y_n^2 + \left(a_3\lambda - 2a^2\lambda^2 + 2\lambda^3 a^2 - \lambda^3 a_3\right) y_n^3 + \ldots,$$

$$a_3\lambda - 2a^2\lambda^2 + 2\lambda^3 a^2 - \lambda^3 a_3 = 0.$$

Therefore if $a_k \neq 0$ then (1.1) can be reduced to (1.3). If mappings (1.2) are non-degenerate in the neighborhood of a point $x = 0$, then a unique trajectory $\{x_n\}$ of equation (1.1) corresponds to any trajectory $\{y_n\}$ of equation (1.3) and vice versa.

Consider the trajectory $\{y_n\} \in (1.3), y_0 = \frac{\lambda}{a}$

$$y_1 = y_0(\lambda - ay_0) = 0,\ y_k = 0,\ k \geq 1.$$

Then $x_0 = \varphi(y_0) \neq 0$, $x_1 = \lambda\varphi(y_0) = \varphi(y_1) = \varphi(0) = 0$. This is impossible.

Let $\{y_n\} \in (1.3)$ be such that $\mu_0 \leq |y_n| \leq \mu_1 n$. Then $x_0 = \varphi(y_0) \neq 0$, $x_2 = \lambda\varphi(y_0), \ldots, x_{n+1} = \lambda^n \varphi(y_0)$. i.e. $x_n \to \infty$ takes place for $n \to \infty$.

Theorem 1. For non-degenerate transformations (2) trajectories $\{y_n\} \in (1.3)$ from the neighborhood $y = 0$ cannot be displayed in the trajectory $\{x_n\} \in (1)$ the neighborhood $x = 0$.

Thus, the topology of the neighborhood of $y = 0$ of the system (1.3) does not transform into the topology of the system (1) in the neighborhood $x = 0$.

The neighborhood $y = 0$ of system (1.3) is very interesting:

$$\left.\begin{array}{l} |\lambda - ay_n| < 1; \\ \end{array}\begin{array}{l} 0 \leq \lambda - ay_n < 1 \\ 0 \leq ay_n - \lambda < 1 \end{array}\right\} \Rightarrow \text{stability zones;}$$

$$\left.\begin{array}{l} |\lambda - ay_n| > 1; \\ \end{array}\begin{array}{l} \lambda - ay_n > 1 \\ ay_n - \lambda > 1 \end{array}\right\} \Rightarrow \text{instability zones.}$$

$t_1 = \frac{\lambda - 1}{a}$, $t_2 = \frac{\lambda}{a}$, $t_3 = \frac{\lambda + 1}{a}$ are singular points of the system (1.3). As shown above, if the trajectory $\{y_n\} \in (1.3)$ falls for some "n" at a neutral singular point $t_2 = \frac{\lambda}{a}$ i.e. $t_n = \frac{\lambda}{a}$, then this trajectory goes to the point $y_n = 0 : \left\{ y_n = \frac{\lambda}{a},\ y_{n+k} = 0, k \geq 1 \right\}$. There are no such trajectories in system (1.1).

Let's consider a more general case: let (1) be converted to

$$y_{n+1} = \left(\lambda - ay_n^{2p}\right) y_n; z_{n+1} = \left(\lambda - az_n\right)^{2p} z_n; |y_n|^{2p} = z_n. \tag{1.4}$$

Let the transformation $x = \varphi(z)$ (1.2) transform the neighborhood $z = 0$ into a neighborhood $x = 0$ one-to-one.

Then in particular the trajectory $\{z_n \in (4)\}; z_0 = \frac{\lambda}{a}; z_k = 0, k \geq 1$ goes into the trajectory $x_0 = \phi\left(\frac{\lambda}{a}\right) \neq 0, x_1 = \lambda\phi\left(\frac{\lambda}{a}\right) = \phi(y_1) = \phi(0) = 0.$ But it is impossible.

Similarly with the trajectories $\mu_0 \leq z_n \leq \mu_1 \forall n$ we have $x_0 = \phi(z_0) \neq 0, x_{n+1} = \lambda^n \phi(z_0), n > 1.$ Since $\lambda > 1$ it is followed $x_n \to \infty$ for $n \to \infty$. And in this case, Theorem 1 holds.

Thus, system (1.1) in a neighborhood of a point $x = 0$ cannot be reduced to the form (1.3) or (1.4) using non-degenerate transformations (1.2).

So, the following contradiction has been obtained: on the one hand, formally (1.1) can be reduced to (1.3) (in the general case, (1.4)) by transformation (1.2), on the other hand, according to statement (1.1), this is impossible.

The reasons for the contradiction. Since we are talking about the transformation of a neighborhood of a point $x=0$ into a neighborhood $y=0$ (in the general case $z=0$), it suffices to consider the transformation

$$x = y + ay^2 \equiv \phi(y);\ y = \frac{1}{2a}\left(\sqrt{1+4ax}-1\right) \equiv \phi^{-1}(x);\ |ax| \le 1, \tag{1.5}$$

where from $y = x - ax^2 + 2a^3x^3 + \alpha_4 a^3 x^4 + \ldots \equiv \varphi^{-1}(x)$.

Moreover, (1) is reduced to the form

$$y_{n+1} \equiv \gamma_1 y_n + \sum_{k=3}^{\infty} \gamma_k (a\lambda)^{k-1} y_n^k;\ \gamma_1 = \lambda - \lambda(\lambda-1)ay_n \tag{1.6}$$

For the map (1.6) to be contracting in a neighborhood $y=0$, it is necessary that for

$$y_{n+1} \equiv \gamma_1 y_n + \sum_{k=3}^{\infty} \gamma_k (a\lambda)^{k-1} y_n^k;\ \gamma_1 = \lambda - \lambda(\lambda-1)ay_n$$

inequalities

$$\omega : ay_n > 0, \quad |\gamma_1| = \lambda\left|1-(\lambda-1)ay_n\right| < 1 \tag{1.7}$$

take place.

Moreover, by virtue of $|y_n| < 1$ the terms in (1.6) should be small in comparison with $\{\gamma_1 y_n\}$.

On the other hand, by virtue of (1.7), we have

a) $0 \le \lambda - \lambda(\lambda-1)ay_n| < 1$;

b) $0 \le \lambda - \lambda(\lambda-1)|ay_n| - \lambda < 1$.

Hence we have

a) $\{\gamma_1 y_n\}$;

b) $\lambda|ay_n| \ge \dfrac{\lambda}{\lambda-1} > 1$, т.е. $(\lambda|ay_n|)^k > 1,\ \forall k \ge 3$.

But then in (1.6) $|\gamma_k|(|\lambda a y_n|)^{k-1}|y_n| > |\gamma_k||y_n|$ takes place, i.e. all terms in expansion (1.6) are comparable with the first term $(\gamma_1 y_n)$.

Direct study of the mapping (5). Based on (5), system (1) is transformed to

$$y_{n+1} = \frac{1}{2a}\left(\sqrt{1+\Delta_n}-1\right),\ \ \Delta_n = 4\lambda\left[ay_n + a^2 y_n^2\right]. \tag{1.8}$$

Let us find out when the map (1.8) is contracting in a neighborhood $y=0$, i.e. inequality

$$|y_{n+1}| = \frac{1}{2|a|}\left|\sqrt{1+\Delta_n}-1\right| < \gamma|y_n|,\ \ y_n \in \omega, \forall n >> 1 \tag{1.9}$$

holds. Let's consider all possible options:

(i) If $ay_n > 0$ then $\Delta_n \ge 0$. We will refine the estimate in (i):

$$|y_{n+1}| = \frac{2\lambda|y_n|(1+|ay_n|)}{1+\sqrt{1+\Delta_n}} < \gamma|y_n|,\ \gamma < 1.$$

From this inequality we find

$$2\lambda(1+z) < \gamma\left(1+\sqrt{1+\Delta_n}\right),\quad \Delta_n = 4\lambda\left(z+z^2\right),\quad z = |ay_n|.\ (*)$$

Take $\alpha = \frac{2\lambda}{\gamma} - 1 = \frac{2\lambda - \gamma}{\gamma} > \frac{2\lambda - \lambda}{\gamma} = \frac{\lambda}{\gamma} > 1,\ a > 1$. Inequality (*) takes the form

$$(\alpha + 2\lambda z) < 1 + 4\lambda\left(z + z^2\right), \quad \left(\alpha^2 - 1\right) + 4\lambda z(\alpha - 1) + 4\lambda z^2(\lambda - 1) < 0.$$

It is impossible for $\alpha = \frac{2\lambda}{\gamma} - 1 = \frac{2\lambda - \gamma}{\gamma} > \frac{2\lambda - \lambda}{\gamma} = \frac{\lambda}{\gamma} > 1,\ a > 1$, i.e.

$$|y_{n+1}| = \frac{1}{2|a|}\frac{|\Delta_n|}{1 + \sqrt{1 + \Delta_n}} < \lambda\left(|y_n| + |a|y_n^2\right) < \gamma|y_n|, \quad \gamma < 1$$

impossible since $\lambda > 1$.

(ii) $ay_n < 0$, $\Delta_n > 0$. Then $ay_{n+1} = \frac{1}{2}\left(\sqrt{1 + |\Delta_n|} - 1\right) > 0,\ \Delta_n > 0$, which by virtue of (i) is impossible.

(iii) $ay_n < 0$, $\Delta_n > 0$ (but certainly $1 + \Delta_n \geq 0$). Then

$$|y_{n+1}| = \frac{1}{2|a|}\left|\sqrt{1 + |\Delta_n|} - 1\right| = \frac{|\Delta_n|}{2|a|\left(1 + \sqrt{1 - |\Delta_n|}\right)} < \gamma|y_n|.$$

From the latter for $y_n \neq 0$ we have

$$\frac{|y_{n+1}|}{|y_n|} \equiv \frac{2\lambda\left(1 - |ay_n|\right)}{1 + \sqrt{1 - |\Delta_n|}} < \gamma < 1, \text{ i.e. } \lambda\left(1 - |ay_n|\right) \leq \frac{|y_{n+1}|}{|y_n|} < \gamma < 1.$$

Thus $|y_n| \geq \alpha_0 = \frac{1}{|a|}\left(1 - \frac{\gamma}{\lambda}\right) > 0, \quad \forall n >> 1,$ which contradicts the compressibility of the map.

Theorem 2. The map (1.8) is not compressive in a neighborhood $y = 0$.

II Analytic difference-dynamical systems and analytic homeomorphisms

Isomorphisms of difference-dynamical systems. Consider difference-dynamical systems on R^1

$$x_{n+1} = \lambda z_n + X(x_n); \quad X(x_n) = \sum_{k=b}^{\infty} b_k x^k, \tag{2.1}$$

Here the function $X(x_n)$ is analytic in a neighborhood of $x = 0$. We apply to (2.1) the analytic homeomorphism $x = \varphi(y)$ of a neighborhood of a point $y = 0$ [4]

$$x = \varphi(y) \equiv y + \Phi(y); \quad \Phi = \sum_{k=z}^{\infty} a_k y^k \tag{2.2}$$

$$y = \varphi^{-1}(y) \equiv x + \Psi(x); \quad \Psi(x) = \sum_{k=2}^{\infty} \alpha_k x^k,$$

Here $\Phi(y)$ and $\Psi(x)$ are respectively analytic in the neighborhoods of $y = 0$ and of $x = 0$. The coefficients a_k of expansion $\Psi(x)$ are uniquely determined through a_k of $\Phi(y)$.

In the new variables, system (1) takes the form

$$y_{n+1} = \lambda y_n + \chi(y_n); \quad \chi(y) = \sum_{k=2}^{\infty} \beta_k y^k \tag{2.3}$$

Here $\chi(y)$ is analytic in a neighborhood of $y = 0$ and its coefficients β_k are uniquely determined in terms b_k of (1) and a_k of (2).

Systems (2.1) and (2.3) are called isomorphic with respect to the analytic homeomorphism (2.2) or simply isomorphic.

ω - compressive *difference-dynamical systems*. System (2.1) is called ω-compressive if there exists a set $\omega \subset M : |x| < \varepsilon$ on which (1) is a compressive manifold

$$|x_{n+1}| \le \gamma |x_n|, \quad 0 < \gamma < 1; \quad x_n \in \omega, \quad \forall n >> 1. \tag{2.4}$$

Obviously, for $|\lambda| < 1$ (stable case) system (2.1) is compressive in a neighborhood $M : |x| < \varepsilon$, i.e. $\omega = M = \{x | |x| < \varepsilon\}$.

Let 's highlight the next non-trivial class of unstable difference-dynamical systems ($|\lambda| > 1$)

$$x_{n+1} = (\lambda - a x_n^q) x_n + X(x_n); \quad X = x_n^{q+2} \sum_{k=0}^{\infty} b_k x_n^k, \quad q \ge 1. \tag{2.5}$$

In the neighborhood $M : |x| < \varepsilon$ we introduce the set

$$\omega = \{x / |\lambda - a x^q| < 1, |x| < \varepsilon\}. \tag{2.6}$$

Obviously, in the unstable case ($|\lambda| > 1$), the set ω does not contain a point $x = 0$, and system (5) is ω-compressive if $\omega \ne \phi$.

Let for definiteness $\lambda > 0$, then $|\lambda - a x^q| < 1$:

а) $0 \le \lambda - a x^q < 1$;

в) $0 \le a x^q - \lambda < 1$.

Let's put $p \equiv \left(\frac{\lambda}{|a|}\right)^{\frac{1}{q}}$, $\underline{p} \equiv \left(\frac{\lambda - 1}{|a|}\right)^{\frac{1}{q}}$, $p \equiv \left(\frac{\lambda + 1}{|a|}\right)^{\frac{1}{q}}$. If the condition

$$p \equiv \left(\frac{\lambda}{|a|}\right)^{\frac{1}{q}} < \varepsilon \tag{2.7}$$

is satisfied then

$$\omega = \underline{\omega} = \left\{ x / 0 < \underline{p} = \left(\frac{\lambda - 1}{|a|}\right)^{\frac{1}{q}} \le |x| \le p \equiv \left(\frac{\lambda}{|a|}\right)^{\frac{1}{q}} \equiv \overline{p} < \varepsilon \right\}, \text{ here } \underline{\omega} = \phi.$$

If the stronger condition

$$\overline{p} = \left(\frac{\lambda - 1}{|a|}\right)^{\frac{1}{q}} < \varepsilon \tag{2.8}$$

is satisfied then $\omega = \underline{\omega} U \overline{\omega}, \quad \overline{\omega} = \{x / p \le |x| \le \overline{p} < \varepsilon\} \ne \phi$.

Thus, when one of the conditions (2.7) or (2.8) is fulfilled, the difference-dynamical system (5) is ω-compressive.

In part I it is proved that (5) is not an isomorphic to the linear system (1) in $(X(x) \equiv 0)$.

Theorem 3. If the difference-dynamical system (2.5) is ω-compressive, then it is isomorphic to the system

$$y_{n+1} = (\lambda - a y_n^p) y_n, \forall p \ge 1. \tag{2.9}$$

Consider the general case of system (1) for $x_n \in R^m, m \ge 1$.

The proof is carried out in two stages. I. We prove first that (2.5) can be reduced to (2.9). For any fixed q (in this case $b \equiv a$) we apply sequentially the transformations

$$x = y + \gamma_i y^{q+i} \equiv \varphi_i(y), \quad i \geq 2 \quad (2.10)$$

We start for $i = 2$ and calculate the inverse transformation

$$y \equiv \phi_2^{-1}(x) = x + \sum_{k=0}^{\infty} \alpha_k x^k = \left(y + \gamma_2 y^{q+2}\right) + \alpha_z \left(y + \gamma_2 y^{q+}\right)^2 + \ldots =$$

$$= y + \alpha_2 y^2 + \ldots + \alpha_{q+1} y^{q+1} + \left(\gamma_2 + \alpha_{q+2}\right) y^{q+2} + \ldots.$$

From here we find $\alpha_k = 0, k = 2, q+1; \alpha_{q+2} = -\gamma_2$. Substituting the transformations $\varphi_2(y)$ and $\varphi_2^{-1}(x)$ to (5), we get

$$y_{n+1} = x_{n+1} + \sum_{k=0}^{\infty} \alpha_k x_{n+1}^k = \lambda x_n - a x_n^{q+2} + X_*(x_n)^3 -$$

$$-\gamma_2 \left(\lambda x_n - a x_n^{q+1} + X(x_n)\right)^{q+2} = \lambda x_n - a x_n^{q+1} + \left(b_0 - \lambda^{q+2}\gamma_2\right) x_n^{q+2} + x_n^{q+3} X^*(x_n),$$

here $X^*(x_n) = \sum_{k=0}^{\infty} \beta_k^* x_n^k, \quad X_*(x_n) = \sum_{k=0}^{\infty} \beta_{k*} x_n^k.$

So

$$y_{n+1} = \lambda\left(y_n + \gamma_2 y_n^{q+2}\right) - a\left(y_n + \gamma_2 y_n^{q+2}\right)^{q+1} + \left(b_0 - \lambda^{q+2}\gamma_2\right)\left(y_n + \gamma_2 y_n^{q+2}\right)^{q+2} +$$

$$+ y_n^{q+3} Y(y_n) = \lambda y_n - a y_n^{q+1} + \left(b_0 + \gamma_2\left(\lambda - \lambda^{q+2}\right)\right) y_n^{q+2} + y_n^{q+3} Y(y_n).$$

Assuming $\gamma_2 = -\left(\lambda - \lambda^{q+2}\right)^{-1} b_0$ we get to the difference-dynamical system (2.5):

$$y_{n+1} = \left(\lambda - a y_n^q\right) y_n + y_n^{q+3} Y(y_n); \quad Y = \sum_{k=0}^{\infty} \mu_k y_n^k \ .$$

Applying the transformation (10) $y = z + \gamma_3 z^{q+3} \equiv \phi_3(z)$ for $i = 3$ to the last difference-dynamical system, we obtain

$$z_{n+1} = \left(\lambda - a z_n^q\right) z_n + z_n^{q+4} Z(z_n)$$

and i.e. As usual, using Newton's method the convergence of this infinite process of "destroying" decomposition members in (2.5) is proved. Note that $Y(y_n)$ do not enter the growing degrees of the "large" parameter $|a| >> 1$.

We show that the system

$$x_{n+1} = \left(\lambda - a x_n^q\right) x_n; \quad \omega(x) \neq \phi, \quad \omega = \left\{x \middle| \lambda - a x^q \right| < 1, |x| < \varepsilon\right\} \quad (2.11)$$

reduced to the following system

$$y_{n+1} = \left(\lambda - b y_n^q\right) y_n + y_n^{q+3} Y(y_n); \quad \omega(y) \neq \phi \quad (2.12)$$

using conversion

$$x = y + \gamma_1 y^{q+1} + \gamma_2 y^{q+2} \equiv \varphi(y).$$

Note that for existence $\varphi^{-1}(x)$ the neighborhood of a point $y = 0$ must be so small as to $\left|\gamma_1 y^{q+1} + \gamma_2 y^{q+2}\right| \leq |y|\mu$.

Consider the inverse transformation $y = x + \sum_{k=2}^{\infty} \alpha_k x^k \equiv \varphi^{-1}(x)$. As before, we make sure that $\widetilde{\alpha}_k = 0, \quad k = \overline{2, q}$. Then

$$\phi^{-1}(x) = y = x + \alpha_1 x^{q+1} + \alpha_2 x^{q+2} + \alpha_3 x^{q+3} + \ldots = \left(y + \gamma_1 y^{q+1} + \gamma_2 y^{q+2}\right) +$$
$$+\alpha_1(\phi)^{q+1} + \alpha_2(\phi)^{q+2} + \alpha_3(\phi)^{q+3} + \ldots = y + (\gamma_1 + \alpha_1) y^{q+1} + (\gamma_2 + \alpha_2) y^{q+2} + \ldots.$$

Hence $\alpha_k = -\gamma_k$, $k = 1,2$ and by that $y = x + \gamma_1 x^{q+1} + \gamma_2 x^{q+2} + \ldots \equiv \varphi^{-1}(x)$. Substituting $\varphi(y)$ and $\varphi^{-1}(x)$ to (2.11) we obtain

$$y_{n+1} = \left(\lambda - a x_n^q\right) x_n - \gamma_1 \left(\lambda - a x_n^q\right)^{q+1} x_n{}^{q+1} - \gamma_2 \left(\lambda - a x_n^q\right)^{q+2} x_n{}^{q+2} + \ldots =$$
$$= \lambda x_n - \left(a + \gamma_1 \lambda^{q+1}\right) x_n^{q+1} - \lambda^{q+2} \gamma_2 x_n^{q+2} + \ldots =$$
$$= \lambda\left(y_n + \gamma_1 y_n^{q+1} + \gamma_2 y_n^{q+2}\right) - \left(a + \gamma_n \lambda^{q+1}\right)\left(\phi(y_n)\right)^{q+1} - \gamma_2 \lambda^{q+2}\left(\phi(y_n)\right)^{q+2} + \ldots =$$
$$= \lambda y_n + \left(\left(\lambda - X^{q+1}\right)\gamma_1 - a\right) y_n^{q+1} + + \left(\lambda - X^{q+2}\right)\gamma_2 y_n^{q+2} + \ldots.$$

Assuming $\gamma_1 = \left(\lambda - \lambda^{q+1}\right)^{-1} a$ and $\left(\lambda - \lambda^{q+2}\right)\gamma_2 \equiv -b$ we obtain (2.12) with arbitrary b (together with arbitrary γ_2), which allows us to obtain $\omega(y) \neq \phi$, $\omega = \left\{y \middle\| \lambda - b y^{q+1}\right| < 1, |y| < \delta\}$.

Note that, due to the ω-compressibility of the considered difference-dynamical systems (conditions (2.7), (2.8)), we have $|\gamma_1| >> 1$. Similarly, the ω-compressibility conditions (2.12) lead to the relation $|\gamma_2| >> 1$.

Therefore, when proving the convergence of decompositions, it is necessary to distinguish the growing degrees of values $p = \left|\lambda - a x_n{}^q\right| < 1$ и $\mu = \left|\lambda - a y_n{}^{q+1}\right| < 1$. The theorem is proved.

Remark. Polynomial difference-dynamical systems

$$x_{n+1} = \sum_{k=1}^{p-1} a_k x_n^k + x_n^p X_p(x_n), \tag{2.13}$$

can be considered. Here continuous function $X_p(x)$ is uniformly bounded

$$\left|X_p(x)\right| \le M, \quad |x| < \varepsilon$$

in the neighborhood of the point $x = 0$.

System (2.13) turns into analytic if $X_p(x)$ is analytic function in the neighborhood of the point $x = 0$, i.e. the series $X_p(x) = \sum_{k=0}^{x} b_k x^k$ converges for $|x| < \varepsilon$.

Similarly, one can consider polynomial homeomorphisms $x = \varphi(y)$ of a neighborhood $y = 0$ into the neighborhood of $x = 0$:

$$x = y + \sum_{k=2}^{p-1} \gamma_k y_k + \Phi_p(y) \equiv \varphi(y); \quad y = x + \sum_{k=1}^{p-1} \alpha_k x^k + \chi_p(x) \equiv \varphi^{-1}(x),$$

here $\Phi_p(y)$ and $\chi_p(x)$ are continuous functions, i.e. they are uniformly bounded functions respectively in the neighborhoods of $y = 0$ and of $x = 0$.

Moreover, the need for proving the convergence of the series in the neighborhood of the points $y = 0$ and $x = 0$ disappears.

К.Б. Бапаев[1], Г.Қ. Василина[1,2], С.С. Сламжанова[3]

[1]Математика және математикалық моделдеу институты, Алматы, Қазақстан;
[2]Алматы энергетика және байланыс университеті, Алматы, Қазақстан;
[3]І. Жансүгіров атындағы Жетісу мемлекеттік университеті, Талдықорған, Қазақстан

ТҰРАҚТЫ ЕМЕС АЙЫРЫМДЫ-ДИНАМИКАЛЫҚ ЖҮЙЕЛЕРДІҢ СЫҒЫМДАЛУ АЙМАҒЫ ТУРАЛЫ ЖӘНЕ ДЕТЕРМИНИСТІК ХАОС

Аннотация. Хаос теориясы белгілі бір жағдайларда хаос (динамикалық хаос, детерминистік хаос) деп аталатын құбылысқа ұшырайтын кейбір сызықты емес динамикалық жүйелердің әрекетін сипаттайтын теория. Мұндай жүйенің өзгерісі кездейсоқ болып көрінеді, тіпті егер жүйені сипаттайтын модель детерминистік болса да.

Қазіргі мағынада, хаос дегеніміз - гидродинамикалық және плазмалық турбуленттілік деп аталатын физикалық процестердің тұрақсыздығы.

Турбуленттілік теориясы толығымен классикалық макроскопиялық теңдеулерге негізделуі керек: Навье-Стокс теңдеулері, газ динамикасы және т.б., дегенмен турбулентті қозғалыстың негізгі сипаттамаларын макроскопиялық теңдеулерден алу әлі мүмкін емес, сондықтан қосымша ойларға жүгінуге тура келеді.

Соңғы кезге дейін Ландау гипотезасы турбуленттіліктің пайда болу теориясында басты орынға ие болды. Ландау теориясы турбуленттіліктің пайда болуын тұрақсыздықпен байланыстырады. Бұл әрине дұрыс, бірақ оны жасау әдісі айтарлықтай жетілдіруді талап етеді. Жаңа көзқарастар тұрғысынан Ландау теориясы толық емес. Бұл турбуленттіліктің пайда болуының мүмкін болатын нұсқаларының тек біреуін ғана көрсетеді және, мүмкін, ең маңыздысынан алыс. Қазіргі бифуркация теориясы Ландау теориясынан басқа сұйықтықтың қозғалысын рандомизация және стохатизациялау жолынан басқа көптеген жолдарды ұсынады.

Ландаудың айтуы бойынша турбуленттіліктің пайда болуы тепе-теңдік күйдің тұрақтылықты жоғалтудың дәйекті тізбегі, пайда болған периодты қозғалыс, пайда болған биполярлық қозғалыс және т.б. нәтижесінде пайда болады, нәтижесінде қозғалыс көп периодты болады.

Рюэль мен Такенс Ландау көрсеткен жолдың тар емес екендігіне, ортақ мүмкіншілік - бейтаныс тартуды қалыптастыру екендігіне назар аударды. Бірақ таңғажайып тартушы қалай пайда болады, олар зерттелмеген.

Ю.И. Неймарктің турбуленттік туралы мәлімдемесі - А. Пуанкаре ашқан гомоклиникалық құрылымдарды зерттеудің нәтижесі.

Лос-Аламостың физигі Митчел Фейгенбаум ашқан хаос теориясының фонындағы турбуленттіліктің ерекше әсемдігімен және маңыздылығымен ерекшеленетіні бір нәтижеден көрінеді. Екі еселенген немесе шанышқы тәрізді бифуркация кезеңінің каскадының бір қызықты аспектісі - оны тәжірибе кезінде байқасаңыз, сіз оны басқа ештеңемен шатастырмайсыз. Сонымен қатар, хаостың каскадтан тыс болатыны белгілі. Демек, Фейгенбаум каскадының гидродинамикада байқалуы режимдердің хаосқа түсетіндігінің нақты дәлелі болып табылады.

Бұл жұмыста біз ерекше нүкте бифуркациясын зерттейміз. Тұрақты және тұрақсыз нүктелердің бифуркация немесе соқтығысуы нәтижесінде олар аймақтан шығатыны көрсетілген. Басқаша айтқанда, олар хаосқа түседі, яғни қарбалас жағдайына. Мұнда бифуркация нүктесін анықтау үшін қалыпқа келтіру әдісі қолданылады. Ляпунов мағынасында тұрақсыз айырымды-динамикалық жүйелер қарастырылған.

Жұмыстың бірінші бөлімінде сызықтық жүйелердің тұрақсыздығы жағдайында олардың түрленуі келтірілген. Диагональды матрицасы бар сызықтық жүйе қарастырылған. Нөлдің айналасында бұл жүйе арнайы түрге азайтылмайтын түрлендірулердің көмегімен төмендетілмейтіндігі көрсетілген. Нерогенді емес түрлендірулер үшін белгілі бір сызықтық жүйе шешімдерінің траекториясында тектік аудандардың траекториялары көрсетілмейтіндігі дәлелденген. Осылайша, арнайы форма жүйесіндегі нөлдік нүктенің аймағының топологиясы берілген жүйенің нөлдік аймағында топологиясына айналмайды. Осы әдісті қолдану арқылы алынған қайшылықтың себептері көрсетілген.

Екінші бөлімде аналитикалық айырымды-динамикалық жүйелер мен аналитикалық гомеоморфизмдер қарастырылған. Сонымен қоса айырымды-динамикалық ω – сығымдалған жүйелер де зерттелген. ω – сығымдалған айырымды-динамикалық жүйелер туралы түсінік берілген. ω – сығымдалған айырымды-динамикалық жүйелер қандай жүйелерге изоморфты болып табылатыны көрсетілген.

Түйін сөздер: динамикалық-айырымдық жүйе, бифуркация, орнықтылық, гомеоморфизм, хаос.

К.Б. Бапаев[1], Г.К. Василина[1,2], С.С. Сламжанова[3]

[1]Институт математики и математического моделирования, Алматы, Казахстан
[2]Алматинский университет энергетики и связи, Алматы, Казахстан
[3]Жетысуский государственный университет им. И. Жансугурова, Талдыкорган, Казахстан

ОБ ОБЛАСТИ СЖИМАЕМОСТИ НЕУСТОЙЧИВЫХ РАЗНОСТНО-ДИНАМИЧЕСКИХ СИСТЕМ И ДЕТЕРМИНИРОВАННЫЙ ХАОС

Аннотация. Теория хаоса есть теория, которая описывает поведение некоторых нелинейных динамических систем, подверженных при определённых условиях явлению, называемому хаос (динамический хаос, детерминированный хаос). Поведение такой системы кажется случайным, даже если модель, описывающая систему, является детерминированной.

В современном понимании хаос означает состояние беспорядка и нерегулярность физических процессов, которое называется гидродинамической и плазменной турбулентностью. Теория турбулентности, казалось бы, должна полностью основываться на классических макроскопических уравнениях: уравнениях Навье-Стокса, газодинамики и др., однако вывести основные характеристики турбулентного движения из макроскопических уравнений пока не представляется возможным и приходится прибегать к дополнительным соображения. До последнего времени в теории возникновения турбулентности безраздельно господствовала гипотеза Ландау.

Теория Ландау связывает возникновение турбулентности с неустойчивостью. Это, безусловно верно, но то, как она это делает, потребует существенных уточнений. С точки зрения новых воззрений теория Ландау не полна. Она указывает лишь на один из возможных вариантов возникновения турбулентности и, по-видимому, далеко не самый важный. Современная теория бифуркаций предлагает много других путей, отличных от теории Ландау, пути хаотизации и стохатизации движения жидкости. По Ландау возникновение турбулентности происходит в результате последовательной серии потери устойчивости состоянием равновесия, возникшим периодическим движением, появившимся двояко периодическим движением и т.д., в результате чего движение становится многопериодическим.

Рюэль и Такенс обратили внимание на то, что путь, указанный Ландау, не общий, что общая возможность – это образование странного аттрактора. Но как возникает странный аттрактор, они не исследовали.

Высказывания Ю.И. Неймарка о турбулентности – результат исследования им гомоклинических структур, открытых еще А. Пуанкаре. Описание турбулентности на фоне теории хаоса, благодаря своей особой красоте и значимости, особенным образом выделяется один результат - каскад удвоения периода, открытый Лос-Аламосским физиком Митчеллом Фейгенбаумом.

Один интересный аспект каскада удвоения периода или вилообразной бифуркации (Сценарий Фейгенбаума) состоит в том, что когда вы заметите его в ходе эксперимента, то не спутаете ни с чем другим. Кроме того, известно, что за каскадом существует хаос. Следовательно, наблюдение каскада Фейгенбаума в гидродинамике является особенно убедительным доказательством того, что моды должны уступать хаосу.

В данной работе исследуется бифуркация типа седловой точки. Показывается, что в результате бифуркации или столкновения устойчивой и неустойчивой точек, они уходят из области. Другими словами, они переходят в хаос, т.е. в состояние беспорядка. Здесь применяется метод нормализации для выявления точки бифуркации. Рассматриваются разностно-динамические системы неустойчивые в смысле Ляпунова.

В первой части работы дается преобразование линейных систем в случае их неустойчивости. Рассматривается линейная система с диагональной матрицей. Показывается, что в окрестности нуля данная система не приводится с помощью невырожденных преобразований к специальному виду. Доказывается, что для невырожденных преобразований траектории системы специального вида из окрестности начала координат не могут отображаться в траектории решений заданной линейной системы. Таким образом, топология окрестности нулевой точки системы специального вида не преобразуется в топологию заданной системы в окрестности нуля. Показываются причины противоречия, получаемого при применении данного метода.

Во второй части рассматриваются аналитические разностно-динамические системы и аналитические гомеоморфизмы. Также исследуются ω – сжимающие разностно-динамические системы. Дается понятие ω – сжимающих разностно-динамических систем. Показывается какой системе изоморфны ω – сжимающие разностно-динамические системы.

Ключевые слова: разностно-динамическая система, бифуркация, устойчивость, гомеоморфизм, хаос.

Information about authors.

Bapaev K.B., Doctor of Physics and Mathematics, Senior Researcher, Institute of Mathematics and Mathematical Modeling, Almaty, Kazakhstan, bapaev41@bk.ru, https://orcid.org/0000-0002-7931-6985;

Vassilina G.K., PhD, Senior Researcher, Institute of Mathematics and Mathematical Modeling, Senior Lecturer, Almaty University of Energy and Communications, Almaty, Kazakhstan, v_gulmira@mail.ru, https://orcid.org/0000-0003-2504-9620;

Slamzhanova S.S., candidate of Physics and Mathematics, associate professor, Zhetysu State University named after I. Zhansugurov, Taldykorgan, Kazakhstan, beksultan.82e@mail.ru, https://orcid.org/0000-0002-7059-0785

REFERENCES

[1] Landau L. D. On the problem of turbulence // Reports of the USSR Academy of Sciences. 1944. Vol. 44, No. 8. P. 339-342.

[2] Landau L. D., Livshits E. M. Hydrodynamics. Moscow, 1988.

[3] Hopf E. A mathematical example displaying features of turbulence // Comm. Pure Appl. Math. 1948. Vol. 1. P. 303-322.

[4] Arnol'd V.I. Small denominators and problems of stability of motion in classical and celestial mechanics // Russian Mathematical Surveys. 1963. 18(6):85. http://dx.doi.org/10.1070/RM1963v018n06ABEH001143.

[5] Arnold V.I., Avets A. Ergodic problems of classical mechanics. Izhevsk, 1999. 160 pp.

[6] Feigenbaum M. Quantitative universality for a class of non-linear transformations // J. Statist. Phys. 1978. 19, 25–52.

[7] Feigenbaum M. The universal metric properties of nonlinear transformations // J. Stat. Phys. 1979. 21, 669.

[8] Lorenz E.N. On the prevalence of aperiodicity in simple systems. In: Grmela M., Marsden J.E. (eds) Global Analysis // Lecture Notes in Mathematics, 1979. Vol. 755.

[9] Manneville P., Pomeau Y. Different ways to turbulence in dissipative dynamical systems // Physica D. 1980. Vol. 1, No. 2. P. 219–226.

[10] Ruelle D., Takens F. On the nature of turbulence // Commun Math Phys. 1971. 20, 167–192.

[11] Neymark Yu.I. The structure of the motions of a dynamical system in the vicinity of a homoclinic curve // Proceedings of the 5th Summer Mathematical School. Kiev, 1968. P. 400-435.

[12] Poincare A. Selected Works. Vol. II. Moscow, 1972.

[13] Bopaev K.B. Normalization of systems of nonlinear difference equations. KazSU, NSU. Almaty-Novosibirsk, 1995. 61 p.

[14] Bapaev K.B., Slamzhanova S.S. On stability and bifurcation of resonant difference-dynamic system // News of the national academy of sciences of the republic of Kazakhstan. Series physico-mathematical. 2015. № 4. P. 250-255.

[15] Bapaev K.B., Vassilina G.K. On Lagrange stability and Poisson stability of the differential-dynamic systems // News of the national academy of sciences of the republic of Kazakhstan. Series physico-mathematical. 2019. Vol. 5, № 327. P. 120-125. https://doi.org/10.32014/2019.2518-1726.66

NEWS
OF THENATIONAL ACADEMY OF SCIENCES OF THE REPUBLIC OF KAZAKHSTAN
PHYSICO-MATHEMATICAL SERIES
ISSN 1991-346X **https://doi.org/10.32014/2020.2518-1726.72**
Volume 4, Number 332 (2020), 114 – 118

УДК 550.383

B.T. Zhumabayev[1], I.V. Vassilyev[2], I.D.Kozin[2], I.N.Fedulina[2]

[1] Institute of Ionosphere, National Center for Space Research and Technology, Almaty, Kazakhstan;
[2] JSC Special Design and Technology Bureau "Granite", Almaty, Kazakhstan.
E-mail: beibit.zhu@mail.ru, iv@granit.kz

THE INFLUENCE OF WATER ON THE FORMATION OF EARTHQUAKE SOURCE

Abstract. A hypothesis is proposed to explain the relationship between the number of earthquakes and geographical latitude. Analysis of ultra-deep well drilling results showed that the boundaries of seismic wave reflection that were taken beyond the boundary between the granite and basalt layers were actually related to the rock decompression zone due to increased porosity and microcracking in the main granite layer. These cracks allow water to penetrate the rocks while being compressed and heated at the same time. Calculations show that at a depth of 30 km the temperature should be 460 degrees, and at 42 kilometers (at the base of the Earth 's crust) - already 580 degrees. The pressure at these depths is 3000 and 4200 atmospheres, respectively. When the temperature reaches 374.3 degrees Celsius and 221 atmospheres, the water changes to a supercritical state. In this state, water has special properties, in particular, increased solubility of various substances and high oxidative capacity. It mixes freely with oxygen, hydrogen, and hydrocarbons. Even with a small change in pressure and temperature, complete dissolution or, conversely, precipitation of oxides and salts can occur. The pressure required to achieve the supercritical state is already reached at a depth of 2.2 kilometers. The required temperature is reached at depths of 20-25 kilometers. However, in areas of magmatic hearths, this temperature can be reached at significantly lesser depths. The dissolution of rocks can lead to the formation of cavities like karst, the collapse of the arches of which leads to the collapse of large arrays of rocks with the formation of new cavities over the filled-in cavity, leading to the formation of sub-vertical clusters of earthquake hypocenters, called seismic "nails". At the same time, a Coriolis force proportional to the cosine of latitude must act on the water moving underground. The distribution of the centers of strong earthquakes shows a more sharp decrease in their latitude, proportional to the third degree of the cosine of latitude. These calculations show that the number of earthquakes correlates fairly well with the cubic root of latitude. An additional factor, which also depends on latitude, may be the increase in rock treadiness, which increases towards the equator in proportion to the square of latitude, reducing rock resistance to fluid movement and resulting in an increase in the speed of movement of the rocks.

Keywords: earthquake, seismic sources, fluids.

In 1927, as a result of the analysis of the locations of the epicenters of 1551 major earthquakes from 1903 to 1920, Moran established a relationship between the number of earthquakes and geographical latitude, these data were subsequently summarized by Polycarpov [1]. However, to date, there are no sufficiently convincing hypotheses explaining the nature of this relationship. Statistical analysis of a wider range of observational data (205311) from 1973 to 2014, added to the NEIC global seismological catalogue for earthquakes with magnitude greater than 4.5, showed a structural correspondence between the geographical location of seismically active zones and the geometry of the main geomagnetic field [2]. The reason for this dependency was not identified. The emergence in 2014 of work [3], which justified the connection of the main geomagnetic field of the Earth with the rotation of polarized silicon dioxide molecules, which form the basis of the Earth 's crust and mantle substance, allowed to put forward a hypothesis on the influence of water on the formation of earthquake sources.

The inner structure of Earth has now been studied very little. Analysis of the results of drilling of ultra-deep wells [4] showed that no ultra-deep well confirmed the geological cut that was expected before drilling began. And that the boundary of seismic wave reflection that was taken beyond the boundary

between the granite and basalt layers is actually related to the rock decompression zone. Decompression has been associated with increased porosity and microcracking in the base granite layer. These cracks allow water to penetrate the rocks.

Starting from depths of about 6-7 kilometers the strength of rocks is violated very much and it is not possible to keep the vertical of wells in practice. The deepest well in the world Kola (12261 meters) deviated from the vertical by 840 meters. The KTB-Oberpfalz well (Bavaria, Germany) remained the most vertical in the world to a depth of 7500 m, but then deviated 300 meters, reaching a depth of 9901 m. Due to high temperatures and high pressure, drill strings were repeatedly destroyed. At a depth of 12 km, the Kola well recorded a temperature of 212 degrees Celsius. Calculations show that at a depth of 30 km the temperature should be 460 degrees, and at 42 kilometers (at the base of the Earth 's crust) - already 580 degrees. The pressure at these depths is 1200, 3000 and 4200 atmospheres, respectively.

At depths of more than 4.5 km, even plastic clays are transformed into brittle argyllites prone to cracking and permeable to liquids and gases. Crack systems form subvertical fluid migration channels [5].

Thus, water penetrating through the fractured channels into the Earth 's interior under the influence of gravity is heated. It can be seen from the water phase diagram (Fig.1) that when the temperature of the 647.3 0K and the pressure of 22.1 MPa (374.3 degrees Celsius, 221 atmosphere) are reached, the water must become supercritical. In this state, water has special properties, in particular, increased solubility of various substances and high oxidative capacity.

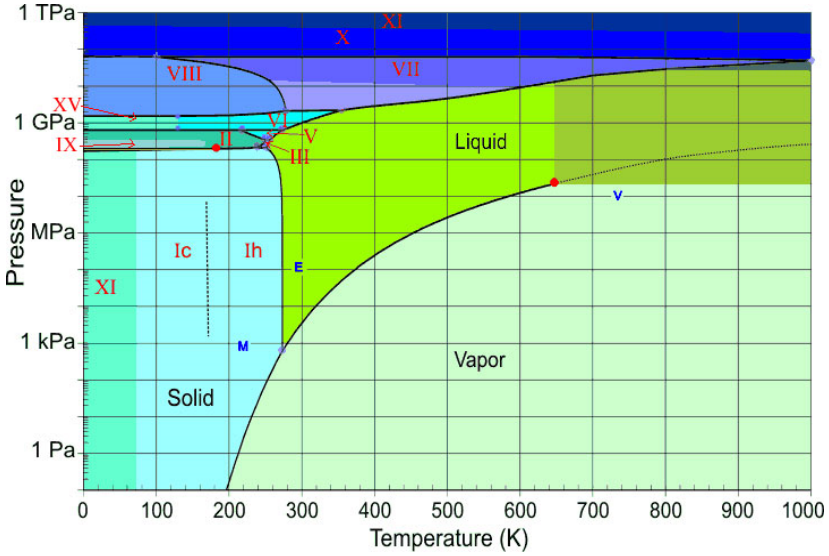

Figure 1

The pressure required to achieve the state of supercriticality is already reached at a depth of 2.2 kilometers. The necessary temperature - on average reached only at depths of 20-25 kilometers. In areas of magmatic hearths, such temperatures can be reached at substantially lesser depths. Thus, a temperature of 223 ^{0}C was recorded on the Tyrnyauz well (North Caucasus, Russia) at a depth of only 4001 meters. This well was drilled to build a geothermal station [4]. And the solubility of various substances in supercritical liquids is primarily influenced by temperature. It has been shown in [6], that even at pressures 4 times higher than supercritical, the best solubility of the substances is observed near the supercritical temperature. The results of the experiments published in [7] show that supercritical water is indefinitely mixed with oxygen, hydrogen and hydrocarbons. Even with a slight change in pressure and temperature, complete dissolution or, conversely, precipitation of oxides and salts may occur. Of the 30 ceramics studied, only pure alumina and alumina with zirconium oxide were not corrosive by supercritical water. At the same time, despite the high concentration of dissolved substances, the electrical conductivity of water in the supercritical state remains quite low and can vary significantly even with small variations in temperature and pressure.

If we accept the presence of water in a sub-and supercritical state in the depth of the earth and its circulation, the dissolution of rocks can lead to the formation of cavities like karst, which are well known

for their ability to collapse with the formation of karst craters. The collapse of the vaults of such cavities in the depth of the earth does not directly lead to the formation of craters, but only to the collapse of large masses of rocks with the formation of new cavities over the filled-in cavity. The sub-vertical clusters of earthquake hypocenters were described in detail in [8], in which they were called the seismic "nail". Such hypocentres are typical mainly for earthquakes with small magnitudes (2-3). The epicentral projection of such "nails" has a diameter of 5-10 kilometers. The time of their formation is from a few days to a month. The authors of this work assumed the connection between the formation of these "nails" with fluids.

In [8] it was shown (from the earthquake analysis for the period 1900-2004) that there are several depths at which severe earthquakes occur most frequently. The figures given in this work show that at a depth of 25 kilometers earthquakes occur most often, although there are several more depths where statistically they are more frequent (10, 33, 40 and further up to 250 km every 10 km). As depths increase, the vertical dimensions of the blocks increase. The data presented in [8] show that, within a century cycle, the accumulated energy is gradually transferred from the deeper layers of the Earth 's substance to the upper layers.

But if there is a circulation of water under the ground, then the Coriolis force must act on this water. Under the influence of this force on the surface of the earth, rivers shift their channels, washing away one of the banks. When water (fluids) moves from the earth's surface to its center, the maximum value of the Coriolis force will be at the equator, but it will be absent at the poles. The Coriolis force for vertically directed fluids decreases from the equator to the poles in proportion to the cosine of latitude. And the distribution of centers of strong earthquakes shows a sharp decrease in their latitude. We will use the data of Moran 's statistics [1] from the work of Polycarpov mentioned at the beginning of the article. It analyzed 542 earthquakes from 1914 to 1920 and 1009 earthquakes from 1903 to 1910.

Table 1 - Distribution of the number of earthquakes by latitude

Latitudes, degrees	Number of earthquakes	Average latitude, degrees	Cosine of average latitude	Cosine cube	Estimated number of earthquakes	Deviation, %
0-10	450	5	0,996	0,988	450	0
10-20	329	15	0,966	0,901	410	20
20-30	244	25	0,906	0,744	339	29
30-40	258	35	0,819	0,549	250	3
40-50	152	45	0,707	0,353	161	6
50-60	87	55	0,574	0,189	86	1
60-70	21	65	0,423	0,076	35	40
70-80	9	75	0,259	0,017	8	12
80-90	1	85	0,087	0,001	0	-

The table shows that the number of earthquakes correlates fairly well with the cosine of the third degree of latitude. So, in addition to the Coriolis force, there must be some other factors that also depend on latitude.

In 2016, a paper [9] was published to explain the causes of vertical cracking of rocks at great depths, which contributes to the penetration of fluids into the earth's interior. It has been calculated tangential mass forces (TMS) and shows that the power of stress horizontal stretching and shear depend on the square of latitude and decrease from the equator to the poles. If we accept this hypothesis and assume that the fracturing of rocks increases to the equator in proportion to the square of latitude, then, accordingly, the resistance of rocks to the movement of fluids should decrease, leading to an increase in the speed of their movement. This may be the additional factor leading to an increase in the Coriolis force, and thus the pressure of fluids on the rocks in the horizontal direction.

The work was carried out on the RBP-008 "Development of space technologies for monitoring and forecasting natural resources, man-made changes in the environment, creation of space technology and ground space infrastructure, research of objects of far and near space" within the framework of the topic "Development of statistical models of spatial and time variations of seismicity characteristics in connection with variations of the structure and dynamics of the radiation belt of the Earth (2018-2020), registration number (RN). 0118RK00797

Б.Т. Жумабаев[1], И.В. Васильев[2], И.Д. Козин [2], И.Н. Федулина[2]

[1]Ионосфера институты, «ҰҒЗТО» АҚ, Алматы, Қазақстан;
[2] «Гранит» АКТБ, Алматы, Қазақстан

ЖЕР СІЛКІНІСІ ОШАҚТАРЫНЫҢ ҚАЛЫПТАСУЫНА СУДЫҢ ӘСЕРІ

Аннотация. Мақалада жер сілкініс санының географиялық кеңдікпен байланысын түсіндіретін гипотеза ұсынылады. Терең ұңғымаларды бұрғылау нәтижесін талдау гранит және базальт қабаттарының шекарасында қабылданған сейсмикалық толқындардың көрініс шекаралары негізінен гранит қабатының кеуектігі мен микрожарығының ұлғаюына байланысты жыныстың тығыздалу аймағымен байланыстығын көрсетті. Жарық суға тау жыныстарының ішіне еніп, қысылады әрі қызады. Есептеу барысында көрсетілгендей, 30 км тереңдікте температура 460 градус, ал 42 километрде (жер қыртысының түбінде) 580 градус болуы тиіс. Осы тереңдіктегі қысым тиісінше 3000 және 4200 атмосфераны құрайды. Температура 374,3 градус Цельсийге және 221 атмосфераға жеткенде су сынақ күйге ауысады. Бұл жағдайда су ерекше қасиетке, атап айтқанда, түрлі заттардың жоғары еруі мен тотығу қабілетіне ие. Ол оттегімен, сутегімен және көмірсутектермен араласады. Тіпті, қысым мен температураның болмашы өзгерісі кезінде де толық еріп немесе керісінше, оксидтер мен тұздардың шөгуі мүмкін. Аса сыни жағдайға жету үшін қажетті қысым 2,2 километр тереңдікте, қажетті температура 20-25 километр тереңдікте жетеді. Алайда, магмалық ошақ аудандарында мұндай температураға айтарлықтай аз тереңдікте қол жеткізуге болады. Тау жыныстарының еруі себебінен карстралық сынды қуыстар пайда болуы мүмкін, олардың күмбездерінің құлауы сейсмикалық «шегелер» деп аталатын жер сілкінісі гипоорталықтарының субвертикальды топтануына әкеледі. Сонымен бірге жер астында қозғалатын суға Кориолис күші әсер етуі тиіс, ендік косинусына пропорционалды. Қатты жер сілкініс ошақтарының таралуы олардың кеңдік шегінің үшінші дәрежесіне пропорционалды кеңдігі арқылы күрт азайғанын көрсетеді. Келтірілген есептеу жұмыстары көрсеткендей, жер сілкіністерінің саны кеңдікте текше тамырымен жақсы корреляцияланады. Әрекет ендікке тәуелді болатын қосымша фактор флюидтер қозғалысына тау жыныстарының кедергісін азайтып және олардың қозғалыс жылдамдығын арттыратын кеңдік квадратына пропорционал экваторға ұлғаятын жынысындағы кеуек өсуі мүмкін.

Түйін сөздер. Жер сілкінісі, жер сілкінісі ошағы, флюидтер

Б.Т. Жумабаев[1], И.В.Васильев[2], И.Д.Козин[2], И.Н.Федулина[2]

[1] Институт ионосферы АО «НЦКИТ», Алматы, Казахстан;
[2] СКТБ «Гранит», Алматы, Казахстан

ВЛИЯНИЕ ВОДЫ НА ФОРМИРОВАНИЕ ОЧАГОВ ЗЕМЛЕТРЯСЕНИЙ

Аннотация. Предлагается гипотеза, объясняющая связь количества землетрясений с географической широтой. Анализ результатов бурения сверхглубоких скважин показал, что границы отражения сейсмических волн, которые принималась за границу между гранитным и базальтовым слоями, на самом деле связана с зоной разуплотнения пород из-за увеличения пористости и микротрещиноватости в основном гранитном слое. Эти трещины позволяют воде проникать внутрь горных пород, при этом подвергаясь сжатию и нагреву одновременно. Расчёты показывают, что на глубине 30 км температура должна быть 460 градусов, а на 42 километрах (у основания земной коры) – уже 580 градусов. Давление же на этих глубинах составляет 3000 и 4200 атмосфер соответственно. При достижении температуры 374,3 градуса Цельсия и 221 атмосфер вода переходит в сверхкритическое состояние. В этом состоянии вода обладает особыми свойствами, в частности, повышенной растворяемостью различных веществ и высокой окислительной способностью. Она неограниченно смешивается с кислородом, водородом и углеводородами. Даже при небольшом изменении давления и температуры может происходить полное растворение или, наоборот, осаждение оксидов и солей. Необходимое для достижения состояния сверхкритичности давление достигается уже на глубине 2,2 километра. Необходимая температура достигается на глубинах 20-25 километров. Однако в районах магматических очагов, такая температура может быть достигнута на существенно меньших глубинах. Растворение горных пород может приводить к образованию полостей наподобие карстровых, обрушение сводов которых приводит к обрушению больших массивов горных пород

с образованием новых полостей над засыпанной полостью, приводя к формированию субвертикальных скоплений гипоцентров землетрясений, называемых сейсмическими «гвоздями». В то же время на движущуюся под землёй воду должна действовать сила Кориолиса, пропорциональная косинусу широты. Распределение очагов сильных землетрясений показывает более резкое уменьшение их с широтой, пропорциональное третьей степени косинуса широты. Приведённые расчёты показывают, что количество землетрясений достаточно хорошо коррелируется с корнем кубическим от широты. Дополнительным фактором, действие которого также зависит от широты, может служить рост трещиноватости пород, которая увеличивается к экватору пропорционально квадрату широты, уменьшая сопротивление горных пород движению флюидов и приводя к увеличению скорости их движения.

Ключевые слова: землетрясение, очаг землетрясения, флюиды.

Information about authors:

Zhumabayev Beibit Tenelovich, candidate of physical and math. sciences, head of laboratory, Almaty, Kamenskoe plato, Institute of Ionosphere, National Center for Space Research and Technology,beibit.zhu@mail.ru, https://orcid.org/0000-0001-7882-0277;

Vassilyev Ivan Veniaminivich, candidate of physical and math. sciences, deputy general director for science, Almaty, JSC Special Design and Technology Bureau “Granite”, iv@granit.kz, https://orcid.org/0000-0002-6216-0443;

Kozin Igor Dmitrievich, doctor of physical and math. science, consultant, Almaty, Special Design and Technology Bureau “Granite”, IDKozin@yandex.kz

Fedulina Inna Nikolaevna, candidate of physical and math. sciences, consultant, Almaty, Special Design and Technology Bureau “Granite”, innafedulina@yandex.kz

REFERENCES

[1] Polycarpov M. On earthquake distribution along latitude// UFN 8, 1928. Page 417-419.

[2] Khachikyan G.J., Zhumabayev B.T., Toishiyev N.S., Kaldybayev A.A., Nurakynov S.M. Variations of solar activity and spatial-temporal distribution of strong earthquakes (M 7.0 1973-2014) on the territory of Eurasia in 2016.// News of the National Academy of Sciences. Page 40-45.

[3] Vasilyev I.V. Influence of Gravity on Formation of Earth Magnetic Field// PEOS Journal, para. 16, vol. 1. 2014. Page 48-55.

[4] Popov V.S., Krenetskiy A.A. Deep and Super Deep Drilling on Continents// Sorosovsky Educational Journal. № 11. 1999. Page 61-68.

[5] Korotkov B.S., Korotkov S.B. Gas potential of deep horizons// Scientific and technical collection "News of gas science," № 3 (8). 2011. Page 26-31.

[6] Humpback Y.E., Bondarenko G.V. Supercritical state of water// Supercritical fluids: Theory and practice. 2007. № 2. Page 5.

[7]. Galkin A.A., Lunin V.V. Water in sub- and supercritical states is a universal medium for carrying out chemical reactions// Success of chemistry, No. 1 (74). 2005. Page 24-40.

[8] Vadkovsky V.N. Subvertical clusters of earthquake hypocenters - seismic "nails"//Journal of ONZ RAS, № 4. 2012. Page 1-8.

[9] Rebetsky Y.L. Assessment of the impact of daily rotation of the earth on the stressed state of the continental crust // Reports of the Russian Academy of Sciences. 2016. T. 469, No. 2. Page 230-234.

NEWS
OF THENATIONAL ACADEMY OF SCIENCES OF THE REPUBLIC OF KAZAKHSTAN
PHYSICO-MATHEMATICAL SERIES
ISSN 1991-346X **https://doi.org/10.32014/2020.2518-1726.73**
Volume 4, Number 332 (2020), 119 – 126

O. Mamyrbayev[1,2], N. Litvinenko[1], A. Shayakhmetova [1,2]

[1] Institute of Information and Computational Technologies, Almaty, Kazakhstan;
[2] Al-Farabi Kazakh National University, Almaty, Kazakhstan.
E-mail: morkenj@mail.ru, n.litvinenko@inbox.ru, asemshayakhmetova@mail.ru

EVIDENCES PROPAGATIONS IN BAYESIAN NETWORKS

Abstract. This paper is devoted to some problems of the distribution of several evidences in Bayesian networks. Currently, there are many different algorithms for calculations in Bayesian networks. Unfortunately, the description of most algorithms is either absent or only the idea of algorithms is described. Not only algorithms but also ideas for constructing these algorithms are quite complex. Many questions arise in the process of considering these algorithms remain unanswered. Some of them can be understood by testing the appropriate software, but many questions remain unanswered.

We use the idea of dividing the set of network vertices into sets by analogy using the concept of “Generation”. The concept of "Generation" is convenient to use in the absence of evidence. The presence of evidence requires a rather complicated adjustment of this concept. However, as a result, the propagation of evidence becomes more visible, and the corresponding algorithms are greatly simplified.

The presence of several evidences in some cases leads to contradictions, which solutions should be provided for by the algorithms of the Bayesian network nodes calculations. The modified concept of “Generation” allows one to find more visual and adequate approaches to resolving contradictions.

Keywords: Bayesian networks, oriented graphs, generation, propagating.

Introduction. Since the beginning of 21st century Bayesian Networks is the most popular tool of artificial intelligence in different researches. Models that use a Bayesian networks are usually insensitive to wrong, incomplete, and redundant data. Bayesian networks allow the use of heterogeneous data in various studies.

Bayesian networks, as a tool for studying models with uncertainties, is considered by many authors. Pearl J. was the first one who considered more completely the Bayesian networks tool in his works [1] and [2]. The Bayesian network theory is described quite well in [3], [4], [5].

The use of Bayesian networks in practice is practically impossible without the use of computer technology and related software. Currently, there are many programs for work with Bayesian networks. For example, BayesiaLab ([6], [7], [8]), AgenaRisk ([9], [10], [11], [12], [13], [14]), Hugin Expert. Unfortunately, we could not find a description of the algorithms for calculations in Bayesian networks which were used in these works.

Main definitions. Bayesian network theory is based on some sections of probability theory and graph theory. The definitions and concepts of graph theory used in BN theory can be found in [15], [16], [17]. The necessary concepts in probability theory can be found in [18], [19], [20]. The basic principles of BN theory can be found in [3], [4], [5].

For brevity, we will not give them here.

Use of the concept «Generation». We can distinguish two types of generations – generations of descendants and generations of ancestors. For a generation of descendants, this is a set of vertices which have parents only from earlier generations (or do not have parents at all), and have children only in later generations (or do not have children at all).

For a generation of ancestors, this concept is similar - it is a set of vertices which have children only in later generations (or do not have children at all) and have parents only from earlier generations (or do not have parents at all).

The only difference is that the construction of generations of descendants begins with nodes that do not have parents, and the construction of generations of ancestors begins with nodes that do not have descendants.

Generations of descendants are constructed, starting from vertices which do not have parents.

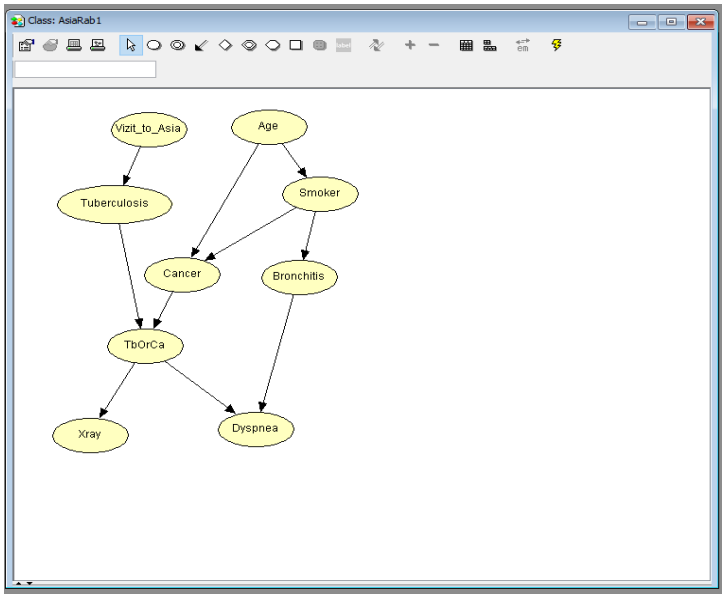

Figure 1 - Partitioning into generations of descendants

Definition. Generations of descendants are defined as follows:

- Nodes without parents belong to the 0 generation of descendants.
- Nodes with only 0 generation of parents belong to 1 generation of descendants.
- Nodes with only 0 and 1 generation of parents belong to 2 generation of descendants.
- ……
- Nodes with 0, 1, 2, … K generation of parents belong to K+1 generation of descendants.
- ……

The example of partitioning into generations of descendants is shown in figure 1.

Generations of descendants for a given Bayesian network:

- Vertices Age and Visit_to_Asia will be assigned to the 0 generation.
- Vertices Smoker and Tuberculosis will be assigned to the 1 generation.
- Vertices Cancer and Bronchitis will be assigned to the 2 generation.
- The only vertex TbOrCa will be assigned to the 3 generation.
- Vertices XRay и Dyspnea will be assigned to the 4 generation.

Generations of ancestors are constructed starting from vertices which do not have children.

Definition. Generations of ancestors are defined as follows:

- Nodes with no children belong to the 0 generation of ancestors.
- Nodes with only 0 generation of children belong to 1 generation of ancestors.
- Nodes with only 0 and 1 generation of children belong to the 2 generation of ancestors.
- ……
- Nodes with only 0, 1, 2, … K generation of children belong to the K+1 generation of ancestors.
- ……

The example of partitioning into generations of ancestors is shown in figure 2.

Generations of ancestors for a given Bayesian network:

- Vertices XRay and Dyspnea will be assigned to the 0 generation.
- Vertices TbOrCa and Bronchitis will be assigned to the 1 generation.

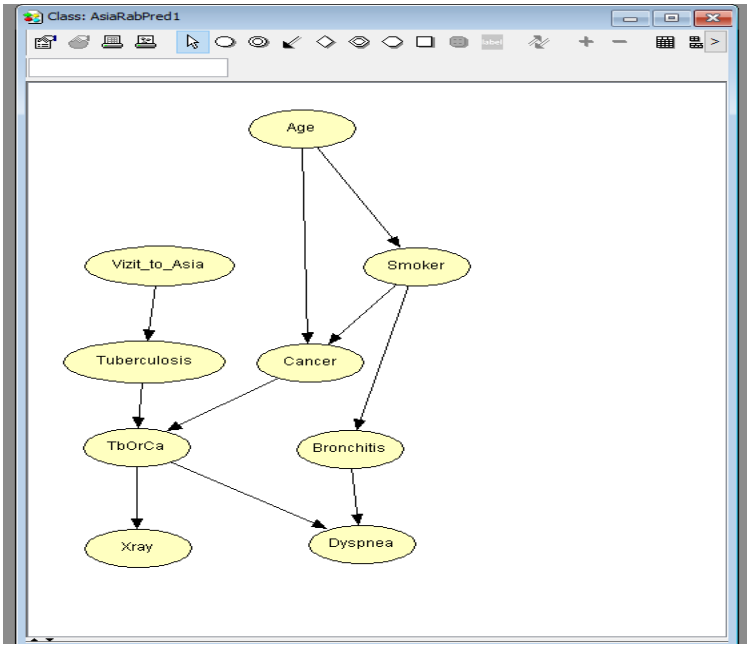

Figure 2 - Partitioning into generations of ancestors

- Vertices Cancer and Tuberculosis will be assigned to the 2 generation.
- Vertices Smoker and Visit_to_Asia will be assigned to the 3 generation.
- The only vertex Age will be assigned to the 4 generation.

In most cases, the partitioning of the set of vertices into generation of descendants and generation of ancestors is significantly different. However, it is not difficult to come up with a graph (Bayesian network) in which the partitioning into generations of descendants and generations of ancestors is completely identical.

Propagation of the several evidences with the use of "Generation" concept

Initialization of a Bayesian network, i.e. calculation of node values from the values of unconditional variables (nodes without parents) and conditional probability tables is a fairly simple task. Nevertheless, we briefly describe the initialization algorithm using the concept of "Generation".

1. We separate the vertices of the BN into generations of descendants, as described above. Recall that the 0 generation consists of vertices without parents. For nodes of 0 generation calculations are not needed.
2. We will calculate the values for all nodes of the 1 generation, using the values of the nodes of the 0 generation and the formula for total probability.
3. We will calculate the values of the nodes of the 2 generation, using the values of the nodes of the 0 generation and the calculated values of the nodes of the 1 generation, as well as the formula for the total probability.
4. Similarly, we will calculate the values of the nodes of the third generation.
5. … etc.

At some point, some nodes in the Bayesian network get evidence. It is required to recalculate the values of the network nodes considering the obtained evidence. One of the difficult issues is determining the order of calculation of Bayesian network nodes. Obviously, the nodes that obtained the evidence do not need calculations. Also, nodes that do not have parents do not need calculations, if among the descendants of these nodes there are no nodes that have obtained evidence.

It would be interesting to collect in one set all the nodes for which we do not need to make calculations. This set will be called the zero level of the Bayesian network nodes.

In the next set we will collect all the nodes for the calculation of the values of which there is enough information from the nodes of the zero level. This set will be called the first level of the Bayesian network nodes.

In the next set we will collect all the nodes, for the calculation of the values of which there is enough information from the nodes of the zero and first levels. This set will be called the second level of the Bayesian network nodes.

In the next set we will collect all the nodes, for the calculation of the values of which there is enough information from the nodes of the zero, first and second levels. This set will be called the third level of the Bayesian network nodes.Etc.

Let us consider in more detail the construction of various levels of Bayesian network nodes. The nodes that do not require calculations (nodes of the zero level):

1. Nodes that obtained evidences.
2. All descendants and ancestors of the nodes that obtained evidences must be recalculated. It is also necessary to recalculate all nodes that are descendants of all the ancestors of the nodes that obtained certificates. These nodes do not belong to 0 level. We remove these nodes from the Bayesian network. We also remove the nodes that obtained evidence. Then we consider the remaining nodes of the Bayesian network. These nodes together with arcs form a certain subnetwork of the studied network. From this subnet, we select nodes that do not have parents. These nodes are also included in the 0 level.

To determine the first, second and other levels, we separate the set of Bayesian network nodes into two subsets (two subnets): BN1 and BN2. BN1 subnet includes nodes that obtained evidences, these nodes' descendants, ancestors, and also the descendants of their ancestors. We assign the remaining nodes to the BN2 subnet. In the BN2 subnet we define "Generations" as described earlier. If the node belongs to some generation, then we will assume that this node belongs to the same level. It is easy to understand that for the calculation of a node of a generation, information on other nodes of a given generation, older generations, as well as on the nodes of the BN1 subnet, is not required. Only data on the nodes of the previous levels (maybe not all) are needed.

Some nodes (BN2 subnet) are already distributed across levels. Then we divide the set of nodes of subnetwork BN1 by levels. First, we replace all the BN1 nodes that are the ancestors of the nodes that obtained evidences with descendant nodes. To do this, we change the direction of the corresponding arcs. Let's denote the new subnet by BN1A. This subnet differs from the BN1 subnet only in the direction of some arcs. The BN1A subnet will no longer have the ancestors of the nodes obtained evidences - all nodes will be descendants of the nodes obtained evidences. We divide the BN1A subnet into generations, as described above. Then we assign a level number equal to a generation number to each node.

The nodes of the original Bayesian network are distributed at the same levels as the same nodes in the auxiliary networks BN1A and BN2.

Thus, all nodes of the Bayesian network will be separated by levels (zero, first, second, etc.). Nodes belonging to level zero do not need calculations. For the calculation of nodes of the first level we need only data of some nodes of the zero level. For the calculation of nodes of the second level, we need only the data of some nodes of the zero and first levels. Etc. For calculations we will mainly use the law of total probability and Bayes formula.

Below we will provide 2 examples of distribution by levels of the training Bayesian network. The network in both examples is the same, but the nodes that obtained evidences are different. Each level in the figure is located on a separate line. The first line contains nodes of the zero level.

Example 1.

Figure 3a shows some Bayesian network. We have obtained 3 evidences for this network for nodes C3, C4 and C6. In what order should we make calculations? To determine the order of calculations, we separate the set of BN nodes into several levels. We refer to the zero level those nodes in which calculations are not necessary. Obviously, these will be the nodes that obtained evidences (nodes C3, C4 and C6), as well as the nodes that do not have parents, and the nodes among whose descendants there are no nodes that obtained evidences (nodes C8 and C10). In figure 3b, the zero level is in the top line.

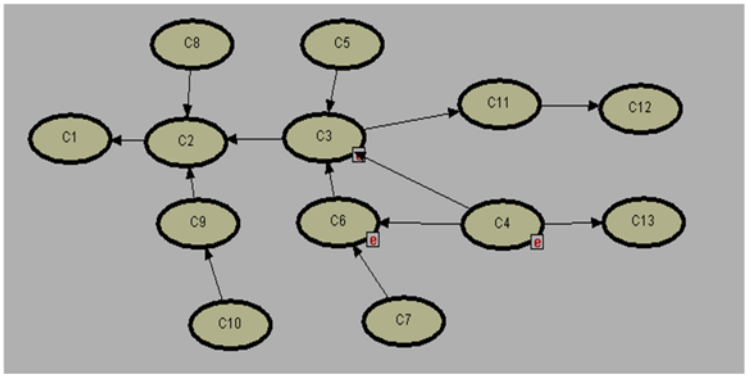

Figure 3a - Example 1

The first level includes nodes which calculation is required the only information of zero level. These will be nodes C5, C11, C13, C7 and C9. In figure 3b, these nodes are in the second line.

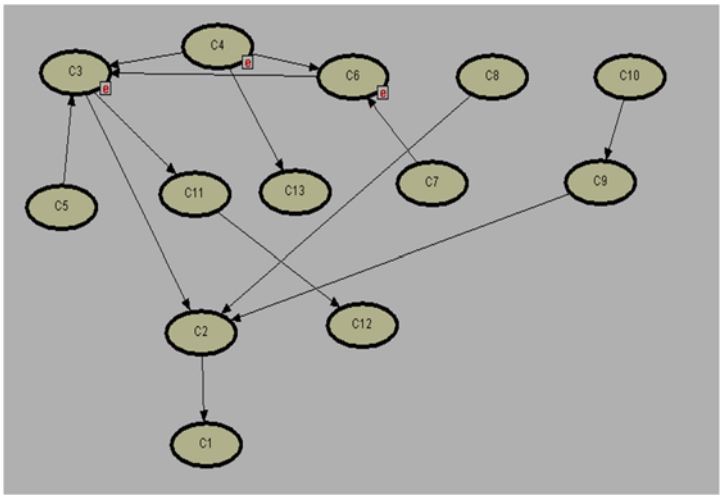

Figure 3b - Example 1

The second level includes nodes which calculation is required information of the zero and first levels. These will be nodes C2 and C12. In figure 3b, these nodes are in the third line.

The third level includes nodes which calculation is required information of the zero, first and second levels. These will be the only node C1. In figure 3b, these nodes are in the fourth line.

The order of calculations:

1. Calculation of nodes of the first level using data from some nodes of the zero level.
2. Calculation of nodes of the second level using data from some nodes of the zero and first levels.
3. Calculation of nodes of the third level using data from some nodes of the zero, first and second levels.

Example 2.

We consider the same Bayesian network as in the figure 3a. However, we obtain 3 evidences for the nodes C8, C10 and C13. To determine the order of calculations, we partition the set of BN nodes into several levels. We refer to the zero level those nodes in which calculations are not necessary. Obviously, it will be nodes, obtained evidences (nodes C8, C10 and C13), as well as the nodes that do not have parents, and the nodes among whose descendants there are no nodes that obtained evidences (nodes C5 and C7). In figure 4a, the zero level is in the top line.

The first level includes nodes which calculation is required the only information of zero level. These will be nodes C9 and C4. In figure 4a, these nodes are in the second line.

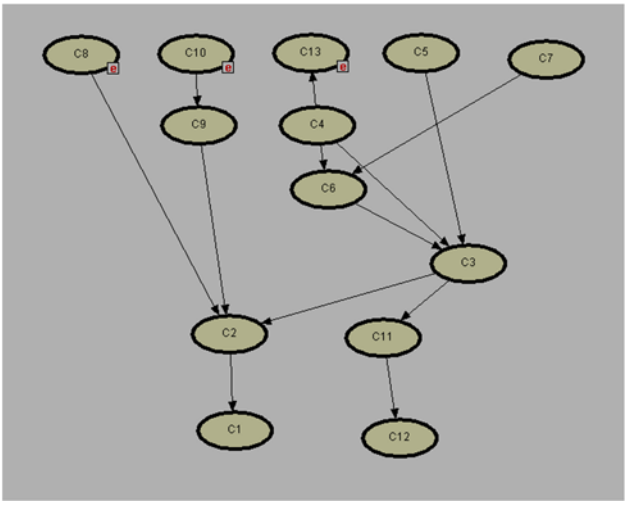

Figure 4a - Example 2

The second level includes nodes which calculation is required information of the zero and first levels. These will be the only node C6. In Figure 4a, these nodes are in the third line.

The third level includes nodes which calculation is required information of the zero, first and second levels. These will be the only node C3. In figure 4a, these nodes are in the fourth line.

The fourth level includes nodes which calculation is required information of the zero, first, second and third levels. These will be nodes C2 and C11. In Figure 4a, these nodes are in the fifth line.

The fifth level includes nodes which calculation is required information of the zero, first, second, third and fourth levels. These will be nodes C1 and C12. In Figure 4a, these nodes are in the sixth line.

The order of calculations:

Steps 1-3 we repeat as in the Example 1

4. Calculation of nodes of the fourth level using data from some nodes of the zero, first, second and third levels.

5. Calculation of nodes of the fifth level using data from some nodes of the zero, first, second, third and fourth levels.

Conclusion. This paper shows one of the options for determining the propagation order of Bayesian network nodes in the process of obtaining evidence with use the idea of partitioning of Bayesian network nodes into independent sets (generations, levels). Nodes, which belong to zero level do not need calculations. For the calculation of nodes of the next level, we use only the data of some nodes of the previously calculated levels.

This method allows to develop simpler algorithms for calculations in networks, some nodes of which have obtained evidences.

Acknowledgement

The work was performed under the grant of the Committee of Science of the Ministry of Education and Science of the Republic of Kazakhstan (2018-2020), on the theme “Development and software implementation of an application package for solving applied problems on Bayesian networks.

Ө. Мамырбаев[1,2], Н. Литвиненко[1], Ә. Шаяхметова [1,2]

[1]Ақпараттық және есептеуіш технологиялар институты, Алматы, Қазақстан;
[2]Әл-Фараби атындағы Қазақ ұлттық университеті, Алматы, Қазақстан

БАЙЕС ЖЕЛІЛЕРІНДЕ КУӘЛІКТЕРДІ НАСИХАТТАУ

Аннотация. Байес желісі көптеген айнымалыларды, сондай-ақ осы айнымалылардың арасындағы әртүрлі ықтималдық тәуелділіктерді сипаттайтын графикалық ықтималдық моделі. Байес желілерінің жалпы математикалық аппаратын американдық ғалым, Тьюринг сыйлығының лауреаты Pearl J құрды.

Байес желісі сұраулардың әртүрлі типтеріне жауап алуға мүмкіндік береді:

- Куәләндірудің ықтималдық бағасы
- Априорлық маргиналдық ықтималдықтарды бағалау.
- Апостериорлық маргиналдық ықтималдықтарды есептеу.
- Апостериорлық максимум есебі.
- Ықтимал болатын оқиғаны түсіндіруді зерттеу.

Байес желілеріндегі есептеулер өте күрделі және көлемді. 10 тораптан тұратын байес желілеріндегі есептеулер, әдетте, есептеу техникасын пайдалануды, алгоритмдерді дайындауды, бағдарламалық кодта алгоритмдерді іске асыруды талап етеді. Байес желілерінде есептеулерді жүргізу кезінде әртүрлі алгоритмдер қолданылады, оларды келесідей жіктеуге болады:

- Толық аралықтар немесе өрескел күш әдісі. Толық таңдаудың кемшіліктеріне, әдетте, тапсырманы шешуге кететін уақыттың жеткілікті үлкен шығындарын жатқызуға болады.
- Кластерлеудің түрлі идеяларын пайдаланатын алгоритмдер. Бұл алгоритмдер жиі өрескел күш әдісімен салыстырғанда жақсы уақыт ұтысын береді. Әдетте, осы алгоритмдерге салынған идеялар жеткілікті ашық және түсінікті.
- Түйіндер арасындағы ақпаратты беру(пропагациялау) идеяларын пайдаланатын алгоритмдер. Бұл алгоритмдер графтар теориясында жақсы білімді талап етеді.
- Әртүрлі сұрыптауды құруда қолданатын алгоритмдер
- Monte Carlo әдісі идеяларын пайдаланатын алгоритмдер

Мақала Байес желілерінде бірнеше дәлелдемелерді таратудың кейбір мәселелеріне арналған. Қазіргі уақытта Байес желілерінде есептеулердің көптеген алгоритмдері бар. Өкінішке орай, алгоритмдердің көпшілігінің сипаттамасы қарастырылмаған немесе тек алгоритм идеялары сипатталған. Алгоритмдер ғана емес, сонымен қатар бұл алгоритмдерді құру идеялары да өте күрделі. Осы алгоритмдерді қарастыру кезінде оқырманға қойылған көптеген сұрақтар жауапсыз қалады. Байес желілерінде алгоритмдерді құру кезінде дәлелдерді тарату мәселесі маңызды болып табылады.

Желілік шыңдардың жиынтығын жиынтықтарға бөлу идеясы аналогия арқылы «Ұрпақ» ұғымын қолданады. «Ұрпақ» ұғымы дәлел болмаған кезде қолдануға ыңғайлы. Дәлелдердің болуы осы тұжырымдаманы едәуір күрделі түзетуді талап етеді. Алайда, нәтижесінде дәлелдердің таралуы айқынырақ болады, сәйкесінше алгоритмдер айтарлықтай жеңілдетілген.

Кейбір жағдайларда бірнеше дәлелдердің болуы қарама-қайшылықтарға әкеледі, олардың шешімі Байес желілеріндегі есептеу алгоритмдерімен қамтамасыз етілуі керек. «Ұрпақ» тұжырымдамасы туындайтын қайшылықтарды шешуге көрнекі және барабар тәсілдерді табуға мүмкіндік береді.

Түйін сөздер: Байестік желілер, бағытталған графтар, генерация, тарату.

О. Мамырбаев[1,2], Н. Литвиненко[1], А. Шаяхметова [1,2]

[1]Институт информационных и вычислительных технологии, Алматы, Казахстан;
[2] Казахский национальный университет имени аль-Фараби, Алматы, Казахстан

ПРОПАГАЦИЯ СВИДЕТЕЛЬСТВ В БАЙЕСОВСКИХ СЕТЯХ

Аннотация. Байесовская сеть представляет собой графовую вероятностную модель, описывающую множество переменных, а также различные вероятностные зависимости между этими переменными. Общий математический аппарат байесовских сетей разработан американским учёным Pearl J, лауреатом премии Тьюринга.

Байесовская сеть позволяет получить ответы на различные типы запросов:

- Вероятностная оценка свидетельств.
- Оценка априорных маргинальных вероятностей.
- Расчет апостериорных маргинальных вероятностей.
- Расчет апостериорного максимума.
- Исследование наиболее вероятного объяснения события.

Расчеты в байесовских сетях достаточно сложны и объемны. Расчеты в байесовских сетях, содержащих более 10 узлов, как правило уже требуют использования вычислительной техники, разработки алгоритмов, реализации алгоритмов в программном коде. При проведении расчетов в байесовских сетях используются различные алгоритмы, которые можно классифицировать, например, следующим образом:

- Полный перебор или метод грубой силы. К недостаткам полного перебора можно отнести, как правило, достаточно большие затраты времени на решение задачи.

- Алгоритмы, использующие различные идеи кластеризации. Данные алгоритмы часто дают хороший выигрыш времени по сравнению с методом грубой силы. Обычно идеи, заложенные в данных алгоритмах достаточно прозрачны и понятны.
- Алгоритмы, использующие идеи передачи(пропагации) информации между узлами. Данные алгоритмы требуют достаточно хороших знаний в теории графов.
- Алгоритмы, использующие построение различных выборок.
- Алгоритмы, использующие идеи метода Monte Carlo.

Статья посвящена некоторым проблемам распространения нескольких свидетельств в байесовских сетях. В настоящее время существует множество различных алгоритмов для расчетов в байесовских сетях. К сожалению описание большинства алгоритмов либо отсутствует, либо описывается лишь идея алгоритмов. Не только алгоритмы, но также и идеи построения данных алгоритмов достаточно сложны. Многие вопросы, возникающие у читателя при рассмотрении данных алгоритмов, остаются без ответа. Что-то можно понять, тестируя соответствующее программное обеспечение, но многие вопросы остаются без ответа.

Используется идея разбиения множества вершин сети на множества по аналогии с использованием понятия «Поколение». Понятие «Поколение» удобно использовать при отсутствии свидетельств. Наличие свидетельств требует достаточно сложной корректировки данного понятия. Однако в результате пропагация свидетельств становится более наглядной, а соответствующие алгоритмы значительно упрощаются.

Наличие нескольких свидетельств в некоторых случаях приводит к противоречиям, решение которых должно быть предусмотрено алгоритмами расчетов узлов байесовской сети. Модифицированное понятие «Поколение» позволяет находить более наглядные и адекватные подходы к разрешению возникающих противоречий.

Ключевые слова: Байесовские сети, ориентированные графы, генерация, распространение.

The information about the authors:

Mamyrbayev O., PhD, deputy general Director, Institute of Information and Computational Technologies, Almaty, Kazakhstan, Al-Farabi Kazakh National University, 050040 Almaty, Kazakhstan. https://orcid.org/0000-0001-8318-3794;

Litvinenko N., junior researcher, Institute of Information and Computational Technologies, Almaty, Kazakhstan, n.litvinenko@inbox.ru, https://orcid.org/0000-0002-0576-8305;

Shayakhmetova A., PhD, senior researcher, Al-Farabi Kazakh National University, 050040 Almaty, Kazakhstan, asemshayakhmetova@mail.ru, https://orcid.org/0000-0002-4072-3671

REFERENCES

[1] Pearl J., How to Do with Probabilities what People Say You Can't // Artificial Intelligence Applications / Ed. Weisbin C.R. IEEE, North Holland. 1985. P. 6–12.

[2] Pearl J., Probabilistic Reasoning in Intelligent Systems. San Francisco: Morgan Kaufmann Publishers. 1988. 552 p.

[3] Jensen F.V., Nielsen T.D. Bayesian Networks and Decision Graphs. Springer. 2007. 447 p.

[4] Barber D., Bayesian Reasoning and Machine Learning. 2017. 686 p. http://web4.cs.ucl.ac.uk/staff/D.Barber/textbook/020217.pdf

[5] Neapolitan R.E., Learning Bayesian Networks. 704 p. http://www.cs.technion.ac.il/~dang/books/Learning%20Bayesian%20Networks(Neapolitan,%20Richard).pdf

[6] Conrady S., Jouffe L., Bayesian Networks and BayesiaLab, A Practical Introduction for Researchers. https://www.researchgate.net/publication/282362899_Bayesian_Networks_ BayesiaLab_-_A_Practical_Introduction_for_Researchers

[7] BayesiaLab User Guide. https://library.bayesia.com/display/BlabC/BayesiaLab+User+ Guide

[8] Litvinenko N., Litvinenko A., Mamyrbayev O., Shayakhmetova A., Work with Bayesian Networks in BAYESIALAB. Almaty: IPIC, 2018. 311 p. (in Rus). ISBN 978-601-332-206-3.

[9] Fenton N. and Neil M., Risk Assessment and Decision Analysis with Bayesian Networks. Queen Mary, University of London and Agena Ltd. CRC Press. ISBN: 9781439809105, ISBN 10: 1439809100

[10] AgenaRisk 7.0 User Manual. https://www.agenarisk.com

[11] Advanced Modelling with AgenaRisk. https://www.agenarisk.com

[12] Agena's Bayesian Network Technology. https://www.agenarisk.com

[13] Basic Modelling with AgenaRisk. https://www.agenarisk.com

[14] N. Litvinenko, A. Litvinenko, O. Mamyrbayev, A. Shayakhmetova, AgenaRisk. Work with Bayesian Networks. Almaty: IPIC, 2019. 236 p. (in Rus). ISBN 978-601-332-335-0.

[15] D.V. Karpov, Graph theory. https://logic.pdmi.ras.ru/~dvk/graphs_ dk.pdf (in Rus)

[16] O. Ore. Graph theory. M.: Science. 1980. 336 p. (in Rus)

[17] Ph. Kharari, Graph theory. M.: Mir. - 1973. 300 p. (in Rus)

[18] Gmurman V.E., Probability Theory and Mathematical Statistics: Manual, M., 2003. 479 p. (in Rus)

[19] Kolmogorov A.N., Basic Concepts of Probability Theory: Manual. M: Science, 1974. 412 p. (in Rus)

[20] Mamyrbayev, O. Zh., Shayakhmetova, A. S., Seisenbekova, P. B. The methodology of creat-ing an intellectual environment of increasing the competence of students based on a bayesian ap-proach // News of the National academy of sciences of the republic of Kazakhstan. Series physico-mathematical. 2019. Vol. 4(326). P. 50-58.

NEWS
OF THENATIONAL ACADEMY OF SCIENCES OF THE REPUBLIC OF KAZAKHSTAN
PHYSICO-MATHEMATICAL SERIES
ISSN 1991-346X **https://doi.org/10.32014/2020.2518-1726.74**
Volume 4, Number 332 (2020), 127 – 134

UDK 524.6-8
МРНТИ 41.27.25

S.A. Shomshekova, E.K. Denissyuk,
R.R Valiullin, A.V. Kusakin, I.V. Reva, M.A. Krugov

V.G. Fesenkov Astrophysical Institute, Almaty, Kazakhstan.
E-mail: shmshekva-saule@mail.ru, eddenis@mail.ru, rashit_valiullin@mail.ru,
un7gbd@gmail.com, reva@aphi.kz, mkrugov@astroclub.kz

PHOTOMETRIC AND SPECTRAL RESEARCHES OF THE SEYFERT GALAXIES NGC 4151 AND NGC 7469

Abstract. Seyfert galaxies are much closer than the rest intergalactic objects and therefore the study of them is the most suitable and it gives an information about the physical processes occurring in objects of this type. Spectra of the Seyfert 1 galaxies (Sy1) are represented by a set of forbidden and permitted emission lines. The latter ones consist of a narrow and a broad (up to 10000 km/s) components. The ionization source is an accretion disk. the energy of which is generated due to the accretion of the surrounding matter onto a central supermassive black hole. The region of formation of the broad hydrogen lines (BLR) consists of dense clouds of gas fibers and jets located near the gravitational center and rotating around it at high velocities. The sizes of BLR are about a few tenths of a parsec. The region of formation of narrow forbidden lines and narrow components of hydrogen lines (NLR) is more extended and farther from the center NLR has a lower density of gas. The extension of NLR in the galaxies is determined by the time delay (reverberation). As it turned out, they are from several light days to several light weeks and depend on the luminosity of the active nucleus of the Seyfert galaxy.

This paper presents the results of photometric and spectral observations of Seyfert galaxies NGC4151 and NGC 7469. Observations were carried out with the 70-cm telescope AZT-8. Eastern and Western 1-meter telescopes of the Tien Shan Astronomical Observatory of the Fesenkov Astrophysical Institute. The estimations of brightness of NGC4151 (in the B V filters) and NGC7469 (in B V R filters) were obtained from 2013 to 2019. Based on the observational data. the light curves of the studied objects were made. Spectra of the galaxies were obtained in the absolute units. Variations of the level of continuum at two wavelengths λ=5100Å and 6300Å were studied.

Key words: seyfert galaxies, photometric variability, spectral variability, light curves, amplitudes.

1. Introduction. The active nuclei galaxies (AGNs) are the brightest objects in the Universe. The reason of the strong energy release of AGN is the accretion of matter into a central compact object, that is, into a “black hole”. Depending on the luminosity, several subclasses of the objects are distinguished: quasars lacertids, Seyfert galaxies (Sy), blazars and radio galaxies. Seyfert galaxies are much closer than the rest objects, and therefore the study of Sy makes it possible to understand the physical processes occurring in objects of this type.

Photometric and spectral observations are the main methods of study of AGN. Researches of the variability of Sy gives an information about the structure nuclei, as well as dynamic processes in the near-nuclear regions of galaxies. Photometric and spectral changes at different time intervals from tens of minutes to several years were observed.

NGC 7469 – SBa spiral galaxy with coordinates α(2000)=$23^h00^m44^s$, δ(2000)=+8°36'16" lying at a distance D = 68 Mpc. The red shift is z=0.0166. The mass of the central body is about (1-6)x$10^7M_\odot$ [1]. Its physical companion. the irregular galaxy IC 5283 lies at an angular distance of 80". The light curve of this galaxy for 1990-2014 was constructed in [2]. Those authors assumed that the light curve describing the variability of the nucleus, consists of two components: a slow component with a period of a few years

and a fast (flare) with a period of a few days. They are known as S and F components. The maximum of S component usually corresponds to the active stage of the galactic nucleus and the F component depends on the accretion rate [2]

NGC4151 – with coordinates α(2000)= 12^h 10^m 32^s, δ(2000)= +39° 24' 24". belongs to Seyfert class 1.5. The red shift z = 0.00332, and the distance D ≈ 19 Mpc [3]. This is one of the brightest Seyfert galaxies in the X-ray, UV and optical ranges. The high degree of X-ray variability in the 0.3 – 50 Kev range makes this galaxy an outstanding object of study. The mass of the central body is estimated to $4.57x10^7 M_\odot$ [4] .

2 Observations. Photometric observations of the galaxies were made with a 1-m Carl Zeiss Jena telescope of the Ritchey-Chretien system. located at the Tyan-Shan Astronomical Observatory (TShAO) of the Fesenkov Institute of Astrophysics (FAI). Equivalent focal distance equals to 6.5 m and a field is 19'×19'. Images are recorded with the U9000D9 CCD camera of the Apogee Alta Company and BVR Astrodon filters. The angular scale of the frame of an image was 0.38"/pixel (until 2016) and 0.56"/pixel (after 2016). All images were dark subtracted and flat fielded. A standard package Maxim DL 6 was used to process the images. Standard stars in the neighborhood of a galaxy were used. The typical errors of the measurements do not exceed $\pm 0^m.01$, and real accuracy of the results depends on the accuracy of the used standards and on the accuracy of the aperture positioning on the centre of an image.

Spectral observations were carried out using diffraction spectrographs mounted on the telescope AZT-8, the 1-meter telescope at the TShAO. The CCD cameras SBIG STT-3200 (2184×1472, 6.8μ 2184x1472. 6.8μ) were used.

During observations. the spectrograms of a galaxy and a standard star with a known energy distribution are performed with a wide slit. which guarantees the pass and registration of the full radiation flux. The file processing consists of subtracting the dark background. taking into account field errors and atmospheric absorption.

3. Results of photometric observations. Photometric observations of the galaxy NGC 7469 have been made since 2013. The results of brightness measurements with the 6" aperture are shown in table 1 and figure 1.

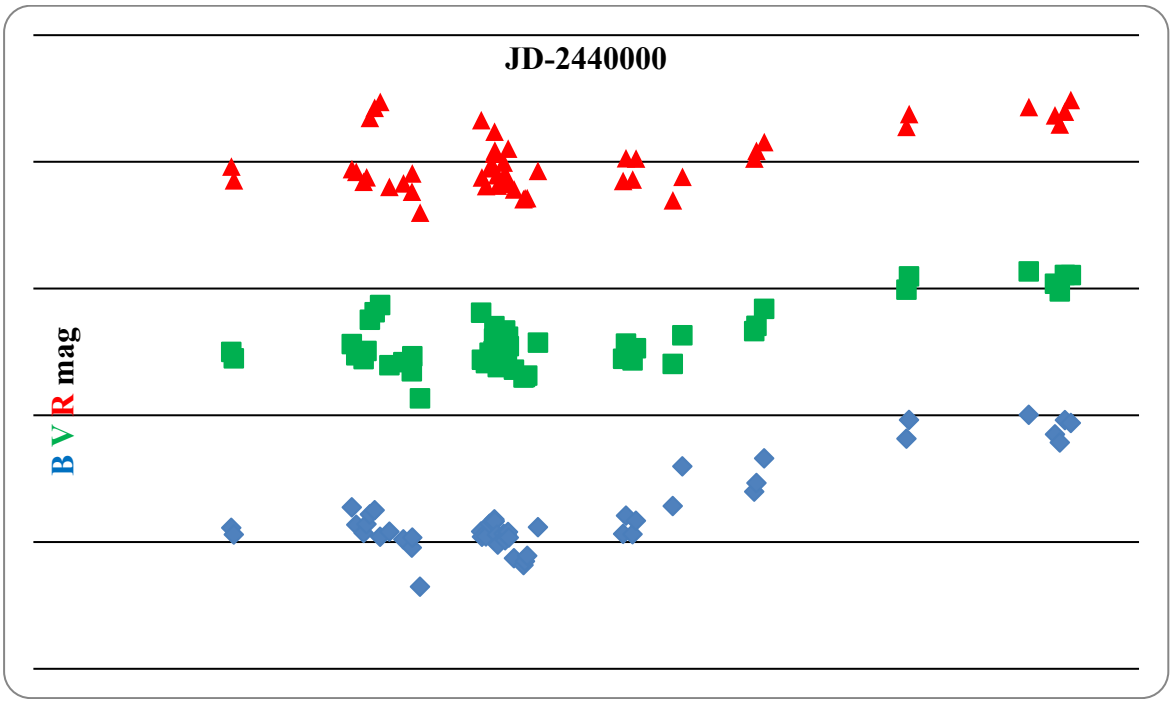

Figure 1

Table 1 - B V R magnitudes of SY NGC 7469. obtained during 2013-2019

Data of Observation	JD-2440000	B	V	R	Data of observation	JD-2440000	B	V	R
1	2	3	4	5	6	7	8	9	10
02.09.2013	16537	13.94	13.25	12.52	12.07.2015	17215	13.96	13.10	12.34
09.09.2013	16544	13.97	13.28	12.53	14.07.2015	17217	13.98	13.28	12.56
26.07.2014	16864	13.86	13.22	12.53	25.07.2015	17228	13.98	13.29	12.60
07.08.2014	16876	13.93	13.26	12.54	04.08.2015	17238	13.93	13.25	12.52
27.08.2014	16896	13.96	13.28	12.58	15.08.2015	17249	13.92	13.25	12.52
04.09.2014	16904	13.93	13.25	12.56	16.08.2015	17250	13.91	13.20	12.47
13.09.2014	16913	13.89	13.12	12.33	17.08.2015	17251	13.91	13.15	12.38
26.09.2014	16926	13.87	13.09	12.29	18.08.2015	17252	13.92	13.23	12.46
11.10.2014	16941	13.98	13.06	12.26	24.08.2015	17258	13.97	13.27	12.55
05.11.2014	16966	13.96	13.30	12.60	26.08.2015	17260	14.01	13.31	12.59
13.12.2014	17004	13.99	13.29	12.58	11.09.2015	17276	13.97	13.26	12.50
05.01.2015	17027	14.02	13.33	12.62	15.09.2015	17280	13.99	13.16	12.55
06.01.2015	17028	13.98	13.27	12.55	20.09.2015	17285	13.97	13.27	12.57
27.01.2015	17049	14.18	13.43	12.70	23.09.2015	17288	13.96	13.19	12.45
25.09.2015	17290	13.98	13.23	12.59	26.08.2016	17626	13.97	13.28	12.57
09.10.2015	17304	14.06	13.32	12.61	04.09.2016	17635	13.92	13.23	12.49
04.11.2015	17330	14.09	13.35	12.65	13.12.2016	17735	13.86	13.30	12.65
08.11.2015	17334	14.08	13.35	12.64	08.01.2017	17761	13.70	13.18	12.56
14.11.2015	17340	14.05	13.34	12.64	22.07.2017	17956	13.80	13.17	12.49
13.12.2015	17369	13.94	13.21	12.54	28.07.2017	17962	13.77	13.15	12.46
31.07.2016	17600	13.97	13.28	12.58	18.08.2017	17983	13.67	13.08	12.42
08.08.2016	17608	13.90	13.22	12.48	08.09.2018	18369	13.59	13.00	12.36
15.09.2018	18376	13.52	12.95	12.31	06.08.2019	18701	13.50	12.93	12.28
16.10.2019	18772	13.575	12.981	12.317	29.10.2019	18785	13.607	13.011	12.353
12.11.2019	18799	13.519	12.946	12.302	28.11.2019	18815	13.53	12.947	12.256

The light curves of the galaxy NGC 7469 (figure 1) indicate a gradual increase of brightness in the three filters, which began in 2016.

Photometric observations of NGC 4151 were carried out since 2013 [6]. The results are presented in table 2.

Table 2 - B V R magnitudes of the Sy NGC 4151. obtained in 2013 – 2019 with the aperture of 8”

Date of observation	JD-2440000	B	V	Date of observation	JD-2440000	B	V
1	2	3	4	5	6	7	8
22.11.2013	16618	12.90	12.21	06.02.2015	17059	12.98	11.78
06.01.2014	16663	12.66	11.84	26.02.2015	17079	12.74	11.43
09.01.2014	16666	12.81	11.77	27.02.2015	17080	12.48	11.18
11.01.2014	16668	12.76	11.95	28.02.2015	17081	12.53	11.19
05.03.2014	16721	12.64	11.56	18.03.2015	17099	12.48	11.15
10.03.2014	16726	12.62	11.60	19.03.2015	17100	12.52	11.20
01.04.2014	16748	12.92	11.68	06.04.2015	17118	12.61	11.82
09.04.2014	16756	12.86	11.91	09.04.2015	17121	12.46	11.11
11.04.2014	16758	12.80	11.78	10.04.2015	17122	12.47	11.20
30.04.2014	16777	12.90	11.69	11.04.2015	17123	12.90	11.81
12.12.2014	17003	12.61	11.60	23.04.2015	17135	12.97	11.83
13.12.2014	17004	12.64	11.69	28.04.2015	17140	12.52	11.54
26.01.2015	17048	12.92	11.86	03.05.2015	17145	12.60	11.51
09.06.2015	17182	12.88	11.72	28.06.2016	17567	12.36	11.27
10.06.2015	17183	12.51	11.32	10.07.2016	17579	12.85	11.81
11.06.2015	17184	12.46	11.12	08.01.2017	17761	12.96	12.15
17.06.2015	17190	12.49	11.28	28.03.2017	17840	13.16	12.26
18.06.2015	17191	12.29	11.26	08.04.2017	17851	13.15	12.29
19.06.2015	17192	12.40	11.23	26.05.2017	17899	13.10	12.19
25.11.2015	17351	12.71	11.76	05.06.2017	17909	13.18	12.23
13.12.2015	17369	12.47	11.30	24.07.2017	17958	13.14	12.17

Continuation of the table

1	2	3	4	5	6	7	8
14.12.2015	17370	12.54	11.36	09.01.2018	18127	13.18	12.21
21.01.2016	17408	12.70	11.63	21.01.2018	18139	13.17	12.33
22.01.2016	17409	12.88	11.94	17.02.2018	18166	13.23	12.40
02.02.2016	17420	12.86	11.83	19.02.2018	18168	13.17	12.26
05.02.2016	17423	12.45	11.33	03.04.2018	18211	13.09	11.97
04.04.2016	17482	12.45	11.36	22.04.2018	18230	13.16	12.17
19.04.2016	17497	12.22	11.12	26.04.2018	18234	13.10	12.25
13.05.2016	17521	12.40	11.32	07.05.2018	18245	13.08	12.03
09.06.2016	17548	12.63	11.58	26.05.2018	18264	13.15	12.16
5.06.2018	18274	12.87	11.78	02.04.2019	18575	13.10	12.30
13.01.2019	18496	13.10	12.29	05.05.2019	18608	12.98	12.24
11.03.2019	18553	13.06	12.26				

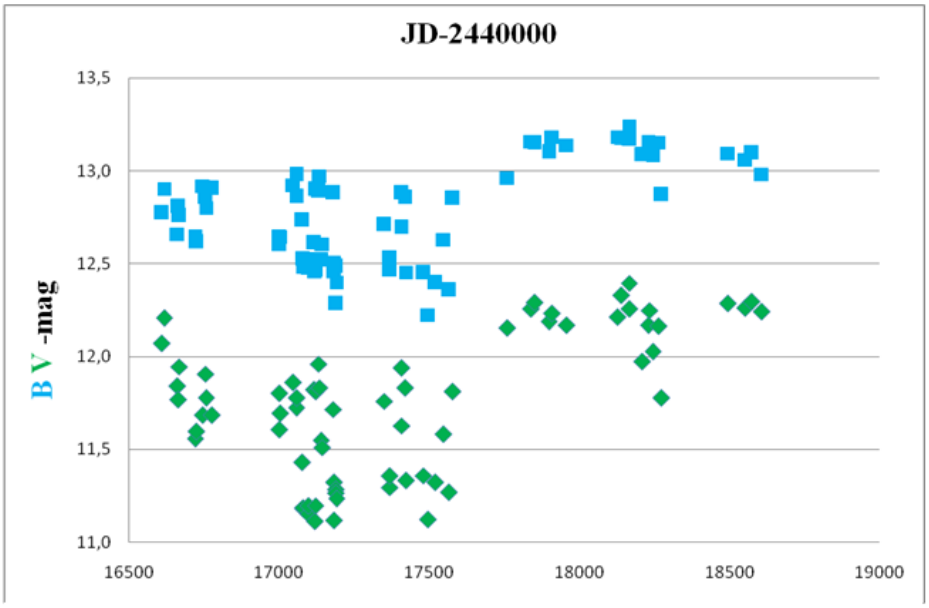

Figure 2 - B and V light curves of the galaxy NGC 4151. The X axis is Julian date JD -2440000 and the Y axis is the stellar magnitude.

The light curves of the galaxy NGC 4151 show that, since 2017, the brightness of the galaxy remains at a fairly low level.

4. Results of spectral observations. Spectra of the Type 1 Seyfert galaxies (Sy1) are represented by a set of forbidden and permitted emission lines. The latter ones consist of a narrow and broad (up to 10.000 km/s) components. The ionization source is an accretion disk, the energy of which is generated due to the accretion of the surrounding substance onto a central supermassive black hole. The region of formation of the broad hydrogen lines (BLR) consists of dense clouds of gas, fibers, and jets located near the gravitational center and rotating around it at high velocities. The region of formation of narrow forbidden lines and narrow components of hydrogen lines has a lower density and greater sizes. The extension of the regions of the emission lines formation are determined by the time delay (reverberation). As it turned out, they are from several light days to several light weeks and depend on the luminosity of the active nucleus of the Seyfert galaxy.

During spectral observations the absolute fluxes in the Hα, [NII] and [SII] emission lines were obtained. In addition, study of changes in the intensity of the continuous spectrum of galaxies was made, Figure 3 illustrates the changes in the intensity of the continuum of the Seyfert galaxy NGC 7469 in 2005-2019. Besides our results. the observational data from the Paper [7] were used.

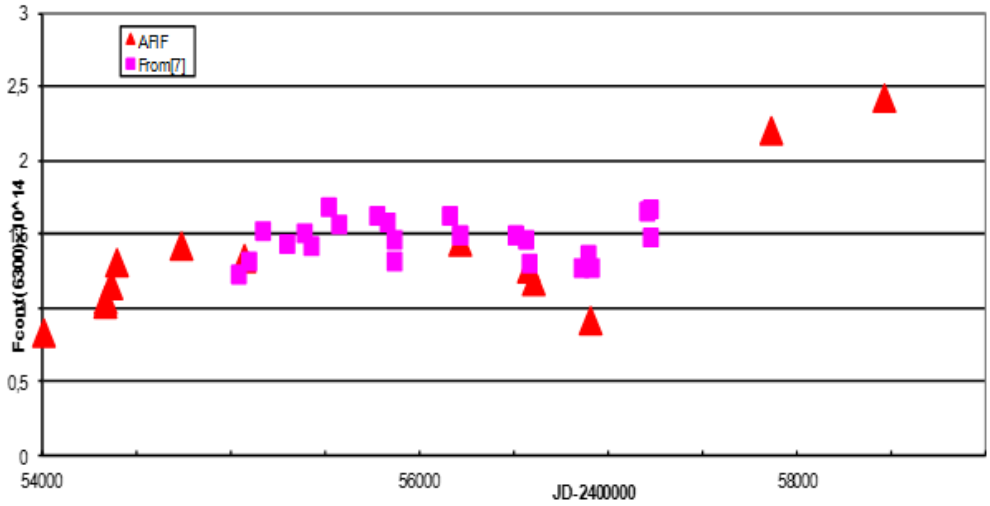

Figure 3 - Change in the intensity of the continuum at $\lambda = 6300 Å$ in the spectrum of NGC 7469. Axis X – Julian dates JD-24000000. Axis Y – in erg / cm^2 sec Å

It can be seen from Figure 3. that over the past two years, the level of continuum in the spectrum of this galaxy has increased significantly. which correlates with an increase in its brightness (see Fig.1). A similar high level of the continuum. about (2-2.5)x10^{-14} erg/cm^{2}secÅ was observed in the spectrum of NGC 7469 in 1997-1998. [7].

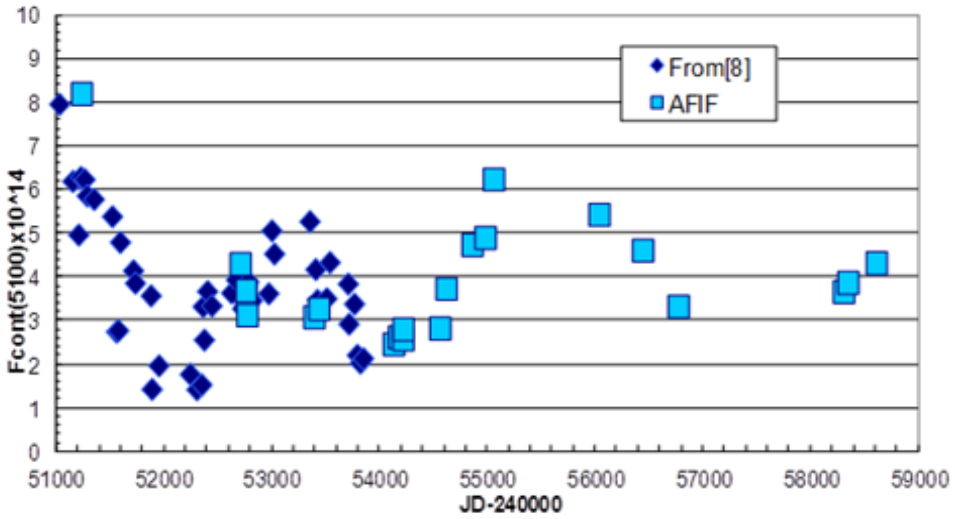

Figure 4 – Change in the intensity of the continuum at λ = 5100 Å in the spectrum of NGC 4151. Axis X – Julian dates JD-24000000. Axis Y – in erg/cm^2 sec A

Figure 4 shows the change in the continuum of the Sy galaxy NGC 4151 on the λ = 5100 Å. Periodic fluctuations in the continuum intensity within the range (1.5-8.3)*10^{-14} erg/cm^2 sec Å are observed. At present, the level of continuum corresponds to the average value.

5. Conclusion. The results of our research confirm the photometric and the spectral variability of the studied galaxies. Irregular fluctuations of the brightness of NGC 4151 are accompanied by the change of the level of its continuum. The light curves of NGC 7469 show the tendency of the brightness increasing during the last year.

Acknowledgments

The work was supported by the funding program BR05236322 of the Ministry of Education and Science of the Republic of Kazakhstan.

С.А.Шомшекова, Э.К. Денисюк, Р.Р. Валиуллин, А.В. Кусакин, И. В. Рева, М.А. Кругов

В.Г. Фесенков атындағы Астрофизика институты, Алматы, Қазақстан

NGC 4151 ЖӘНЕ NGC 7469 СЕЙФЕРТ ҒАЛАМДАРЫНЫҢ ФОТОМЕТРЛІК ЖӘНЕ СПЕКТРЛІК ЗЕРТТЕУЛЕРІ

Аннотация. Ғаламдардың белсенді ядролары (ҒБЯ) кең диапазонды толқын ұзындығындағы күшті сәулелену көзі болып табылады. Кезінде сейферт ғаламдары келесі шарттар бойынша жеке классқа бөлінген болатын: ядроның өте жоғарғы жарқырауы, объектілердің спектрлеріндегі кең эмиссиялық сызықтары және сәулеленуінің айнымалылығы. Жарқырауының айнымалылығы әртүрлі уақыт аралығында байқалады: бірнеше мнуттан (рентген аймағында) бірнеше жылға дейін.

ҒБЯ зерттеуде спектрлік және фотометрлік бақылаулар негізгі әдістер болып қалады. Соңғы кездерде ҒБЯ зерттеуде рентген аймағындағы бақылауларға көп көңіл бөлінеді. Сонымен бірге, оптикалық аймақтағы алынған мәліметтер өзектілігін жоғалтпайды.

Әртүрлі аймақта алынған спектрлердің нәтижелерін салыстыру ғаламдардың ішінде болып жатқан процестердің толық сипатын береді.

В. Г. Фесенков атындағы Астрофизика институтында ҒБЯ спектрлік зерттеулері бірнеше он жыл болды. Ғаламдардың белсенді ядроларын фотометрлік бақылаулары шамамен он жыл аралығында жалғасуда.

Берілген мақалада Астрофизика институтында екі сейферт ғаламы NGC 7469 және NGC 4151 зерттеу нәтижелері ұсынылған.

Фотометрлік зерттеулер ФАФИ Тянь-Шань обсерваториясында орналасқан (ТШАО) Карл Цейсс Йена 1-метрлік телескобының көмегімен жүргізілді. Сәулелелік қабылдағыш ретінде ЗБА Apogee Alta Company U9000D9 камерасы, BVR Astrodon фильтрлері қолданылды. Алыған мәліметтерді өңдеуге стандартты пакет Maxim Dl 6 бағдарламасы қолданылды. Стандарт жұлдыздар ретінде зерттелетін объектілерге жақын орналасқан. жұлдыздық шамалары белгілі жұлдыздар таңдап алынды. Жарқырауды өлшеудегі қателіктері $\pm 0.^{m}01$ аспайды.

Спектрлік бақылаулар АЗТ-8 және Тянь-Шань обсерваториясындағы 1-метрлік телескобында жүргізілді. Спектрограф SBIG STT-3200 (2184x1472. 6.8μ) ЗБА камерасымен жабдықталған. Бақылау барысында зерттелетін ғаламның және стандарт жұлдыздың спектрлері белгі энергияның таралуы бойынша алынады. Ғаламдардың спектрлерін абсолютті калибровкалауға қоданылады.

NGC 7469 – 68 Мпс қашықтықта орналасқан. координаталары $\alpha(2000)=23^{h}00^{m}44^{s}$, $\delta(2000)=+8°36'16"$. иірімді ғаламдар. Қызыл ығысуы z=0.0166, орталық дененің массасы шамамен $(1\text{-}6)x10^{7}M_{\odot}$ тең. Ғаламнан 80" бұрыштық қашықтықта физикалық тұрғыдағы серігі ретсіз ғалам - IC 5283 орналасқан. Уголькова және тағы басқа авторлар 1999-2014 аралығында NGC 7469 жарқырау қисығын тұрғызған, одан екі компонент анықталды: бірнеше жылдан тұратын жәй периодты және бірнеше периодтан тұратын тез период. Жәй компонент ЦД белсенділігіне сәйкес орналасқан, ал тез компонент ядро маңы аймағындағы аккреция жылдамдығына тәуелді.

ФАФИ NGC 7469 фотометрлік бақылаулары 2013 жылдан басталады. Жарқырауын өлшеу 6" белгілеп алынған апертура бойынша орындалады. Жарқырау қисығы оның жарқырау деңгейінің біртіндеп жоғарлағанын көрсетеді. NGC 7469 спектрлерінде HI, [OIII], [NII] және [SII] эмиссиялық сызықтар бақыланады. Біз жүргізген соңғы екі жылдық үздіксіз спектрлердің (λ=6300A) зерттеулері объектінің жарқырау қисығына сәйкес анағұрлым өскен. 1997-1998 жылдары NGC 7469 спектрлерінде осындай жоғарғы мәндегі $(\sim (2\text{-}2.5)x10^{-14}$эрг/см^{2}сек Å) интисивті континуум бақыланған.

NGC 4151 ғаламы, координаталары $\alpha(2000)= 12^{h}\ 10^{m}\ 32^{s}$, $\delta(2000)= +39°\ 24'\ 24"$ Сейферт 1.5 типіне жатады. Қызыл ығысуы z = 0.00332. қашықтығы D ≈ 19 Мрс, ЦД массасы $4.57x10^{7}M_{\odot}$. УК. рентген және оптика аймағындағы ең жарық сейфер ғаламдарының бірі.

2013 жылдан бастап ФАФИ NGC 4151 фотометрлік бақылаулары жүргізілуде. Жарқырауын өлшеу 8" белгілеп алынған апертура бойынша орындалады. 2017 жылдан бастап B және V фильтрлерінде амплитуданың тербелісі орташа деңгейден $\sim 0^{m}.7$ шамамен өзгереді. NGC 4151 континуум деңгейі λ=5100A толқын ұзындығында $\sim (1.5\text{-}8.3)x10^{-14}$эрг/см^{2}сек Å кездейсоқты ауытқуларға ұшырайды.

Түйін сөздер: Сейферт ғаламдары, фотометрлік айнымалылық, спектрлік айнымалылық, жарқырау қисығы. Амплитудалар.

С.А. Шомшекова, Э.К. Денисюк, Р.Р. Валиуллин, А.В.Кусакиню, И.В. Рева, М.А. Кругов

V.G. Fesenkov Astrophysical Institute, Almaty, Kazakhstan

ФОТОМЕТРИЧЕСКИЕ И СПЕКТРАЛЬНЫЕ ИССЛЕДОВАНИЯ СЕЙФЕРТОВСКИХ ГАЛАКТИК NGC 4151 И NGC 7469

Аннотация. Галактики с активными ядрами (АЯГ) являются источниками мощного излучения в широком диапазоне длин волн. Серфертовские галактики в свое время были выделены в отдельный класс по следующим критериям: высокая светимость ядра, переменность излучения и широкие эмиссионные линии в спектрах объектов. Переменность блеска проявляется в разных временных интервалах: от нескольких минут (в рентгеновском диапазоне) до нескольких лет.

Спектральные и фотометрические наблюдения до сих пор остаются основными методами исследования АЯГ. Последнее время много внимания уделяется рентгеновским наблюдениям АЯГ. Вместе с тем, данные, полученные в оптическом диапазоне. не теряют своей актуальности. Именно сопоставление результатов исследований, полученных в разных областях спектра, дает наиболее полную картину процессов. происходящих в галактиках.

В Астрофизическом Институте им. Фесенкова (АФИФ) спектральные наблюдения АЯГ проводятся на протяжении нескольких десятков лет. Примерно десять лет тому назад начались регулярные фотометрические наблюдения активных галактик.

В данной статье приводятся результаты исследования двух сейфертовских галактик NGC 7469 и NGC 4151, проведенных в Астрофизическом Институте.

Фотометрические наблюдения выполняются на 1-метровом телескопе Карл Цейсс Йена. расположенном на Тянь-Шанской обсерватории (ТШАО) АФИФ. Приемником излучения служит ПЗС камера Apogee Alta Company U9000D9, используются BVR Astrodon фильтры. Для обработки изображений используется стандартный пакет программ Maxim Dl 6. В качестве стандартов выбирались звезды с известными оценками блеска в непосредственной близости от исследуемого объекта. Типичные ошибки измерений блеска не превышают $\pm 0.^{m}01$.

Спектральные наблюдения проводятся на телескопе АЗТ-8 и 1-метровом телескопе Тянь-Шанской обсерватории. Спектрографы оборудованы ПЗС камерами SBIG STT-3200 (2184x1472. 6.8μ). В процессе наблюдений. получаются спектры исследуемых галактик и спектры звезд с известными распределениями энергии. Последние используются для абсолютной калибровки спектров галактик.

NGC 7469 - спиральная галактика с координатами $\alpha(2000)=23^{h}00^{m}44^{s}$, $\delta(2000)=+8°36'16"$. расположенная на расстоянии 68 Мпс. Красное смещение z=0.0166, масса центрального тела (ЦТ) составляет примерно $(1\text{-}6)x10^{7}M_{\odot}$. На угловом расстоянии 80" от галактики расположен ее физический компаньон – нерегулярная галактика IC 5283. На кривой блеска NGC 7469 за 1999 – 2014гг. построенной Угольковой и др. удалось выделить две составляющие: медленную с периодом в несколько лет и быструю с периодом несколько дней. Медленная компонента находится в соответствии с активностью ЦТ, а быстрая компонента зависит от скорости аккреции в околоядерной зоне.

Фотометрические наблюдения NGC 7469 проводятся в АФИФ, начиная с 2013г. Измерения блеска выполняются с фиксированной апертурой 6". Кривые блеска объекта указывают на постепенное повышение уровня блеска. В спектре NGC 7469 наблюдаются эмиссионные линии HI, [OIII], [NII] и [SII]. Проведенные нами исследования показали, что в течение двух последних лет уровень непрерывного спектра (λ=6300A) значительно вырос в соответствии с кривой блеска объекта. Подобные высокие значения интенсивности континуума ~ $(2\text{-}2.5)x10^{-14}$эрг/см^{2}сек Å) наблюдались в спектре NGC 7469 в 1997 – 1998гг.

Галактика NGC 4151 с координатами $\alpha(2000)= 12^{h}\ 10^{m}\ 32^{s}$, $\delta(2000)= +39°\ 24'\ 24"$, принадлежит к типу Сейферт 1.5. Красное смещение z = 0.00332, расстояние D ≈ 19 Мрс, масса ЦТ $4.57x10^{7}M_{\odot}$. Это одна из самых ярких сейфертовских галактик в рентгеновском. УФ и оптическом диапазонах.

В АФИФ фотометрические наблюдения NGC 4151 проводятся. начиная с 2013г. Измерения блеска выполняются с фиксированной апертурой 8". Представленные фотометрические данные свидетельствуют о том, что, начиная с 2017г. блеск объекта на среднем уровне с амплитудой колебаний в фильтрах B и V $\sim 0^{m}.7$. Уровень континуума NGC 4151 на длине волны λ=5100A испытывает флуктуации в диапазоне ~ $(1.5\text{-}8.3)x10^{-14}$эрг/см^{2}сек Å.

Ключевые слова: Сейфертовские галактики, фотометрическая переменность, спектральная переменность, кривые блеска, амплитуды.

Information about authors:

Shomshekova S.A., Magister. Researcher. V.G. Fesenkov Astrophysical Institute. shmshekva-saule@mail.ru, https://orcid.org/0000-0002-9841-453X;

Denissyuk E.K., Doctor of Physical and Mathematical Sciences. V.G. Fesenkov Astrophysical Institute. eddenis@mail.ru, https://orcid.org/0000-0001-5020-2557;

Valiullin R.R., Doctor of Physical and Mathematical Sciences. V.G. Fesenkov Astrophysical Institute. rashit_valiullin@mail.ru, https://orcid.org/0000-0001-8073-8715;

Kusakin A.V., Leader researcher V.G. Fesenkov Astrophysical Institute. un7gbd@gmail.com, https://orcid.org/0000-0002-7756-546X;

Reva I.V., Junior researcher. V.G. Fesenkov Astrophysical Institute . reva@aphi.kz, https://orcid.org/0000-0001-9944-8398;

Krugov M.A., Engineer. V.G. Fesenkov Astrophysical Institute. mkrugov@astroclub.kz, https://orcid.org/0000-0002-2788-2176

REFERENCES

[1] Shapovalova A.. Popovic L.. et al. **(2016)** MNRAS. Vol.466. P.4. 4759. (in Engl).

[2] Ugol'kova L.. Artamonov B.. Shimanovskaya E**. (2017)** Study of the Nuclear Activity of the Seyfert GalaxyNGC 7469 over the Period of Observations 2008–2014. arXiv 1707.06290.

[3] Honig S.. Watson D.. Kishimoto M.. et al. **(2014)** Nature. 515. 528. 2014.

[4]]Bentz M.. Denney K.. Cackett E.. et al. **(2006)** ApJ. 651. 775. 2006.

[5] DoroshenkoV.. Sergeev S..Merkulova N.. et al. **(2005)** BVRI CCD-photometry of comparison stars in the neighborhoods of Galaxies with active nuclei. I // Astrofizika. Vol. 48. No. 2. P. 191-211

[5] Shomshekova S.. Denissyuk E.. Valiullin R.. et al. **(2005)** Photometric studies of the seyfert galaxies NGC 3516. NGC 5548. NGC 3227. NGC 4051. NGC 4151 and NGC 7469. Astrophysics V. 62 No 2. P.163 -176 (IF=0.920) DOI 10.1007/s10511-019-09571-w.

[6] Shapovalova A.. Popovic L.. et al. **(2017)** arXiv 1701.01490 v1. 2017.

]7] Shapovalova A.. Popovic L.. Burenkov A. **(2009)** arXiv 0910.2980. 2009

NEWS
OF THENATIONAL ACADEMY OF SCIENCES OF THE REPUBLIC OF KAZAKHSTAN
PHYSICO-MATHEMATICAL SERIES
ISSN 1991-346X **https://doi.org/10.32014/2020.2518-1726.75**
Volume 4, Number 332 (2020), 135 – 144

UDC 66.023

V.N. Koleskin[1], A.A.Yunusov[2], A.A. Yunusova[2], P.G. Shtern[1], A.V. Lukyanova[1], M.A.Amandikov[2], D.K. Zhumadullayev[3]

[1]State Budgetary Educational Institution "Yaroslavl State Pedagogical University named after K. D. Ushinsky", Yaroslavl, Russia;
[2] Kazakhstan Engineering Pedagogical University of Friendship of Peoples, Shymkent, Kazakhstan;
[3]M. Auezov South Kazakhstan State University, Shymkent, Kazakhstan.
E-mail**:** daulet_ospl@mail.ru

THE MODELING OF A FLOW IN FLAT AND RADIAL CONTACT UNITS WITH A STILL GRANULAR LAYER. THE SOLVING OF THE PROBLEM IN II DOMAIN (THE COLLECTING MANIFOLD). (PART- 2)

Abstract. Heterogeneous catalytic processes conducted in axial or radial type reactors with a still catalytic layer are some of the most important elements of the chemical technology. The attention of scientists and manufacturers to the investigation and application of these contact units deals with the following advantages: a highly developed surface of a phase separation, a possibility to provide a high flow velocity and hence to decrease sizes and a material consumption, a construction simplicity and a reliability of an exploit. Improving an operation of contact units may be achieved by refining present technologies, catalysts, disperse system structures and by creating new ones. Nevertheless, in some cases large scale hydrodynamic heterogeneities in a working zone of the unit cancel out efforts to increase an efficiency of chemical, heat/mass transfer and other processes. The exploration of reasons of the hydrodynamic heterogeneities formation requires an investigation of liquid and gas motion physics features in granular layers. A practice of a chemical reactors exploitation reveals that technical and economical indicators of an industrial process are as a rule lower than the calculated ones, derived on a stage of the process design. Now it can be considered proven that one of the reasons affecting the reactor output is the heterogeneity of a reagents flow in a granular catalyst layer. The article deals with a mathematical modeling of an incompressible liquid flow in flat and radial contact units with the still granular layer and a creation of numerical realization methods for the model

We propose a cycle of articles dealt with a model of a real reactor that consists of three parts: a distributing manifold, a collecting manifold and a working zone, where the still layer of a granular catalyst is loaded. An input and an output are made with a Z-shaped scheme. We consider processes and their equations in each reactor zone in detail.

Keywords: chemical reactor, still granular layer, catalyst, Ergun law, stream function, granular layer resistance factor, Green's function, pressure field, velocity field, layer resistance.

The vast amounts of works are dealt with revealing the equations of an incompressible liquid motion in the still granular layer. These equations are constructed by phenomenological and statistical methods [1-4]. In the first case equations are written down phenomenologically and an interpretation of some parts is conducted using the averaging of a microscopic model [1,2]. The statistical method is based on time, ensemble and space ways of averaging correspondent micro-equations, that describe a continuous one-phase medium motion and the motion of several one-phase media with account for boundary conditions on inter-phase surfaces [3,4]. For deriving the averaging equations the kinetic theory of a disperse media and Vokker-Planck differential equation were applied. As a result of these approaches there were obtained either different modifications of Darcy and Ergun equations or, as in a turbulence theory, non-closed systems of equations that may be closed with account for a structure and physical properties of phases in the mixture [5-7]. This is the main problem in modeling heterogeneous media.

Contact units of a radial type with the still granular material are widely used in technological processes of different industries. A chemical reactor with the still layer of a tableted catalyst that is used in a large-capacity petrochemical industry can be mentioned as an example. One of the reasons that decreases the efficiency of such units is a heterogeneity of a reagents flow in a reactor working zone. It is known that the appearance of heterogeneities in a steam and raw mixture flow is caused by two factors. The first factor is the heterogeneity of the catalyst layer structure, for example, its porosity (or density) that appears during the process of a layer making (in filling the unit) [8-10] and during the further operation as a result of packing by gravity, vibration, breaking catalyst granules and so on. The second one is a bad choice of a ratio between geometrical and hydraulic parameters of a unit during its design.

It is considered that the heterogeneity of the reagents flow in the reactor working zone sufficiently influences process indicators only if a chemical reaction takes place either near the catalyst surface or on it. Indeed, at these conditions the velocity of reacting products directly defines the time of a contact with the catalyst. Main characteristic parameters of the reaction depend on this time. If the reaction takes place inside a porous space of catalyst granules then the contact time is defined by a diffusive reagents velocity and does not depend on a flow velocity near the granule. In the case it is assumed that the flow heterogeneity does not influence the chemical reaction kinetics.

Indeed that is not so. The majority of practically using reactions are accompanied by heat consumption or emission, so they are endothermic or exothermic. Hence if the reaction takes place in an interdiffusive area then some heat should be brought in or out, because the efficiency of the reaction often depends upon a temperature. To hold the specified temperature regime of the catalyst layer a neutral heat carrier, for example an overheated steam, is added to source reactants. It is well known that the flow heterogeneity of such steam-raw mixture causes an inhomogeneous temperature field and therefore leads to an appearance of overcooled or overheated parts in the catalyst layer. In addition to decreasing the output of a target product that results in sintering the catalyst or losing its catalytic properties.

Heterogeneities in the catalyst layer structure may be removed by using special ways of loading [11-16] or by an application a modular catalyst, where it is possible. By now these ways of loading and the technology of the catalyst module production have been already invented and continue to be developed. The flow nonuniformity that is caused by the reactor construction may be investigated and removed on the base of hydroaerodynamic calculations which allow to define the velocity and pressure fields in the unit in dependence on its geometrical and hydraulic parameters.

Let us consider the calculating of flow parameters in the collecting manifold on a boundary between *II* and *III* domains. Let the outside collector consists of two sub-domains *A* and *B* (fig. 1). The *B* domain is a semi-restricted pipe of R_2 radius. The *A* domain is a semi-restricted coaxial domain with an outer radius R_{an} and the inner radius R_2. A boundary between a working zone and the outer collector is denoted as Γ_2 and the boundary between *A* and *B* is denoted as Γ_3. Deviations of a real geometry from the selected scheme cannot lead to a significant change of the velocity flow near the Γ_2 boundary at distances much more than the collector width $R_{an} - R_2$.

The problem of finding the flow in the collecting manifold can be divided into three parts:

1) the finding of the flow in the *A* domain upon the velocity normal component specified at Γ_2 and Γ_3 boundaries;

2) the finding of the flow in the *B* domain upon the velocity normal component specified at Γ_3 boundary;

3) the finding of the velocity normal component at Γ_3 upon a condition of the velocity tangential component continuity at the boundary.

The solution of the problem 2 is accomplished like the solution of the problem for the distribution manifold since the *B* domain is the semi-restricted pipe, too. To solve the problem 3 it is necessary to parameterize the velocity normal component υ_r with *N* parameters C_n:

$$v_r(z)|_{\Gamma_3} = \sum_{n=1}^{N} C_n \varphi_n(z), \qquad (1)$$

where $\varphi_n(z)$ are some specified functions. The solutions of 1 and 2 problems allow find the velocity tangential components $\upsilon_z^{(AB)}$ in *A* and *B* domains that will be linear functions of C_n due to a linearity of the task:

$$v_z^{(A)}|_{\Gamma_3} = \varphi_0^{(A)}(z) + \sum_{n=1}^{N} C_n \varphi_n^{(A)}(z),$$

$$v_z^{(B)}|_{\Gamma_3} = \sum_{n=1}^{N} C_n \varphi_n^{(B)}(z). \quad (2)$$

A free term $\varphi_0^{(A)}$ is related to a flow that enters in the A domain through Γ_2 boundary. Equating the tangential components $\upsilon_z^{(A)}$ and $\upsilon_z^{(B)}$ at some N points of Γ_2 boundary, we obtain the system of linear equations for the determination of the velocity normal component parameters. A numerical solution of a linear equation system is a well-known task and is conducted via standard computer programs that do not need many computing time. The most consuming part of solving the problem of finding the flow in the outer collector is the problem 1, i.e. the determination of the flow in the A domain.

Green's function of a coaxial pipe

To solve the problem of finding the flow of the incompressible liquid in a semi-restricted coaxial domain with a porous inner boundary Green's functions were used [17]. Using modified Green's and Hankel's functions [18-21] and expressing the solution as a Fourier integral we have obtained:

$$v(r,z) = \int \left(v_1^{(R)}(r,z)\Phi_1^{(R)} v_2^{(R)}(r,z)\Phi_2^{(R)} \right) dk \quad (3)$$

$\Phi_1^{(R)}$ and $\Phi_2^{(R)}$ coefficients are defined from the conditions that the normal component of the velocity equals to zero on the outer boundary at $r = R_{an}$ and $v_r(R_2, z)$ equals to the specified $v_n(z)$ function on the inner boundary.

After transformations the desired expression for the velocity looks like:

$$v(r,z) = \int_{-\infty}^{\infty} G(r, z-\tilde{z}) \cdot v_n(\tilde{z}) d\tilde{z}, \quad (4)$$

where $G(r, z) \equiv \{G_r(r, z), G_z(r, z)\}$ is Green's function of an unbounded coaxial domain.

Since Green's function must be real a real part of the integrand in the formula for G_r is an even function of k, and an imaginary one is odd while in the formula for G_z this is backwards: the real part is odd and the imaginary part is even. At this reason we rewrite expressions for Green's function without imaginary values:

$$G_r(r,z) = \frac{1}{p}\int_0^{\infty} \frac{J_1(kR_{an})K_1(kr) - J_1(kr)K_1(kR_{an})}{J_1(kR_{an})K_0(kR_2) - J_0(kR_2)K_1(kR_{an})} \cdot coskzdk,$$

$$G_z(r,z) = \frac{1}{p}\int_0^{\infty} \frac{J_1(kR_{an})K_0(kr) - J_0(kr)K_1(kR_{an})}{J_1(kR_{an})K_1(kR_2) - J_1(kR_2)K_1(kR_{an})} \cdot sinkzdk. \quad (5)$$

To find the flow in the semi-restricted domain let us extend it to the unbounded one by a reflection relative to a $z = 0$ plane.

In this unbounded domain the solution is defined by (4), where $v_z(z)$ is a symmetrical function of z. Hence,

$$v(r,z) = \int_{-\infty}^{0} G(r, z-\tilde{z}) v_n(\tilde{z}) d\tilde{z} + \int_0^{\infty} G(r, z-\tilde{z}) v_n(\tilde{z}) d\tilde{z},$$

Replacing $\tilde{z}$ by $-\tilde{z}$ we obtain that in the $\tilde{z} < 0$ domain the solution looks like

$$\boldsymbol{v}(r,z) = \int_{-\infty}^{0} \{\boldsymbol{G}(r, z-\tilde{z}) + \boldsymbol{G}(r, z-\tilde{z})\} \cdot v_n(\tilde{z}) d\tilde{z} \quad (6)$$

Equations (5) and (6) are the solutions of the problem of finding the flow in a semi-restricted coaxial pipe.

The analytic expression (5) for Green's function is valid in any coaxial domain. But a procedure of the numerical calculating of integrals (5) for a narrow coaxial domain has some features. They deal with the fact that the geometry of a narrow domain is characterized by two sharply different sizes: R_2 radius and a width $\Delta = R_{an} - R_2$ and $\Delta << R_2$. To calculate integrals (5) with a proper accuracy we should choose the upper limit of the integration $\tilde{k} >> 1/\Delta$ (for example, $\tilde{k} = 10/\Delta$).

The integration step Δk should be so tiny that $\Delta k << 1/R_2$ (for example, $\Delta k = 1/10R_2$). Then a net will consists of $N = \frac{\tilde{k}}{\Delta k} = \frac{100R_2}{\Delta}$ points and $N = 10^3$ at $\frac{R_2}{\Delta} = 10$. Since the integral should be calculated at

different r and z, in each net point the special functions must be calculated and the time for finding Green's functions becomes extremely large. Moreover an argument value of special functions $\widetilde{k}R_2$ reaches $10R_2/\Delta \approx 100$, and as special functions grow exponentially their values exceed maximum allowed ones and integrals (5) cannot be calculated at all.

To avoid these difficulties the integration domain [0; +∞] should be divided into three parts: from zero to $\widetilde{k}_1$, from $\widetilde{k}_1$ to $\widetilde{k}_2$ and from $\widetilde{k}_2$ to the infinity. The full integral will be a sum of integrals over these domains

$$\boldsymbol{G} = \boldsymbol{G^{(1)}} + \boldsymbol{G^{(2)}} + \boldsymbol{G^{(3)}} \tag{7}$$

The $\widetilde{k}_1$ value is chosen so that $\widetilde{k}_1 >> R_2^{-1}$ (but $\widetilde{k}_1$ may be less then Δ^{-1}). For calculating $G^{(1)}$ we will use the following:

$$G_r{}^{(1)}(r,z) = \frac{1}{p}\int_0^{R_1} \frac{J_1(kR_{an})K_1(kr) - J_1(kr)K_1(kR_{an})}{J_1(kR_{an})K_0(kR_2) - J_0(kR_2)K_1(kR_{an})} \cdot \cos kz dk\,, \tag{8}$$

$$G_z{}^{(1)}(r,z) = \frac{1}{p}\int_0^{\infty} \frac{J_1(kR_{an})K_0(kr) - J_0(kr)K_1(kR_{an})}{J_1(kR_{an})K_1(kR_2) - J_1(kR_2)K_1(kR_{an})} \cdot \sin kz dk.$$

At k → 0 terms under integrals contain an indeterminate form 0/0 that should be evaluated analytically. Since

$$з \to 0, K_0(з) \to ln\, з, K_1(з) \to з^{-1}, j_0(з) \to 1,, j_1(з) \to \frac{1}{2}\, з,$$

then at k = 0 the term under the integral for $G_r^{(1)}$ equals to:

$$G_r^{(1)} = R_2(R_{an}^2 - r^2)\left[[r(R_{an}^2 - R_2^2)]\right]^{-1},$$

and for $G_z^{(1)}$ equals to:

$$G_z^{(1)} = (-2zR_2)(R_{an}^2 - R_2^2)^{-1}.$$

At $k > \widetilde{k}_1$ Bessel functions are much more than 1 and asymptotic expansions are valid [19]:

$$J_0(з)|_{з\to\infty} \to \frac{1}{\sqrt{2pз}} \cdot e^{з}(1 + \frac{1}{8}з^{-1} + \cdots),$$
$$J_1(з)|_{з\to\infty} \to \frac{1}{\sqrt{2pз}} \cdot e^{з}(1 - \frac{3}{8}з^{-1} + \cdots), \tag{9}$$
$$K_0(з)|_{з\to\infty} \to \sqrt{\frac{p}{2з}} \cdot e^{з}(1 - \frac{1}{8}з^{-1} + \cdots),$$
$$K_1(з)|_{з\to\infty} \to \sqrt{\frac{p}{2з}} \cdot e^{з}(1 + \frac{3}{8}з^{-1} + \cdots). \tag{10}$$

Correspondingly the expression for $G^{(2)}$ will be

$$G_r^{(2)} = \frac{1}{p}\sqrt{\frac{R_2}{r}}\int_{\tilde{k}_1}^{\tilde{k}_2}\left\{e^{k(R_{an}-r)} \cdot \left[1 - \frac{3}{8k}(\frac{1}{R_{an}} - \frac{1}{r})\right] - e^{-k(R_{an}-r)} \cdot \left[1 + \frac{3}{8k}(\frac{1}{R_{an}} - \right.\right.$$
$$\left.\left. - \frac{1}{r}\right]\right\} D^{-1} \cdot \cos kz dk \tag{11}$$

$$G_z^{(2)} = -\frac{1}{p}\sqrt{\frac{R_2}{r}}\int_{\tilde{k}_1}^{\tilde{k}_2}\left\{e^{k(R_{an}-r)} \cdot \left[1 - \frac{3}{8k}(\frac{1}{R_{an}} + \frac{1}{r})\right] + e^{-k(R_{an}-r)} \cdot \left[1 + \frac{3}{8k}(\frac{1}{R_{an}} + \right.\right.$$
$$\left.\left. + \frac{1}{r}\right]\right\} D^{-1} \cdot \sin kz dk \tag{12}$$

where

$$D = e^{k(R_{an}-R_1)} \cdot \left[1 - \frac{3}{8k}\left(\frac{1}{R_{an}} - \frac{1}{R_2}\right)\right] - e^{-k(R_{an}+R_2)} \cdot \left[1 + \frac{3}{8k}\left(\frac{1}{R_{an}} - \frac{1}{R_2}\right)\right].$$

Taking into account two terms of asymptotic expansions is necessary so that even at $\eta = \tilde{k}_1 R_1 \approx 10$ the accuracy was about $(\tilde{k}_1 R_2)^{-2} \approx 1\%$.

Green's function is a flow that forms in the infinite coaxial domain at $\upsilon_n(z)$ equaled to $\delta(z)$ — the Dirac delta function, that is if the finite liquid flow equaled to $2\pi R_2$ enters the domain through an infinitely narrow ring slot set at z = 0. It is obvious that at moving away from the slot the flow should level off and r component of the velocity must turn into zero and z component tends to a constant. It is explicitly from the physics and numerical calculations confirm that this aligning should occur at distances comparable with the width of the domain, i.e. at $|z| \sim \Delta$. Therefore the only characteristic size — Δ — enters the integral (12) and in its calculating the net should be chosen so that $\Delta k << \Delta$ (but Δk may be more than $1/R_2$).

The necessity of the third integration domain from R_{an} to ∞ deals with the fact that at $r \to R_2$ the terms under integral approach zero very slowly and at $r = R_2$ they don't reach zero at all and become oscillating. Thus a numerical determination of these integrals is not possible and it is necessary to make an analytic evaluation. This is not difficult if $\tilde{k}_2 >> 1/\Delta$. Then the number of terms with $e^{-k\Delta}$ is much less then the number of terms with $e^{-k\Delta}$ and may be neglected. After that the analytic integration is made by standard techniques. We have:

$$G_r^{(3)} = \frac{1}{\mathrm{p}}\left\{\sqrt{\frac{R_2}{r}} \cdot e^{-\tilde{k}_2(r-R_2)} \cdot \frac{(r-R_2)\cos\tilde{k}_2 z - z\sin\tilde{k}_2 z}{(r-R)^2 + z^2} - \sqrt{\frac{rR_2}{R_{an}^2}} \cdot \right.$$
$$\left. \cdot e^{-\tilde{k}_2(2R_{an}-R_2-r)} \cdot \frac{(2R_{an}-R_2-r)\cos\tilde{k}_2 z - z\sin\tilde{k}_2 z}{(2R_{an}-R_2-r)^2}\right\} \quad (13)$$

$$G_r^{(3)} = \frac{1}{\mathrm{p}}\left\{\sqrt{\frac{R_2}{r}} \cdot e^{-\tilde{k}_2(r-R_2)} \cdot \frac{(r-R_2)\sin\tilde{k}_2 z + z\cos\tilde{k}_2 z}{(r-R)^2 + z^2} + \sqrt{\frac{rR_2}{R_{an}^2}} \cdot \right.$$
$$\left. \cdot e^{-\tilde{k}_2(2R_{an}-R_2-r)} \cdot \frac{(2R_{an}-R_2-r)\sin\tilde{k}_2 z + z\cos\tilde{k}_2 z}{(2R_{an}-R_2-r)^2}\right\}$$

Note that $G^{(3)}$ contains all singularities that appear in the flow at $r \to R_2$ and $z \to 0$. Denoting $r \to R_2 = \varepsilon > 0$ we have that at $z \to 0$, $\varepsilon \to 0$:

$$G_r(r,z) \to \frac{1}{\mathrm{p}} \cdot \frac{\mathrm{e}}{\mathrm{e}^2 + z^2}\Big|_{\mathrm{e}\to 0} \to \text{д}(z) \quad (14)$$

$$G_r(r,z) \to \frac{1}{\mathrm{p}} \cdot \frac{z}{\mathrm{e}^2 + z^2}\Big|_{\mathrm{e}\to 0} \to \frac{1}{\mathrm{p}z}$$

The numerical finding of Green's function was carried out for the outer manifold of Nizhnekamsk reactor for the styrene production. Results are presented in the fig. 2. One of the qualitative conclusions is that at $z = R_{an} - R_2 = \Delta$ the flow may be considered as homogeneous with 10% accuracy that is the influence of a disturbance on the manifold boundary spreads out the distance about Δ.

Let us analyze the spreading of the flow leaving the collecting manifold. Consider that the normal component of the velocity has rectangular profile at the boundary between the working zone and the outer manifold (Γ_2 boundary, fig. 1).

A parameterization of the normal component of the velocity on the boundary Γ_3 is carried out under the following reasons:

$$v_r(z)|_{\Gamma_3} = e^{-z/l_1}(a_0 + a_1 z + a_2 z^2 + \cdots) + \\ + e^{-z/l_2}(b_0 + b_1 z + b_2 z^2 + \cdots), \quad (15)$$

where Γ_3 is the boundary between A and B domains; l_1 and l_2 are the characteristic sizes of the task ($l_1 < l_2$), z ∈ (0; ∞). Parameters a_0, a_1, … b_0, b_1… are defined under the condition of the continuity of the tangential component on the boundary Γ_3 and the conservation of the full flow. The last condition is the following:

$$\int_{\Gamma_3} v_r dz = -R_2 R_{\text{ап}}^{-2} \quad (16)$$

or taking into account that integrals from $e^{-z/l_{1,2}} \cdot z^n$ are taken in explicit form

$$l_1 б_0 - 1!\, l_1^2 б_1 + 2!\, l_1^3 a_2 - 3!\, l_1^4 a_3 + \cdots + \\ + l_2 b_0 - 1!\, l_2^2 b_1 + 2!\, l_2^3 b_2 - \cdots = -R_2 R_{\text{ап}}^{-2}. \quad (17)$$

The eq. (15) provides the continuity of the tangential component at $x \to \infty$.

At numerical finding parameters of normal component of the velocity on the boundary we used requirements of the continuity of the normal component at $z = 0$ and $z = \Delta/2$ in addition to eq. (15). Under these three conditions parameters a_0, a_1 and b_0 were obtained by solving the system of linear equations.

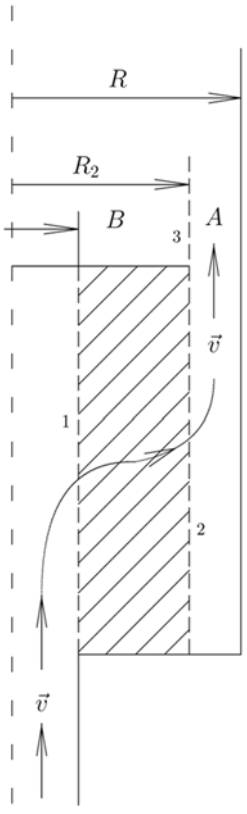

Figure 1 - The outer manifold

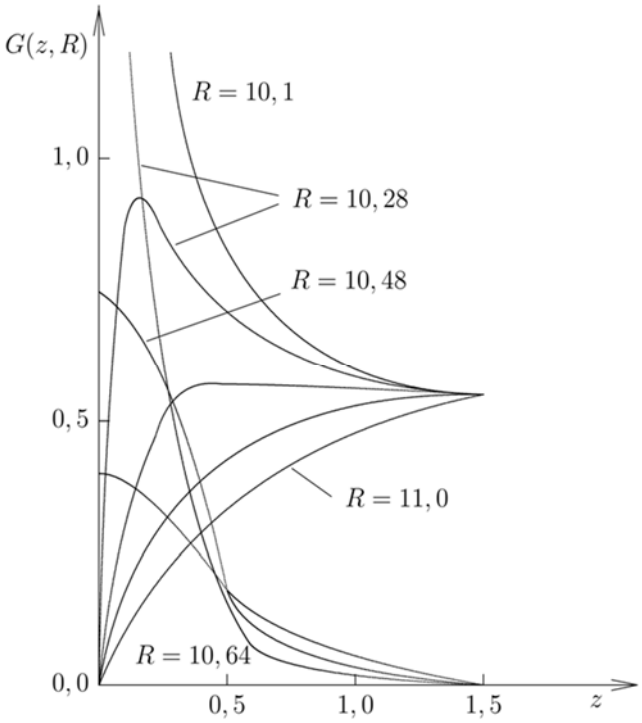

Figure 2 - The universal Green's function for various *R* values

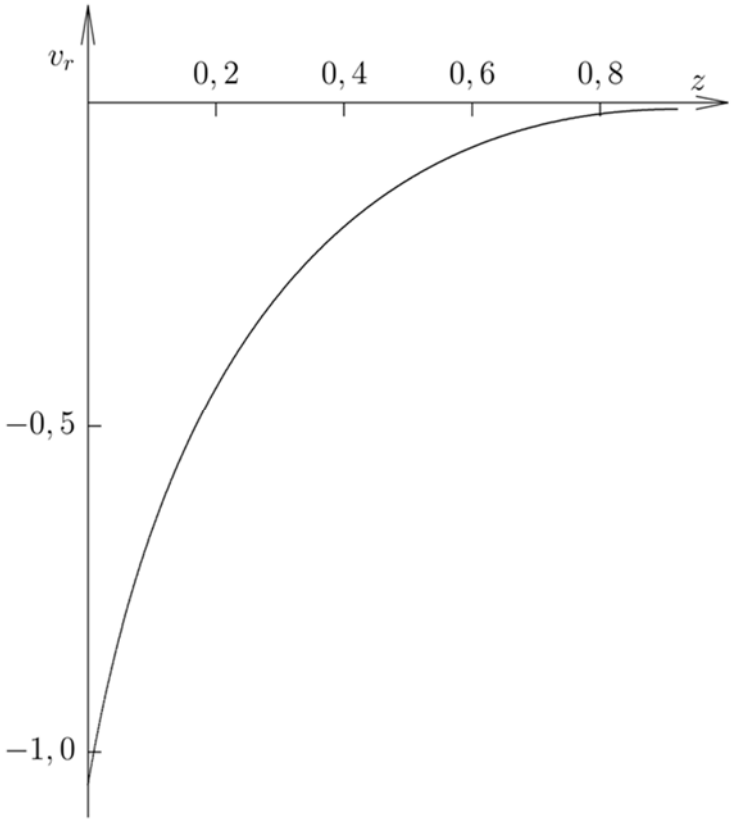

Figure 3 - The profile of the normal component of the relative velocity

Dimensionless coefficients $c_1 = \frac{l_1}{\Delta}$ and $c_2 = \frac{l_2}{R_2}$ were determined under the condition that the parameterization provides the continuity of the tangential component of the velocity in average on the boundary the best way. We made a functional equaled to the average square of a jump of the tangential component of the velocity on the boundary

$$F(c_1, c_2) = \int_{\Gamma_3} (v_z^A - v_z^B)^2 \, dz \tag{18}$$

and parameters c_1 and c_2 were defined under the condition of the F functional minimum. It results in

$$c_1 = 0{,}69 \text{ and } c_2 = 0{,}31 \tag{19}$$

Parameters a_0, a_1 and b_0 were

$$a_0 = -0{,}70,\ a_1 = -2{,}79 \text{ and } b_0 = -0{,}53 \tag{20}$$

(a normalization of these coefficients is determined by an amplitude of the normal component of the velocity on the boundary Γ_2 and may be considered arbitrary). At these parameter values the calculation error of the tangential component was about 5%. A profile of the normal component of the velocity is shown in the fig. 3. The fig. 3 shows that the profile of the normal component of the velocity on the boundary Γ_3 (i.e. in the output hole of the outer manifold) is mainly determined by the characterized size Δ and therefore the disturbance related to a sudden widening has the size of the same order. The part of the profile that has the characterized size R_2 has an amplitude less or about 5%, if exists at all.

В.Н. Колескин[1], А.А. Юнусов[2], А.А. Юнусова[2], П.Г. Штерн[1], А.В. Лукьянова[1], М.А. Амандыков[2], Д.К. Жумадуллаев [3]

[1]ФБГОУ «Ресей ЖБҒМ К.Д.Ушинский атындағы Ярославль мемлекеттік педагогикалық университеті», Ярославль, Ресей;
[2] Қазақстан инженерлі-педагогикалық Халықтар достығы университеті, Шымкент, Қазақстан;
[3]М.Әуезов атындағы Оңтүстік Қазақстан мемлекеттік университеті, Шымкент, Қазақстан

АҒЫНДЫ ҚОЗҒАЛМАЙТЫН ТҮЙІРШІКТІ ҚАБАТЫ БАР ЖАЗЫҚ ЖӘНЕ РАДИАЛДЫ БАЙЛАНЫС АППАРАТТАРДА МОДЕЛЬДЕУ. II САЛАДАҒЫ ЕСЕПТЕРДІ ШЕШУ(ЖИНАУШЫ КОЛЛЕКТОР). (2 бөлім)

Аннотация. Химиялық технологияның маңызды элементтерінің бірі катализатордың қозғалмайтын қабаты бар аксиальді немесе радиалды түрдегі реакторларда іске асырылатын гетерогенді каталитикалық процестер болып табылады. Ғалымдар мен өндірушілердің назарына осындай байланыс құрылғыларын зерттеу мен қолдануға бірқатар артықшылықтар себеп болған: фазалар бөлімінің жоғары дамыған беті, ағындардың жоғары жылдамдықтарын қамтамасыз ету мүмкіндігі, демек, габариттер мен материал сыйымдылығын азайту, конструкцияның қарапайымдылығы мепайдаланудағы сенімділік. Байланыс аппараттарының жұмысын жақсартуға қолданыстағы технологияларды жетілдіру және жаңа технологияларды, катализаторлар мен дисперсиялық жүйелердің құрылымдарын құру есебінен қол жеткізілуі мүмкін. Алайда, бірқатар жағдайларда аппараттың жұмыс аймағында ірі масштабты гидродинамикалық біртекті еместіктердің болуы химиялық, жылу-масса алмасу және басқа да процестердің тиімділігін арттыру бойынша іс-әрекетті жоққа шығарады. Гидродинамикалық біртекті емес құбылыстардың пайда болу себептерін анықтау түйіршікті қабаттарда сұйықтық пен газдың қозғалыс физикасының ерекшеліктерін зерттеуді талап етеді. Химиялық реакторларды пайдалану тәжірибесі өнеркәсіптік процестің техникалық-экономикалық көрсеткіштері, әдетте, осы процесті жобалау сатысында алынған есептік мәндерден төмен екендігін куәландырады. Қазіргі уақытта реактордың өнімділігіне әсер ететін себептердің бірі түйіршікті катализатордың қабатындағы реагенттер ағынының біртекті еместілігі болып табылатыны дәлелденген деп санауға болады. Жұмыс қозғалмайтын түйіршікті қабаты бар жазық және радиалды контактілі аппараттарда қысылмайтын сұйықтықтың ағынын математикалық моделдеуге және осы модельді сандық іске асыру әдістерін құруға арналған. Үш бөліктен тұратын нақты реактордың моделі бойынша жұмыс циклі ұсынылды: таратушы коллектор, жинайтын коллектор және түйіршікті катализатордың қозғалмайтын қабаты жүктелетін жұмыс аймағы. Газ ағынын модельге енгізу және шығару Z - бейнелі схема

бойынша жүзеге асырылады. Реактордың әрбір аймағындағы процестер мен олардый сипаттайтын теңдеулерді егжей-тегжейлі қарастырайық.

Түйін сөздер: химиялық реактор, қозғалмайтын түйіршікті қабат, катализатор, Эрган заңы, ток функциясы, түйіршікті ортаның кедергі факторы, Грин функциясы, қысым өрісі, жылдамдық өрісі, қабат кедергісі.

В.Н. Колескин[1], А.А. Юнусов [2], А.А. Юнусова[2], П.Г. Штерн[1], А.В. Лукьянова[1], М.А. Амандыков[2], Д.К. Жумадуллаев [3]

[1]ФБГОУ «Ярославский государственный педагогический университет им. К.Д.Ушинского Минвышобрнауки России» Ярославль, Россия;
[2]Университет Дружбы народов имени академика А.Куатбекова, Шымкент, Казахстан;
[3]Южно-Казахстанский государственный университет им.М.Ауэзова, Шымкент, Казахстан

МОДЕЛИРОВАНИЕ ТЕЧЕНИЯ В ПЛОСКИХ И РАДИАЛЬНЫХ КОНТАКТНЫХ АППАРАТАХ С НЕПОДВИЖНЫМ ЗЕРНИСТЫМ СЛОЕМ. РЕШЕНИЕ ЗАДАЧИ В ОБЛАСТИ II (СОБИРАЮЩИЙ КОЛЛЕКТОР). (Часть 2)

Аннотация. Одними из важнейших элементов химической технологии являются гетерогенные каталитические процессы, реализуемые в реакторах аксиального или радиального типа с неподвижным слоем катализатора. Вниманию учёных и производственников к исследованию и применению таких контактных устройств обусловлено рядом преимуществ: высокоразвитой поверхностью раздела фаз, возможностью обеспечения высоких скоростей потоков и, следовательно, уменьшения габаритов и материалоёмкости, простотой конструкции и надёжностью в эксплуатации. Улучшение работы контактных аппаратов может быть достигнуто за счёт усовершенствования существующих и создания новых технологий, катализаторов и структур дисперсных систем. Однако, в ряде случаев наличие крупномасштабных гидродинамических неоднородностей в рабочей зоне аппарата сводит на нет усилия по повышению эффективности химических, тепло-массообменных и других процессов. Выяснение причин возникновения гидродинамических неоднородностей требует изучения особенностей физики движения жидкости и газа в зернистых слоях. Опыт эксплуатации химических реакторов свидетельствует о том, что технико-экономические показатели промышленного процесса как правило ниже расчётных значений, полученных на стадии проектирования этого процесса. В настоящее время можно считать доказанным, что одной из причин, влияющих на производительность реактора, является неоднородность потока реагентов в слое зернистого катализатора. Работа посвящена математическому моделированию течения несжимаемой жидкости в плоских и радиальных контактных аппаратах с неподвижным зернистым слоем и построению методов численной реализации этой модели. Предложен цикл работ по модели реального реактора, состоящего из трех частей: раздающего коллектора, собирающего коллектор и рабочей зоны в которую загружается неподвижный слой зернистого катализатора. Ввод и вывод газового потока в модели осуществлен по Z-образной схеме. Рассмотрим подробно процессы и описываемые их уравнения в каждой зоне реактора.

Ключевые слова: химический реактор, неподвижный зернистый слой, катализатор, закон Эргана, функция тока, фактор сопротивления зернистой среды, функция Грина, поле давлений, поле скоростей, сопротивление слоя.

Information about authors:

Yunusov Anarbay Aulbekovich, Candidate of Physical and Mathematical Sciences, assistant professor, Kazakhstan Engineering and Pedagogical University of Peoples' Friendship, Shymkent, Kazakhstan, e-mail: yunusov1951@mail.ru, https://orcid.org/0000-0002-0647-6558;

Yunusova Altynai Anarbaevna, Candidate of Technical Sciences, assistant professor, Kazakhstan Engineering and Pedagogical University of Peoples' Friendship, Shymkent, Kazakhstan, e-mail: altyn_79@mail.ru, https://orcid.org/0000-0002-4215-4062;

Amandykov Madamin Aldamuradovich, Candidate of Technical Sciences, assistant professor, Kazakhstan Engineering and Pedagogical University of Peoples' Friendship, Shymkent, Kazakhstan, e-mail: Madamin01@mail.ru, https://orcid.org/0000-0001-6378-0540;

Shtern Pavel Gennadevich, Doctor of Technical Sciences, Professor, Yaroslavl State Pedagogical University named after K.D.Ushinsky, Yaroslavl, Russia https://orcid.org/0000-0002-5513-3068;

Lukyanova Antonina Vladimirovna, Candidate of Physical and Mathematical Sciences, Yaroslavl State Pedagogical University named after K.D.Ushinsky, Yaroslavl, Russia, https://orcid.org/0000-0002-7647-4910;

Koleskin Vladimir Nikolaevich, Candidate of Technical Sciences, assistant professor, Yaroslavl State Pedagogical University named after K.D.Ushinsky, Yaroslavl, Russia, https://orcid.org/0000-0003-2426-2817;

Zhumadullayev Daulet Koshkarovich, PhD, senior teacher of the Department of Technological Machines and Equipment, M.Auezov South Kazakhstan State University, e-mail:daulet_ospl@mail.ru, https://orcid.org/0000-0002-6552-2817

REFERENCS

[1] Slattery J. (1978) Theory of the impulse, mass and energy transfer in continuous medium [Teoriya perenosa impul'sa, energii i massy w sploshnykh sredakh]. Energiya, Moscow (in Russian).

[2] Sedow L.I. (1970) Mechanics of the continuous medium [Mekhanika sploshnykh sred]. Nauka, Moscow (in Russian).

[3] Goldshtik M.A. (1984) Transfer processes in a granular layer [process perenosa w zernistoms sloe]. Institute of thermophysics SO AN USSR, Novosibirsk (in Russian).

[4] Nesterowich M.I. (1979) Equations for a turbulent motion of heterogeneous mixtures [Urawneniya turbulentnogo dwizheniya geterogennykh smesej]. Novosibirsk, Preprint ITPM SO AN USSR № 8 (in Russian).

[5] Berdichewskij V.L. (1987) Variational principles of a continuous medium mechanics [Varaitsionnye printsypy mekhaniki sploshnykh sred]. - P. 447–461, Nauka, Moscow (in Russian).

[6] Sergeev S.P. (1990) Radial catalytic reactors with a still granular layer : thesis for the Ph. D. degree in technical science [Radial'nye kataliticheskie reaktora s nepodwizhnym zernistym sloem: diss. … dokt. tekhn. nauk]. NIFKHI by LY Karpov, Moscow (in Russian).

[7] Koleskin V.N. (1992) The structure and organization of a still granular layer in in cylindrical devices : thesis for the Ph. D. degree in technical science [Struktura I organizatsiya nepodvizhnogo zernistogo sloya v tsilindricheskikh apparatakh : diss. … kand. techn. nauk]. IONH RAN, Moscow (in Russian).

[8] Koleskin V.N. (2018) Methods of investigating and obtaining a homogeneous structure of granular layer [Metody izucheniya i polucheniya odnirodnoj struktury zernistogo sloya]. Eurasian Union of scientists (EUS), 7(52), p.15–19.

[9] Shtern P.G., Koleskin V.N. (2018) Hydrodynamics and evaluation of chemical reactors with a still layer of granular catalyst [Gidrodinamika i raschet khimicheskikh reaktorov s nepodvizhnym sloem zernistogo katalizatora]. Monograph: YSPU, Yaroslavl (in Russian).

[10] Koleskin V.N., et al (1982) Influence of bounding surfaces on a porosity distribution in a granular medium [Vliyanie ogranichivayuschikh poverkhnostej na raspredelenie poroznosti v zernistoj srede]. Journal of Engineering Physics [Inzhenerno-fizicheskij journal]. V. 42, № 4, p. 578–581 (in Russian).

[11] Koleskin V.N., et al. (1992) Structural and hydrodynamical heterogeneities of a still granular layer in axial units [Strukturnye i gidrodinamicheskie heodnorodnosti nepodvizhnogo zernistogo sloya v aksial'nykh apparatakh] / Theoretical Foundations of Chemical Engineering [Teoreticheskie osnovy khimicheskoj tekhnologii]. V. 26, № 6, p. 800–811 (in Russian).

[12] Shtern P.G., et al. (1989) The isothermal axisymmetric flow of an incompressible liquid in contact units of a radial type [Izotermicheskoe techenie neszhimaemoj zhidkosti v kontaktnykh apparatakh radial'nogo tipa]. Journal of Engineering Physics [Inzhenerno-fizicheskij journal]. V. 56, № 1, p. 555 (in Russian).

[13] Luk'yanenko I.S. (1995) Mathematical model of processes taking place in radial reactors [Matematicheskaya model' protsessov, protekayuschikh v radial'nykh reaktorakh]. Chemical Industry [Khimicheskaya promyshlennost'], 31, p. 72 (in Russian).

[14] Dil'man V.V., et al. (1971) Description of a flow in a channel with porous walls upon an energy equation [Opisanie potoka v kanale s pronitsaemymi stenkami na osnove uravnenuya energii]. Theoretical Foundations of Chemical Engineering [Teoreticheskie osnovy khimicheskoj tekhnologii]. V. 5, № 4, p. 564–571 (in Russian).

[15] Nazarov A.S. (1981) Flow distribution in perforated channels with a porous end [Raspredelenie potokow w perforirowannykh kanalakh s pronichaemym tortsem]. Journal of Engineering Physics [Inzhenerno-fizicheskij journal]. V. 41, № 6, p. 1009–1016 (in Russian).

[16] Idel'chik I.K. (1975) Reference book of hydraulic resistances [Sprawochnik po gidrawlicheskim soprotiwleniyam]. Mashinostroenie, Moscow (in Russian).

[17] Shtern P.G. (1995) Development of evaluation methods for industrial chemical reactors : thesis for the Ph. D. degree in technical science [Postroenie metodow rascheta promyshlennykh khimicheskikh reaktorow : diss. … dokt. tekhn. nauk] NIFKHI by LY Karpov, Moscow (in Russian).

[17] Shtern P.G. (1995) Development of evaluation methods for industrial chemical reactors : thesis for the Ph. D. degree in technical science [Postroenie metodow rascheta promyshlennykh khimicheskikh reaktorow : diss. … dokt. tekhn. nauk] NIFKHI by LY Karpov, Moscow (in Russian).

[18] Korn T. (1968) Mathematics reference book for scientists and engineers [Sprawochnik po matematike dlya nauchnykh sotrudnikow i ingenerow]. Nauka, Moscow (in Russian).

[19] Bateman H., et al. (1966) Higher transcendental functions. Bessel's functions, functions of a parabolic cylinder, orthogonal polynomials [Wyschie transtsendentnye funktsii. Funktsii Besselya, funktsii parabolicheskogo tsilindra, ortogonal'nye mnogochleny]. V.2. Nauka, Moscow (in Russian).

[20] Godunov S.K., et al. (1973) Difference schemes [Raznostnye schemy]. Nauka, Moscow (in Russian).

[21] Zhohov A.L., et. al. (2019) The possibility of creating learning situations and learning tasks in learning mathematics at school // NEWS of the national academy of sciences of the Republic of Kazakhstan Physico-mathematical series. №1(323), -2019, P. 22-27. https://doi.org/10.32014/2019.2518-1726.5 (in English)

МАЗМҰНЫ

СОДЕРЖАНИЕ

CONTENTS

Publication Ethics and Publication Malpractice
in the journals of the National Academy of Sciences of the Republic of Kazakhstan

For information on Ethics in publishing and Ethical guidelines for journal publication see **http://www.elsevier.com/publishingethics** and **http://www.elsevier.com/journal-authors/ethics**.

Submission of an article to the National Academy of Sciences of the Republic of Kazakhstan implies that the described work has not been published previously (except in the form of an abstract or as part of a published lecture or academic thesis or as an electronic preprint, see **http://www.elsevier.com/postingpolicy**), that it is not under consideration for publication elsewhere, that its publication is approved by all authors and tacitly or explicitly by the responsible authorities where the work was carried out, and that, if accepted, it will not be published elsewhere in the same form, in English or in any other language, including electronically without the written consent of the copyright-holder. In particular, translations into English of papers already published in another language are not accepted.

No other forms of scientific misconduct are allowed, such as plagiarism, falsification, fraudulent data, incorrect interpretation of other works, incorrect citations, etc. The National Academy of Sciences of the Republic of Kazakhstan follows the Code of Conduct of the Committee on Publication Ethics (COPE), and follows the COPE Flowcharts for Resolving Cases of Suspected Misconduct (**http://publicationethics.org/files/u2/New_Code.pdf**). To verify originality, your article may be checked by the Cross Check originality detection service **http://www.elsevier.com/editors/plagdetect**.

The authors are obliged to participate in peer review process and be ready to provide corrections, clarifications, retractions and apologies when needed. All authors of a paper should have significantly contributed to the research.

The reviewers should provide objective judgments and should point out relevant published works which are not yet cited. Reviewed articles should be treated confidentially. The reviewers will be chosen in such a way that there is no conflict of interests with respect to the research, the authors and/or the research funders.

The editors have complete responsibility and authority to reject or accept a paper, and they will only accept a paper when reasonably certain. They will preserve anonymity of reviewers and promote publication of corrections, clarifications, retractions and apologies when needed. The acceptance of a paper automatically implies the copyright transfer to the National Academy of Sciences of the Republic of Kazakhstan.

The Editorial Board of the National Academy of Sciences of the Republic of Kazakhstan will monitor and safeguard publishing ethics.

(Правила оформления статьи для публикации в журнале смотреть на сайтах:

www:nauka-nanrk.kz

http://physics-mathematics.kz/index.php/en/archive

ISSN 2518-1726 (Online), ISSN 1991-346X (Print)

Редакторы: *М. С. Ахметова, Д. С. Аленов, А. Ахметова*
Верстка на компьютере *А.М. Кульгинбаевой*

Подписано в печать 12.08.2020.
Формат 60x881/8. Бумага офсетная. Печать – ризограф.
9,25 п.л. Тираж 300. Заказ 4.

Национальная академия наук РК
050010, Алматы, ул. Шевченко, 28, т. 272-13-18, 272-13-19

Уважаемые авторы научных журналов НАН РК!

Президиумом НАН РК принято решение, в целях повышения международного рейтинга академических изданий, объединить следующие 3 журнала, начиная с № 5 (сентябрь-октябрь), 2020 г., с высокорейтинговыми журналами НАН РК, входящими в международные базы Scopus, WoS и др.:

1. **«Известия НАН РК. Серия биологических и медицинских наук»** объединить с журналом «Доклады НАН РК»;

2. **«Известия НАН РК. Серия аграрных наук»** – «Доклады НАН РК»;

3. **«Известия НАН РК. Серия общественных и гуманитарных наук»** – с журналом «Вестник НАН РК».

Статьи, которые публиковались в журналах «Известия НАН РК. Серия биологических и медицинских наук» и «Известия НАН РК. Серия аграрных наук», впредь будут публиковаться в журнале **«Доклады НАН РК»**, а статьи, публикуемые в журнале «Известия НАН РК. Серия общественных и гуманитарных наук», – в журнале **«Вестник НАН РК»**.

При подаче статей просим указывать название журнала и отрасль науки, согласно представленного перечня (см. ниже) в данном журнале:

I. Научный журнал **«Вестник НАН РК»** посвящен исследованиям фундаментальной науки (гуманитарные и естественные):

Редакционная коллегия принимает статьи по следующим отраслям науки:

1. Гуманитарные (экономика, юриспруденция, история и археология, политология и социология, философия, филология, педагогика и психология, литературоведение, искусствоведение)
2. Естественные (астрономия, физика, химия, биология, география и технические науки). Примеры технических наук: космонавтика, кораблестроение, машиностроение, системотехника, электротехника, электросвязь, радиоэлектроника, ядерная энергетика и т.д.

Адрес сайта «**Вестник НАН РК**» – http://www.bulletin-science.kz/index.php/en/arhive

II. Научный журнал **«Доклады НАН РК»** посвящен исследованиям в области получения наноматериалов, биотехнологии и экологии.

Редакционная коллегия принимает статьи по следующим отраслям науки:

1. Получение наноматериалов в области естественных наук, медицины и сельского хозяйства.
2. Биотехнология в земледелии, растениеводстве и зоотехнике.
3. Общая биология и биотехнология в медицине.
4. Экология.

Адрес сайта «**Доклады НАН РК**» – http://reports-science.kz/index.php/en/archive

Кроме того, в журналах «Известия НАН РК. Серия физико-математическая», «Известия НАН РК. Серия химии и технологий» и «Известия НАН РК. Серия геологии и технических наук» также указаны отрасли науки, по которым будут приниматься научные статьи для экспертизы и дальнейшего опубликования:

III. Научный журнал **«Известия НАН РК. Серия физико-математическая»** посвящен исследованиям в области математики, физики и информационной технологии.

Редакционная коллегия принимает статьи по следующим отраслям науки:

1. Математика.
2. Информатика.
3. Интеллектуальный анализ данных и распознавание образов.
4. Математическое моделирование социальных и экономических процессов.
5. Механика.
6. Механика машин и роботов.
7. Теория управления и космические исследования.
8. Физика.
9. Ядерная физика.
10. Теоретическая физика.
11. Астрономия.
12. Ионосфера.

Адрес сайта «**Известия НАН РК. Серия физико-математическая**» –
http://physics-mathematics.kz/index.php/en/archive

IV. Научный журнал **«Известия НАН РК. Серия химии и технологий»** посвящен исследованиям в области химии и технологий новых материалов.

Редакционная коллегия принимает статьи по следующим отраслям науки:

1. Органическая химия.
2. Неорганическая химия.
3. Высокомолекулярные соединения.
4. Физическая химия (катализ, электрохимия).
5. Технология новых материалов.
6. Технология органических веществ.
7. Технология неорганических веществ.
8. Технология химических удобрений.
9. Технология полимерных и строительных материалов и силикаты.
10. Технология пищевых продуктов.
11. Фармацевтическая химия.

Адрес сайта **«Известия НАН РК. Серия химии и технологии» –**

http://chemistry-technology.kz/index.php/en/arhiv

V. Научный журнал **«Известия НАН РК. Серия геологии и технических наук»** посвящен исследованиям в области геологии и технических наук:

Редакционная коллегия принимает статьи по следующим отраслям науки:

1. Геология.
2. Региональная геология.
3. Петрология.
4. Геология нефти и газа.
5. Геология и генезис рудных месторождений.
6. Гидрогеология.
7. Горное дело и геомеханика.
8. Фундаментальные проблемы обогащения минерального сырья.
9. Инженерная геология.
10. Геофизика и сейсмология.
11. География.

Адрес сайта **«Известия НАН РК. Серия геологии и технических наук» –**
http://www.geolog-technical.kz/index.php/en/archive